

# Sheffield Hallam University

*Stress-strain properties and micro-structural change in metal deformed at strain rates of upto  $10^5$  per second.*

HAQUE, Md. Mohafizul.

Available from the Sheffield Hallam University Research Archive (SHURA) at:

<http://shura.shu.ac.uk/19752/>

## A Sheffield Hallam University thesis

This thesis is protected by copyright which belongs to the author.

The content must not be changed in any way or sold commercially in any format or medium without the formal permission of the author.

When referring to this work, full bibliographic details including the author, title, awarding institution and date of the thesis must be given.

Please visit <http://shura.shu.ac.uk/19752/> and <http://shura.shu.ac.uk/information.html> for further details about copyright and re-use permissions.

POLYTECHNIC LIBRARY  
POND STREET  
SHEFFIELD S1 1WB

6987

79 3236101X

**Sheffield City Polytechnic Library**

**REFERENCE ONLY**

ProQuest Number: 10697054

All rights reserved

INFORMATION TO ALL USERS

The quality of this reproduction is dependent upon the quality of the copy submitted.

In the unlikely event that the author did not send a complete manuscript and there are missing pages, these will be noted. Also, if material had to be removed, a note will indicate the deletion.



ProQuest 10697054

Published by ProQuest LLC (2017). Copyright of the Dissertation is held by the Author.

All rights reserved.

This work is protected against unauthorized copying under Title 17, United States Code  
Microform Edition © ProQuest LLC.

ProQuest LLC.  
789 East Eisenhower Parkway  
P.O. Box 1346  
Ann Arbor, MI 48106 – 1346

STRESS-STRAIN PROPERTIES AND MICRO-STRUCTURAL CHANGE IN  
METAL DEFORMED AT STRAIN RATES OF UPTO  $10^5$  PER SECOND

By

MD. MOHAFIZUL HAQUE, M. Sc

A Thesis submitted to the COUNCIL FOR  
NATIONAL ACADEMIC AWARDS in partial  
fulfilment for the degree of  
DOCTOR OF PHILOSOPHY

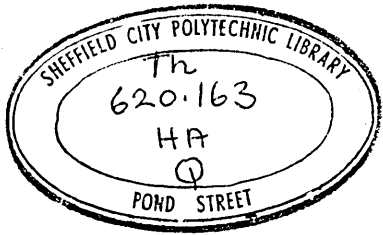
SPONSORING ESTABLISHMENT:

Department of Mechanical and Production Engineering  
Sheffield City Polytechnic  
Sheffield, U.K.

COLLABORATING ESTABLISHMENT:

British Steel Corporation  
Sheffield Laboratories

December 1983



7932361-01

## DECLARATION

All the work reported in this thesis was carried out by the candidate at Sheffield City Polytechnic during the period of October 1980 to December 1983.

The candidate has not been a registered student for any other CNAA award or for any University degree, during the period of registration for the CNAA degree of Ph.D.

To the best of his knowledge, the results presented in the thesis originated from the present study, except where references have been made. No part of this thesis has been submitted for a degree at any other institution.

Signature of Candidate:

(MD. MOHAFIZUL HAQUE)

## ACKNOWLEDGEMENTS

The author wishes to express his sincere gratitude to Dr. M S J Hashmi, Principal Lecturer, for his supervision and guidance and to Dr. F B Pickering, Reader in Metallurgy, for his constructive suggestions and comments during the course of this project.

The author is indebted to Mr. O Bardsley, the former Head of the Department of Mechanical and Production Engineering for his kind support and to the Authority of Sheffield City Polytechnic for the approval to carry out this work.

Sincere thanks are also extended to Messrs. R Wilkinson, P Fisher and D McKay and other technical staff for their support at various stages of this work.

Finally, a word of thanks to my wife for her patience and support towards completion of my work, sometimes at the expense of her own pleasure.

STRESS-STRAIN PROPERTIES AND MICRO-STRUCTURAL CHANGE IN  
METAL DEFORMED AT STRAIN RATES OF UPTO  $10^5$  PER SECOND

M. M. Haque

ABSTRACT

A ballistic test equipment has been designed, constructed and commissioned to facilitate firing of cylindrical projectiles at speeds varying from 30 to 300 m/s on to small cylindrical test specimen placed on to a rigid anvil. Compressed air was used to propel the projectile the speed of which before impact was measured using laser-beam interruption device. An IMACON high speed camera was used to continuously record the deformation-time history of the specimen and these records were then used to obtain the prevailing force, strain, stress and strain rate histories during the entire deformation process.

The stress-strain curves over large strain ranges were obtained from tests carried out on specimen statically pre-strained to different levels. The effect of strain rate history on the pre-strained specimen was found to be negligibly small and hence ignored. The temperature rise during highspeed deformation and material inertia were assumed to have mutually cancelling effect on the deduced stress values. The effect of friction was found to be significant and appropriate corrections were introduced to account for this effect.

Following the above procedure, the stress-strain characteristics of structural steel (En-8) at strain rates of up to  $10^5$  per second at  $-30^\circ\text{C}$ , room temperature and at  $235^\circ\text{C}$  have been established. The structural steel has shown a strong strain rate sensitivity within the strain rate range of about  $10^3$  to about  $10^5$  per second. Comparative studies showed that copper was more strain rate sensitive than aluminium and steel used in the present investigation.

There were no marked differences observed in the micro-structures of the structural steel specimen deformed quasi-statically and dynamically at  $-30^\circ\text{C}$ , room temperature and at  $235^\circ\text{C}$ . There was also no distinguishable micro-structural change observed in the structure of aluminium specimen deformed at low and high strain rates but mechanical twinning was observed in the micro-structure of copper specimens deformed at high strain rates.

## CONTENTS

	<u>Page No.</u>
DECLARATION	(i)
ACKNOWLEDGEMENT	(ii)
ABSTRACT	(iii)
CHAPTER 1	
INTRODUCTION	1
1.1 Importance of Stress-Strain Data at High Strain Rates	1
1.1.1 Blast load resistance and demolition of structures	1
1.1.2 Forming of metals	3
1.1.3 Dynamic compaction of metal powders	4
1.2 Review of Previous Works and Deficiencies	5
1.3 Selection of Test Materials	8
1.4 Aim and Plan of the Present Project	9
CHAPTER 2	
DESIGN, DEVELOPMENT AND COMMISSIONING OF THE EXPERIMENTAL RIG	11
2.1 Introduction	11
2.2 Load Cell and Anvil Unit	11
2.3 Barrel and Loading Throat Unit	12
2.4 2-Way Ball Valve and Reservoir Unit	13
2.5 Construction of the Experimental Rig	14
2.6 Commissioning and Synchronization of the Experimental Set-up	15
2.6.1 Firing of the Projectile	15
2.6.1.1 Calibration of pressure transducer	16
2.6.1.2 Calibration of the projectile speed	16
2.6.2 Recording the Load-Time History	16

2.6.3	Calibration of Speed Measuring Technique by Laser-Beam	17	
2.6.4	Recording Deformation-Time History	18	
2.6.4.1	Positioning of the laser and photo-cell units	18	
2.6.4.2	Delay timing and selection of lens aperture	19	
2.6.4.3	Modification of the optical extension tube	20	
CHAPTER 3			
EXPERIMENTAL TECHNIQUE AND PREPARATION OF THE PROJECTILES AND BALLISTIC TEST SPECIMENS			21
3.1	Introduction	21	
3.2	Preparation of the Projectiles	21	
3.3	Preparation of the Ballistic Test Specimens	22	
3.4	Operational Technique of the Camera	24	
3.5	Technique for Recording Time- Deformation History	26	
3.6	Calibration of Streak Unit	27	
3.7	Loading, Firing and Recording Procedure	28	
3.8	Other Electronic Instrumentations for Recording	29	
3.9	Reading under Travelling Microscope	30	
3.10	Selection of Curve Fitting Equation	31	
3.11	Construction of the Stress-Strain Curves	32	
3.11.1	Initial approach	32	
3.11.2	Alternative arrangement	35	
3.11.3	Technique of the construction of dynamic stress-strain curve	37	
3.11.4	Effect of total deformation	38	
3.12	Arrangement for Conducting Tests at Sub-zero and at Warm Temperatures	39	
3.12.1	Arrangement for low temperature tests	39	
3.12.2	Arrangement for high temperature tests	41	

	<u>Page No.</u>
3.13 Metallography	43
CHAPTER 4	
RESULTS OF THE EXPERIMENTS	44
4.1 Introduction	44
4.2 Results of the Preliminary Tests	44
4.2.1 Effect of strain rate history	44
4.2.2 Effect of total deformation	48
4.2.3 Effect of specimen geometry	50
4.2.4 Effect of friction	51
4.3 Results from the Main Test Programme	54
4.3.1 Stress-strain characteristics of structural steel	54
4.3.2 Stress-strain characteristics of aluminium and copper	58
4.3.3 Proposed constitutive equation	59
4.4 Micro-examination of Structures	61
4.4.1 Micro-examination of structural steel	61
4.4.2 Micro-examination of aluminium and copper	62
4.5 Error Analysis	63
CHAPTER 5	
DISCUSSION OF RESULTS	64
5.1 Introduction	64
5.2 Effect of Strain Rate History	64
5.3 Effect of Pre-straining	66
5.4 Effect of Specimen Geometry	67
5.5 Effect of Radial Inertia	69
5.6 Effect of Friction	71
5.7 Temperature Rise during Deformation	72
5.8 Comparison of Dynamic and Static Stress-Strain Characteristics of En-8 Steel at Different Temperatures	74

	<u>Page No.</u>
5.8.1 Quasi-static stress-strain characteristics	74
5.8.2 Dynamic stress-strain characteristics	76
5.8.3 Strain rate sensitivity	76
5.9 Comparison of Dynamic and Static Stress-Strain Characteristics of Aluminium and Copper	78
5.10 Metallographic Studies	81
5.10.1 For En-8 steel	81
5.10.2 For aluminium and copper	83
 CHAPTER 6	
CONCLUSIONS	85
 LIST OF TABLES	88
 LIST OF FIGURES	149
 REFERENCES	238
 APPENDIX	A-I

## CHAPTER 1

### INTRODUCTION

#### 1.1 Importance of Stress-Strain Data at High Strain Rates

Data on the mechanical behaviour of metals at very high strain rates are required for a variety of reasons. From the theoretical stand point, there is a need to study the rate-controlled mechanism for plastic flow which, in many materials has been found to change when the strain rate exceeds about  $10^4$  per second (1). From the practical stand point, strain rates of this order, and above are encountered in many real engineering situations and applications. The broad band of practical topics are in the field of the following:

- (i) Spalling, fracture, elastic wave propagation, cracking and deformation in the field of demolition,
- (ii) High energy rate metal forming processes,
- (iii) Dynamic metal powder compaction.

##### 1.1.1 Blast load resistance and demolition of structures:

Materials are often subjected to rapidly applied loading when used as construction material in certain structures which may undergo high intensity impulsive or shock loading. Due to rapid unloading and the reflection of compressive stress-waves from a free surface, scabs or

spalls may be formed in hard concrete or steel which may acquire speeds of the order of 100 m/s (2), and hence be lethal. Also fracture due to unloading - even more than loading in a (composite) concrete building structure may lead to large scale dynamic, catastrophic "knock on" collapse.

The demand in recent years for large and relatively cheaper building structures has promoted the development of several new varieties of design and the imaginative structural use of concrete which may be reinforced, pre-stressed or post-tensioned, with steel bar. This has given rise to buildings with a considerable sophistication in the structural design. The ability of these buildings to withstand blast loading effect require to be assessed which in turn requires high strain rate data. The demolition of such buildings at the end of their useful life is also a complex operation. The non-critical severing or removal of only some stressed elements in some of these modern, large and continuous structures may well lead to disastrous dynamic collapse. Demolition work therefore, must be approached with great caution; straightforward demolition, for example, by swinging a heavy steel ball, will often be quite inadequate for these modern structures whether it be accompanied by the use of explosives and drilling or not.

For demolition of other structures such as railway bridges, factory chimneys and the removal of foundations

and buildings shot-hole charges tend to be used (3). In the breaking up of heavy plant such as acid pots, retorts and boilers etc. by concussion charges and the cutting of concrete, steel and wood etc. "lay on" charges are usually employed. However, from an engineering point of view, this has important design aspects for a variety of structures which may go shock loading.

#### 1.1.2 Forming of metals:

The principal use which metal processing engineers have for conventional strain rate data is to facilitate predictive calculations for tool pressures or loads developed in causing a certain operation or process to take place. In structural applications, small plastic strains in metals, beams or frames and the like, would be of interest whereas in the case of metal forming, large plastic strains are involved. But in both kinds of applications, interest in mechanics of fracture and stress-wave or shock effects is always present. The structural engineer very occasionally meets with cleavage fracture and elastic waves, but the manufacturing engineer may come across ductile fracture processes, problems of tensile instability (especially in sheet metal) and plastic waves or plastic shock fronts during forming. It has been recognised that strain rate as well as temperature affect many materials properties, including those governing the fracture initiation. The rate effect can be due to either mechanical (inertia) or metallurgical

reasons such as ageing and change of failure modes (4). Strain rate has greater effect on the flow stress in hot working range and relatively smaller effect in cold working range, this applies especially when large strains are imposed. The choice of appropriate strain rate is also important in superplastic metal forming processes. The amount of plastic flow in this case is usually very high. Interest in impressing a super-alloy composite (5) arises from the need to use new materials for turbine discs and the like, so that they can operate successfully in advanced high temperature turbo-plant. It is important to know the strain rates and temperatures in order to avoid excessive damage in the forming of such materials.

#### 1.1.3 Dynamic compaction of metal powders:

In recent years, metal powders have been prepared and made commercially available on a large scale, for conversion into engineering components directly by means of quasistatic compaction processes. Powder metallurgical fabrication techniques have been developed because (a) for some components and materials, established forming methods are unsuitable, e.g. there are difficulties with refractory metals in melting and cutting; (b) savings on material wastage or in machining costs are possible and worthwhile, e.g. with many iron-based alloys; and (c) they afford greater control of structure, e.g. grain size and component distributions are more homogenous.

However, dynamic compaction appears to have

originated in about the 1950's in the belief that compact properties such as uniform density, improved green strength and lower ejection forces from dies and containers, as well as increased production rates, could be secured by this means. Uniaxial and isodynamic compaction systems are found to be most suitable arrangements for industry. Ballistic and explosive uniaxial compaction presses are said to operate at strain rates of upto  $10^2$  to  $10^3$  per second respectively (6). Magnetic and explosive isodynamic compaction systems have been tried but details of press design and product properties are not available. Therefore, fundamental informations about the stress-strain properties of metal powders at high strain rates are necessary to secure better compaction systems.

## 1.2 Review of Previous Works and Deficiencies

As early as the 1930's and probably earlier, investigators (7-9) attempted to measure the effects of deformation rate upon the resultant mechanical properties of the deformed metals. Since then, however, there has been significant developments in forming processes involving high strain rates at large values of strains. Electro-magnetic, explosive-hydraulic and some of the conventional forming processes are said to generate strain rates of upto  $10^5$  per second (10). The conventional tensile and compression tests are normally made at strain rates between  $10^{-3}$  and  $10^{-1}$  per second. In

contrast, many forming and machining processes are said to be carried out at strain rates in the range  $10^3$  to  $10^6$  per second or even higher (11). Although tensile and compression tests have been performed successfully at strain rates upto  $10^3$  per second, but difficulties are encountered with these methods in making the necessary measurements in the extremely limited time during which the applied load acts.

A review of recent literature shows that since the introduction of split Hopkinson pressure bar by Kolsky (12), considerable efforts by various investigators (13-15) have been directed to evaluate the stress-strain characteristics of metals at high rates of strain, usually between  $10^4$  and  $10^5$  per second. In this respect, various high speed impact apparatus and associated techniques have been devised to affect and record the deformation-time and load-time histories. Flat ended mild steel projectiles as test specimens fired against a rigid anvil enabled others (16,17) to derive the yield stress from known impact velocity and the final shape of the projectile. However, recent experimental efforts consisted of uniaxial compression using specially designed drop hammer (14,18) and ballistic tests (15) on strong material. Holzer and Brown (14) tried to obtain the deformation-time history using fibre optics non-contacting transducer which required elaborate computation for interpolation purpose while the use of high speed camera in framing mode in conjunction with separate optical system

by Gorham (15) involved tedious measurement on each frame. In addition, with the fast loading rates and limited test durations that are encountered in such situations, frequency dispersions of the stress pulse in the load measuring system is significant. Consequently, converting these raw data by various mathematical and computer manipulations, into useable form introduces the possibility of incurring errors of unknown degree. Furthermore, the variation of strain rate during deformation was not properly accounted for in the processing of the data and in the presentation of results.

However, a review of previous works (13 - 23) also shows that the material inertia (19), stress wave propagation (20), highly localised temperature effect (13,14), adiabatic shear bands (21,22) and the bulk effects (23) appear to have caused many conflicting observations and contradictory conclusions.

On the basis of the information available in the upto-date literature, it appears that there is no definite mechanism of predicting macro-deformation and failure modes of engineering components at high strain rates. Therefore, analysis of the forming and cutting processes and prediction of structural collapse and catastrophic failure, require more data and better understanding of the material behaviour at high strain rates. To analyse these processes effectively, the corresponding stress-strain properties must be known but unfortunately, at the present

time very little reliable published information is available. However, a consideration of the past works suggest that an attempt, employing new experimental technique as well as the displacement-time measuring equipments, is necessary. These were the main motivating factors behind the present study to explore further investigation on the subject.

### 1.3 Selection of Test Materials:

For the present investigation, three different materials were chosen, (i) structural steel (En-8), (ii) aluminium and (iii) copper. Aluminium and copper have been selected arbitrarily to conduct experiments at room temperature only. However, the En-8 steel has been selected because of the following applications:

The En-8 steel resembles one of the important varieties of steels, which is subjected to stresses in machine parts. This type of medium carbon steel is also used for both the construction and transportation industries for making components which are directly or indirectly subjected to dynamic loading. The main advantage of this steel is that it enables people to build lighter but relatively high strength structures while retaining the highly desirable properties of easy workability and adaptability. The structural steel is also easily available in plate, slab, bar and rod forms in the hot rolled conditions. Furthermore, a uniform strength over a range of section thickness is provided by

varying the amount of carbon, manganese and silicon contents and it does not necessarily include the alloying elements such as chromium, vanadium etc.

#### 1.4 Aim and Plan of the Present Project

The present research project has been undertaken with the following aims of investigation:

To (a) develop a suitable testing technique and method of processing the displacement-time data for establishing the stress-strain properties of metals and alloys at strain rates of upto  $10^5$  per second,

(b) establish the stress-strain characteristics of structural steel, aluminium and copper at these high rates of strain at room temperature,

(c) establish the stress-strain characteristics of structural steel at sub-zero and at warm temperatures, and compare with those at room temperature,

(d) study micro-structural changes corresponding to these high strain rate deformations, and finally

(e) compare the results with the existing data available in the literature.

In order to achieve the above objectives, it was necessary to design and develop a dynamic compression test rig capable of firing projectiles to impact on to the specimen directly. Therefore, the basic experimental

technique used in this study involved firing of a cylindrical projectile on to small disc shaped specimen placed on a rigid anvil. Compressed air was used to propel the projectile and as of interest the load-time history was also measured by using a high frequency piezo-electric load-cell and pressure bar arrangement. This measured load-time history was not used for actual derivations of the final results. In order to facilitate recording of deformation-time history, a high speed image converter (IMACON) type camera was used which is capable of recording the event at a framing rate of upto  $10^6$  frames per second and also in a continuous streak mode.

## CHAPTER 2

### DESIGN, DEVELOPMENT AND COMMISSIONING OF THE EXPERIMENTAL RIG

#### 2.1 Introduction

A schematic diagram of the experimental rig with its other accessories is shown in Fig. 1, whilst Fig. 2 shows a photograph of the experimental set-up. The test rig mainly consisted of (a) Load-Cell and Anvil Unit, (b) Barrel and Loading Throat Unit and (c) 2-Way Ball Valve and Reservoir Unit. For convenience, assembly drawing of the experimental rig was grouped into three sections. Details of each sub-assembly drawing are shown by line diagrams in Figs. 3 to 5 and the sectional drawing of the individual components are shown in Figs. 6 to 10 inclusive, all dimensions being in millimetre. The fundamental design calculations are shown in Appendix A to E.

#### 2.2 Load-Cell and Anvil Unit

A schematic diagram of this section in assembled condition is shown in Fig. 3. This unit is composed of 8 individual components listed as follows: (i) Base plate, (ii) Back-up anvil, (iii) Holder plate, (iv) Pressure bar, (v) Middle anvil, (vi) Load-cell, (vii) Top anvil and (viii) Cover plate. The detail line diagrams of these parts are shown in Figs. 6 and 7.

A robust cylindrical alloy steel (En-32) bar was used as the main pressure bar or anvil column. The top end of which is recessed to incorporate a 80 kHz piezo-electric load-cell and the top and middle anvil pieces which are made of tool steel (FMP-338). All the anvil pieces including the pressure bar were hardened by special heat treatment. The load cell is placed in between the middle and top anvil pieces. These parts are held in place by means of the top cover plate and a holder plate which in turn is fastened to the base plate at the bottom end of the pressure bar. The whole arrangement was put under 2 kN of compressive pre-load and securely attached to the base plate. The base plate is a rectangular solid En-12 steel plate having a central recess for the insertion of the back-up anvil, which is also fixed onto the reinforced concrete foundation of the test rig. All the mating surfaces of the assembly were machined and ground to a mirror finish.

### 2.3 Barrel and Loading Throat Unit

Assembled drawing of this section in line diagram is shown in Fig. 4. This unit is composed of 8 individual components listed as follows: (i) Extension barrel, (ii) Surge suppressor cap, (iii) Coupling sleeve, (iv) Loading throat, (v) Split cover, (vi) Sliding collar, (vii) Collar nut and (viii) Projectile gripper mechanism. The detailed line diagrams of these parts are shown in Fig. 8.

The extension barrel is made of En-16 steel at one end of which is attached a surge suppressor cap. The suppressor also permits the laser beam to pass through it. The other end of the extension barrel is connected to the loading throat (primary barrel) by means of a threaded and knurled coupling sleeve. The loading throat is made of En-32 alloy steel and its top end is fixed to the air release valve nut. There is a cut-out segment of the primary barrel through which the projectile can be loaded and pushed upwards inside the projectile gripper mechanism. A close fitting split cover made of En-32 alloy steel is used to close the cut-out segment, and a sliding collar and nut is used to firmly hold the assembly in place, thus preventing escape of the high pressure air upon release of the valve.

The projectile gripper mechanism consists of three grab screw and spring operated smooth pins (hardened En-32 alloy steel) incorporated at the upper end of the loading throat. The projectile holding pressure may thus easily be adjusted to suit projectiles of different masses. The coupling sleeve provides two holes in order to fix stop pins used to prevent the collar nut from sliding down.

#### 2.4 2-Way Ball Valve and Reservoir Unit

The line diagram of this section in assembled condition is shown in Fig. 5 and those of the individual

parts are shown in Figs. 9 and 10. The two main components are (a) the high pressure reservoir unit and (b) a 2-way ball valve. The ball valve of 1" B.S.P. (Part No: 012-25-34) specification is suitable for operation at pressures of upto 4700 psi at temperatures in between  $-30^{\circ}\text{C}$  to  $+100^{\circ}\text{C}$ , and is manually operated by turning a handle through  $90^{\circ}$ . This valve is firmly fixed to the bottom end of the pressure chamber by means of the valve nut. Copper gasket is used to make the assembly leak proof. The pressure chamber and valve assembly is rigidly secured to the frame of the rig by means of the holder plates specially designed for this purpose. The top end of the pressure chamber was made with appropriate connection facilities to the high pressure (2000 psi) air cylinder.

### 2.5 Construction of the Experimental Rig

Once the individual components were made, they were then assembled together and fixed to the frame of the rig.

This frame was made of welded and bolted mild steel angles and is 2 metres high overall and about half a metre square in plan area. Two platforms were provided, each on the opposite side of the rig in order to fix the laser beam generator and receiver. A small safety chamber was built using wire mesh material and perspex sheet to contain the projectile and the deformed specimen after

impact. Two Xenon flash units were placed outside this safety chamber. The front wall of the chamber was made with 20 mm thick armour glass plate. This was necessary to focus the specimen as well as to prevent any possible damage to the camera by the deformed specimen. The back wall can be easily opened and closed in order to place the specimen onto the anvil as well as to remove the specimen and the projectile after each test.

The entire rig with its frame was erected on a cubical reinforced concrete foundation built over the cemented floor.

## 2.6 Commissioning and Synchronization of the Experimental Set-up

Commissioning of the testing rig was carried out by conducting initial tests in order to standardise and calibrate the facilities for (a) firing of the projectile onto the compression test specimen, (b) recording the load-time history using 80 kHz piezo-electric load cell and pressure bar arrangement, (c) measuring the initial impact speed and (d) recording the deformation-time history using high speed image converter (IMACON) camera.

### 2.6.1 Firing of the projectile

For trial operation, a number of projectiles were made from tool steel. These were fired at different speeds onto the specimens prepared from mild steel. The rig was found to be satisfactory for firing the projectile

in order to deform the specimen upto 80% reduction in height. This facilitated selection of the appropriate size of the projectile and specimens to be used in proper testing programmes.

#### 2.6.1.1 Calibration of pressure transducer:

The pressurised air reservoir was fitted with a pressure transducer which was connected to a Roband Digital Voltmeter through a Direct Reading Transducer Meter (Type C-52). A Budenberg Gauge Tester was used to calibrate the system and the results are given in Table 1, in terms of pressure and voltage reading.

#### 2.6.1.2 Calibration of projectile speed:

Projectiles of different masses were fired at different air pressures and the corresponding speeds were measured. Fig. 11 shows a calibration chart where the broken line demonstrates how to arrive at an indicated voltage and hence the chamber air pressure corresponding to a desired projectile speed of 200 m/s. This calibration chart is used as a rough guide and the actual impact speed is obtained from the photographic record in a manner discussed later in Chapter 3.

#### 2.6.2 Recording the Load-Time History

The initial arrangement for direct load measurement consisted of a composite pressure bar contained in a tubular chamber and a high frequency piezo-electric load-

cell (80 kHz) which could be located at different positions along the length of the pressure bar. The load-time traces obtained from similar tests with the load-cell at different positions along the composite pressure bar are shown in Fig. 12. It is evident that the load-time trace is affected if the position of the load cell is changed. However, all of these measured loads produced stress values even lower than those obtained from static tests. Subsequently, it was decided that the measured load would not be used to calculate the stress values but for reference only.

In order to check the repeatability of the load-time history and that of the projectile speed, a projectile was fired at the same air-pressure to obtain a desired speed of 132 m/s for a given set of experiments. Fig. 13 shows the repeatability of load-time traces during impact whereas Fig. 14 shows the repeatability of the elapsed time covered by the projectile (19.07 mm long) before impact.

### 2.6.3 Calibration of Speed Measuring Technique by Laser Beam

In order to assess the accuracy of speed measurement by laser beam, first a thin rigid disc (15 cm dia.) of aluminium was firmly attached to a motor whose r.p.m. was controlled by a Servo Motor Controller (Type MC-43). A small hole (3 mm dia.) was made at a known radius from the

centre of the disc to allow the laser beam to pass through. A photo-cell unit of response time of 5 ns was positioned to receive the beam through the hole in the disc. A schematic diagram is shown in Fig. 15. The photo-cell unit was connected to a pre-calibrated storage oscilloscope. As soon as the motor was run at a known r.p.m, the beam remained obstructed intermittently by the disc and the photo-cell unit received signal only when the beam passed through the hole after each revolution. Instantaneously, the photo-cell unit transferred the signal to the oscilloscope screen. The elapsed time during which the beam was obstructed by the solid disc was recorded on the oscilloscope screen. From the known distance covered and the elapsed time, it was possible to calculate the speed of the disc. Now, comparison was made with this calculated speed and the actual speed of the motor as precisely regulated by the speed controller, which showed only 3% variation.

#### 2.6.4 Recording Deformation-Time History

##### 2.6.4.1 Positioning of the laser and photo-cell units:

In order to obtain a useful photographic record, it was necessary to synchronise the camera and the flashing of the flash units with the impact. The flashing time was controlled by the Trigger Delay Generator (TDG) unit and this timing was again dependent on the height of the

laser beam from the top of the test specimen as well as on the speed of the projectile. In order to maintain a constant beam height throughout the experiment, it was therefore, necessary to fix the laser and the photo-cell units at a certain position. The beam was positioned at a height of about 35 mm from the top of the specimen and the flash units were then attached to the frame one at opposite side of it as shown in Fig. 1.

#### 2.6.4.2 Delay timing and selection of lens aperture:

Once the beam height was fixed, it was possible to determine the expected time of impact and accordingly the delay time was adjusted using the TDG unit. When the beam is cut off by the high speed projectile, the TDG unit starts counting and the Xenon flash lamp flashes just after the pre-selected delay period. As soon as the event becomes luminous, a photo-cell detector triggers the camera to record the sequence of deformation.

Since it was not possible to control the intensity of light produced by the Xenon flash lamps, the aperture disc opening of the camera was chosen and adjusted by trial and error method, at position mark 16, which gave a better picture. A typical photograph is shown in Fig. 16. This same aperture position was used throughout the rest of the experiments.

#### 2.6.4.3 Modification of the optical extension tube:

Fig. 16(a) shows the sequence of pictures taken by the IMACON camera in framing mode. As the field of view was too wide to show important details of the events, it was therefore necessary to magnify the field of view such that the test specimen becomes more prominent. In order to achieve this, the optical extension tube of the camera was replaced by another 250 mm long tube which was designed and made at the Polytechnic from duralumin. Black matt paint was then sprayed over its surface to match with the original part of the camera. After attaching the optical extension tube, it was possible to obtain magnified framing sequences (about  $2\frac{1}{2}$  times of the original) as shown in Fig. 16(b).

## CHAPTER 3

### EXPERIMENTAL TECHNIQUE AND PREPARATION OF THE PROJECTILES AND BALLISTIC TEST SPECIMENS

#### 3.1 Introduction

A series of experiments were carried out in order to standardise the testing procedure to obtain accurate results using the experimental set-up described in the previous chapter. For each experiment, attempts were made to maintain identical conditions in order to compare the results for establishing most appropriate test procedures. Details of the experimental procedure are described in the following sub-sections.

#### 3.2 Preparation of the Projectiles

For the projectile, tool steel (type FMP-338) was chosen, since this material has very high strength and high resistance to impact. Furthermore, it was heat-treated to induce desired hardness and was found to be about 800 Hv 30. The composition of this material is shown in Table 2(a).

The projectile was machined to a diameter of  $9.52 \pm .001$  mm to fit closely within the loading throat.

The length of the projectile was made about 19.00 mm.

It was finely ground and polished resulting in a mirror finish surface. Using this projectile, it was

only possible to obtain stress-strain results corresponding to strain rates ranging from about  $1 \times 10^4$  to about  $2.5 \times 10^4$  per second. In order to obtain results corresponding to strain rates in excess of about  $2.5 \times 10^4 \text{ sec}^{-1}$  some lighter projectiles were subsequently made from the same material. The projectile was made lighter by drilling a 5 mm diameter blind hole into it as shown in Fig. 17. Using this lighter projectile results corresponding to strain rates of upto about  $4 \times 10^4 \text{ sec}^{-1}$  were obtained. In order to carry out comparatively low strain rate experiments, between  $7 \times 10^3 \text{ sec}^{-1}$  and  $1 \times 10^4 \text{ sec}^{-1}$ , 30 mm long projectiles were used. A threaded hook was screwed on the top of the projectile to facilitate its upward lifting by a string through the hole of the extension barrel. This extra arrangement was necessary because of the shorter length (22 mm) of the cut-out segment in the primary barrel.

In order to obtain stress-strain results in excess of  $4 \times 10^4 \text{ sec}^{-1}$ , it was necessary to use a different loading throat - extension barrel unit which facilitated 8 mm diameter projectiles. Furthermore, it was made lighter by drilling a 5 mm diameter blind hole into it. Using this smaller projectile, it was possible to obtain stress-strain results at strain rates of upto about  $1 \times 10^5$  per second.

### 3.3 Preparation of the Ballistic Test Specimens

The ballistic test specimens were prepared from

structural steel (En-8), aluminium and copper. The compositions of these metals and alloy are shown in Table 2. All the specimens in the present work were machined from as-received 15 mm round bar. In order to avoid barrelling or buckling, all the compression test specimens were made to a length to diameter ratio of less than one for both dynamic and quasi-static tests. The specimen surface was finely ground and the end faces were made as flat and parallel as possible.

For making specimens from pre-strained material, small samples of 15 mm diameter and 14 mm long were cut from the as-received 15 mm round bar. These were quasi-statically compressed to different strain levels using a 50 Ton Universal Machine and a sub-press fitted with a dial gauge. During pre-straining, graphite in grease was used as lubricant to minimise friction at the specimen-platen interface and thus induce deformation more uniformly throughout the specimen. After each 10% of strain, the test was interrupted and the interfaces were cleaned and relubricated. Ballistic test specimens of different sizes were then prepared out of these compressed samples. For carrying out comparatively low strain rate ( $7 \times 10^3 \text{ sec}^{-1}$ ) tests, specimens of 6.5 mm diameter and 6.00 mm long were used whereas, for medium high strain rate ( $2 \times 10^4 \text{ sec}^{-1}$ ) tests and very high strain rate (in excess of  $4 \times 10^4 \text{ sec}^{-1}$ ) tests, specimens of 7.00 mm diameter and 3.00 mm long and 6.50 mm diameter and 1.65 mm long were used, respectively. The dimensions

of each specimen were measured individually by a micrometer and the specimens were put in separate envelopes having appropriate notes for identification. Before a dynamic test was conducted, the contacting faces of the specimen, the anvil and the projectile were cleaned with acetone.

### 3.4 Operational Techniques of the Camera

For recording the deformation history of any specimen the following steps were undertaken.

After positioning the test specimen on to the anvil, the camera was directed towards it and aligned by switching to the focus mode. For focussing purpose, some lighting was necessary. Two desk lamps were used to provide adequate illumination of the specimen. At this stage, if the capping shutter was opened, the image could be viewed on the output screen. The fine focussing was carried out with a magnifier inside the viewing hood and adjusting the lens focus by means of a remote control. The cross point graticule was then inserted into the left slot of the Imacon tube. It was necessary to locate the exact position, where the operating streak optics needed to be placed. After fixing the position, the cross point graticule was removed and a streak optic with a slit opening of 100 micron was placed. A pre-calibrated slow streak unit (SS/CV type) was used and the streak speed was selected at 1 micro-second per 2.00 millimetre of the

sweep. After fitting the streak optic, the camera was switched to operate mode. By turning the lens aperture disc, it was set at position marked 16 which was found to give a better quality picture. The film backing unit was then loaded with high speed polaroid film (type 47) and pushed upto the appropriate position for recording the deformation-time history. During these steps, it was essential to take the following operational safety precautions in order to obtain better and consistent results from the IMACON high speed camera.

(a) It was noticed during the operation of the camera that about 2 minutes delay was necessary after switching the camera from focus to operate mode, otherwise a square shape white shade (fog) was observed on the photographic trace of the polaroid film. It is believed that with a static image in focus mode, the phosphor (photo luminescent) of the image tube stores the image for a while. In normal incident light, this is not visible but is bright enough to cause an image on the film when a picture is taken. After being in focus mode for a considerable time, it is advisable to leave the camera in operate mode for a few minutes to allow the image to disappear.

(b) When the plug-in units (either framing or streak) operate at a very high voltage, the capacitors within these units retain the charge even after being disconnected. It was therefore necessary to discharge this

voltage into a conducting medium. This was usually achieved by placing the pins of the plug-in units on a flat conductive surface.

(c) Before each re-loading of the polaroid film, it is essential to clean-up the rollers of the film backing unit with a soft cloth to remove any dirt or chemical from the previous film which may damage the subsequent film.

### 3.5 Technique for Recording Time-Deformation History

The framing photography as shown in Fig. 16 was found to be inadequate to give a continuous record of the interaction between the projectile and the specimen. Furthermore, measurements on each frame, in order to construct the strain history of a specimen, were found to be tedious and sometimes unreliable due to the change in datum between the frames. Many accurate measurements of deformation in one axis over a very short time are possible by operating the camera in streak mode. The line diagram shown in Fig. 18(a) describes the principle of streak photography. A detailed time-deformation history can be obtained with this arrangement. The camera looks through a 0.1 mm wide slit perpendicular to the projectile-specimen contact faces and records the event of the projectile impacting on to the specimen and deforming it. The result is an accurate and continuous record of time-displacement history of the projectile and strain history of the specimen as both the projectile and

the anvil are considered to be rigid. The rigidity of the anvil was confirmed by investigating streak photographs under travelling microscope which revealed no measurable deviation of the anvil top face during compression of the specimen. A clear band and continuous picture of the projectile-specimen contact interface is shown in Fig. 18(b). Hence, framing unit was replaced by streak unit to carry out the main experiments. The framing mode of photography was used to study the mode of overall deformation of the specimen during high strain rate experiments.

### 3.6 Calibration of Streak Unit

The streak mode unit of the IMACON camera was accurately calibrated before the dynamic test programme was started. This was done by first feeding pulses of mark/space ratio of 1:10 from a pulse generator (type TSA 628) into a storage oscilloscope to obtain time/distance values. The streak optic of the camera was then carefully masked to provide an aperture opening of about 100 micron in diameter. The pulse generator was then connected to the input terminal of the camera. The storage oscilloscope was left connected to the pulse generator so that the input pulses to the camera could be monitored. The camera was operated in streak mode, the switching action being affected by the cutting of the laser beam. This produced a streak photograph of the input pulses. By comparing the time/distance values of

the input pulses to those measured from the photograph, the actual operating speed of a streak unit was determined. This actual streak speed was then used to measure the time-displacement data from the photograph obtained during dynamic tests. Throughout the test programme, the streak speed was checked several times using the same procedure and the necessary correction, if any, was made accordingly.

### 3.7 Loading, Firing and Recording Procedure

Once the camera was set to take pictures and the 2-way ball valve was in closed position, the projectile was then put inside the loading throat through the entrance slot and pushed up into the gripper mechanism and kept in suspension. The slot opening was then closed with the split cover and the sliding collar was slid over and clamped using the collar-nut as shown in Fig. 4. The valve of the compressed air cylinder was then opened slowly and kept open until the reservoir air pressure reached the predetermined level as indicated by the pressure transducer meter attached to it.

The whole system i.e. the charge amplifier, the oscilloscope, the flash and the TDG units were then reset and it was made sure that the laser beam was in correct position. The whole set-up was then ready to receive signals. Checking was done once again prior to firing which was achieved by pressing down the handle of the valve. In the course of its travel through the barrel at

a very high velocity, the projectile cut off the laser beam before impacting onto the specimen and deforming it within a few micro-seconds.

As soon as the beam was cut off by the projectile the whole system responded instantaneously. The camera recorded the events for about 35 micro-seconds of duration. The film holder was then pushed down and the film was pulled out of the camera after a delay of about 20 seconds and the developing solution was applied on to the picture.

### 3.8 Other Electronic Instrumentations for Recording

(a) Charge amplifier: A Kiag Swiss 5001 type charge amplifier was used for amplifying the load signal from the piezo-electric load cell of maximum capacity of 60 kN.

(b) Oscilloscope: A Philips PM 3310 type (0-60 MHz) oscilloscope was used for recording the load-time history. As soon as the projectile struck the specimen, the load produced due to impact was transmitted through the load cell to the oscilloscope. On the oscilloscope screen, the analog signal represented the magnitude of the load in the Y-axis and that of the deformation time in the X-axis. The recorded trace was then transferred via the X-Y recorder onto the graph using a suitable scale. The speed of the projectile just before impact was also obtained from the recordings on the oscilloscope of the interception of the laser beam.

(c) Recorder: A Bryans (26000 series, model A4) portable X-Y recorder was used for plotting the load-time curves and the elapsed time recordings during which the beam was obstructed by the projectile.

### 3.9 Reading under Travelling Microscope

The photograph obtained from the IMACON camera represents the time-deformation history of the specimen and also the time-displacement history of the projectile. The time ( $t$ ) in the horizontal and the displacement ( $d$ ) in the vertical directions were calibrated with respect to the operating streak speed and the magnifying factor respectively. Since the streak speed was known, therefore, it was possible to determine the displacement covered in a given time period. The photograph was firmly attached to the platform of the travelling microscope and it was aligned with the horizontal vernier before taking any measurement. On the photographic trace, the straight part represents the zone of free flight just before impact. The slope of this straight part was used to determine the speed of the projectile before impact. Starting from the specimen-projectile contact point ( $t = 0, d = 0$ ), the displacement co-ordinates were measured at every micro-second interval. It was necessary to establish the magnifying factor for each and every set of tests and analyse the photographic record accordingly. The magnifying factor was obtained by dividing the height

of the specimen in the photograph, by the actual original height of the specimen. All the displacements from the photograph were then divided by the magnifying factor to obtain actual displacements.

### 3.10 Selection of Curve Fitting Equation

Table 3 shows a comparative chart of the displacement-time values calculated using different mathematical expressions for 0% pre-strained specimen. In order to obtain the values of the unknown constants of these equations which give closest fit of the displacement data to those measured experimentally, an iterative computer program was necessary.

Fig. 19 shows the values obtained by equation No: 4 i.e.  $Y = C_1t + C_2t^n$  are the closest to the measured values compared to those obtained according to curves 1, 2 and 3. For this curve, the value of 'n' should be greater than 2 but for low total deformation good matching becomes difficult for 'n' greater than 2. Therefore, finally a fourth order polynomial equation of the following form  $Y = C_1t + C_2t^2 + C_3t^3 + C_4t^4$  was chosen.

The experimental displacement-time data were then used to feed directly into a desk-top computer and the following calculations were carried out by using a computer program.

$$\text{Velocity of compression at time } t, V_t = \frac{d(Y)}{dt}$$

$$\text{Force on the specimen at time } t, F_t = \text{Mass of projectile} \times \frac{dV_t}{dt}$$

Stress on the specimen at time  $t$ ,  $\sigma_t = \frac{F_t}{A_t}$  where,  
 $A_t$  is the cross-sectional area of the specimen at  
time  $t$ ,

Strain of the specimen at time  $t$ ,  $\epsilon_t = \ln(h_0/h_t)$  where,  
 $h_0$  and  $h_t$  are the original height and the height at  
time ' $t$ ' of the specimen respectively, and

Strain rate at time  $t$ ,  $\dot{\epsilon}_t = \frac{V_t}{h_t}$

Following the above calculations, the stress-strain results obtained by using equations (4) and (5) are shown in Fig. 20. It shows that, although the displacement-time data given by equations (4) and (5) were very close to those obtained experimentally, as shown in Fig. 19, the stress-strain results calculated based on them differ considerably. However, for the present study the equation No. 5, has been selected and the reasons for this already described above.

### 3.11 Construction of the Stress-Strain Curves

#### 3.11.1 Initial Approach:

The original aim was to derive the strain-time, velocity time, strain rate-time and area-time values from the photographic record. The corresponding force-time traces obtained from the load cell would then be used in conjunction with the area-time values to calculate the stress-time values for a known strain rate which remains fairly constant during the initial part of the total deformation-time history.

The measured force-time trace for a typical test is shown in Fig. 21, indicating severe distortion, attenuation and phase-shift, especially during the first few vital microseconds. It is envisaged that the following possible factors might affect the recorded load-time history during high speed deformation.

(a) Effect of stress wave: When one end of a long bar is impacted by means of a rigid striker, a longitudinal stress wave is generated at the point of impact which propagates through the bar. In the present study, when the projectile struck the specimen, the load produced due to impact was recorded using a load-cell and was stored in a storage oscilloscope, the signal being transmitted through a charge amplifier to the oscilloscope and displayed on to the screen. It is thought that the stress waves reflected from the projectile caused the distortions and may be explained by considering the propagation of stress wave through the projectile soon after impact.

The speed of the elastic stress wave,  $C_e = \sqrt{E/\rho}$  for steel was found to be about 5.167 mm/ $\mu$ s, using  $E = 210 \times 10^9$  N/m<sup>2</sup> and  $\rho = 7.862 \times 10^3$  Kg/m<sup>3</sup>. Immediately after impact, a compressive stress wave will travel through the 19 mm long steel projectile which is subsequently reflected from its free surface as a tensile stress wave. This tensile stress is an unloading wave and thus the reflected tensile wave will have a reducing effect on the

incident compressive wave. Let 'L' be the length of the projectile. At the end of the time  $t = 2L/C_e$ , therefore a slightly reduced compressive force will be experienced at the projectile-specimen interface. The calculated time 't' in the present case was found to be about 7.5  $\mu\text{s}$  using  $L = 19 \text{ mm}$  and  $C_e = 5.167 \text{ mm}/\mu\text{s}$ . Hence, the magnitude of the force after this period would be affected and the recorded force-time history shown in Fig. 21 clearly demonstrates this effect. It is also noticeable from this figure that the fluctuation is repeated several times after each 7.5  $\mu\text{s}$  interval making a hump on the force-time trace. The stress wave space-time diagram may be constructed as shown in Fig. 22. Only the first stage of stress wave propagation is shown in this figure, since after this stage, the stress wave propagation becomes even more complex.

(b) Effect of size of the top anvil and position of the load cell: In order to establish the effect of the length of the anvil piece and the position of the load cell on the recorded load-time trace, several experiments were carried out by altering the position of the load cell and the length of the top part of the pressure bar. Fig. 12 shows that there was no real consistency in the results, although the overall pattern of the load-time traces was the same.

Furthermore, the projectile strikes a specimen of different dimensions and material which is placed upon an

anvil of different dimensions and material. It is believed that these dimensional and material differences would also have some attenuation effect on the recorded force-time history.

(c) Effect of inherent response characteristics of the recording devices: The inherent response characteristics of the charge amplifier and the storage oscilloscope may also affect the recorded load-time trace. It was observed during the calibration of the oscilloscope that when a monitor square shaped signal was fed into it, the output signal was found to be somewhat distorted.

Therefore, all the aforesaid factors were either directly or indirectly affecting the true force-time trace during the high speed deformation and these traces could not be used to deduce the stress values. Indeed the stress values calculated using this measured force values were found to be lower than those obtained from the quasi-static test as shown in Fig. 23. The technique was, therefore, abandoned and an alternative method of obtaining the force-time histories was sought and developed.

### 3.11.2 Alternative arrangements

Subsequently, alterations were made to the anvil and pressure bar assembly, replacing the composite pressure bar system with a massive rigid block (hardened alloy tool steel, En-32). The load cell and the smaller top anvil were also incorporated so that the load-time

histories could still be recorded despite their distorted shapes, for the purpose of comparison only. After spending a considerable length of time and effort to rectify the situation, it was finally decided that the force-time histories should be deduced from the photographic record of the displacement-time histories of the projectile (i.e. deformation-time histories of the specimen).

Assuming the projectile and anvil to be rigid, the deceleration-time curve of the projectile was deduced from displacement-time records. Knowing the mass of the projectile, the force-time histories were established from Newton's Second Law of Motion. Fig. 24 shows a comparison of the force-time histories derived from the displacement-time curve and measured force using the load cell incorporated in the rigid anvil. It is clear from this figure that the new arrangement of the load cell has reduced the phase shift and distortions to the measured load-time history and also has shifted the position of the maximum load towards the left-hand side, i.e. towards early stages of deformation. It also indicates that the maximum load obtained from the computer calculations (on the basis of the photographic records of the displacement-time histories) is comparable to that measured experimentally with load cell.

### 3.11.3 Technique of the construction of dynamic stress-strain curves:

Once the force-time histories have been obtained, these were then used to obtain the stress-time values. Fig. 25 shows a typical stress-time and strain rate-time histories corresponding to a single test in which the acceptable part of the curve is clearly marked. It is noticed that from a single test, only a limited amount of results could be said to correspond to the same strain rate. Therefore, in order to complete the stress-strain diagram over a wide range of strain values, the tests on a number of pre-strained specimens are necessary.

Fig. 26 illustrates how a complete stress-strain curve is achieved from the results of tests carried out on a number of specimens each pre-strained quasi-statically to different strain levels before testing. The dynamic stress-strain values thus obtained for various pre-strained specimens were then used to plot for a constant strain rate starting at the appropriate pre-strain values on the same scale as that of the stress-strain curve for quasi-static compression test. The maximum acceptable stress values for strain rates within about  $\pm 10\%$  of the initial strain rate for each curve were then used to construct the complete dynamic stress-strain curve over large strain values (Fig. 26).

#### 3.11.4 Effect of total deformation:

The effect of large total deformation on a single test is neglected in the present technique, because of the following reasons:

(a) It has been observed that for large total deformation, the displacement-time curve appears almost to be a straight line (Fig. 27) because of very high energy of the projectile and comparatively low resistance and hence lower deceleration of the projectile. Hence, it becomes difficult to accurately determine the profile of the displacement-time curve especially during its initial stages due to the limitation of how accurately the photographic records could be analysed under the microscope. But with lower total deformation, it becomes easier to determine the profile much more accurately since the deceleration is comparatively higher.

(b) It has also been observed that for large total deformation, the strain rate increases considerably immediately after impact and decreases at a later stage of deformation as shown in Fig. 28(a). In such cases, the material is deformed at a faster rate than the velocity drop of the projectile. Therefore, the strain rate which is a function of the ratio of current velocity of the projectile to current height of the specimen, does not remain constant. An important aspect of the technique under consideration is that only the data within reasonably

constant strain rate is accepted.

(c) Fig. 28(b) shows the stress-strain curves where the effect of total deformation on a single test is clarified. When the deformation is larger, accurate determination of the displacement-time curve which, as explained earlier, is used to calculate the force becomes difficult. As a result, the calculated force and hence the stress values are found to be very much underestimated during the initial stages of deformation. This underestimation, however, becomes rectified as the total deformation is reduced. A number of tests were carried out at various total deformation levels (described in results section) but with the same initial strain rate. It was observed that for tests in which the total deformation is less than about 20 percent, the underestimation disappears and produces almost the same stress-strain curve. This pattern starts to change as soon as the total deformation becomes higher than about 30 percent. All the tests were therefore carried out such that the total deformation was less than 30 percent.

### 3.12 Arrangement for Conducting Tests at Sub-zero and at Warm Temperatures

#### 3.12.1 Arrangement for low temperature tests

Before proceeding to conduct any test at low temperature, arrangements were made to reduce the temperature of the specimen as well as the top anvil and the pressure bar.

The pressure bar was covered with a suitable fibre glass insulating jacket leaving about 20 mm circumferential gap which was filled with dry ice produced by passing gaseous carbon dioxide. This arrangement is shown schematically in Fig. 29. As the anvil was in direct contact with the pressure bar, it also cooled down along with the bar.

The temperature of the anvil was measured by a single strand (36 swg) PTFE insulated Cu/Constantan (type T) thermocouple connected to a Comark electronic (type 1621) thermometer. After about an hour, the anvil temperature reached about  $10^{\circ}\text{C}$  and remained steady. The evaporated carbon dioxide ice (CARDICE) was replenished intermittently to make up the loss. In addition, the aerosol freezer (type BS 3914) was sprayed on the anvil to reduce the temperature of  $10^{\circ}\text{C}$  down to  $-40^{\circ}\text{C}$ .

A fine hole was drilled upto the centre of a specimen and the thermocouple tip was inserted into the centre of the specimen. The gap around the tip was filled with thermally conductive interface compound (Thermopath 167). Finally, the entrance of the hole was closed with non-conductive silicon rubber (Silastic) so that the thermocouple can measure only the temperature within the body of the specimen. This arrangement is shown in Fig. 30. The specimen was dipped in liquid nitrogen and kept inside a thermoflask. After a few minutes the specimen reached a temperature of about  $-70^{\circ}\text{C}$ . The specimen was

brought out and immediately placed onto the anvil which was previously cooled. Furthermore, the 'insitu' cooling was continued by spraying aerosol freezer to lower the temperature down to  $-40^{\circ}\text{C}$ . The rise in temperature with time inside and at the surface of the specimen was recorded. This procedure was repeated several times and the average time versus temperature rise is shown in Fig. 30.

This set of experiments was designed to simulate the ballistic test situation and it was noted that the time taken from the moment the 'insitu' cooling by aerosol freezer was stopped to the completion of the ballistic test varied between 15 to 30 seconds. This interval is termed as "Test Regime" in Fig. 30 which indicates that the test temperature should be at  $-30^{\circ}\text{C}$  ( $\pm 5^{\circ}\text{C}$ ).

The specimens for quasi-static tests were also cooled in liquid nitrogen down to  $-70^{\circ}\text{C}$  and the platens of the sub-press were cooled by spraying aerosol freezer to reduce the temperature down to  $-40^{\circ}\text{C}$ . Then the specimen was brought out of the flask and placed in between the platens. While the specimen was being compressed slowly, the spraying with aerosol freezer was continued on the specimen-platen interface to maintain a constant temperature of about  $-30^{\circ}\text{C}$ .

### 3.12.2 Arrangement for high temperature tests:

The top anvil was heated up by Oxy-acetylene flame in such a way that the anvil temperature did not exceed

350°C. As soon as the flame was removed, the temperature decreased and reached to about 250°C within half a minute and remained steady for a minute. In order to protect the armour glass plate and perspex flash window of the safety chamber from heat, a semi-circular steel sheet (5 mm thick) with a fire brick (35 mm) barrier was placed in front of the flame. The specimens for high temperature tests were heated to about 400°C for one hour in a muffle furnace placed near the experimental rig. The specimen was then brought out of the furnace and placed onto the pre-heated anvil within 10 seconds. The ballistic tests were performed within 30 to 50 seconds. The arrangement for temperature measurement is shown in Fig. 31. This is an average result of several tests carried out before doing any scheduled experiment. The thermocouple tip was introduced into the 1mm diameter hole drilled upto the centre of the specimen. The inside temperature was recorded to about 250°C within 20 seconds of removal of the specimen from the furnace. This temperature remained steady for a minute as shown in Fig. 31. The temperature at the surface of the specimen was also measured which showed about 15°C lower than the inside temperature. Therefore, the test temperature at which the dynamic compression tests were conducted should be about 235°C ( $\pm 5^\circ\text{C}$ ).

Quasi-static tests were also carried out in a similar way as the dynamic tests were performed. The platens of

the sub-press were heated up by the EPI gas flame while the specimen was being heated in the muffle furnace. As soon as the flame was removed, the specimen was placed in between the platens and compressed slowly. At the same time, the specimen and platens were both kept hot by intermittent application of the flame to maintain a constant temperature of about 235°C throughout the experiment.

### 3.13 Metallography

Metallographic samples were prepared from as-received material as well as from the specimens deformed both quasi-statically and dynamically. These were polished in the usual manner and then the steel, aluminium and copper specimens were etched in 2% Nital solution, 0.5% HF acid solution (freshly made) and alcoholic ferric chloride solution (100 cc alcohol, 5 cc HCl and 3 gms anhydrous ferric chloride) respectively. The etching time for steel and copper was about 30 - 40 seconds, whereas for aluminium repeated etching and polishing was necessary to reveal the structure. The micro-structures were examined by optical microscopy to observe the structural difference at different magnifications. A Universal microscope and a Zeiss Ultraphot were used for this micro-examination and for photographically recording the representative structures. A Vickers projection microscope was used for counting the number of grains in the micro-structures of the specimens.

## CHAPTER 4

### RESULTS OF THE EXPERIMENTS

#### 4.1 Introduction

Following the experimental procedure described in the previous chapter, the results are divided into two parts. The first part deals with preliminary tests carried out to standardise some of the experimental techniques used in the main investigation. The second part comprises the results obtained from the main experiments and deals mainly with the stress-strain characteristics of structural steel, aluminium and copper at high strain rate ( $10^3 \sim 10^5 \text{ sec}^{-1}$ ) and at low strain rate (quasi-static) as well as with the photomicrographs which show the structures of the specimens deformed at these strain rates.

#### 4.2 Results of the Preliminary Tests

In the preliminary tests, the effects of the following were investigated to establish the experimental technique and the method of processing the results:

- (a) Effect of strain rate history
- (b) Effect of total deformation
- (c) Effect of specimen geometry, and
- (d) Effect of friction.

##### 4.2.1 Effect of strain rate history:

The first set of the preliminary experiments were

carried out to compare the stress strain curves as well as to see any differences due to pre-straining as affected by different strain rates. A series of tests were conducted in order to assess this effect and the summarised results are shown in Tables 4 to 8 and graphically presented in Figs. 32 to 39.

The first set of tests for this series were conducted on a number of similar specimens, each being tested in either dynamic-static-dynamic (DSD) or static-dynamic-static (SDS) sequences. Fig. 32 shows results obtained from a typical test carried out on a specimen in DSD sequence. Curve No. 1 in this figure was obtained from the dynamic compression of the specimen at an initial strain rate of  $1.9 \times 10^4 \text{ sec}^{-1}$  to about 15 percent strain. The solid part of the curve represents results at constant strain rate and the dashed part of the curve represents decreasing strain rate results. The specimen was then compressed quasi-statically to about 31 percent strain giving curve No. 2. Finally, it was compressed dynamically at an initial strain rate of  $2.1 \times 10^2 \text{ sec}^{-1}$  to a total of about 40 percent strain giving a curve No. 3. Curve No. 4 was obtained by compressing a single specimen quasi-statically upto about 45 percent strain. It is evident that the stress-strain curve from this test corresponds very closely to curve No. 2 which was obtained from a dynamically pre-strained specimen.

The results shown in Fig. 33 correspond to a specimen

subjected to compression tests in SDS sequence. The specimen was initially compressed quasi-statically upto a strain level of 15 percent, the result from which is shown in curve No. 1. The specimen was then dynamically compressed to a total strain level of 31 percent at an initial strain rate of  $1.9 \times 10^4 \text{ sec}^{-1}$ . The result of this dynamic compression is shown by curve No. 2, the part of the curve in solid line representing results at constant strain rate. Finally, the same specimen was compressed quasi-statically to a total strain level of about 40 percent, the result of which is shown by curve No. 3. A separate but similar specimen was then compressed quasi-statically upto a total strain level of 40 percent and the results of this test are shown by curve No. 4. It was found that the quasi-statically obtained stress-strain curves for both specimens correspond very closely, indicating that the variable strain rate deformation of the first specimen did not influence the stress-strain property given by curves numbered 1, 3 and 4.

Fig. 32 and 33, when superimposed, facilitated construction of two stress-strain curves over the total strain range of about 45 percent, one at strain rate of about  $2 \times 10^4 \text{ sec}^{-1}$  and the other corresponding to quasi-static compression rate as illustrated in Fig. 34. These resulting two curves are shown separately in Fig. 35 for better clarity.

The second set of tests for this series were carried

out with dissimilar specimens pre-strained (i) quasi-statically, (ii) dynamically with different and variable strain rates and (iii) dynamically at constant strain rate. In the last case, hardened alloy tool steel rings were used to limit the reduction in height during deformation. All these pre-strained specimens were then subjected to dynamic tests carried out at the same constant strain rate. The stress values for different strains within acceptable range of constant strain rate for these tests were found to be almost the same as given in Tables 6 to 8 and diagrammatically shown in Figs. 36 to 39.

Fig. 36 shows a number of stress-strain curves obtained from dynamic compression tests at an initial strain rate of about  $1.8 \times 10^4 \text{ s}^{-1}$  carried out on quasi-statically pre-strained specimens. From these curves the complete stress-strain curve is obtained over a total strain range of about 40 percent which correspond to an initial strain rate of about  $1.8 \times 10^4 \text{ sec}^{-1}$ . Similarly, two other complete stress-strain curves were constructed over total strain range of about 40 percent and at initial strain rate of about  $1.8 \times 10^4 \text{ sec}^{-1}$  but from tests carried out on specimens pre-strained dynamically at variable and constant strain rates as shown in Figs. 37 and 38, respectively.

These final stress-strain diagrams at strain rates of about  $1.8 \times 10^4 \text{ sec}^{-1}$  have been superimposed in Fig. 39

from which it is evident that very little difference is observed in the derived stress strain curves inspite of different modes of pre-straining of the specimens. In the same figure a quasi-statically obtained stress-strain curve is also shown for comparison.

#### 4.2.2 Effect of total deformation:

The second set of the preliminary trials were carried out to establish the acceptable level of total deformation for which the displacement-time histories could be determined accurately enough to obtain the stress-strain curves corresponding to the same initial strain rate. In order to achieve this, the projectiles of different masses were fired on the dimensionally similar specimens of the same material and with the same initial speed. The results of this set of experiments are summarised in Table 9 and graphically shown in Figs. 40 to 43.

Fig. 40 shows the displacement-time curves of three projectiles having masses of 6.4, 8.3 and 10.2 gms, respectively fired onto dimensionally similar specimens of the same material at initial impact velocity of 62 m/s. These displacement curves, when analysed in the manner described previously, produced strain-time, force-time and strain rate-time curves as shown in Figs. 41 and 42.

It was observed that, as the mass of the projectile increased, the total deformation was also increased. However, for each test the range of constant strain rate was

considered to be within 10% of the initial strain rate and the strain rate fell out of this range after only about 2.3, 3.2 and 3.8 micro-seconds from the start of deformation. Therefore, in the present investigation, the first five micro-seconds was considered as a vitally important stage of total deformation sequence. Hence, the displacement-time, strain-time and strain rate-time histories are presented for this period only in the results of the main investigation.

It can be seen from Fig. 42(a) in the force-time histories that slight discrepancy arises at the moment of impact. This is because of the variation of the projectile speed and hence variation of the acceleration, since the force is calculated as mass of the projectile multiplied by its instantaneous acceleration. It can be seen from Table 9 (top value of the 2nd column) that the impact speed for 6.4 gms projectile was found to be 61.293 m/s whereas for 10.2 gms projectile, it was found to be 61.647 m/s.

It is also noticeable from Fig. 43 that the stress values upto the level of constant strain rate were found as  $\sigma_1 = 1.455 \text{ kN/mm}^2$ ,  $\sigma_2 = 1.496 \text{ kN/mm}^2$  and  $\sigma_3 = 1.505 \text{ kN/mm}^2$  for 11.93%, 14.79% and 17.13% total deformation, respectively. The maximum variation of stress values was found to be about 3% which could be considered to be within the limit of the experimental error. Therefore, it is evident from this finding that for the extent of total

deformation (about 20%), the stress-strain curves obtained using projectiles of different masses corresponding to the same initial strain rate do not show any marked difference. It was shown in Section 3.11.4 that, if the total deformation imparted to the specimen is in excess of about 30%, then the results cannot be deduced accurately and underestimation of the stress during the early part of strain becomes evident (see Fig. 28).

#### 4.2.3 Effect of specimen geometry:

The third set of the preliminary experiments were conducted to select the appropriate size of the specimens to be used in the main investigation. In order to carry out this set of experiments, the same projectile was fired with the same initial speed onto the specimens of different aspect ratios (height/diameter). The deformation-time history was recorded by means of framing mode of photography to study the overall deformation sequence. Figs. 44(a) and (b) shows series of high speed photographs of two specimens taken at a framing rate of 500,000 frames per second, the aspect ratio being more than unity for both specimens. Careful inspection of these photographs would show that slight barrelling occurs towards the end of the deformation, but no barrelling effect is evident during the initial stages of deformation which is of interest in this study. Similar tests were carried out with specimens having aspect ratio less than unity. The photographic records of the deformation of

these specimens taken at 500,000 frames per second are shown in Figs. 45(a) and (b). From these photographs also, it is evident that during the initial period of deformation of interest in this study, there is no noticeable localised uneven deformation in the specimen. For the proper test programmes, however, specimens of aspect ratio less than one were used in order to reduce the chance of any non-cylindrical deformation.

#### 4.2.4 Effect of friction:

The final set of the preliminary tests were carried out to estimate the effect of friction on the stress-strain properties of structural steel obtained from tests carried out under dry condition and thus to determine the frictionless stress-strain curves. A major source of error in dynamic uniaxial compression tests is the frictional restraint at the ends of the specimen. In the present investigation, an attempt has been made to quantify the effect of this frictional restraint. All the dynamic tests have been performed without using any lubricant and hence, friction correction was necessary for the dynamic tests. The results from the dry dynamic tests were converted to those under frictionless condition in the following way. From reference (26), the compressive flow stress using lubrication may be expressed as

$$\sigma_s = Y \left( 1 + \frac{2}{3} \mu \frac{r}{h} \right) \dots \dots \dots (1)$$

where,  $\sigma_s$  = quasi-static compressive flow stress using lubricant,

$Y$  = frictionless flow stress of specimen material,

$\mu$  = coefficient of friction,

$r$  = current specimen radius,

$h$  = current specimen height.

During a test, the current radius 'r' corresponding to the current height 'h' was found using volume constancy. A number of experiments were carried out quasi-statically under dry and lubricated conditions with the same aspect ratio (height/diameter) as that used for the dynamic tests. The results from the quasi-static compression tests listed in Table 10 are the average of three experiments.

Now, taking the coefficient of friction for graphite mixed with grease as 0.01 (Ref. 27) and using stress values from quasi-static test carried out with this lubricant, the frictionless flow stress,  $Y$ , can be calculated from equation 1, for different strains and hence different values of  $\left(\frac{r}{h}\right)$  from curves (1) and (2) in Figs. 46 and 47, respectively. The coefficient of friction,  $\mu_D$ , during dry quasi-static test was then found from equation (2):

$$\mu_D = \left( \frac{\sigma_{SD}}{Y} - 1 \right) / \left( \frac{2}{3} \frac{r}{h} \right) \dots\dots\dots(2)$$

where  $\sigma_{SD}$ ,  $r$  and  $h$  have the same meaning as before but refer to curves (3) and (4) in Figs. 46 and 47 for the

quasi-static tests carried out under dry condition at room and high temperatures, respectively.

Finally, the dynamic frictionless flow stress,  $\sigma_D$ , was deduced from equation (3):

$$\sigma_D = \sigma_{DD} / \left( 1 + \mu_D \frac{2}{3} \frac{r}{h} \right) \dots \dots \dots (3)$$

where,  $\sigma_{DD}$ ,  $r$  and  $h$  now refer to curves (5) and (6) in Figs. 46 and 47 for the dynamic tests carried out under dry condition at room and high temperatures, respectively. The results obtained following the above procedures are presented in Figs. 46 and 47 by solid curves (7) and (8) respectively.

This friction correction technique was applied to all the experiments carried out under dry condition and hence the stress-strain curves obtained from the main investigation represent results under frictionless test condition.

It was observed during the quasi-static tests in the present investigation that the stress values at  $-30^\circ\text{C}$  were lower than those obtained at  $22^\circ\text{C}$  and  $235^\circ\text{C}$ . The only reason found during several experiments was that of the formation of ice dew on the specimen surface at  $-30^\circ\text{C}$  because of condensation which acted as an active lubricant. During high speed impact test, it was also revealed that the condensed particles melted and jettisoned out during impact. Therefore, no friction correction was applied to the results of the tests conducted at  $-30^\circ\text{C}$ . Hence, the

results presented in Fig. 48 and in the main investigation for  $-30^{\circ}\text{C}$  are those obtained directly from the tests without any friction correction.

#### 4.3 Results from the Main Test Programme

In the main test programme, experiments were carried out to determine the stress-strain characteristics of structural steel at various strain rates and at room temperature ( $22^{\circ}\text{C}$ ), sub-zero temperature ( $-30^{\circ}\text{C}$ ) and high temperature ( $235^{\circ}\text{C}$ ). Similar experiments were also carried out with aluminium and copper but conducted only at room temperature. The detailed results are described in the following sub-sections:

##### 4.3.1 Stress-strain characteristics of structural steel:

The following experiments were conducted at room temperature at constant strain rates of (a)  $7.32 \times 10^3 \text{ sec}^{-1}$ , (b)  $1.86 \times 10^4 \text{ sec}^{-1}$ , (c)  $4.94 \times 10^4 \text{ sec}^{-1}$  and (d)  $8.75 \times 10^4 \text{ sec}^{-1}$ . The detailed results of these tests given in Tables 11 to 15 and graphically presented in Figs. 49 to 54 inclusive.

Three sets of experiments were conducted at  $-30^{\circ}\text{C}$  and at constant strain rates of (a)  $1.83 \times 10^4 \text{ sec}^{-1}$ , (b)  $4.89 \times 10^4 \text{ sec}^{-1}$  and (c)  $8.65 \times 10^4 \text{ sec}^{-1}$ . Results of these experiments are given in Tables 16 to 19 and graphically shown in Figs. 55 to 58 inclusive.

The detailed results of the high temperature tests are given in Tables 20 to 23 and graphically presented in Figs. 59 to 62. In this case, it was not possible to obtain results of the tests conducted above strain rate of about  $6 \times 10^4 \text{ sec}^{-1}$  because of the higher total deformation (more than 30%) imparted onto the specimen. As explained previously, the total deformation in excess of 30 percent produces almost linear displacement-time curve, making it increasingly difficult to accurately detect the change of its slope with time which is necessary for the calculation of force and hence the stress values.

However, different values of strain rate were obtained by changing impact speed of the projectile while the total strain imposed on a specimen was kept to about 30% by using projectiles of different masses. The details of the specimen dimensions and the masses of different projectiles are mentioned in the tables for different test conditions.

Figs. 49, 55 and 59 show the displacement-time curves obtained during deformation at various strain rates for 0% pre-strained material tested at room temperature,  $-30^\circ\text{C}$  and  $235^\circ\text{C}$  respectively. When these curves were analysed in the manner described previously, the initial part of the stress-strain curves shown in Figs. 51, 56 and 60 were obtained. In order to complete the stress-strain curves upto about 45 to 50 percent strain level as shown in those

figures, similar displacement-time curves for 20% and 40% pre-strained samples needed to be analysed in the same manner. The quasi-static stress-strain curves of structural steel obtained at different temperatures are also presented with those obtained from the dynamic tests for comparison only. It can be seen from Figs. 51, 56 and 60 that, as the strain rate increased, the stress values at different strains also increased.

Fig. 50 shows the strain-time histories derived from the displacement-time histories of Fig. 49 corresponding to initial strain rates varying from  $7.68 \times 10^3 \text{ sec}^{-1}$  to  $9.00 \times 10^4 \text{ sec}^{-1}$ . The corresponding strain rate-time histories are shown in Fig. 52 in which the range of constant strain rate ( $\pm 10\%$  of the initial strain rate) is marked off for each test. For example, for initial strain rate of  $5.16 \times 10^4 \text{ sec}^{-1}$ , only the data contained within the range of  $5.16 \times 10^4 \text{ sec}^{-1}$  and  $4.64 \times 10^4 \text{ sec}^{-1}$  were used for constructing the relevant stress-strain curve. This figure also shows the extents of strain values within this constant strain rate range for different initial strain rates. It was found that the strain rate remained constant upto 14.75% strain, i.e. about 46% of total deformation for high initial strain rate ( $9 \times 10^4 \text{ sec}^{-1}$ ) experiments whereas the strain rate remained constant upto 1.85% strain i.e. 40% of total deformation for comparatively low strain rate ( $7 \times 10^3 \text{ sec}^{-1}$ ) experiments carried out at room temperature.

A similar trend was also observed for the experiments conducted at  $-30^{\circ}\text{C}$  and at  $235^{\circ}\text{C}$  except that at  $-30^{\circ}\text{C}$  the total deformation was lesser and at  $235^{\circ}\text{C}$ , the total deformation was greater than the room temperature tests, as can be seen from Fig. 63, a typical displacement-time graph obtained during deformation at strain rate of about  $1.8 \times 10^4$  per second.

The variation of flow stress with strain rate for strain values of 5 to 40 percent are shown in Figs. 53, 57 and 61 whilst the variation of the ratio of dynamic to quasi-static stress with strain rate for strain values of 5 to 40 percent are shown in Figs. 54, 58 and 62 respectively for room temperature,  $-30^{\circ}\text{C}$  and  $235^{\circ}\text{C}$ . It is evident that for higher strain levels the effect of strain rates on the stress ratio decreases for all the experiments conducted at different temperatures.

Few more experiments were also carried out at  $0^{\circ}\text{C}$  and at  $100^{\circ}\text{C}$  which showed that there was no significant difference in total deformation due to impact when compared with the tests carried out at room temperature ( $22^{\circ}\text{C}$ ) and also that it was not possible, even under the travelling microscope, to distinguish displacement-time curves from the ones obtained for the tests at room temperature. Hence, the results of these sets of experiments were not processed.

#### 4.3.2 Stress-strain characteristics of aluminium and copper:

The following three sets of experiments were conducted at room temperature and at constant strain rates of (a)  $6.7 \times 10^3 \text{ sec}^{-1}$ , (b)  $1.04 \times 10^4 \text{ sec}^{-1}$  and (c)  $3.3 \times 10^4 \text{ sec}^{-1}$  for both aluminium and copper. The experiments using strain rates higher than  $3.3 \times 10^4 \text{ sec}^{-1}$  were not conducted because of higher total deformation (more than 30%) in both cases. The results of the experiments are summarised in Tables 24 to 33 and graphically presented in Figs. 64 to 75 inclusive.

Figs. 64 and 70 show the displacement-time curves obtained during deformation at various strain rates for aluminium and copper, respectively for 0% pre-strained material. When these curves were analysed in the manner described previously, they produced strain-time and strain rate-time histories as shown in Figs. 65 and 67 for aluminium and Figs. 71 and 73 for copper, respectively. In order to complete the stress-strain curves upto about 50% strain from the dynamic tests as shown in Figs. 66 and 72 for aluminium and copper, respectively, the displacement-time curves for 20% and 40% pre-strained specimens were also needed to be analysed.

It can be seen from Figs. 67 and 73 that at low strain rate tests, the range of constant strain rate continued upto 2.2% and 2.4% strain for aluminium and copper, respectively. At high strain rate tests, this

range remained constant upto 10.90% and 11.10% strain for aluminium and copper, respectively.

It can be seen from Figs. 68 and 74 that the higher stress values were obtained at higher rates of strain for aluminium and copper, respectively. Figs. 69 and 75 show the variation of the ratio of dynamic to quasi-static stress at different strains for aluminium and copper, respectively. It is noticeable from these figures that this ratio was decreased at higher strains for aluminium as well as for copper.

#### 4.3.3 Proposed constitutive equation:

In order to represent the derived stress-strain properties at strain rates between  $10^3$  to  $10^5$  per second, an attempt has been made to develop a suitable constitutive equation of all the three materials tested at room temperature. Thus a strain rate sensitivity equation of the following form had to be proposed (Appendix F):

$$\sigma_D = A \epsilon^{n\alpha} (1 + Bf^3) \dots\dots\dots(4)$$

where  $f = \ln(\dot{\epsilon}/\dot{\epsilon}_0)$ ,

$\dot{\epsilon}$  = prevailing strain rate,

$\dot{\epsilon}_0$  = constant at 1 per second,

$\epsilon$  = natural strain,

B = constant,

A = material constant,

n = material strain hardening index,

$\sigma_D$  = dynamic flow stress,

$$\alpha = e^{-f \cdot 25}$$

The value of 'A' was derived from the quasi-static stress-strain curve for each material at natural strain = 1. The constant 'n' was determined by trial and error attempt until a close fit of the quasi-static curve was obtained. The value of the constant 'B' was determined again by trial and error using the stress values at strain rates ranging from  $10^3$  to  $10^5$  per second. All these values for different materials are listed in Table 34.

Applying the values of the constants to equation (4), the stress values for structural steel were calculated in the manner described in Appendix F for different strains and strain rates. These values are shown in Table 35 and graphically presented in Fig. 76 by the broken curves where the solid curves represent actual results determined experimentally. It can be seen that the experimental curves and the curves obtained by using the proposed equation are very close at strain rates between about  $10^3$  to  $10^5$  per second. The variation of the stress values using proposed flow rule with those obtained experimentally at various strains (upto 40%) and strain rates ( $\sim 10^3$  to  $\sim 10^5/s$ ), was found to be about 3 to 4%.

Similarly, the stress-strain results obtained for aluminium and copper using the derived constitutive equation are shown in Tables 36 and 37 and the stress-strain curves are presented in Figs. 77 and 78, respectively. It can be seen from these tables and figures that

the stress values obtained on the basis of the proposed equation correspond closely with those obtained experimentally within the strain rates of about  $6.7 \times 10^3$  to  $3.3 \times 10^4$  per second for strains of upto 40%.

#### 4.4 Micro-examination of Structures

In order to investigate the effect of different temperatures on the stress-strain characteristics of structural steel, steel samples were deformed at  $-30^{\circ}\text{C}$ , room temperature and at  $235^{\circ}\text{C}$ , both dynamically and quasi-statically. The effect of different testing temperatures on the micro-structures of deformed steel was also studied. The stress strain characteristics of aluminium and copper were investigated only at room temperature and hence the micro-structures were also examined for these metals after deforming at room temperature. Since the main investigation was carried out at different strain rates using a total deformation within 30%, the samples for metallographic examination were also deformed to this same extent.

##### 4.4.1 Micro-examination of structural steel:

Fig. 79 shows the normal micro-structure of the as-received En-8 steel, whereas Figs. 80 to 83 show the micrographs of the samples deformed at different temperatures using different strain rates. It can be seen from Fig. 79 that the structure consists of a uniform distribution of ferrite (white) and pearlite (dark) with

a more or less uniform grain size. When this material was deformed either quasi-statically or dynamically, the grains were slightly deformed and this effect was found to be enhanced with the total deformation. This was confirmed by counting the number of grains in the microstructures of the deformed and undeformed specimens by Vickers projection microscope.

#### 4.4.2 Micro-examination of aluminium and copper:

Fig. 84(a) shows the microstructures of as-received aluminium, whereas Figs. 84(b) and (c) show the structures of the samples deformed quasi-statically and dynamically, respectively. Figs. 84(a) to (c) are all from longitudinal sections and show the elongated grains and a uniform dispersion of particles (dark dots) which may be particles of insoluble phases such as  $\text{FeAl}_3$  and Al-Mn-Si. Some flow lines and sub-grains are also seen in the structures of the deformed samples.

Fig. 85(a) shows the structure of as-received high purity copper (99.99%), whereas Fig. 85(b) shows the structure of the quasi-statically deformed copper specimen.

It can be seen that the structures consist of equiaxed grains with some twinned regions together with particles of cuprous oxide (dark dots). Figs. 86(a) and (b) show the structures of copper specimens deformed at strain rates of  $6.6 \times 10^3 \text{ sec}^{-1}$  and  $3.3 \times 10^4 \text{ sec}^{-1}$ , respectively. Both structures show mechanical twinning

within the grains together with the original annealed twinned grains of copper as well as a few particles of cuprous oxide (dark dots). Mechanical twinning was also observed in the longitudinal section of copper specimen deformed at these high strain rates.

#### 4.5 Error Analysis

Errors, however small they may be, always occur owing to the inaccuracies involved during a test on which the final results depend. Estimation of probable error is therefore necessary before results can be considered with some degree of confidence.

##### (a) Error due to the assumption of rigid anvil and projectile

Experiments were carried out on the basis of the assumption that the projectile and the top anvil are rigid. These were made from alloy steel (F.M.P.-338) and were heat-treated which gave rise to a hardness number of about 800 Hv 30. This is about four times higher than that for the steel (En-8) and about eight times higher than those for aluminium and copper used in the present study (Table 2). It should, therefore, be reasonable to assume that during the experiment there would not be any localised permanent indentation of the anvil and the projectile. Furthermore, it has been observed after repeating the high strain rate experiments several times that there was no visible permanent indentation mark on either the anvil

or the projectile. Extensive study of the photographic trace under a travelling microscope also revealed no measurable deviation of the anvil face, even after repeated tests. Error due the elastic deformation of the projectile may be ignored since the specimen and the projectile were of comparable diameters and the readings were measured with reference to the interface. It was estimated by means of average elastic stress calculations that there may be elastic depression of the anvil piece of about 0.0075 mm at maximum load, the error due to neglecting this elastic depression would be about 3 per cent.

(b) Error due to the assumption of cylindrical deformation

In the present study, it was also assumed that the plane sections of the specimen remain plane especially during initial stages of total deformation sequence. Some justification of this assumption can be found from Figs. 44 and 45, from which it is evident that there is no non-cylindrical unevenness noticed when the aspect ratio is less than unity. Furthermore, in the present study only the data under constant strain rate were considered in presenting the final results. It was found that the strain rate remained fairly constant upto a strain range of about 2 to 15% for 3.5 to 1 micro-seconds depending on the strain rates ( $10^3$  to  $10^5$  per second) induced during impact.

(c) Error in processing the photographic record:

Results presented in this report are based on the experimental displacement-time curve obtained during high speed deformation. In measuring these displacement-time data from the recorded photographic trace under the travelling microscope (which has an accuracy of about  $\pm 0.0001$  mm), there would be some human error. Estimation of such error was done by repeating the reading several times under travelling microscope from the same photographic trace and the maximum variation was found to be about 2.7% on the deduced stress-strain results.

(d) Error due to ignoring the effect of specimen mass:

Another source of error could be that in calculating the force acting on the specimen during a deformation, only the mass of the projectile and its instantaneous deceleration were considered and that the effect of the mass of the specimen was ignored. In the present study, it was assumed that since the force at the projectile-specimen interface is required and hence it should be calculated based on only the projectile mass and its instantaneous deceleration. However, if the force acting on the anvil is to be considered, then the effect of mass of the specimen should be included in calculating the force. Thus there would be some discrepancy between the force calculated at the top of the specimen and that at the top of the anvil. In the present study the force at the projectile-specimen interface will depend on the deceleration of the projectile

which in turn will be determined by the strength of the specimen material. The initial speed of the projectile immediately after impact will, of course, be affected by the mass of the specimen.

Considering all the above possible sources of error in the present study, the estimated overall error of about  $\pm 5\%$  could occur in the final results, which is believed to be within the limit of any experimental tolerances.

DISCUSSION OF THE RESULTS

5.1 Introduction

The theme of the present work was mainly confined to develop a suitable technique and method of recording and processing experimental data to determine the stress-strain properties of metals and alloys at different temperatures and at strain rates of upto  $10^5 \text{ sec}^{-1}$ . In order to establish and assess the various aspects of the technique, a number of preliminary trial tests were carried out. Results from these preliminary tests greatly helped to optimise the test conditions to be used in the main investigation. Further investigations were carried out to study the micro-structural changes corresponding to these high strain rate deformations. All these aspects are discussed in the following sub-sections.

5.2 Effect of Strain Rate History

The dynamic stress-strain curves were constructed on the basis of the assumption that the strain rate sensitivity of the materials under consideration is insensitive to strain rate history. This assumption was verified for steel at room temperature shown in Fig. 34 which shows stress-strain curves constructed from specimens pre-strained at different strain rates. The comparison of these results from both high-low and low-high strain rate modes of test sequences showed, for the present test

material (En-8 steel), that the effect of strain rate history on uniaxial stress-strain characteristics was negligible. Similar results were obtained by Barraclough (28) and Wilson et al (29) during torsion and shear jump tests respectively. Their low and high strain rate modes of test sequence on steel showed insensitivity to strain rate history.

On the other hand, Smith (30) and Nicholas (31) showed strain rate history effect was pronounced in steel. No explanation for this effect, however, has been given in the literature by them. The strain rate history effect was also investigated by Campbell and DUBY (32). In their study, the static reloading in compression of dynamically pre-strained specimen of mild steel was investigated. It was found that the stress required to produce a given amount of plastic strain was less for the specimen pre-strained dynamically than for those pre-strained statically.

In an attempt to put some more light on the aforesaid contradictory conclusions, another set of experiments were carried out during the present investigation. Results of this set of dynamic compression tests were systematically presented in Fig. 39. It can be seen that the stress-strain curves constructed after joining the points from different specimens pre-strained either quasi-statically or dynamically at constant or variable strain rates, were found to be almost the same. This finding suggests that

the strain hardening due to pre-straining is independent of the strain rate history. Thus, the present method of obtaining the stress-strain curve for a constant strain rate over large strain values should be considered as quite satisfactory.

### 5.3 Effect of Pre-straining

It has been observed in the present investigation that the total deformation was smaller and the stress values were greater for pre-strained specimens deformed at the same projectile speed. This is easily understandable since the material becomes work-hardened due to pre-straining. This work-hardening effect is reflected on the deformation-time recording and hence the force-time histories of the material. It can be seen from Table 11 that the stress value for 0% pre-strained (i.e. as-received) steel is 1.185 kN/mm<sup>2</sup> whereas for 20% and 40% pre-strained material, stresses are found to be about 1.34 kN/mm<sup>2</sup> and 1.41 kN/mm<sup>2</sup>, respectively for almost the same strain increment of about 1.5 percent at strain rate of  $7 \times 10^3 \text{ sec}^{-1}$ . This is in accordance with the results obtained by Campbell (33) who used 0%, 7.5%, 21% and 28% pre-strained mild steel samples and found higher stress values for different levels of pre-straining. The effect of pre-straining was also investigated by Ohlson (34) on crack initiation under dynamic loading conditions who mentioned that work-hardening increased the yield stress of the material and hence the degree of tri-axiality

of the stress state as compared with that under non-work-hardening plane stress conditions. Brown and Watson (35) have shown substantial increase in stress value due to torsional pre-straining (twisted to 1/8 revolution) on 0.51% C steel bar at same strain rate.

In the present investigation, it was noticed that for 0% pre-strained material the range of constant strain rate from the same test was longer, whereas for 20% and 40% pre-strained material the range of constant strain rate was found to be comparatively shorter. This suggests that the higher the pre-straining, i.e. harder the material, the shorter is the range of constant strain rate for a given speed of the projectile.

#### 5.4 Effect of Specimen Geometry

In the present technique, different values of strain rate were obtained by changing the impact speed of the projectile and also by reducing the height of the specimen. In each case, the total reduction on the specimen was kept under 30% by using projectiles of lighter masses. A number of investigators (14, 36-39) obtained scattered results when different strain rates were achieved by reducing the specimen height. Because of these non-conclusive results, the overall deformation sequence was extensively studied in the preliminary experiments of the present investigation. The results from these tests are shown in Figs. 44 and 45. It is

evident from these figures that no barrelling was observed during deformation when the aspect ratio (height/diameter) was less than unity but some barrelling did appear when the aspect ratio was more than one, but only after 10 micro-seconds after the onset of the deformation.

In the present investigation, the deformation-time histories corresponding to the first 7 micro-seconds were considered and the aspect ratio was kept always under unity. In addition, only the data under constant strain rate was accepted. The range of constant strain rate varied between 1.5 to 4.0 micro-seconds depending on the strain rate and total deformation imposed on the specimen during impact. Therefore, the present observation advocates that, as long as the aspect ratio is kept under unity and the total reduction imposed on the specimen is kept within 30%, there should not be any discrepancy in the results of the tests at high strain rates. Furthermore, any slight discrepancy of results will also be diminished if correction for the frictional effect is carried out. All stress-strain results determined from the present investigation are those obtained after correcting for frictional effect. One explanation for the scatter in results reported elsewhere might be the fact that they used mean strain rate (36, 37) for stress calculation at different strain rates imposing total strain in excess of 60% on the specimen in a single impact (14, 38, 39).

## 5.5 Effect of Radial Inertia

Further considerations in high strain rate tests must be made regarding radial inertia and prevailing friction. Kolsky (12) showed that the actual stress necessary to produce deformation in an infinitesimal specimen is less than that measured, because part of the axial stress goes to produce radial kinetic energy in the specimen. To assess the inertia effect during the fast compression of a cylindrical billet, it is to be assumed (40) that frictional resistance at the billet-platen interfaces is absent and the deformation is homogeneous. Furthermore, the effects of stress wave propagation are considered to be insignificant implying that the speed of compression is in the range of 10 to 300 m/s (40).

The axial force,  $F$ , exerted on a cylindrical specimen by the platens may be expressed (40) by the following equation:

$$F = \pi r^2 Y \left[ 1 + \frac{3}{16} \rho \left( \frac{V^2}{Y} \right) \left( \frac{r}{h} \right) \right]$$

where,  $r$  = current radius of the specimen,

$h$  = current height of the specimen,

$Y$  = current yield stress,

$\rho$  = density of the material,

$V$  = constant velocity of upper platen.

The inertia effect on the axial force required to achieve fast compression of the cylindrical specimen is

expressed by the second term on the right hand side of the above equation which is characterised by the dimensionless parameter,  $\rho \frac{V^2}{Y}$ .

Applying the above analysis to the present study, the contribution due to inertia effect to the total force was found to be between 0.08 to 9.7% (Appendix G) corresponding to the strain rates of  $10^3$  to  $10^5 \text{ sec}^{-1}$ , respectively for deformation at constant strain rates. This is in accordance with the results obtained by Maiden (41). He found that the inertia contribution to the actual measured stress was about 10% and considered as negligible effect for his experiments at strain rates of upto  $10^4 \text{ sec}^{-1}$ . In the present study, no correction was made for the inertia effect since any stress raising effect should more or less be cancelled out by the stress diminishing effect due to localised temperature rise during deformation (see section 5.7).

Samanta (42) mentioned that for constant strain rate experiments, the contribution from the radial inertial stress would be minimum for the specimen dimensions satisfying  $\frac{r}{h} \approx 2.3$  and not  $\frac{r}{h} \approx 1.0$  as found by Davies and Hunter (20). Lindholm (43) used specimen dimensions of  $\frac{r}{h} \approx 2.3$ , whereas Maiden (41) used radius to height ratio about 0.375 for their high strain rate experiments. In the present study, for lower strain rate ( $7.3 \times 10^3 \text{ sec}^{-1}$ ) experiments,  $\frac{r}{h}$  was about 0.5, whereas for comparatively higher strain rate ( $9 \times 10^4 \text{ sec}^{-1}$ ) experiments, it was

about 2. Therefore, from the above discussion, it is reasonable to claim that the specimen dimensions used in the present investigation were quite satisfactory.

### 5.6 Effect of Friction

Frictional contribution during dynamic and static uniaxial compression tests under dry condition is generally considered to be significant and for large deformations, a major source of error is the possibility of frictional constraint at the top and bottom ends of the specimen. In the present case of high speed compression, the exact nature of frictional behaviour was difficult to assess due to complex mechanism with which the topography of the contacting surfaces changed as the deformation continued. From the available information, (44, 45), it is however, reasonable to assume that during the initial stages of deformation with which the present study is specifically concerned, the frictional mechanisms remained almost similar in all the tests.

Following the procedure described in section 4.2.4, the average coefficient of friction was found to be about 0.14 and 0.15 at room temperature and 235°C, respectively, over a strain of 40% (Appendix H) using specimen of  $\frac{r}{h} = 1.15$ . Similar observations were made by Samanta (37), who found that the coefficient of friction was about 0.145 for 40% reduction of a specimen of  $\frac{r}{h} = 1$ . These values are quite low as compared to 0.3 quoted by Rowe (46) from the work

of Male (47), who used specimen having  $\frac{r}{h} = 0.375$  and compressed the specimens by 44% reduction in height.

### 5.7 Temperature Rise during Deformation

All the results presented in this report, were obtained from the experiments conducted at specified test temperature giving rise to maximum strain of about 14.75% within the range of the constant strain rate. An implicit assumption made in the present study is that the temperature within the specimen during deformation to this strain level did not change appreciably from the initial test temperature. In other words, the tests could be described to have taken place isothermally and the resultant characteristics are truly temperature independent. Some justification of this assumption can be found in reference (14).

An approximate estimation of the adiabatic temperature rise was made on the basis of the approximately known friction conditions. A number of solutions have been suggested by Mohitpour (48) and Lahoti (49) for the temperature distribution in axisymmetric compression but their results are in disagreement. In particular, the temperature rise at the specimen-die interfaces was shown to increase with increasing friction in one instance (48) and to decrease with increasing friction in the other (49). Also, the temperature rise within the deforming specimen was found to be much less than at the interface in one case (48), and much greater in the other (49).

In view of this disagreement, in the present study the temperature rise, ' $\Delta T$ ' was calculated by considering the plastic work done only (14). Thus the temperature rise may be given by the following equation:

$$\Delta T = \frac{0.865}{\rho S} \int_0^{\epsilon_f} \sigma d\epsilon \dots\dots\dots(1)$$

where,  $\rho$  is the density of steel taken as 7862 Kg/m<sup>3</sup>,  $\epsilon_f$  is the final strain,  $\sigma$  is the true stress and  $\epsilon$  is the true strain. The factor 0.865 is the portion of the work of deformation converted to heat energy for steel as evaluated by Farren and Taylor (50). The specific heat 'S', is calculated from the following equation, given by ref. (51):

$$S(\text{J/Kg}^\circ\text{K}) = 420 + 0.504T \dots\dots\dots(2)$$

where, T ( $^\circ\text{C}$ ) is taken as the starting test temperature.

The maximum temperature rise in the present case was found to be about 62 $^\circ\text{K}$  (Appendix I) corresponding to a strain rate of  $\sim 10^5 \text{ sec}^{-1}$  for 14.75% strain tested at room temperature. Samanta (37) found the maximum values of rise in temperature to be between 60 $^\circ\text{C}$  and 70 $^\circ\text{C}$  for constructional steel at mean strain rate of  $4.3 \times 10^2 \text{ sec}^{-1}$  and thought it to be modest. In a high-speed tensile test of pure iron, an instantaneous temperature rise of about 50 $^\circ\text{C}$ , due to the conversion of the work of deformation was observed by Nadai and Manjoine (52) at strain rates of upto about  $10^3 \text{ sec}^{-1}$ . However, Muller (53) found the

maximum temperature rise to be  $24^{\circ}\text{C}$  for iron tested at room temperature at strain rate of  $10^4 \text{ sec}^{-1}$ , at a true strain of about 15% and that the corresponding stress correction for this was only  $0.05 \text{ kN/mm}^2$ . Similar results were also obtained by Holzer and Brown (14). No correction due to the effect of temperature rise in the present case has therefore been made on the basis of the assumption that the temperature rise and inertia have mutually cancelling effect on the deduced stress values (see section 5.5).

## 5.8 Comparison of Dynamic and Static Stress-Strain Characteristic of En-8 Steel at Different Temperatures

### 5.8.1 Quasi-static stress-strain characteristics:

The stress-strain characteristics of structural steel at low rates of strain were extensively studied in the present investigation at temperatures of  $-30^{\circ}\text{C}$ ,  $22^{\circ}\text{C}$  and at  $235^{\circ}\text{C}$ . During the tests conducted under dry condition, it was found that the stress values at  $-30^{\circ}\text{C}$  were lower than those obtained at room temperature and at  $235^{\circ}\text{C}$ . The reason (as explained before in section 4.2.4) was that the tests at  $-30^{\circ}\text{C}$  were not conducted truly under dry condition due to the formation of ice dew on the surface of the specimen and hence the frictional constraint between the specimen surface and platens was virtually nil. However, the quasi-static stress values at  $235^{\circ}\text{C}$  were observed lower than those results obtained by Samanta (37) and

Eleiche (54), who all find higher stresses at 200°C for low carbon (0.1 - 0.125% C) steel. It is reported (37) that the ductility is very low for low-carbon steel between temperature range of 100 to 300°C. This low ductility range is known as the "blue-brittle range" and is characterised by an increase in strength and by the presence of serrated (jerky flow) stress-strain curves (37, 54) during quasi-static tests. Conard (55) also mentions that for low-carbon steels, the yield-point phenomena, work-hardening characteristics and ductility are all markedly affected by temperature. From the above discussion, therefore, it appears that the presence of impurities, especially the carbon content in the En-8 steel (0.41% C) did not bring about the so-called "blue brittleness" and hence the observation of the lower stress values at 235°C than those obtained at room temperature.

Furthermore, "blue brittleness" is a dynamic strain ageing effect due to the diffusion of interstitial carbon and nitrogen atoms to dislocations during straining at moderate (100-300°C) temperatures. It is a phenomenon associated with ferrite, and thus might be expected more obvious in low carbon steel than in the En-8 steel studied here. Also, with a very rapid strain rate, the diffusion of carbon and nitrogen atoms is not rapid enough for them to migrate to the moving dislocations during the test, as these dislocations are moving at very high speeds. Hence, it is not surprising that the higher carbon content steel

(En-8) did not show "blue brittleness".

### 5.8.2 Dynamic stress-strain characteristics

From the dynamic tests, it was found that for a given strain rate the stress value at  $-30^{\circ}\text{C}$  was higher and at  $235^{\circ}\text{C}$  was lower than that at room temperature at any strain level. Because, the rate of work-hardening during deformation has increased as the temperature was reduced from  $235^{\circ}\text{C}$  to  $-30^{\circ}\text{C}$ . Similar comparative studies were performed by Costin et al (56), who systematically investigated the effect of temperature on the stress-strain properties of 0.26% carbon steel under dynamic torsional loading at temperatures between  $-157^{\circ}\text{C}$  to  $107^{\circ}\text{C}$  at strain rate of about  $10^3$  per second and observed a positive work-hardening rate at all temperatures and maximum stress values at  $-157^{\circ}\text{C}$  and minimum at  $107^{\circ}\text{C}$ . Hockett and Zukas (57) also investigated the effect of temperature on stress-strain properties of iron and found higher stresses at  $22^{\circ}\text{C}$  and comparatively lower values at  $180^{\circ}\text{C}$  at strain rate of about  $10^2$  per second. Their findings are in accordance with the results obtained in the present study.

### 5.8.3 Strain rate sensitivity:

The stress-strain characteristics of structural steel at various strain rates and at temperatures between  $-30^{\circ}\text{C}$  and  $235^{\circ}\text{C}$  showed that the stress values obtained by dynamic tests were about 1.8-2.5 times higher than those

obtained quasi-statically at a strain of about 10%. It was also observed that the strain rate sensitivity decreased with the increase in strain. In order to compare the strain rate sensitivity of the steel under consideration with those reported elsewhere, results obtained in the present study have been shown with others in Fig. 87. It can be seen that the dynamic stress values obtained in the present study are higher than those reported by Hashmi (10), Oxley (11), Gorham (15) and Woodward (38) but lower than those reported by Symonds (58, 59) and Dowling et al (60) at room temperature.

It should be mentioned here that Gorham (15) used work-hardened high strength tungsten alloy which could be less sensitive to high strain rate than the medium carbon steel used in the present study. Furthermore, he deformed the specimen upto a strain level of 30% in about 8 micro-seconds at strain rate of about  $4 \times 10^4 \text{ sec}^{-1}$ . Gorham (15) employed framing mode of photography to record the strain-time history of the specimen during deformation, which was found to be inadequate to obtain a continuous record of the interaction between the projectile and the specimen. In addition, the variation of strain rate during deformation was not accounted for in the processing of the experimental data and hence obtaining the results.

However, other investigators (33, 52, 60-65), pointed out that the yield or the flow stress,  $\sigma$ , of steel is considerably affected by the strain rate, and the stresses

at high strain rates ( $\dot{\epsilon} = 10^2 \sim 10^3 \text{ sec}^{-1}$ ) become 2 to 4 times larger than those at low strain rates ( $\dot{\epsilon} = 10^{-4} \sim 10^{-2} \text{ sec}^{-1}$ ). A very rapid increase in flow stress above a critical strain rate of about  $10^3 \text{ sec}^{-1}$ , at room temperature was reported by Dowling et al (60) in mild steel and Nagata et al (63) in low carbon iron. Campbell (33) found the rate sensitivity of mild steel to increase markedly at strain rates exceeding about  $5 \times 10^3 \text{ sec}^{-1}$  at temperatures in the range of  $20^\circ\text{C}$  to  $440^\circ\text{C}$ .

However, when the dynamic to static flow stress ratio is considered as a measure of strain rate sensitivity, then it can be concluded that the 0.41% carbon steel under present test condition is highly strain rate sensitive. Comparative studies were also made by Campbell (61) and Tanaka (64, 66) in low carbon and medium carbon steel, who all found strong strain rate sensitivity in steel at strain rate of about  $10^3 \text{ sec}^{-1}$  and at temperatures between  $20^\circ\text{C}$  and  $-30^\circ\text{C}$ .

#### 5.9 Comparison of Dynamic and Static Stress-Strain Characteristics of Aluminium and Copper

Results of the quasi-static and dynamic tests showed that the low purity aluminium (97.5%, supplied at fully heat-treated condition) was stronger than the high purity copper (99.99%). This is because aluminium used in the present investigation contained numerous impurity elements (composition shown in Table 2) which made it harder. It

has been reported elsewhere (67-70) that strength as well as hardness of aluminium decrease with increase purity. Hardness for both the metals was also measured in the as-received condition and the comparative studies in Table 2 showed that aluminium used in this study was harder than copper.

However, the dynamic flow stress was always higher than the quasi-static one showing strain rate dependence at any strain value for both aluminium and copper. Similar observations were made by Lindholm (43), Samanta (42), Dowling et al (60) and Senseny et al (71), who all found higher stresses for high strain rate tests than those obtained from quasi-static tests at any strain value in each case. Experiments conducted by Yoshida (72) and Carden et al (73) with aluminium and by Sundararajan (74) with copper also showed that an increase in the rate of strain raised the dynamic flow stress. Wulf (75) observed a marked increase in the flow stress for strain rates in excess of about  $10^3$  per second, followed by a change to a lower rate of increase at strain rates above  $10^4$  per second for both aluminium and copper. It was again reported elsewhere (76) that the data was too scattered to establish a definite trend.

However, during the present investigation, a strong strain rate sensitivity was observed for both the metals at any strain level employing strain rates from  $6.7 \times 10^3$  to  $3.3 \times 10^4 \text{ sec}^{-1}$ . Figs. 88 and 89 show the comparison

of the ratio of dynamic to quasi-static stress with various strain rates for aluminium and copper, respectively between the values obtained by the present study and those reported by others (77-80). It can be seen that the ratio of dynamic to quasi-static stress was found to be about 1.9 to 2.3 for aluminium and 2.0 to 2.5 for copper at the above strain rate range over a strain of about 10%. This ratio was slightly decreased for higher strain values. Similar linear dependence of the flow stress was observed by Dowling et al (60) at strain rates of upto  $10^4$  per second for both metals.

It was also noticed during the present study that the ratio of dynamic to quasi-static stress was always higher for copper than aluminium for any value of strain, although the stress value at any strain and strain rate was found to be higher for aluminium than those for copper. The probable reason might be the purity of copper as it has been reported elsewhere (74, 81) that pure metals which are softer than metals containing impurity elements and alloying additions, exhibit the highest strain rate sensitivity. Similar conclusion could also be drawn from the work of Davies and Hunter (20), who found the ratio of dynamic to static yield point for mild steel to be about 2.6, whereas for dead soft iron it was about 3.6 at room temperature at strain rates of upto  $10^4$  per second.

## 5.10 Metallographic Studies

### 5.10.1 For En-8 steel:

The overall features of the micrographs as shown in Figs. 80 to 83 did not show any marked changes of the structure of steel specimen whether the material was deformed at high strain rates ( $10^3 - 10^5 \text{ sec}^{-1}$ ) or at low strain rate (quasi-static). During metallographic examination, the longitudinal sections were also seen under the microscope but no distinguishable difference was observed in the micro-structures of the specimens deformed either quasi-statically or dynamically. It was also observed that the deformation effect was slightly masked by "banding" of the ferrite and this was especially noticeable when the extent of total deformation was larger. It was anticipated that there might be some mechanical twins or Newmann bands in the ferritic structure of the structural steel specimen compressed at high strain rates. This is because metals that do not twin by conventional deformation at ambient temperature can often be made to twin by shock loading (82). It could be that the initiation of twinning in En-8 steel during impact was affected by the presence of alloying elements and inclusions, despite its high strain rate sensitivity.

However, among the several factors involved to cause twinning in metals, the effect of pulse duration during impact was systematically investigated by Champion and

Rohde (83) for an austenitic steel. They found twins at pulse durations of 2  $\mu\text{s}$ , while no twinning was present at 0.065  $\mu\text{s}$ . Stone et al (84) found an increase in twin density as the pulse duration was increased from 0.5  $\mu\text{s}$  to 1.0  $\mu\text{s}$ , in both the low carbon (0.04% C) steel and Armco magnetic ingot iron. Rohde (85) observed twinning in shock loaded commercially pure iron but did not observe it at lower stresses, employing strain rates of  $3 \times 10^{-4}$  to  $10^5 \text{ sec}^{-1}$  over a temperature range of  $-197^\circ\text{C}$  to  $300^\circ\text{C}$ . Hockett and Zukas (57) observed twins in annealed iron which was compressed at the strain rate of  $1.2 \times 10^2$  per second at  $140^\circ\text{C}$ . They also mentioned that twinning occurred in the early stages of deformation and was essentially complete at a true strain of 0.1 (10% reduction).

In the present study, the total deformation time varied between 7  $\mu\text{s}$  to 20  $\mu\text{s}$  depending on the strain rates ( $10^5$  to  $10^3 \text{ sec}^{-1}$ ) used during impact. There is no sign of twinning in the structures (Fig. 81) of the specimens which were compressed at different temperatures to 10% reduction using strain rate of  $10^3 \text{ sec}^{-1}$ . No twins were also observed in the structures (Figs. 82 and 83) of the specimens compressed at strain rates of either  $10^4 \text{ sec}^{-1}$  or  $10^5 \text{ sec}^{-1}$ .

Other investigators (53, 57, 83-87) however, used either pure iron or low carbon (0.04% C) steel which were tough and highly strain rate sensitive (74, 81) compared

to the steel used in the present investigation. It may therefore be possible that the inherent impurities present in the En-8 steel might be one of the factors preventing deformation twin formation in the deformed samples. Murr et al (88) shows that thoria particles in TD-Ni or in TD-NiCr prevents the formation of twins in the shock loaded alloy. Leslie (81) also recommends for further study the effect of inclusions on the formation of twinning in a shock loaded metal structure. Orava (89) shows that the limiting carbon content above which mild steels will be unlikely to twin at strain rates of  $10^2$  to  $10^4$   $\text{sec}^{-1}$  is 0.2%.

From the foregoing discussion, it appears that there is a threshold time (57, 83, 84), stress (57, 85, 90, 91) and some critical temperature (57, 86) for the initiation of twinning. It also appears that the inherent inclusion (88) or carbon content (89) in the alloy affects or at least inhibits the initiation of twinning during deformation process. On the basis of these observations, it is perhaps not surprising that no deformation twins were observed in the En-8 steel which contained 0.41%C and fairly numerous non-metallic inclusions.

#### 5.10.2 For aluminium and copper:

It can be seen from Figs. 84(b) and (c) that the grains were more distorted in the structure of the shocked aluminium than those of the quasi-statically deformed

specimen. On the other hand, the flow lines in the structure of the specimen deformed dynamically showed weaker contrast than those in the structure of the specimen deformed at a low strain rate. It is however, difficult to distinguish clearly the strain rate effect on the patterns. Similar observations were made by Yoshida and Nagata (72), who deformed high purity (99.99%) aluminium at room temperature using strain rates of upto  $10^4 \text{ sec}^{-1}$ . Dhere et al (92) found no noticeable change in the texture of shock loaded commercial purity aluminium, while conventional deformation induced significant changes. Therefore, from the above discussion and from the findings in the present work, it can be concluded that any distinguishable structural change or twinning is not induced in aluminium during deformation at high strain rates.

It has been reported elsewhere (81, 93-97) that mechanical twins can be generated in copper by shock loading. During metallographic examination in the present investigation, twins were indeed found in the structure of the high purity copper specimen deformed at high strain rates, as shown in Figs. 86(a) and (b). It can be seen that, as the strain rate was increased from  $6.6 \times 10^3$  to  $3.3 \times 10^4 \text{ sec}^{-1}$ , more severe twinning was observed in the structure. This suggests that high strain rate deformation favours mechanical twinning in the high purity copper.

CONCLUSIONS

In the present investigation, the following conclusions have been drawn from the experiments conducted under quasi-static and dynamic constant strain rates over a strain range of upto about 50 percent.

- (i) A high strain rate compression test rig has been designed, constructed and commissioned to enable testing materials at strain rates of  $10^3$  to  $10^5$  per second.
- (ii) A suitable testing technique and method of processing the data have been developed.
- (iii) The high speed streak photographic technique has been found to have the unique ability of recording strain-time history of a test material with a high degree of sensitivity.
- (iv) It has been found that the strain-hardening in steel was essentially independent of strain rate history.
- (v) A method has been established following which the stress-strain characteristics of any metallic material could be obtained for a constant strain rate over a wide range of strain value.

- (vi) It has been shown that the specimen geometry during impact test did not affect the results (after friction correction) as long as the height to diameter ratio was kept under unity and the total strain imposed on the specimen was less than 30 percent.
- (vii) The stress-strain characteristics of structural steel at strain rates of upto  $10^5$  per second at  $-30^{\circ}\text{C}$ , room temperature and at  $235^{\circ}\text{C}$  have been established.
- (viii) Structural steel has shown a strong strain rate sensitivity within the strain rate range of about  $10^3$  to about  $10^5 \text{ sec}^{-1}$ , which decreased with the increase in strain at any temperature between  $-30^{\circ}\text{C}$  to  $235^{\circ}\text{C}$ .
- (ix) Like structural steel, both the aluminium and copper have shown a strong strain rate sensitivity within the strain rate range of about  $10^3$  to about  $10^4 \text{ sec}^{-1}$  at room temperature.
- (x) Comparative studies showed that copper was more strain rate sensitive than aluminium and steel used in the present investigation.
- (xi) A constitutive equation has been proposed for the steel, aluminium and copper used in

the present study incorporating the effects of work-hardening and strain rate sensitivity of the material.

- (xii) There were no marked differences observed in the micro-structures of the structural steel specimen deformed quasi-statically and dynamically at  $-30^{\circ}\text{C}$ , room temperature and at  $235^{\circ}\text{C}$ .
- (xiii) It is believed that the initiation of twinning during impact could be affected by the presence of alloying elements and inclusions in the En-8 steel; and the higher the alloying elements and the more the inclusion content, the less is the possibility of mechanical twinning.
- (xiv) There was no distinguishable micro-structural changes observed in the structure of aluminium specimen deformed at low and high strain rates.
- (xv) Mechanical twinning was found in the micro-structure of the high purity copper specimen deformed at high strain rates and this increased with increasing strain rate.

Table 1, Calibration chart of air pressure versus voltmeter reading.

Budenberg gauge tester reading (psi)	Roband digital voltmeter reading (volts)
10	0.003
20	0.006
50	0.015
100	0.034
150	0.050
200	0.068
250	0.085
300	0.101
350	0.118
400	0.134
450	0.152
500	0.169
600	0.202
700	0.236
800	0.270
900	0.303
1000	0.340
1200	0.404

Table 2, Chemical composition and comparative hardness of different materials used in the present study.

Material specification and Chemical composition (wt %)			
a	b	c	d
Tool steel (F.M.P.-338)	Structural steel (En-8)	Aluminium (BS 1474- HE 30 TF)	Copper (BS 1433- C 101)
C - 2.05 Mn - 0.40 Si - 0.30 Cr - 13.00 Fe - Rem.	C - 0.41 Mn - 0.78 Si - 0.26 P - 0.018 Ni - 0.13 Mo - 0.02 Al - 0.012 Fe - Rem.	Mn - 0.55 Si - 1.02 Cr - 0.006 Ni - 0.001 Fe - 0.30 Cu - 0.01 Mg - 0.55 Zn - 0.03 Al - Rem.	High purity copper (99.99)
Hardness No. (Hv 30)			
800 (after heat treatment)	214	112	104

Table 3, Comparative chart of displacement-time values calculated by different equations.

Time ( $\mu$ s)	Measured displacement reading (mm)	Curve Fitting Equations			
		1	2	3	4
		$Y = d_0 (1 - e^{-\alpha t})$ where, $Y =$ displacement at time $t$ , $d_0 =$ max. reduction $= 0.4$ mm $T = \frac{d_0}{V_0} = \frac{.4}{.0343} \mu s^{-1}$ $V_0 =$ velocity $= .0343$ mm/ $\mu s$	$Y = d_0 e^{-\alpha t} \sin \omega t$ where, $\omega = \frac{V_0}{d_0} = \frac{.0343}{.4} \mu s^{-1}$ $\alpha = \frac{\ln(\sin \omega t_f)}{t_f}$ $t_f =$ final time $= 19 \mu s$ .	$Y = d_0 \sin At$ where, $A = \frac{V_0}{d_0}$ $= \frac{.0343}{.4} \mu s^{-1}$	$Y = C_1 t + C_2 t^n$ where, $C_1$ and $C_2$ are constants, $C_1$ is related to $V_0$ and $C_2$ is available when value of $n$ found out by iteration (until best fit is obtained) and here $n = 2.29$
0	0	0	0	0	0
1	0.0338	0.0328	0.03426	0.03426	0.033964
2	0.0665	0.0630	0.06827	0.06826	0.06695
3	0.0985	0.0907	0.10179	0.10176	0.09874
4	0.1290	0.1161	0.13457	0.13452	0.12917
5	0.1585	0.1394	0.16636	0.16629	0.15811
6	0.1865	0.1609	0.19694	0.19683	0.18548
7	0.2135	0.1805	0.22608	0.22593	0.21118

Table 4, Results of the (a) dynamic, (b) quasi-static and (c) dynamic tests for D-S-D testing sequence.  
Table 4 (a)

Specimen specification	Values of $C_1, C_2, C_3$ & $C_4$ respectively; where $C_1$ related to impact velocity (m/s)	Time (μs)	Displacement (mm)	Force, $F = Mx - \frac{dv}{dt}L$ (kN) where, $M = 5.1800$ gms.	Stress, $\sigma$ (kN/mm <sup>2</sup> )	Stress, $\sigma$ after friction correction (kN/mm <sup>2</sup> )	Strain, $\epsilon$ ( $\ln h_0/h_t$ )	Strain rate, $\dot{\epsilon} = v_t/h_t$ ( $\times 10^4/s$ )	Strain rate constant ( $\times 10^4/s$ )
a) 0 %	96.446	0	0				0	1.9682	1.9459
b) $H_0 = 4.90$	480051196	1	.0950	20.003	0.998	0.7990	.0197	1.9744	over 3
$\phi_0 = 5.00$	$-9.4626 \times 10^{14}$	2	.1890	36.112	1.768	1.5280	.0392	1.8951	points
$H_f = 4.20$		3	.2750	43.356	2.084	1.7796	.0575	1.7613	
		4	.3500	41.732	1.973	1.6963	.0743	1.6075	
		5	.4200	31.242	1.454	1.2528	.0897	1.4719	
T.D. = 15.41%		6	.4850				.1040		
		7	.5450				.1179		

continued

Table 4 (b)

Mode of tests	Specimen dimensions (mm)	Reduction in height (mm)	Current height, $h_f$ (mm)	Strain, $\epsilon$ ( $\ln h_0/h_f$ )	Applied load, $F_f$ (kN)	Stress, $\sigma = F_f / A_f$ $= \frac{F_f \times h_f}{\text{Volume}}$ (kN/mm <sup>2</sup> )
Dynamic	$H_0 = 4.20$	0	4.20	0.1541	0	0
		0.10	4.10	0.1781	10.50	0.4475
		0.20	4.00	0.2029	14.00	0.5821
Static	$\phi_0 = 5.40$	0.30	3.90	0.2282	17.75	0.7195
		0.40	3.80	0.2541	19.50	0.7702
		0.50	3.70	0.2808	20.50	0.7885
Dynamic	$H_f = 3.60$	0.60	3.60	0.3082	21.30	0.7970

continued

Table 4 (c)

Specimen specification	Values of $C_1, C_2, C_3$ & $C_4$ respectively; where $C_1$ related to impact velocity (m/s)	Time; Displacement (mm)	Force, $F = Mx - \frac{dv}{dt}$ (kN) where, $M = 5.1800$ gms.	Stress, $\sigma$ (kN/mm <sup>2</sup> )	Stress, $\sigma$ after friction correction (kN/mm <sup>2</sup> )	Strain, $\epsilon$ ( $\ln h_0/h_t$ )	Strain rate, $\dot{\epsilon} = v_t/h_t$ ( $\times 10^4/s$ )	Strain rate constant ( $\times 10^4/s$ )
a) 30.83%	78.660	0	53.340	1.956	1.6544	.3083	2.1850	2.0933
b) $E_0 = 3.60$	-2.7935	1	67.916	2.445	2.0531	.3293	2.0017	over 2
$\phi_0 = 5.83$	-9.4305	2	72.671	2.577	2.1599	.3479	1.6964	points
$H_f = 3.30$	7.9007	3	67.603	2.370	1.9895	.3630	1.3194	
T.D. = 8.7%		4	52.713	1.834	1.5382	.3742	0.9278	
		5				.3817	0.5829	
		6				.3862		
		7				.3892		

Table 5, Detailed results of the (a) quasi-static, (b) dynamic and (c) quasi-static tests for S-D-S testing sequence.  
 Table 5 (a)

Mode of tests	Specimen dimensions (mm)	Reduction in height (mm)	Current height, $h_t$ (mm)	Strain, $\epsilon$ ( $\ln h_0/h_t$ )	Applied load, $F_t$ (kN)	Stress, $\sigma = F_t / A_t$ $= \frac{F_t \times h_t}{\text{Volume}}$ (kN/mm <sup>2</sup> )
Static	$H_c = 4.90$	0	4.90	0	0	0
		0.10	4.80	0.0206	8.50	0.4241
		0.20	4.70	0.0416	11.75	0.5740
Dynamic	$\phi_0 = 5.00$	0.30	4.60	0.0631	13.60	0.6503
		0.40	4.50	0.0851	15.00	0.7016
		0.50	4.40	0.1076	15.85	0.7249
Static	$H_f = 4.20$	0.60	4.30	0.1306	16.50	0.7375
		0.70	4.20	0.1541	17.30	0.7553

continued

Table 5 (b)

Specimen specification	Values of $C_1, C_2, C_3$ & $C_4$ respectively; where $C_1$ related to impact velocity (m/s)	Time (μs)	Displacement (mm)	Force, $F = Mx - \frac{dv}{dt}t$ (kN) where, $M = 5.1800$ gms.	Stress, $\sigma$ (kN/mm <sup>2</sup> )	Stress, $\sigma$ after friction correction (kN/mm <sup>2</sup> )	Strain, $\epsilon$ ( $\ln h_0/h_t$ )	Strain rate, $\dot{\epsilon}$ ( $v_t/h_t$ ) ( $\times 10^4/s$ )	Strain rate constant ( $\times 10^4/s$ )
a) 15 %	85.530	0	0				.1541	2.0364	1.9533
b) $H_0 = 4.20$	-86.8175973	1	.0830	30.203	1.292	1.0977	.1742	1.9833	over 3
$\phi_0 = 5.40$	-7.9372 $\times 10^{14}$	2	.1630	44.494	1.867	1.5802	.1934	1.8404	points
$H_f = 3.60$	5.5654 $\times 10^{19}$	3	.2325	51.866	2.139	1.8110	.2108	1.6355	
T.D. = 15.41%		4	.2900	52.319	2.125	1.7957	.2260	1.4004	
		5	.3425	45.853	1.839	1.5546	.2389	1.1700	
		6	.3825				.2496		
		7	.4175				.2588		

continued

Table 5 (c)

Mode of tests	Specimen dimensions (mm)	Reduction in height (mm)	Current height, $h_f$ (mm)	Strain, $\epsilon$ ( $\ln h_0/h_f$ )	Applied load, $F_f$ (kN)	Stress, $\sigma = F_f / A_f$ $= \frac{F_f \times h_f}{\text{Volume}}$ (kN/mm <sup>2</sup> )
Static	$H_0 = 3.60$	0	3.60	0.3082	0	0
		0.05	3.55	0.3221	12.50	0.4612
		0.10	3.50	0.3364	15.75	0.5730
Dynamic	$\phi_0 = 5.83$	0.15	3.45	0.3508	19.00	0.6813
		0.20	3.40	0.3654	22.00	0.7775
Static	$H_f = 3.30$	0.25	3.35	0.3802	23.25	0.8096
		0.30	3.30	0.3953	24.00	0.8232

Table 6, Detailed results of the dynamic test carried out on specimens pre-strained quasi-statically.

Specimen specification a) Pre-straining (%) b) Dimensions (mm)	Values of $C_1, C_2, C_3$ & $C_4$ respectively; where, $C_1$ related to impact velocity (m/s)	Time (μs)	Displacement (mm)	Force, F $= Mx \frac{dv}{dt}$ (kN) where, M = 10.3770 gms.	Stress, σ (kN/mm <sup>2</sup> )	Stress, σ after friction correction (kN/mm <sup>2</sup> )	Strain, ε (ln h <sub>0</sub> /ht)	Strain rate $\dot{\epsilon} = v_t/ht$ ( $\times 10^4/s$ )	Strain rate constant ( $\times 10^4/s$ )
a) 0 %	57.254	0	0				0	1.9084	1.8426
b) $H_0 = 3.00$ $\phi_0 = 7.00$	330492210 -8.7151 $\times 10^{14}$ 6.0775 $\times 10^{19}$	1 2 3 4 5 6 7	.0560 .1095 .1585 .1925 .2225 .2475 .2635	39.834 71.392 87.814 89.100 75.250	1.015 1.787 2.163 2.165 1.809	0.8087 1.5093 1.8342 1.8552 1.5436	.0191 .0372 .0534 .0668 .0774	1.8871 1.7321 1.4863 1.1983 0.9214	over 3 points
a) 10 %	56.502	0	0				.1000	1.8834	1.7971
b) $H_0 = 3.00$ $\phi_0 = 7.00$	-119100896 -7.8811 $\times 10^{14}$ 5.4408 $\times 10^{19}$	1 2 3 4 5 6 7	.0560 .1065 .1520 .1875 .2150 .2350 .2500	44.766 73.510 88.704 90.348 78.442	1.141 1.841 2.188 2.200 1.892	0.9808 1.5720 1.8590 1.8706 1.6002	.1187 .1363 .1518 .1645 .1743	1.8380 1.6699 1.4177 1.1253 0.8404	over 3 points

continued

Table 6 continuation

Specimen specification a) Pre-straining (%) b) Dimensions (mm)	Values of $C_1, C_2, C_3$ & $C_4$ respectively; where, $C_1$ related to impact velocity (m/s)	Time (ms)	Displacement (mm)	Force, F $\frac{dvt}{dt}$ $= Mx - \frac{d^2t}{dt^2}$ (kN) where, M = 10.3770 gms.	Stress, $\sigma$ (kN/mm <sup>2</sup> )	Stress, $\sigma$ after friction correction (kN/mm <sup>2</sup> )	Strain, $\epsilon$ (ln $h_0/h_t$ )	Strain rate $\dot{\epsilon} = v_t/h_t$ ( $\times 10^4/s$ )	Strain rate constant ( $\times 10^4/s$ )
a) 22 % b) $H_0 = 3.00$ $\phi_0 = 7.00$	59.105 -2.6029 $\times 10^9$ -3.6909 $\times 10^{14}$ 2.9418 $\times 10^{19}$	0 1 2 3 4 5 6 7	0 .0555 .1055 .1475 .1775 .2025 .2200 .2300	73.339 85.330 89.994 87.331 77.342	1.870 2.139 2.224 2.134 1.873	1.5805 1.7928 1.8624 1.7875 1.5732	.2200 .2388 .2557 .2699 .2814 .2899	1.9701 1.7973 1.5616 1.2860 0.9958 0.7186	1.8837 over 2 points
a) 34 % b) $H_0 = 3.00$ $\phi_0 = 7.00$	58.112 -2.0836 $\times 10^9$ -6.1504 $\times 10^{14}$ 4.9478 $\times 10^{19}$	0 1 2 3 4 5 6 7	0 .0550 .1045 .1425 .1725 .1925 .2050 .2125	75.376 95.186 102.674 97.839 80.682	1.922 2.387 2.540 2.396 1.961	1.6004 1.9796 2.1046 1.9824 1.6186	.3400 .3586 .3751 .3888 .3991 .4063	1.9370 1.7761 1.5185 1.2022 0.8695 0.5658	1.8565 over 2 points

Table 7, Detailed results of the dynamic test carried out on specimens pre-strained dynamically at different and variable strain rates.

Specimen specification a) Pre-straining (%) b) Dimensions (mm)	Values of $C_1, C_2, C_3$ & $C_4$ respectively; where, $C_1$ related to impact velocity (m/s)	Time (μs)	Displacement (mm)	Force, F $= M \frac{dv}{dt}$ (kN) where, M = 10.3770 gms.	Stress, $\sigma$ ( $kN/mm^2$ )	Stress, $\sigma'$ after friction correction ( $kN/mm^2$ )	Strain, $\epsilon$ ( $\ln h_0/h_t$ )	Strain rate $\dot{\epsilon} = v_t/h_t$ ( $\times 10^4/s$ )	Strain rate constant ( $\times 10^4/s$ )
a) 10 %	56.497	0	0						1.8021
b) $H_0=3.00$ $\phi_0=7.00$	18952269 $-8.1299 \times 10^{14}$ $5.4386 \times 10^{19}$	1 2 3 4 5 6 7	.0560 .1065 .1535 .1875 .2150 .2350 .2480	43.453 73.755 90.512 93.724 83.392	1.108 1.847 2.232 2.282 2.011	0.9525 1.5771 1.9027 1.9403 1.7008	.1000 .1187 .1364 .1520 .1647 .1744	1.8832 1.8447 1.6786 1.4232 1.1219 0.8225	over 3 points
a) 22 %	58.637	0	0						1.8669
b) $H_0=3.00$ $\phi_0=7.00$	$-2.5970 \times 10^9$ $-3.9711 \times 10^{14}$ $3.4584 \times 10^{19}$	1 2 3 4 5 6 7	.0550 .1055 .1435 .1770 .2000 .2175 .2300	74.317 86.123 89.315 83.894 69.860	1.895 2.160 2.208 2.051 1.694	1.6065 1.8104 1.8490 1.7180 1.4235	.2200 .2387 .2553 .2694 .2806 .2890	1.9545 1.7793 1.5398 1.2631 0.9793 0.7206	over 2 points

continued

Table 7 continuation

Specimen specification a) Pre-straining (%) b) Dimensions (mm)	Values of $C_1, C_2, C_3$ & $C_4$ respectively, where $C_1$ related to impact velocity (m/s)	Time (ms)	Displacement (mm)	Force, F $= Mx \frac{dv}{dt}$ (kN) where, M = 10.3770 gms.	Stress, $\sigma$ (kN/mm <sup>2</sup> )	Stress, $\sigma$ after friction correction (kN/mm <sup>2</sup> )	Strain, $\epsilon$ (ln $h_0/ht$ )	Strain rate $\dot{\epsilon} = v_t/ht$ ( $\times 10^4/s$ )	Strain rate constant ( $\times 10^4/s$ )
a) 34 %	58.293	0	0	76.985	1.963	1.6322	.3400	1.9431	1.8522
b) $H_0 = 3.00$	$-2.6392 \times 10^9$	1	.0545	90.008	2.258	1.8726	.3585	1.7614	over 2
$\phi_0 = 7.00$	$-4.3051 \times 10^{14}$	2	.1040	93.844	2.322	1.9257	.3749	1.5103	points
	$3.6891 \times 10^{19}$	3	.1425	88.491	2.166	1.7939	.3886	1.2184	
		4	.1725	73.951	1.796	1.4870	.3993	0.9182	
		5	.1945				.4071	0.6437	
		6	.2100						
		7	.2195						

Table 8, Detailed results of the dynamic test carried out on specimens pre-strained dynamically at constant strain rate.

Specimen specification a) Pre-straining (%) b) Dimensions (mm)	Values of $C_1, C_2, C_3$ & $C_4$ respectively, where, $C_1$ related to impact velocity (m/s)	Time (μs)	Displacement (mm)	Force, F $\frac{dv}{dt}$ (kN) where M = 10.2740 gms.	Stress, $\sigma$ (kN/mm <sup>2</sup> )	Stress, $\sigma'$ after friction correction (kN/mm <sup>2</sup> )	Strain, $\epsilon$ (ln $h_0/h_t$ )	Strain rate $\dot{\epsilon} = v_t/h_t$ ( $\times 10^4/s$ )	Strain rate constant ( $\times 10^4/s$ )
a) 0 %	70.558	0	0				0	1.7639	1.7080
b) $H_0 = 4.00$	-980870741	1	.0685	37.930	1.318	1.0880	.0175	1.7223	over 3
$\phi_0 = 6.00$	$-3.2113 \times 10^{14}$	2	.1360	51.664	1.765	1.5008	.0343	1.6378	points
$H_f = 3.60$	$1.6389 \times 10^{19}$	3	.1950	61.358	2.064	1.7637	.0501	1.5185	
		4	.2500	67.009	2.221	1.9099	.0645	1.3732	
		5	.2985	68.620	2.245	1.9216	.0775	1.2118	
		6	.3400						
		7	.3750						
a) 10 %	64.374	0	0				.1000	1.7881	1.6988
b) $H_0 = 3.60$	$-1.2149 \times 10^9$	1	.0615	46.303	1.447	1.2467	.1175	1.7200	over 3
$\phi_0 = 6.325$	$-4.0885 \times 10^{14}$	2	.1215	59.912	1.842	1.5766	.1342	1.5985	points
$H_f = 3.20$	$3.1349 \times 10^{19}$	3	.1755	65.790	1.992	1.6966	.1494	1.4427	
		4	.2190	63.938	1.910	1.6280	.1630	1.2737	
		5	.2580	54.357	1.605	1.3608	.1749	1.1148	
		6	.2970						
		7	.3255						

continued

Table 8 continuation

Specimen specification a) Pre-straining (%) b) Dimensions (mm)	Values of $C_1, C_2, C_3$ & $C_4$ respectively; where, $C_1$ related to impact velocity (m/s)	Time (ms)	Displacement (mm)	Force, F $= Mx \frac{dv}{dt}$ (kN) where, M = 10.2740 gms.	Stress, $\sigma$ (kN/mm <sup>2</sup> )	Stress, $\sigma$ after friction correction (kN/mm <sup>2</sup> )	Strain, $\epsilon$ (ln $h_0/h_t$ )	Strain rate $\dot{\epsilon} = v_t/h_t$ ( $\times 10^4/s$ )	Strain rate constant ( $\times 10^4/s$ )
a) 22 %	61.437	0	0				.2200	1.9199	1.8432
b) $H_0 = 3.20$ $\phi_c = 6.71$ $H_f = 2.85$	$-2.5656 \times 10^9$ $-3.0852 \times 10^{14}$ $2.8814 \times 10^{19}$	1 2 3 4 5 6 7	.0570 .1125 .1550 .1915 .2225 .2475 .2675	68.185 76.546 77.802 71.954 59.000	1.892 2.089 2.093 1.912 1.552	1.5933 1.7529 1.7547 1.6035 1.3060	.2384 .2551 .2697 .2819 .2920	1.7666 1.5664 1.3408 1.1131 0.9084	over 2 points
a) 34 %	60.115	0	0				.3400	2.1093	2.0210
b) $H_0 = 2.85$ $\phi_c = 7.10$ $H_f = 2.62$	$-2.1772 \times 10^9$ $-6.7066 \times 10^{14}$ $5.6906 \times 10^{19}$	1 2 3 4 5 6 7	.0550 .1085 .1495 .1750 .1965 .2135 .2200	79.063 99.358 105.621 97.852 76.052	1.956 2.415 2.529 2.317 1.787	1.6306 2.0008 2.0903 1.9155 1.4822	.3603 .3782 .3930 .4042 .4119	1.9328 1.6471 1.2983 0.9381 0.6220	over 2 points

Table 9, Detailed results of the dynamic test carried out using projectiles of different masses.

Specimen specification a) Pre-straining (%) b) Dimensions (mm)	Values of $C_1, C_2, C_3$ & $C_4$ respectively; where, $C_1$ related to impact velocity (m/s)	Time (ms)	Displacement (mm)	Force, F $= M \frac{dv}{dt}$ (kN) where, M = 6.4017 & 8.2750 gms.	Stress, $\sigma$ (kN/mm <sup>2</sup> )	Stress, $\sigma$ after friction correction (kN/mm <sup>2</sup> )	Strain, $\epsilon$ (in ho/ht)	Strain rate $\dot{\epsilon} = v_t/ht$ ( $\times 10^4/s$ )	Strain rate constant ( $\times 10^4/s$ )
a) 0 %	61.293	0	0	14.599	1.344	1.0824	0	1.5323	1.4739
b) $H_0 = 4.00$	$-1.1402 \times 10^9$	1	.0600	21.715	1.620	1.4170	.0151	1.4829	over 3
$\phi_c = 4.50$	$-2.1502 \times 10^{14}$	2	.1160	26.547	1.752	1.5397	.0431	1.3177	points
$H_f = 3.55$	$1.4871 \times 10^{19}$	3	.1700	29.095	1.745	1.5127	.0557	1.2068	
T.D. = 11.93%		4	.2165	29.357	1.606	1.3916	.0673	1.1016	
M = 6.4017 gms.		5	.2600	27.334	1.339	1.1588	.0778	1.0062	
		6	.3000	23.027	0.946	0.8245	.0875	0.9311	
		7	.3350	16.435					
a) 0 %	61.587	0	0	15.109	1.317	1.0747	0	1.5396	1.4733
b) $H_0 = 4.00$	$-912949644$	1	.0605	21.283	1.570	1.3570	.0152	1.5070	over 4
$\phi_c = 4.50$	$-1.4166 \times 10^{14}$	2	.1185	25.740	1.712	1.4935	.0300	1.4559	points
$H_f = 3.45$	$8.6515 \times 10^{18}$	3	.1735	28.478	1.750	1.5185	.0443	1.3907	
T.D. = 14.79%		4	.2250	29.498	1.687	1.4683	.0578	1.3164	
M = 8.2750 gms.		5	.2725	29.800	1.527	1.3346	.0706	1.2384	
		6	.3175	26.384	1.273	1.1110	.0826	1.1623	
		7	.3585	22.250			.0939	1.0943	

continued

Table 9 continuation

Specimen specification a) Pre-straining (%) b) Dimensions (mm.)	Values of $C_1, C_2, C_3$ & $C_4$ respectively; where, $C_1$ related to impact velocity (m/s)	Time (ms)	Displacement (mm)	Force, F $= Mx - \frac{dv}{dt}$ (kN) where, M = 10.2010 gms.	Stress, $\sigma$ (kN/mm <sup>2</sup> )	Stress, $\sigma'$ after friction correction (kN/mm <sup>2</sup> )	Strain, $\epsilon$ (ln $h_0/h_t$ )	Strain rate $\dot{\epsilon} = v_t/h_t$ ( $\times 10^4/s$ )	Strain rate constant ( $\times 10^4/s$ )
a) 0 %	61.647	0	0	17.656	1.373	1.1203	0	1.5411	1.4900
b) $H_0 = 4.00$	-865431666	1	.0605	22.385	1.574	1.3605	.0152	1.5148	over 4 points
$\phi_0 = 4.52$	-8.6075 $\times 10^{13}$	2	.1190	26.035	1.704	1.4752	.0302	1.4763	
$H_f = 3.37$	4.4069 $\times 10^{18}$	3	.1760	28.606	1.768	1.5348	.0447	1.4276	
T.D. = 17.13%		4	.2280	30.098	1.769	1.5357	.0587	1.3713	
M = 10.2010 gms.		5	.2780	30.511	1.708	1.4881	.0721	1.3097	
		6	.3265	29.845	1.589	1.3795	.0849	1.2458	
		7	.3700	28.101			.0971	1.1825	

Table 10, Results of the quasi-static tests carried out at different temperatures on structural steel under dry and lubricated condition.

Strain, $\epsilon$ ( $\ln h_0/h_f$ )	Stress, $\sigma$ (kN/mm <sup>2</sup> )				
	Room temperature		-30° C	235° C	
	Dry	Lubricated		Dry	Lubricated
.020	.5116	.4325	.4212	.5101	.4241
.040	.6615	.5823	.5815	.6175	.5625
.062	.7900	.6519	.6875	.6920	.6312
.084	.8025	.7015	.7221	.7605	.6700
.106	.8415	.7250	.7925	.8145	.6906
.130	.8613	.7362	.8025	.8312	.7150
.162	.8910	.7602	.8381	.8602	.7356
.198	.9025	.7715	.8625	.8805	.7475
.223	.9113	.7792	.8725	.8879	.7575
.259	.9255	.7835	.8775	.9013	.7685
.287	.9407	.7932	.8850	.9127	.7745
.314	.9519	.8006	.8956	.9216	.7850
.356	.9660	.8110	.9125	.9325	.7910
.400	.9725	.8205	.9300	.9665	.8100
.446	.9853	.8356	.9425	.9768	.8212
.494	.9910	.8415	.9523	.9925	.8300
.544	1.1036	.8580	.9650	1.0657	.8415

Table 11, Detailed results of the experiment carried out at  $\dot{\epsilon} = 7.3 \times 10^3$  /s on structural steel at room temperature.

Specimen specification a) Pre-straining (%) b) Dimensions (mm)	Values of $C_1, C_2, C_3$ & $C_4$ respectively; where, $C_1$ related to impact velocity (m/s)	Time (μs)	Displacement (mm)	Force, F $= Mx \frac{dv}{dt}$ (kN) where, M = 16.39 gms.	Stress, $\sigma$ (kN/mm <sup>2</sup> )	Stress, $\sigma$ after friction correction (kN/mm <sup>2</sup> )	Strain, $\epsilon$ (ln $h_0/ht$ )	Strain rate $\dot{\epsilon} = v_t/ht$ ( $\times 10^3$ /s)	Strain rate constant ( $\times 10^3$ /s)
a) 0 % b) $H_0 = 6.00$ $\phi_0 = 6.50$	46.131 -770994865 -1.6231 $\times 10^{14}$ 9.5876 $\times 10^{19}$	0 1 2 3 4 5 6 7	0 .0460 .0870 .1280 .1650 .1965 .2265 .2525	39.349 49.655 56.189 58.951 57.943	1.176 1.474 1.657 1.727 1.688	1.1845	0 .0075 .0147 .0215 .0277 .0333	7.688 7.412 7.003 6.498 5.933 5.349	7.368 over 3 points
a) 20 % b) $H_0 = 6.00$ $\phi_0 = 6.50$	45.744 -529505105 -2.3392 $\times 10^{14}$ 1.3884 $\times 10^{19}$	0 1 2 3 4 5 6 7	0 .0460 .0865 .1275 .1635 .1950 .2225 .2475	37.630 52.442 61.793 65.682 64.110	1.125 1.557 1.822 1.925 1.869	1.3403	.2000 .2075 .2147 .2214 .2275 .2330	7.624 7.395 6.979 6.428 5.796 5.141	7.332 over 3 points

continued

Table 11 continuation

Specimen specification a) Pre-straining (%) b) Dimensions (mm)	Values of $C_1, C_2, C_3$ & $C_4$ respectively; where, $C_1$ related to impact velocity (m/s)	Time (μs)	Displacement (mm)	Force, F $= Mx \frac{dv}{dt}$ (kN) where, M = 16.39 gms.	Stress, σ (kN/mm <sup>2</sup> )	Stress, σ after friction correction (kN/mm <sup>2</sup> )	Strain, ε (ln h <sub>0</sub> /h <sub>t</sub> )	Strain rate $\dot{\epsilon} = v_t/h_t$ (x 10 <sup>3</sup> /s)	Strain rate constant (x 10 <sup>3</sup> /s)
a) 40 %	44.792	0	0				.4000	7.465	7.282
b) H <sub>0</sub> =6.00	188151088	1	.0455	30.153	0.901		.4074	7.389	over 3
φ <sub>0</sub> =6.50		2	.0860	55.485	1.647	1.4083	.4146	6.991	points
	-4.2522 x 10 <sup>14</sup>	3	.1275	69.828	2.059		.4213	6.377	
	2.7937 x 10 <sup>19</sup>	4	.1625	73.181	2.145		.4273	5.659	
		5	.1925	65.544	1.911		.4326	4.951	
		6	.2200						
		7	.2440						

Table 12, Detailed results of the experiment carried out at  $\dot{\epsilon} = 1.8 \times 10^4$  /s on structural steel at room temperature.

Specimen specification a) Pre-straining (%) b) Dimensions (mm)	Values of $C_1, C_2, C_3$ & $C_4$ respectively, where, $C_1$ related to impact velocity (m/s)	Time ( $\mu$ s)	Displacement (mm)	Force, F $\frac{dvt}{dt}$ (kN) where $M = 10.3770$ gms.	Stress, $\sigma$ (kN/mm <sup>2</sup> )	Stress, $\sigma$ after friction correction (kN/mm <sup>2</sup> )	Strain, $\epsilon$ ( $\ln h_0/ht$ )	Strain rate $\dot{\epsilon}_{svt}/ht$ ( $\times 10^4$ /s)	Strain rate constant ( $\times 10^4$ /s)	
e) 0 % b) $H_0 = 3.00$ $\phi_0 = 7.00$	57.254 330492210 $-8.7151 \times 10^{14}$ $6.0775 \times 10^{19}$	0	0				0			
		1	.0560	39.834	1.015		.0191	1.9084	1.8425	
		2	.1095	71.392	1.787	1.5038	.0372	1.8871	over 3	
		3	.1585	87.814	2.163		.0534	1.7321	points	
		4	.1925	89.100	2.165		.0668	1.4863		
		5	.2225	75.250	1.809		.0774	1.1983		
		6	.2475							
		7	.2635							
a) 22 % b) $H_0 = 3.00$ $\phi_0 = 7.00$	59.105 $-2.6029 \times 10^9$ $-3.6909 \times 10^{14}$ $2.9418 \times 10^{19}$	0	0				.2200	1.9701	1.8837	
		1	.0555	73.339	1.870	1.5730	.2388	1.7973	over 2	
		2	.1055	85.330	2.139		.2557	1.5616	points	
		3	.1475	89.994	2.224		.2699	1.2860		
		4	.1775	87.331	2.134		.2814	0.9958		
		5	.2025	77.342	1.873		.2899	0.7186		
		6	.2200							
		7	.2300							

continued

Table 12 continuation

Specimen specification a) Pre-straining (%) b) Dimensions (mm)	Values of $C_1, C_2, C_3$ & $C_4$ respectively; where, $C_1$ related to impact velocity (m/s)	Time (μs)	Displacement (mm)	Force, F $= Mx \frac{dv}{dt}$ (kN) where, M = 10.3770 gms.	Stress, σ (kN/mm <sup>2</sup> )	Stress, σ - after friction correction (kN/mm <sup>2</sup> )	Strain, ε (ln h <sub>0</sub> /ht)	Strain rate $\dot{\epsilon}_{av} / ht$ ( $\times 10^4 / s$ )	Strain rate constant ( $\times 10^4 / s$ )
a) 34 %	58.112	0	0				.3400	1.9370	1.8565
b) H <sub>0</sub> = 3.00	-2.0836 x 10 <sup>9</sup>	1	.0550	75.376	1.922	1.6004	.3586	1.7761	over 2
φ <sub>0</sub> = 7.00	-6.1504 x 10 <sup>14</sup>	2	.1045	95.186	2.387		.3751	1.5185	points
	4.9478 x 10 <sup>19</sup>	3	.1425	102.674	2.540		.3888	1.2022	
		4	.1725	97.839	2.396		.3991	0.8695	
		5	.1925	80.682	1.961		.4063	0.5658	
		6	.2050						
		7	.2125						

Table 13, Detailed results of the experiment carried out at  $\dot{\epsilon} = 4.9 \times 10^4$ /s on structural steel at room temperature.

Specimen specification a) Pre-straining (%) b) Dimensions (mm)	Values of $C_1, C_2, C_3$ & $C_4$ respectively; where, $C_1$ related to impact velocity (m/s)	Time (μs)	Displacement (mm)	Force, F $= M \frac{dv}{dt}$ (kN) where, M = 4.6250 gms.	Stress, σ (kN/mm <sup>2</sup> )	Stress, σ - after friction correction (kN/mm <sup>2</sup> )	Strain, ε (ln h <sub>0</sub> /h <sub>t</sub> )	Strain rate $\dot{\epsilon} = v_t/h_t$ ( $\times 10^4$ /s)	Strain rate constant ( $\times 10^4$ /s)
a) 0 %	103.358	0	0				0	5.1679	4.9777
b) $H_0 = 2.00$ $\phi_0 = 6.50$	-5.0318 $\times 10^9$ -8.4196 $\times 10^{14}$ 7.8093 $\times 10^{19}$	1 2 3 4 5 6 7	.0935 .1850 .2500 .2950 .3350 .3600 .3750	65.575 75.936 77.630 70.655 55.012	1.879 2.081 2.048 1.810 1.380	1.6480	.0500 .0949 .1326 .1619 .1830	4.7875 4.1578 3.3607 2.5092 1.7376	over 2 points
a) 20% b) $H_0 = 2.00$ $\phi_0 = 6.50$	102.855 -4.9541 $\times 10^9$ -1.0827 $\times 10^{15}$ 1.0299 $\times 10^{20}$	0 1 2 3 4 5 6 7	0 .0930 .1825 .2450 .2850 .3200 .3400 .3525	70.155 83.053 84.518 74.550 53.150	2.011 2.279 2.237 1.921 1.345	1.6969	0 .2496 .2936 .3295 .3562 .3740	5.1427 4.7350 4.0272 3.1316 2.1988 1.4046	4.9388 over 2 points

continued

Table 13 continuation

Specimen specification a) Pre-straining (%) b) Dimensions (mm)	Values of $C_1, C_2, C_3$ & $C_4$ respectively; where $C_1$ related to impact velocity (m/s)	Time (μs)	Displacement (mm)	Force, F $= Mx - \frac{dv}{dt}t$ (kN) where, M = 4.6250 gms.	Stress, $\sigma$ (kN/mm <sup>2</sup> )	Stress, $\sigma$ , after friction correction (kN/mm <sup>2</sup> )	Strain, $\epsilon$ ( $\ln h_0/h_t$ )	Strain rate, $\dot{\epsilon}$ ( $= v_t/h_t$ ) ( $\times 10^4/s$ )	Strain rate constant ( $\times 10^4/s$ )
a) 40%	102.963	0	0				.4000	5.1481	4.9054
b) $H_0 = 2.00$	$-5.9046 \times 10^9$	1	.0925	75.032	2.152	1.7970	.4493	4.6627	over 2 points
$\phi_0 = 6.50$	$-9.1518 \times 10^{14}$	2	.1800	85.484	2.348		.4923	3.9063	
		3	.2400	85.972	2.282		.5268	2.9812	
		4	.2775	76.497	1.980		.5518	2.0239	
		5	.3100	57.058	1.453		.5677	1.1920	
		6	.3250						
		7	.3325						

Table 14, Detailed results of the experiment carried out at  $\dot{\epsilon} = 9.0 \times 10^4/s$  on structural steel at room temperature.

Specimen specification a) Pre-straining (%) b) Dimensions (mm)	Values of $C_1, C_2, C_3$ & $C_4$ respectively, where, $C_1$ related to impact velocity (m/s)	Time (ms)	Displacement (mm)	Force, F $= Mx - \frac{dv}{dt}$ (kN) where M = 3.1160 gms.	Stress, $\sigma$ (kN/mm <sup>2</sup> )	Stress, $\sigma'$ after friction correction (kN/mm <sup>2</sup> )	Strain, $\epsilon$ ( $\ln h_0/h_t$ )	Strain rate $\dot{\epsilon} = v_t/h_t$ ( $\times 10^4/s$ )	Strain rate constant ( $\times 10^4/s$ )
a) 0 % b) $H_0 = 1.65$ $\phi_0 = 6.50$	148.662 -4.7133 $\times 10^9$ -2.7174 $\times 10^{15}$ 2.3850 $\times 10^{20}$	0 1 2 3 4 5 6 7	0 .1400 .2620 .3500 .4050 .4350 .4450 .4500	71.124 95.129 101.333 89.734 60.334	1.959 2.414 2.406 2.038 1.339	1.6969	0 .0896 .1718 .2380 .2827 .3059	9.0098 8.7527 7.5447 5.5954 3.3428 1.3964	8.8812 over 2 points
a) 20 % b) $H_0 = 1.65$ $\phi_0 = 6.50$	148.944 -7.4340 $\times 10^9$ -2.1544 $\times 10^{15}$ 2.0017 $\times 10^{20}$	0 1 2 3 4 5 6 7	0 .1390 .2550 .3375 .3900 .4150 .4200 .4200	78.971 96.761 99.610 87.518 60.485	2.178 2.466 2.386 2.013 1.364	1.8331	.2000 .28331 .3672 .4292 .4698 .4894	9.0269 8.5017 7.1468 5.1667 2.9610 1.0611	8.7643 over 2 points

continued

Table 14 continuation

Specimen specification a) Pre-straining (%) b) Dimensions (mm)	Values of $C_1, C_2, C_3$ & $C_4$ respectively; where $C_1$ related to impact velocity (m/s)	Time ( $\mu$ s)	Displacement (mm)	Force, $F = Mx - \frac{dv}{dt}$ (kN) where, $M = 3.1100$ gms.	Stress, $\sigma$ (kN/mm <sup>2</sup> )	Stress, $\sigma'$ after friction correction (kN/mm <sup>2</sup> )	Strain, $\epsilon$ ( $\ln h_0/h_t$ )	Strain rate, $\dot{\epsilon}$ ( $v_t/h_t$ ) ( $\times 10^4/s$ )	Strain rate constant ( $\times 10^4/\dot{\epsilon}$ )
a) 40 % b) $H_0 = 1.65$ $\phi_0 = 6.50$	147.952 -8.6510 x 10 <sup>9</sup> -2.2860 x 10 <sup>15</sup> 2.3110 x 10 <sup>20</sup>	0 1 2 3 4 5 6 7	0 .1375 .2475 .3200 .3700 .3800 .3825 .3825	87.843 104.627 104.161 86.446 51.481	2.427 2.681 2.524 2.026 1.192	1.9415	.4000 .4868 .5619 .2178 .2509 .2617	8.9668 8.2443 6.6493 4.4672 2.1946 0.4367	8.6055 over 2 points

Table 15 Stress and stress ratio at different strains and at various strain rates for structural steel at room temperature.

Strain rate, $\dot{\epsilon} \left( \frac{v_f}{h_f} \right)$	Strain, $\epsilon$ ( $\ln h_o/h_f$ )	Stress, $\sigma$ ( $\text{kN/mm}^2$ )	Ratio of dynamic to quasi-static stress ( $\sigma_D/\sigma_S$ )
Quasi-static	0.05	0.61	
	0.10	0.72	
	0.20	0.78	
	0.30	0.80	
	0.40	0.82	
$7.32 \times 10^3/\text{s}$	0.05	1.24	2.03
	0.10	1.31	1.82
	0.20	1.34	1.71
	0.30	1.36	1.70
	0.40	1.40	1.70
$1.86 \times 10^4/\text{s}$	0.05	1.51	2.47
	0.10	1.54	2.13
	0.20	1.57	2.01
	0.30	1.59	1.98
	0.40	1.61	1.96
$4.94 \times 10^4/\text{s}$	0.05	1.64	2.68
	0.10	1.67	2.32
	0.20	1.70	2.18
	0.30	1.73	2.16
	0.40	1.77	2.15
$8.75 \times 10^4/\text{s}$	0.05	1.66	2.72
	0.10	1.75	2.43
	0.20	1.82	2.33
	0.30	1.86	2.32
	0.40	1.90	2.31

Table 16, Detailed results of the experiment carried out at  $\dot{\epsilon} = 1.8 \times 10^4$  /s on structural steel at  $-30^\circ$  C.

Specimen specification a) Pre-straining (%) b) Dimensions (mm)	Values of $C_1, C_2, C_3$ & $C_4$ respectively; where, $C_1$ related to impact velocity (m/s)	Time ( $\mu$ s)	Displacement (mm)	Force, F $= Mx \frac{dv}{dt}$ (kN) where, M = 10.3770 gms.	Stress, $\sigma$ (kN/mm <sup>2</sup> )	Strain, $\epsilon$ ( $\ln h_0/h_t$ )	Strain rate $\dot{\epsilon} = v_t/h_t$ ( $\times 10^4$ /s)	Strain rate constant ( $\times 10^4$ /s)
a) 0 %	57.327	0	0			0	1.9109	1.8147
b) $H_0 = 3.00$ $\phi_0 = 7.00$	-746934457	1	.0555	45.530	1.160	.0188	1.8449	1.8147
	-5.5356 $\times 10^{14}$	2	.1075	66.683	1.670	.0365	1.6885	over 3
	3.5638 $\times 10^{19}$	3	.1550	78.960	1.946	.0524	1.4664	points
		4	.1900	82.361	2.003	.0658	1.2069	
		5	.2200	76.887	1.850	.0765	0.9413	
		6	.2450					
		7	.2600					
a) 20 %	58.035	0	0			.2000	1.9345	1.8493
b) $H_0 = 3.00$ $\phi_0 = 7.00$	-2.5323 $\times 10^9$	1	.0550	72.464	1.848	.2185	1.7642	over 2
	-3.7816 $\times 10^{14}$	2	.1035	85.099	2.135	.2350	1.5294	points
	2.9204 $\times 10^{19}$	3	.1435	90.461	2.238	.2490	1.2527	
		4	.1750	88.549	2.166	.2600	0.9593	
		5	.1975	79.364	1.926	.2682	0.6763	
		6	.2135					
		7	.2225					

continued

Table 16 continuation

Specimen specification a) Pre-straining (%) b) Dimensions (mm)	Values of $C_1, C_2, C_3$ & $C_4$ respectively; where, $C_1$ related to impact velocity (m/s)	Time (μs)	Displacement (mm)	Force, F $= Mx \frac{dv}{dt}$ (kN) where, M = 10.3770 gms.	Stress, σ (kN/mm <sup>2</sup> )	Strain, ε (ln $h_0/ht$ )	Strain rate $\dot{\epsilon} = v_t/ht$ ( $\times 10^4/s$ )	Strain rate constant ( $\times 10^4/s$ )
a) 40 %	57.289	0	0			.4000	1.9096	1.8248
b) $H_0 = 3.00$	$-2.3370 \times 10^9$	1	.0545	75.035	1.914	.4183	1.7401	over 2
$\phi_0 = 7.00$	$-5.0731 \times 10^{14}$	2	.1020	91.458	2.295	.4345	1.4889	points
	$4.0590 \times 10^{19}$	3	.1400	97.772	2.421	.4479	1.1873	
		4	.1700	93.978	2.303	.4582	0.8703	
		5	.1900	80.074	1.948	.4654	0.5752	
		6	.2025					
		7	.2100					

Table 17, Detailed results of the experiment carried out at  $\dot{\epsilon} = 4.9 \times 10^4$  /s on structural steel at  $-30^\circ$  C.

Specimen specification a) Pre-straining (%) b) Dimensions (mm)	Values of $C_1, C_2, C_3$ & $C_4$ respectively, where, $C_1$ related to impact velocity (m/s)	Time (ms)	Displacement (mm)	Force, F $= Mx \frac{dv}{dt}$ (kN) where, M = 4.6250 gms.	Stress, $\sigma$ (kN/mm <sup>2</sup> )	Strain, $\epsilon$ (ln $h_0/h_t$ )	Strain rate $\dot{\epsilon} = v_t/h_t$ (x 10 <sup>4</sup> /s)	Strain rate constant (x 10 <sup>4</sup> /s)
a) 0 % b) $H_0 = 2.00$ $\phi_0 = 6.50$	102.224 -4.6266 x 10 <sup>9</sup> -9.2341 x 10 <sup>14</sup> 8.2677 x 10 <sup>19</sup>	0 1 2 3 4 5 6 7	0 .0925 .1840 .2485 .2925 .3325 .3560 .3700	63.833 75.691 78.373 71.878 56.205	1.830 2.075 2.070 1.844 1.412	0 .0495 .0942 .1317 .1607 .1813	5.1112 4.7566 4.1361 3.3345 2.4692 1.6807	4.9339 over 2 points
a) 20 % b) $H_0 = 2.00$ $\phi_0 = 6.50$	101.419 -4.1323 x 10 <sup>9</sup> -1.3232 x 10 <sup>15</sup> 1.2273 x 10 <sup>20</sup>	0 1 2 3 4 5 6 7	0 .0920 .1815 .2430 .2825 .3150 .3350 .3475	68.133 84.419 87.083 76.123 51.540	1.954 2.318 2.307 1.965 1.308	.2000 .2492 .2930 .3285 .3544 .3714	5.0709 4.7100 4.0025 3.0790 2.1160 1.3184	4.8905 over 2 points

continued

Table 17 continuation

Specimen specification a) Pre-straining (%) b) Dimensions (mm)	Values of $C_1, C_2, C_3$ & $C_4$ respectively, where, $C_1$ related to impact velocity (m/s)	Time (μs)	Displacement (mm)	Force, F $\frac{dV}{dt}$ $= Mx \frac{dV}{dt}$ (kN) where, M = 4.6250 gms.	Stress, σ (kN/mm <sup>2</sup> )	Strain, ε (in $h_0/h_t$ )	Strain rate $\dot{\epsilon} = v_t/h_t$ (x 10 <sup>4</sup> /s)	Strain rate constant (x 10 <sup>4</sup> /s)
a) 40 % b) $H_0 = 2.00$ $\phi_c = 6.50$	101.367 -4.8726 x 10 <sup>9</sup> -1.2126 x 10 <sup>15</sup> 1.1382 x 10 <sup>20</sup>	0 1 2 3 4 5 6 7	0 .0915 .1790 .2385 .2750 .3050 .3200 .3275	72.406 87.106 89.173 78.605 55.403	2.077 2.394 2.369 2.038 1.415	.4000 .4488 .4917 .5259 .5502 .5652	5.0683 4.6434 3.8893 2.9310 1.9358 1.0971	4.8558 over 2 points

Table 18, Detailed results of the experiment carried out at  $\dot{\epsilon} = 9.0 \times 10^4 / \text{s}$  on structural steel at  $-30^\circ \text{C}$ .

Specimen specification a) Pre-straining (%) b) Dimensions (mm)	Values of $C_1, C_2, C_3$ & $C_4$ respectively; where $C_1$ related to impact velocity (m/s)	Time (μs)	Displacement (mm)	Force, F $= Mx - \frac{dv}{dt}$ (kN) where, $M = 3.1100$ gms.	Stress, $\sigma$ (kN/mm <sup>2</sup> )	Strain, $\epsilon$ (in $h_0/h_t$ )	Strain rate $\dot{\epsilon} = v_t/h_t$ ( $\times 10^4/\text{s}$ )	Strain rate constant ( $\times 10^4/\text{s}$ )	
a) 0 % b) $H_0 = 1.65$ $\phi_0 = 6.50$	148.097 $-4.3063 \times 10^9$ $-2.8937 \times 10^{15}$ $2.5498 \times 10^{20}$	0	0			0	8.9756	8.8561	
		1	.1395	71.266	1.963	.0894	8.7367	over 2	
		2	.2615	96.715	2.455	.1713	7.5035	points	
		3	.3485	103.132	2.452	.2369	5.5046		
		4	.4025	90.516	2.060	.2804	3.2110		
		5	.4300	58.868	1.311	.3023	1.2707		
		6	.4400						
		7	.4450						
a) 20 % b) $H_0 = 1.65$ $\phi_0 = 6.50$	146.569 $-6.1580 \times 10^9$ $-2.555 \times 10^{15}$ $2.3422 \times 10^{20}$	0	0			.2000	8.8830	8.6588	
		1	.1370	77.241	2.132	.2874	8.4346	over 2	
		2	.2535	98.698	2.520	.3655	7.0641	points	
		3	.3330	102.673	2.467	.4263	5.0106		
		4	.3850	89.165	2.061	.4650	2.7346		
		5	.4050	58.175	1.321	.4823	0.8407		
		6	.4100						
		7	.4100						

continued

Table 18 continuation

Specimen specification a) Pre-straining (%) b) Dimensions (mm)	Values of $C_1, C_2, C_3$ & $C_4$ respectively; where, $C_1$ related to impact velocity (m/s)	Time (μs)	Displacement (mm)	Force, F $= M \frac{dv_t}{dt}$ (kN) where, M = 3.1100 gms.	Stress, $\sigma$ (kN/mm <sup>2</sup> )	Strain, $\epsilon$ (ln $h_0/h_t$ )	Strain rate $\dot{\epsilon} = v_t/h_t$ ( $\times 10^4/s$ )	Strain rate constant ( $\times 10^4/s$ )
a) 40 %	145.181	0	0			.4000	8.7382	8.4444
b) $H_0 = 1.65$	$-6.9435 \times 10^9$	1	.1350	82.378	2.279	.4852	8.1506	over 2
$\phi_0 = 6.50$	$-2.6014 \times 10^{15}$	2	.2450	102.861	2.641	.5598	6.6284	points
	$2.5063 \times 10^{20}$	3	.3165	104.636	2.541	.6156	4.4626	
		4	.3675	87.704	2.061	.6486	2.1702	
		5	.3765	52.065	1.208	.6605	0.3895	
		6	.3785					
		7	.3785					

Table 19, Stress and stress ratio at different strains and at various strain rates for structural steel at  $-30^{\circ}$  C.

Strain rate, $\dot{\epsilon} \left( \frac{v_f}{h_f} \right)$	Strain, $\epsilon$ ( $\ln h_0/h_f$ )	Stress, $\sigma$ ( $\text{kN/mm}^2$ )	Ratio of dynamic to quasi-static stress ( $\sigma_D/\sigma_S$ )
Quasi-static	0.05	0.68	
	0.10	0.79	
	0.20	0.87	
	0.30	0.90	
	0.40	0.93	
$1.83 \times 10^4/\text{s}$	0.05	1.68	2.47
	0.10	1.74	2.20
	0.20	1.82	2.09
	0.30	1.86	2.06
	0.40	1.90	2.04
$4.89 \times 10^4/\text{s}$	0.05	1.83	2.69
	0.10	1.87	2.37
	0.20	1.94	2.23
	0.30	1.98	2.20
	0.40	2.04	2.19
$8.65 \times 10^4/\text{s}$	0.05	1.87	2.75
	0.10	1.97	2.49
	0.20	2.07	2.38
	0.30	2.14	2.37
	0.40	2.20	2.36

Table 20, Detailed results of the experiment carried out at  $\dot{\epsilon} = 7.2 \times 10^3$  /s on structural steel at 235° C.

Specimen specification a) Pre-straining (%) b) Dimensions (mm)	Values of $C_1, C_2, C_3$ & $C_4$ respectively; where, $C_1$ related to impact velocity (m/s)	Time (μs)	Displacement (mm)	Force, F $\frac{dvt}{dx \cdot dt}$ (kN) where, M = 16.3900 gms.	Stress, $\sigma$ (kN/mm <sup>2</sup> )	Stress, $\sigma$ after friction correction (kN/mm <sup>2</sup> )	Strain, $\epsilon$ (ln $h_0/h_t$ )	Strain rate $\dot{\epsilon} = v_t/h_t$ (x 10 <sup>3</sup> /s)	Strain rate constant (x 10 <sup>3</sup> /s)
a) 0 %	44.923	0	0				0	7.487	7.272
b) $\epsilon_0 = 6.00$ $\phi_0 = 6.50$	134646760 -2.5302 x 10 <sup>14</sup> 1.3817 x 10 <sup>19</sup>	1 2 3 4 5 6 7	.0450 .0885 .1300 .1695 .2050 .2375 .2675	17.750 34.479 45.773 51.632 52.055	0.530 1.023 1.349 1.512 1.515	1.1407	.0075 .0148 .0219 .0286 .0347	7.470 7.251 6.881 6.412 5.901	over 4 points
a) 20 %	44.241	0	0				.2000	7.373	7.188
b) $\epsilon_0 = 6.00$ $\phi_0 = 6.50$	254024185 -2.6399 x 10 <sup>14</sup> 1.2203 x 10 <sup>19</sup>	1 2 3 4 5 6 7	.0445 .0875 .1285 .1675 .2025 .2330 .2610	15.234 33.995 47.955 57.115 61.476	0.455 1.009 1.414 1.673 1.790	1.2004	.2074 .2147 .2217 .2282 .2342	7.389 7.184 6.805 6.296 5.706	over 4 points

continued

Table 20 continuation

Specimen specification a) Pre-straining (%) b) Dimensions (mm)	Values of $C_1, C_2, C_3$ & $C_4$ respectively; where, $C_1$ related to impact velocity (m/s)	Time (μs)	Displacement (mm)	Force, F $= Mx \frac{dv_t}{dt}$ (kN) where, M = 16.3900 gms.	Stress, $\sigma$ (kN/mm <sup>2</sup> )	Stress, $\sigma$ after friction correction (kN/mm <sup>2</sup> )	Strain, $\epsilon$ (ln $h_0/h_t$ )	Strain rate $\dot{\epsilon} = v_t/h_t$ ( $\times 10^3/s$ )	Strain rate constant ( $\times 10^3/s$ )
a) 40 %	44.878	0	0				.4000	7.430	7.120
b) $E_0 = 6.04$	-45100622	1	.0450	23.922	0.715		.4074	7.351	over 4
$\phi_0 = 6.50$	-2.5590 $\times 10^{14}$	2	.0875	40.922	1.215		.4146	7.067	points
	1.3839 $\times 10^{19}$	3	.1280	52.479	1.547	1.2966	.4214	6.629	
		4	.16665	58.591	1.717		.4278	6.090	
		5	.2000	59.260	1.726		.4336	5.505	
		6	.2300						
		7	.2575						

Table 21, Detailed results of the experiment carried out at  $\dot{\epsilon} = 1.8 \times 10^4$ /s on structural steel at 235° C.

Specimen specification a) Pre-straining (%) b) Dimensions (mm)	Values of $C_1, C_2, C_3$ & $C_4$ respectively; where, $C_1$ related to impact velocity (m/s)	Time (μs)	Displacement (mm)	Force, F $= Mx - \frac{dvt}{dt}$ (kN) where, M = 10.3770 gms.	Stress, $\sigma$ (kN/mm <sup>2</sup> )	Stress, $\sigma$ after friction correction (kN/mm <sup>2</sup> )	Strain, $\epsilon$ (ln $h_0/h_t$ )	Strain rate $\dot{\epsilon} = v_t/h_t$ ( $\times 10^4$ /s)	Strain rate constant ( $\times 10^4$ /s)	
c) 0 % b) $H_0 = 3.00$ $\phi_0 = 7.00$	56.521 $1.5186 \times 10^9$ $-1.0442 \times 10^{15}$ $6.5985 \times 10^{19}$	0	0				0	1.8840	1.8723	
		1	.0570	25.279	0.644		.0192	1.9263	over 3	
		2	.1110	65.643	1.642	1.3826	.0379	1.8065	points	
		3	.1620	89.573	2.203		.0549	1.5694		
		4	.2000	97.070	2.353		.0691	1.2659		
		5	.2300	88.133	2.113		.0802	0.9529		
		6	.2550							
		7	.2700							
a) 20 % b) $H_0 = 3.00$ $\phi_0 = 7.00$	56.091 $1.5602 \times 10^9$ $-1.1048 \times 10^{15}$ $6.9773 \times 10^{19}$	0	0				.2000	1.8697	1.8513	
		1	.0565	27.716	0.706		.2190	1.9085	over 3	
		2	.1100	70.439	1.762	1.4826	.2375	1.7757	points	
		3	.1600	95.784	2.357		.2541	1.5186		
		4	.1950	103.752	2.519		.2677	1.1915		
		5	.2250	94.344	2.267		.2779	0.8547		
		6	.2450							
		7	.2575							

continued

Table 21 continuation

Specimen specification a) Pre-straining (%) b) Dimensions (mm)	Values of $C_1, C_2, C_3$ & $C_4$ respectively; $C_3$ where, $C_1$ related to impact velocity (m/s)	Time ( $\mu$ s)	Displacement (mm)	Force, F $=Mx \frac{dv}{dt}$ (kN) where, M = 10.3770 gms.	Stress, $\sigma$ (kN/mm <sup>2</sup> )	Stress, $\sigma$ after friction correction (kN/mm <sup>2</sup> )	Strain, $\epsilon$ (ln $h_0/h_t$ )	Strain rate $\dot{\epsilon} = v_t/h_t$ ( $\times 10^4/s$ )	Strain rate constant ( $\times 10^4/s$ )
a) 40 %	56.157	0	0				.4000	1.8719	1.8080
b) $H_0 = 3.00$	390706478	1	.0560	38.677	0.986	1.5046	.4187	1.8537	over 3 points
$\phi_0 = 7.00$		2	.1060	72.274	1.810		.4366	1.6986	
		3	.1565	92.683	2.285		.4523	1.4427	
	$-8.5735 \times 10^{14}$	4	.1875	99.904	2.431		.4652	1.1274	
	5.2956	5	.2160	93.935	2.264		.4748	0.7990	
		6	.2355						
		7	.2450						

Table 22, Detailed results of the experiment carried out at  $\dot{\epsilon} = 5.9 \times 10^4$  /s on structural steel at 235° C.

Specimen specification a) Pre-straining (%) b) Dimensions (mm)	Values of $C_1, C_2, C_3$ & $C_4$ respectively, where, $C_1$ related to impact velocity (m/s)	Time (μs)	Displacement (mm)	Force, F $= M \frac{dv}{dt}$ (kN) where, M = 4.6250 gms.	Stress, $\sigma$ (kN/mm <sup>2</sup> )	Stress, $\sigma$ after friction correction (kN/mm <sup>2</sup> )	Strain, $\epsilon$ (ln $h_0$ /ht)	Strain rate $\dot{\epsilon} = v_t/ht$ ( $\times 10^4$ /s)	Strain rate constant ( $\times 10^4$ /s)
a) 0 %	119.764	0	0				0	5.9882	5.9393
b) $H_0 = 2.00$ $\phi_0 = 6.50$	-328424881	1	.1170	43.409	1.230	1.6193	.0607	6.0845	over 3
	-1.6786 $\times 10^{15}$	2	.2275	71.356	1.906		.1202	5.7453	points
	1.1193 $\times 10^{20}$	3	.3200	86.878	2.199		.1744	5.0334	
		4	.3950	89.975	2.175		.2200	4.0633	
		5	.4500	80.648	1.882		.2553	3.0043	
		6	.4900						
		7	.5150						
a) 20 %	118.995	0	0				.2000	5.9497	5.8336
b) $H_0 = 2.00$ $\phi_0 = 6.50$	-938156868	1	.1160	48.252	1.369	1.6839	.2600	5.9791	over 3
	-1.6505 $\times 10^{15}$	2	.2225	75.371	2.018		.3181	5.5721	points
	1.1221 $\times 10^{20}$	3	.3150	90.034	2.288		.3702	4.7969	
		4	.3825	92.241	2.245		.4132	3.7743	
		5	.4350	81.992	1.933		.4454	2.6798	
		6	.4700						
		7	.4900						

continued

Table 22 continuation

Specimen specification a) Pre-straining (%) b) Dimensions (mm)	Values of $C_1, C_2, C_3$ & $C_4$ respectively; where, $C_1$ related to impact velocity (m/s)	Time (ms)	Displacement (mm)	Force, F $= Mx \frac{dx}{dt}$ (kN) where, M = 4.6250 gms.	Stress, $\sigma$ (kN/mm <sup>2</sup> )	Stress, $\sigma$ after friction correction (kN/mm <sup>2</sup> )	Strain, $\epsilon$ (ln $h_c/h_t$ )	Strain rate $\dot{\epsilon} = v_t/h_t$ (x 10 <sup>4</sup> /s)	Strain rate constant (x 10 <sup>4</sup> /s)
a) 40 %	118.400	0	0				.4000	5.9200	5.7962
b) $\phi_0 = 2.00$	-381590482	1	.1155	50.041	1.420		.4598	5.9626	
$\phi_0 = 6.50$	-1.9621 x 10 <sup>15</sup>	2	.2215	80.676	2.161	1.7264	.5175	5.5060	over 3
	1.4303 x 10 <sup>20</sup>	3	.3125	95.434	2.429		.5686	4.6507	points
		4	.3775	94.316	2.304		.6098	3.5635	
		5	.4250	77.321	1.833		.6399	2.4748	
		6	.4600						
		7	.4800						

Table 23, Stress and atress ratio at different strains and at various strain rates for structural steel at 235° C.

Strain rate, $\dot{\epsilon} \left( \frac{v_f}{h_f} \right)$	Strain, $\epsilon$ (ln $h_0/h_f$ )	Stress, $\sigma$ (kN/mm <sup>2</sup> )	Ratio of dynamic to quasi-static stress ( $\sigma_D/\sigma_S$ )
Quasi-static	0.05	0.58	
	0.10	0.68	
	0.20	0.75	
	0.30	0.78	
	0.40	0.81	
$7.2 \times 10^3/s$	0.05	1.16	2.00
	0.10	1.17	1.72
	0.20	1.19	1.59
	0.30	1.24	1.58
	0.40	1.29	1.58
$1.84 \times 10^4/s$	0.05	1.39	2.40
	0.10	1.42	2.08
	0.20	1.45	1.93
	0.30	1.48	1.89
	0.40	1.50	1.85
$5.85 \times 10^4/s$	0.05	1.54	2.65
	0.10	1.60	2.35
	0.20	1.64	2.19
	0.30	1.68	2.15
	0.40	1.71	2.11

Table 24, Results of the quasi-static tests carried out at room temperature on as-received aluminium under dry and lubricated condition.

Strain, $\epsilon$ ( $\ln h_0/h_f$ )	Stress, $\sigma = F_t/A_t$ ( $\text{kN/mm}^2$ )	
	Dry	Lubricated
0.0093	0.2305	0.2200
0.0140	0.2415	0.2365
0.0219	0.2600	0.2500
0.0315	0.2895	0.2755
0.0508	0.3225	0.3100
0.0723	0.3450	0.3325
0.1062	0.3695	0.3560
0.1324	0.3767	0.3648
0.1685	0.3825	0.3712
0.2059	0.3914	0.3724
0.2447	0.3951	0.3742
0.2851	0.4024	0.3765
0.3272	0.4079	0.3774
0.3712	0.4138	0.3816
0.4171	0.4220	0.3847
0.4654	0.4308	0.3866
0.5160	0.4417	0.3885
0.5694	0.4560	0.3930
0.6257	0.4721	0.3975

Table 25, Detailed results of the experiment carried out at  $\dot{\epsilon} = 6.7 \times 10^3/s$  on aluminium at room temperature.

Specimen specification a) Pre-straining (%) b) Dimensions (mm)	Values of $C_1, C_2, C_3$ & $C_4$ respectively; where, $C_1$ related to impact velocity (m/s)	Time (ms)	Displacement (mm)	Force, F $= Mx \frac{dv}{dt}$ (kN) where, M = 10.2207 gms.	Stress, $\sigma$ (kN/mm <sup>2</sup> )	Stress, $\sigma$ after friction correction (kN/mm <sup>2</sup> )	Strain, $\epsilon$ (ln $h_0/h_t$ )	Strain rate $\dot{\epsilon} = v_t/h_t$ ( $\times 10^3/s$ )	Strain rate constant ( $\times 10^3/s$ )
a) 0 %	45.061	0	0				0	6.932	6.677
b) $\epsilon_0 = 6.50$	-14672683	1	.0450	13.304	.299		.0069	6.873	over 4
$\phi_0 = 7.50$	-2.3719 $\times 10^{14}$	2	.0880	23.226	.518		.0136	6.637	points
	1.2564 $\times 10^{19}$	3	.1300	30.067	.667	.6185	.0201	6.267	
		4	.1680	33.825	.745		.0261	5.807	
		5	.2030	34.501	.756		.0317	5.305	
		6	.2350						
		7	.2635						
a) 20 %	44.521	0	0				.2000	6.849	6.612
b) $\epsilon_0 = 6.50$	208318511	1	.0445	12.156	.273		.2068	6.832	over 4
$\phi_0 = 7.50$	-2.9797 $\times 10^{14}$	2	.0875	24.854	.555		.2135	6.591	points
	1.5151 $\times 10^{19}$	3	.1290	33.836	.750	.6907	.2199	6.177	
		4	.1660	39.101	.862		.2259	5.646	
		5	.2000	40.650	.891		.2312	5.052	
		6	.2300						
		7	.2560						

continued

Table 25 continuation

Specimen specification a) Pre-straining (%) b) Dimensions (mm)	Values of $C_1, C_2, C_3$ & $C_4$ respectively; where, $C_1$ related to impact velocity (m/s)	Time (μs)	Displacement (mm)	Force, F $= N \frac{dv}{dt}$ (kN) where, M = 10.2207 gms.	Stress, σ (kN/mm <sup>2</sup> )	Stress, σ after friction correction (kN/mm <sup>2</sup> )	Strain, ε (ln h <sub>0</sub> /h <sub>t</sub> )	Strain rate $\dot{\epsilon} = v_t/h_t$ ( $\times 10^3/s$ )	Strain rate constant ( $\times 10^3/s$ )
a) 40 %	44.136	0	0				.4000	6.790	6.549
b) $H_0 = 6.50$	30098266	1	.0440	12.217	.274		.4068	6.785	over 4
$\phi_0 = 7.50$		2	.0870	26.210	.585		.4134	6.531	points
	$-3.3523 \times 10^{14}$	3	.1280	35.827	.795	.7204	.4198	6.091	
	$1.7841 \times 10^{19}$	4	.1640	41.067	.906		.4256	5.527	
		5	.1975	41.932	.920		.4308	4.906	
		6	.2265						
		7	.2515						

Table 26, Detailed results of the experiment carried out at  $\dot{\epsilon} = 1.0 \times 10^4/s$  on aluminium at room temperature.

Specimen specification a) Pre-straining (%) b) Dimensions (mm)	Values of $C_1, C_2, C_3$ & $C_4$ respectively; where, $C_1$ related to impact velocity (m/s).	Time (μs)	Displacement (mm)	Force, F = $Mx \frac{dv}{dt}$ (kN) where, M = 4.6750 gms.	Stress, (kN/mm <sup>2</sup> )	Stress, σ after friction correction (kN/mm <sup>2</sup> )	Strain, ε (ln h <sub>0</sub> /ht)	Strain rate $\dot{\epsilon} = vt/ht$ ( $\times 10^4/s$ )	Strain rate constant ( $\times 10^4/s$ )	
a) 0 % b) H <sub>0</sub> = 4.75 φ <sub>0</sub> = 5.00	51.207 -41683808 -2.7019 x 10 <sup>14</sup> 1.5151 x 10 <sup>19</sup>	0	0				0	1.0780	1.0431	
		1	.0510	7.118	0.358		.0107	1.0720	over 4	
		2	.1000	12.147	0.605		.0213	1.0384	points	
		3	.1475	15.477	0.763	.7154	.0314	0.9841		
		4	.1910	17.106	0.836		.0409	0.9164		
		5	.2300	17.035	0.825		.0497	0.8430		
		6	.2675							
		7	.3000							
a) 20 % b) H <sub>0</sub> = 4.75 φ <sub>0</sub> = 5.00	51.505 -286090236 -2.2133 x 10 <sup>14</sup> 9.1893 x 10 <sup>18</sup>	0	0				.2000	1.0843	1.0400	
		1	.0510	8.367	0.421		.2107	1.0705	over 4	
		2	.1000	13.029	0.649		.2213	1.0322	points	
		3	.1470	16.660	0.822	.7511	.2313	0.9733		
		4	.1900	19.260	0.941		.2407	0.8978		
		5	.2275	20.829	1.009		.2492	0.8103		
		6	.2635							
		7	.2925							

continued

Table 26 continuation

Specimen specification a) Pre-straining (%) b) Dimensions (mm)	Values of $C_1, C_2, C_3$ & $C_4$ respectively; where, $C_1$ related to impact velocity (m/s)	Time ( $\mu$ s)	Displacement (mm)	Force, $F$ $= M \frac{dv}{dt}$ (kN) where; $M = 4.6750$ gms.	Stress, $\sigma$ (kN/mm <sup>2</sup> )	Stress, $\sigma$ after friction correction (kN/mm <sup>2</sup> )	Strain, $\epsilon$ (ln $h_0/h_t$ )	Strain rate $\dot{\epsilon} = v_t/h_t$ ( $\times 10^4$ /s)	Strain rate constant ( $\times 10^4$ /s)
a) 40 % b) $H_0 = 4.75$ $\phi_0 = 5.00$	51.471 -308782310 -2.4141 $\times 10^{14}$ 1.0545 $\times 10^{19}$	0 1 2 3 4 5 6 7	0 .0510 .0995 .1465 .1885 .2250 .2600 .2875	9.067 14.064 17.877 20.508 21.955	0.456 0.701 0.882 1.003 1.064	.7855	.4000 .4107 .4212 .4312 .4404 .4487	1.0836 1.0677 1.0253 0.9608 0.8793 0.7858	1.0343 over 4 points

Table 27, Detailed results of the experiment carried out at  $\dot{\epsilon} = 3.3 \times 10^4$  /s on aluminium at room temperature.

Specimen specification a) Pre-straining (%) b) Dimensions (mm)	Values of $C_1, C_2, C_3$ & $C_4$ respectively, where, $C_1$ related to impact velocity (m/s)	Time (μs)	Displacement (mm)	Force, F $\frac{dvt}{dt} = Mx$ (kN) where, M = 2.9650 gms.	Stress, $\sigma$ (kN/mm <sup>2</sup> )	Stress, $\sigma$ after friction correction (kN/mm <sup>2</sup> )	Strain, $\epsilon$ (ln $h_0/h_t$ )	Strain rate $\dot{\epsilon} = v_t/h_t$ ( $\times 10^4$ /s)	Strain rate constant ( $\times 10^4$ /s)
a) 0 % b) $H_0 = 2.95$ $\phi_0 = 6.00$ $H_f =$	97.938 729464853 $-9.6449 \times 10^{14}$ $6.2263 \times 10^{19}$	0 1 2 3 4 5 6 7	0 .0980 .1925 .2775 .3600 .4250 .4865 .5400	10.617 21.129 27.211 28.862 26.082	.363 .698 .871 .897 .789	.8154	0 .0337 .0673 .0995 .1292 .1560	3.3199 3.3921 3.3095 3.1078 2.8320 2.5370	3.2823 over 4 points
a) 20 % b) $H_0 = 2.95$ $\phi_0 = 6.00$ $H_f =$	97.425 $-831761542$ $-1.0502 \times 10^{15}$ $7.1195 \times 10^{19}$	0 1 2 3 4 5 6 7	0 .0975 .1915 .2750 .3565 .4200 .4800 .5335	11.218 22.302 28.320 29.271 25.157	.383 .737 .907 .911 .762	.8280	.2000 .2335 .2669 .2986 .3278 .3540	3.3025 3.3730 3.2774 3.0585 2.7694 2.4743	3.2528 over 4 points

continued

Table 27 continuation

Specimen specification a) Pre-straining (%) b) Dimensions (mm)	Values of $C_1, C_2, C_3$ & $C_4$ respectively, where, $C_1$ related to impact velocity (m/s)	Time (μs)	Displacement (mm)	Force, $F = Mx \frac{dv}{dt}$ (kN) where, $M = 2.9650$ gms.	Stress, $\sigma$ (kN/mm <sup>2</sup> )	Stress, $\sigma$ after friction correction (kN/mm <sup>2</sup> )	Strain, $\epsilon$ ( $\ln h_0/h_t$ )	Strain rate $\dot{\epsilon} = v_t/h_t$ ( $\times 10^4/s$ )	Strain rate constant ( $\times 10^4/s$ )
a) 40 %	97.428	0	0				.4000	3.3026	3.2254
b) $H_0 = 2.95$ $\phi_c = 6.00$	591059651	1	.0970	12.718	.435		.4334	3.3553	over 4
	-1.0596 $\times 10^{15}$	2	.1910	23.683	.783		.4665	3.2405	points
	7.3684 $\times 10^{19}$	3	.2725	29.391	.942	.8342	.4978	3.0034	
		4	.3525	29.842	.930		.5263	2.7005	
		5	.4150	25.034	.760		.5518	2.3991	
		6	.4725						
		7	.5250						

Table 28, Stress and stress ratio at different strains and at various strain rates for aluminium at room temperature.

Strain rate, $\dot{\epsilon} \left( \frac{V_f}{h_f} \right)$	Strain, $\epsilon$ ( $\ln h_0/h_f$ )	Stress, $\sigma$ (kN/mm <sup>2</sup> )	Ratio of dynamic to quasi-static stress ( $\sigma_D/\sigma_S$ )
Quasi-static	0.05	0.3100	
	0.10	0.3550	
	0.20	0.3700	
	0.30	0.3770	
	0.40	0.3840	
$6.7 \times 10^3/s$	0.05	0.6450	2.08
	0.10	0.6700	1.88
	0.20	0.6890	1.86
	0.30	0.7015	1.86
	0.40	0.7155	1.86
$1.04 \times 10^4/s$	0.05	0.7130	2.30
	0.10	0.7350	2.07
	0.20	0.7490	2.02
	0.30	0.7635	2.02
	0.40	0.7790	2.02
$3.25 \times 10^4/s$	0.05	0.7850	2.53
	0.10	0.8160	2.30
	0.20	0.8210	2.22
	0.30	0.8290	2.20
	0.40	0.8325	2.17

Table 29, Results of the quasi-static tests carried out at room temperature on as-received copper under dry and lubricated condition.

Strain, $\epsilon$ ( $\ln h_0/h_f$ )	Stress, $\sigma = F_f/A_f$ ( $\text{kN/mm}^2$ )	
	Dry	Lubricated
0.0093	0.2100	0.2000
0.0140	0.2265	0.2180
0.0219	0.2400	0.2300
0.0315	0.2645	0.2550
0.0476	0.2900	0.2715
0.0723	0.3125	0.3015
0.0976	0.3200	0.3025
0.1324	0.3220	0.3104
0.1685	0.3232	0.3125
0.2059	0.3288	0.3165
0.2447	0.3341	0.3180
0.2851	0.3363	0.3200
0.3272	0.3405	0.3255
0.3712	0.3455	0.3289
0.4171	0.3486	0.3321
0.4654	0.3544	0.3358
0.5160	0.3614	0.3396
0.5690	0.3677	0.3413
0.6257	0.3762	0.3435

Table 30, Detailed results of the experiment carried out at  $\dot{\epsilon} = 6.7 \times 10^3$  /s on copper at room temperature.

Specimen specification a) Pre-straining (%) b) Dimensions (mm)	Values of $C_1, C_2, C_3$ & $C_4$ respectively; where, $C_1$ related to impact velocity (m/s)	Time (ms)	Displacement (mm)	Force, F $= M \frac{dv}{dt}$ (kN) where, M = 10.2207 gms.	Stress, $\sigma$ (kN/mm <sup>2</sup> )	Stress, $\sigma$ after friction correction (kN/mm <sup>2</sup> )	Strain, $\epsilon$ (ln $h_0/h_t$ )	Strain rate $\dot{\epsilon} = v_t/h_t$ ( $\times 10^3$ /s)	Strain rate constant ( $\times 10^3$ /s)
a) 0 % b) $H_0 = 6.50$ $\phi_0 = 7.50$	45.319 36542760 -2.3487 $\times 10^{14}$ 1.3183 $\times 10^{19}$	0 1 2 3 4 5 6 7	0 .0450 .0890 .1315 .1700 .2060 .2400 .2700	12.039 21.592 27.911 30.996 30.848	.270 .482 .619 .683 .676	.5672	0 .0070 .0138 .0203 .0265 .0322	6.972 6.931 6.718 6.377 5.957 5.076	6.749 over 4 points
a) 20 % b) $H_0 = 6.50$ $\phi_0 = 7.50$	45.017 13282703 -2.2269 $\times 10^{14}$ 9.2705 $\times 10^{18}$	0 1 2 3 4 5 6 7	0 .0445 .0885 .1305 .1680 .2030 .2350 .2615	12.247 22.493 30.464 36.161 39.584	.275 .502 .675 .797 .867	.6411	.2000 .2069 .2137 .2201 .2262 .2317	6.925 6.880 6.659 6.292 5.813 5.254	6.689 over 4 points

continued

Table 30 continuation

Specimen specification a) Pre-straining (%) b) Dimensions (mm)	Values of $C_1, C_2, C_3$ & $C_4$ respectively; where, $C_1$ related to impact velocity (m/s)	Time ( $\mu$ s)	Displacement (mm)	Force, F $= Mx \frac{dv}{dt}$ (kN) where, M = 10.2207 gms.	Stress, $\sigma$ (kN/mm <sup>2</sup> )	Stress, $\sigma$ after friction correction (kN/mm <sup>2</sup> )	Strain, $\epsilon$ (ln $h_0/h_t$ )	Strain rate $\dot{\epsilon} = v_t/h_t$ ( $\times 10^3/s$ )	Strain rate constant ( $\times 10^3/s$ )
a) 40 %	44.610	0	0				.4000	6.863	6.598
b) $H_0 = 6.50$	-17442846	1	.0440	13.460	.302		.4068	6.802	over 4
$\phi_0 = 7.50$	-2.3524 $\times 10^{14}$	2	.0875	23.919	.534		.4135	6.559	points
	1.0781 $\times 10^{19}$	3	.1290	31.734	.704	.6623	.4199	6.170	
		4	.1650	36.904	.814		.4258	5.673	
		5	.2000	39.429	.865		.4312	5.108	
		6	.2305						
		7	.2565						

Table 31, Detailed results of the experiment carried out at  $\dot{\epsilon} = 1.0 \times 10^4$  /s on copper at room temperature.

Specimen specification a) Pre-straining (%) b) Dimensions (mm)	Values of $C_1, C_2, C_3$ & $C_4$ respectively; $C_4$ is related to impact velocity (m/s)	Time ( $\mu$ s)	Displacement (mm)	Force, F $= Mx \frac{dv}{dt}$ (kN) where, M = 4.6750 gms.	Stress, $\sigma$ ( $kN/mm^2$ )	Stress, $\sigma$ after friction correction ( $kN/mm^2$ )	Strain, $\epsilon$ ( $\ln h_0/h_t$ )	Strain rate $\dot{\epsilon} = v_0/h_t$ ( $\times 10^4$ /s)	Strain rate constant ( $\times 10^4$ /s)
a) 0 %	51.582	0	0				0	1.0859	1.0531
b) $H_0 = 4.75$ $\phi_0 = 5.00$	-263392779	1	.0510	6.889	.347		.0108	1.0761	over 4
	-1.7348 $\times 10^{14}$	2	.1010	10.437	.520		.0214	1.0474	points
	7.8334 $\times 10^{18}$	3	.1485	13.106	.646	.6090	.0317	1.0031	
		4	.1925	14.896	.727		.0414	0.9469	
		5	.2350	15.807	.765		.0506	0.8825	
		6	.2725						
		7	.3075						
a) 20 %	51.570	0	0				.2000	1.0814	1.0437
b) $H_0 = 4.75$ $\phi_0 = 5.00$	-256407429	1	.0510	7.571	.381		.2107	1.0700	over 4
	-2.0514 $\times 10^{14}$	2	.1000	11.586	.577		.2213	1.0369	points
	1.0339 $\times 10^{19}$	3	.1475	14.440	.712	.6691	.2314	0.9865	
		4	.1905	16.134	.788		.2410	0.9238	
		5	.2315	16.668	.807		.2499	0.8539	
		6	.2680						
		7	.3015						

continued

Table 31 continuation

Specimen specification a) Pre-straining (%) b) Dimensions (mm)	Values of $C_1, C_2, C_3$ & $C_4$ respectively; where, $C_1$ related to impact velocity (m/s)	Time ( $\mu$ s)	Displacement (mm)	Force, F $= Mx \frac{dv}{dt}$ (kN) where, M = 4.6750 gms.	Stress, $\sigma$ (kN/mm <sup>2</sup> )	Stress, $\sigma$ after friction correction (kN/mm <sup>2</sup> )	Strain, $\epsilon$ (ln $h_0/h_t$ )	Strain rate $\dot{\epsilon} = v_t/h_t$ ( $\times 10^4/s$ )	Strain rate constant ( $\times 10^4/s$ )
a) 40%	51.318	0	0				.4000	1.0803	1.0370
b) $H_0 = 4.75$	-326372631	1	.0510	8.332	.419		.4107	1.0657	over 4
$\phi_0 = 5.00$	-2.0842 $\times 10^{14}$	2	.0995	12.481	.622		.4212	1.0286	points
	1.0081 $\times 10^{19}$	3	.1465	15.500	.765	.7103	.4312	0.9735	
		4	.1890	17.387	.850		.4406	0.9052	
		5	.2290	18.144	.879		.4493	0.8285	
		6	.2640						
		7	.2960						

Table 32, Detailed results of the experiment carried out at  $\dot{\epsilon} = 3.3 \times 10^4$ /s on copper at room temperature.

Specimen specification a) Pre-straining (%) b) Dimensions (mm)	Values of $C_1, C_2, C_3$ & $C_4$ respectively; where, $C_1$ related to impact velocity (m/s)	Time (µs)	Displacement (mm)	Force, $F = Mx \frac{dv}{dt}$ (kN) where, $M = 2.9650$ gms.	Stress, $\sigma$ (kN/mm <sup>2</sup> )	Stress, $\sigma$ after friction correction (kN/mm <sup>2</sup> )	Strain, $\epsilon$ (ln $h_0/bt$ )	Strain rate $\dot{\epsilon} = v_t/ht$ ( $\times 10^4$ /s)	Strain rate constant ( $\times 10^4/\epsilon$ )
a) 0 %	99.695	0	0				0	3.3794	3.3192
b) $H_0 = 2.95$ $\phi_c = 6.00$	-96743230	1	.0985	12.276	.419		.0340	3.4172	over 4
	-7.5681 $\times 10^{14}$	2	.1950	20.456	.675	.7571	.0679	3.3309	points
	4.9499 $\times 10^{19}$	3	.2800	25.114	.803		.1003	3.1491	
		4	.3625	26.249	.814		.1307	2.9076	
		5	.4325	23.862	.720		.1584	2.6499	
		6	.4950						
		7	.5525						
a) 20 %	98.869	0	0				.2000	3.3559	3.2836
b) $H_0 = 2.95$ $\phi_0 = 6.00$	-524590049	1	.0980	12.770	.436		.2338	3.3908	over 4
	-7.9393 $\times 10^{14}$	2	.1930	21.464	.709	.7906	.2673	3.2932	points
	5.7635 $\times 10^{19}$	3	.2775	26.309	.842		.2993	3.0946	
		4	.3590	27.303	.848		.3290	2.8349	
		5	.4250	24.448	.739		.3560	2.5624	
		6	.4875						
		7	.5420						

continued

Table 32 continuation

Specimen specification a) Pre-straining (%) b) Dimensions (mm)	Values of $C_1, C_2, C_3$ & $C_4$ respectively; where $C_1$ related to impact velocity (m/s)	Time Displacement ( $\mu$ s)	Force, $F = Mx - \frac{dv}{dt}t$ (kN) where, $M = 2.9650$ gms.	Stress, $\sigma$ (kN/mm <sup>2</sup> )	Stress, $\sigma$ after friction correction (kN/mm <sup>2</sup> )	Strain, $\epsilon$ ( $\ln h_0/h_t$ )	Strain rate, $\dot{\epsilon} = v_t/h_t$ ( $\times 10^4/s$ )	Strain rate : constant ( $\times 10^4/s$ )
a) 40 %	98.869	0				.4000	3.3515	3.2358
b) $H_0 = 2.95$	-524590049	1	15.184	.519		.4336	3.3540	over 4
$\phi_0 = 6.00$	-7.9393 $\times 10^{14}$	2	23.156	.766		.4666	3.2281	points
	5.7635 $\times 10^{19}$	3	27.026	.866	.8051	.4979	3.0098	
		4	26.796	.834		.5266	2.7441	
		5	22.463	.681		.5528	2.4841	
		6						
		7						

Table 33, Stress and stress ratio at different strains and at various strain rates for copper at room temperature.

Strain rate, $\dot{\epsilon} \left( \frac{V_f}{h_f} \right)$	Strain, $\epsilon$ ( $\ln h_0/h_f$ )	Stress, $\sigma$ (kN/mm <sup>2</sup> )	Ratio of dynamic to quasi-static stress ( $\sigma_D/\sigma_S$ )
Quasi-static	0.05	0.2715	
	0.10	0.3025	
	0.20	0.3165	
	0.30	0.3240	
	0.40	0.3315	
$6.7 \times 10^3/s$	0.05	0.5750	2.11
	0.10	0.6050	2.00
	0.20	0.6315	2.00
	0.30	0.6500	2.00
	0.40	0.6600	2.00
$1.04 \times 10^4/s$	0.05	0.6250	2.30
	0.10	0.6400	2.11
	0.20	0.6675	2.11
	0.30	0.6900	2.11
	0.40	0.7025	2.11
$3.3 \times 10^4/s$	0.05	0.7150	2.63
	0.10	0.7575	2.50
	0.20	0.7780	2.45
	0.30	0.7910	2.44
	0.40	0.8000	2.41

Table 34, Values of the constants for the derived constitutive equation for different material under investigation.

Material	Constants		
	A (kN/mm <sup>2</sup> )	n	B
Structural steel (En - 8)	1.00	0.18	$5.85 \times 10^{-4}$
Aluminium	0.50	0.20	$6.50 \times 10^{-4}$
Copper	0.45	0.22	$7.00 \times 10^{-4}$

Table 35, Comparison of the dynamic stress values obtained by using the proposed equation with those obtained experimentally at room temperature at various strains and strain rates for structural steel.

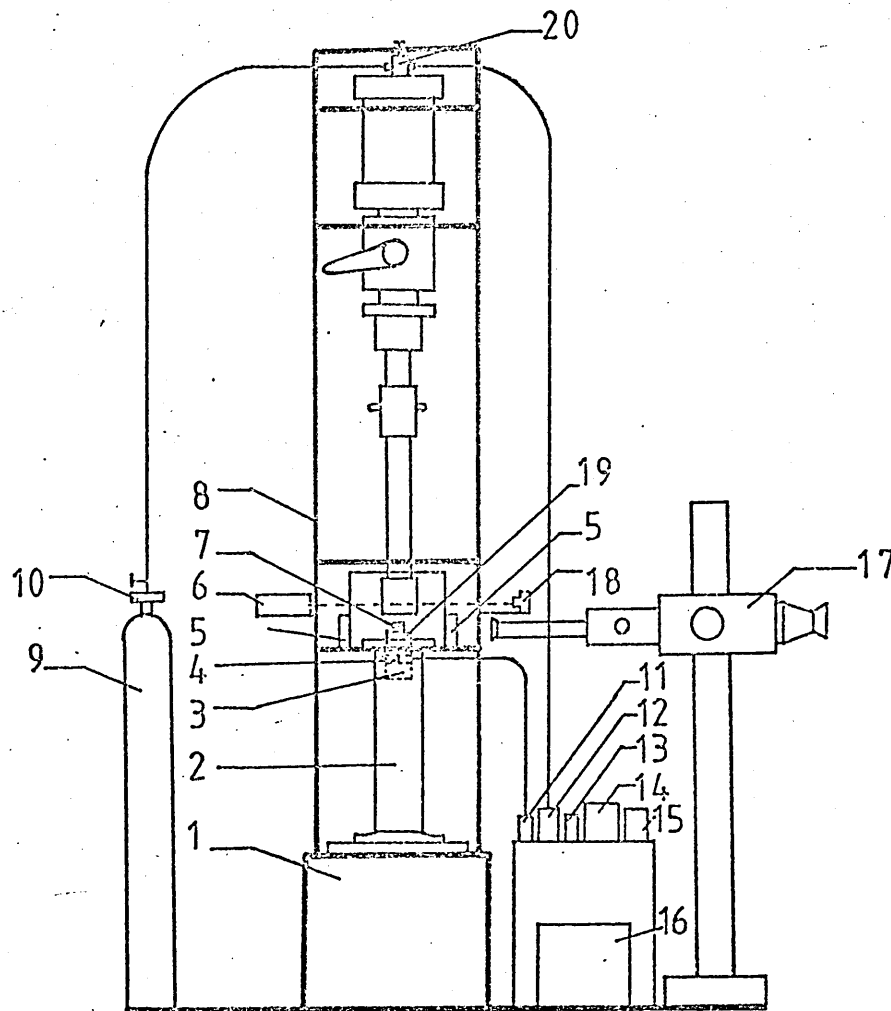
Strain rate	Strain	Dynamic stress (kN/mm <sup>2</sup> )	
		Experimental	: Equation (4)
7.32 x 10 <sup>3</sup> /s	•05	: 1.26	: 1.28
	•20	: 1.34	: 1.34
	•40	: 1.40	: 1.37
8.75 x 10 <sup>4</sup> /s	•05	: 1.66	: 1.70
	•20	: 1.82	: 1.78
	•40	: 1.90	: 1.82

Table 36, Comparison of the dynamic stress values obtained by using proposed equation with those obtained experimentally at room temperature at various strains and strain rates for aluminium.

Strain rate	Strain	Dynamic stress (kN/mm <sup>2</sup> )	
		Experimental	Equation (4)
$6.70 \times 10^3/s$	•05	•6450	•6481
	•20	•6890	•6812
	•40	•7155	•6981
$3.25 \times 10^4/s$	•05	•7850	•7835
	•20	•8210	•8205
	•40	•8325	•8396

Table 37, Comparison of the dynamic stress values obtained by using proposed equation with those obtained experimentally at room temperature at various strains and strain rates for copper.

Strain rate	Strain	Dynamic stress (kN/mm <sup>2</sup> )	
		Experimental	Equation (4)
$6.70 \times 10^3/s$	•05	•5750	•5908
	•20	•6315	•6239
	•40	•6600	•6412
$3.30 \times 10^4/s$	•05	•7150	•7210
	•20	•7780	•7585
	•40	•8000	•7780



- |                           |                               |
|---------------------------|-------------------------------|
| 1 Concrete base           | 11 Charge amplifier           |
| 2 Pressure bar            | 12 Pressure transducer meter  |
| 3 Middle anvil            | 13 Digital voltmeter          |
| 4 Load cell               | 14 Oscilloscope               |
| 5 Flash                   | 15 X-Y recorder               |
| 6 Laser                   | 16 Trigger delay generator    |
| 7 Specimen                | 17 High speed (IMACON) camera |
| 8 Rig frame               | 18 Photo cell                 |
| 9 Compressed air cylinder | 19 Top anvil                  |
| 10 Cylinder valve         | 20 Pressure transducer        |

Fig.1 Schematic diagram of the experimental apparatus.

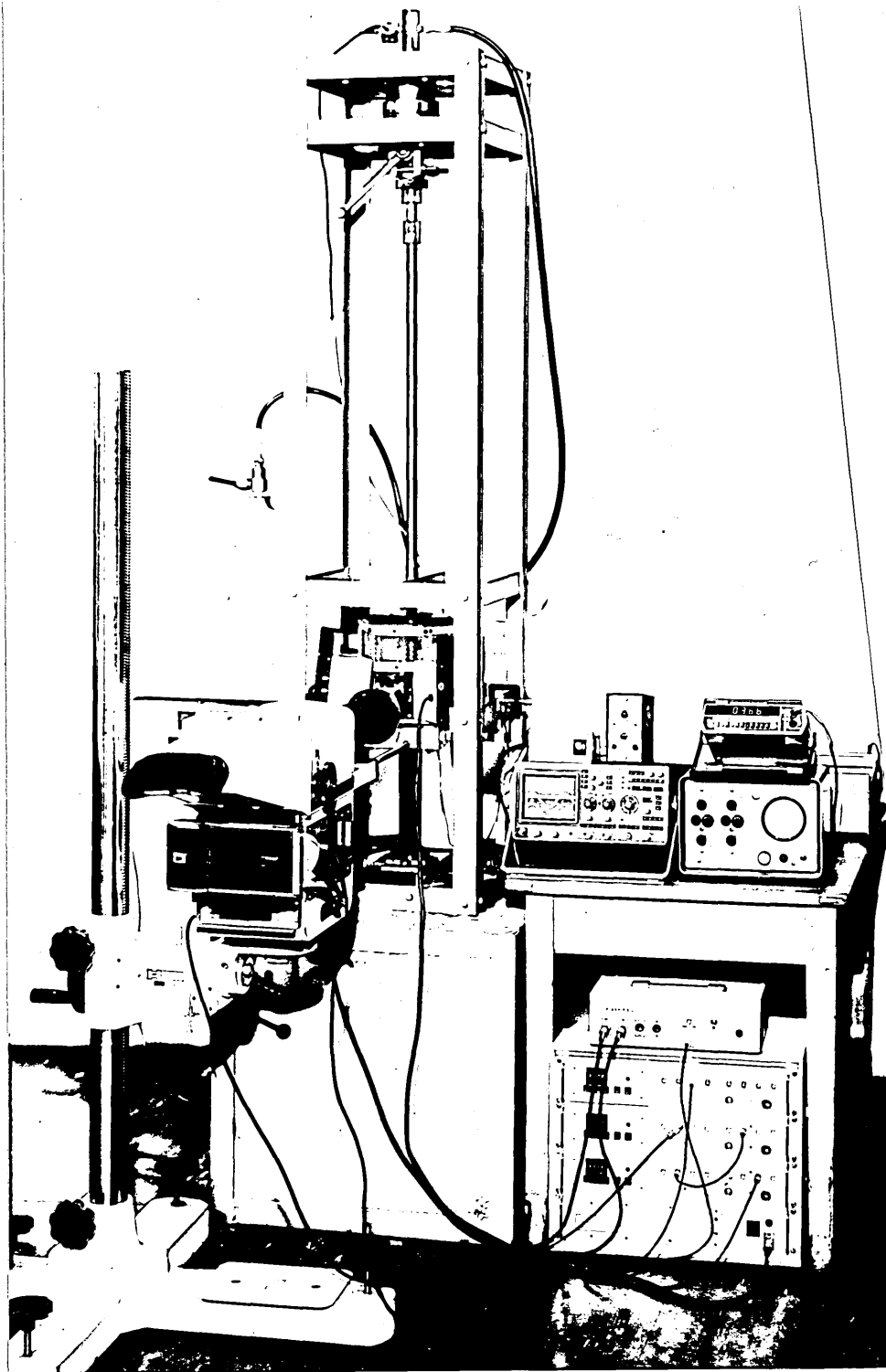


Fig.2 Photograph of the experimental set-up.

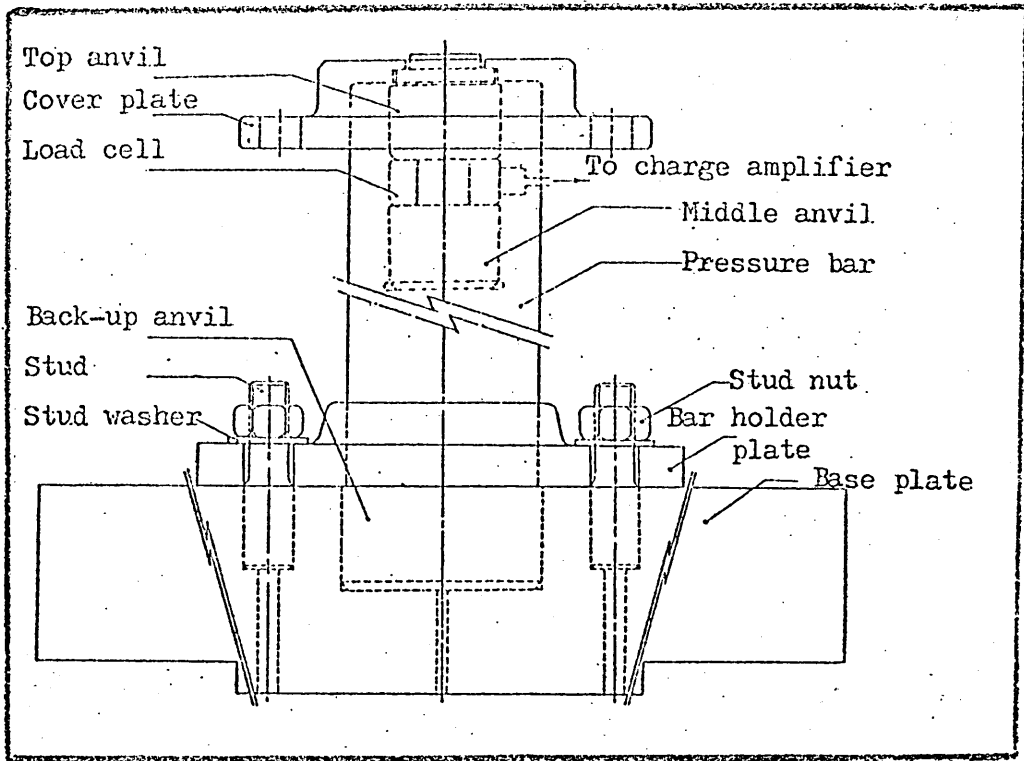


Fig.3 Line diagram of load cell and anvil unit in assembled condition.

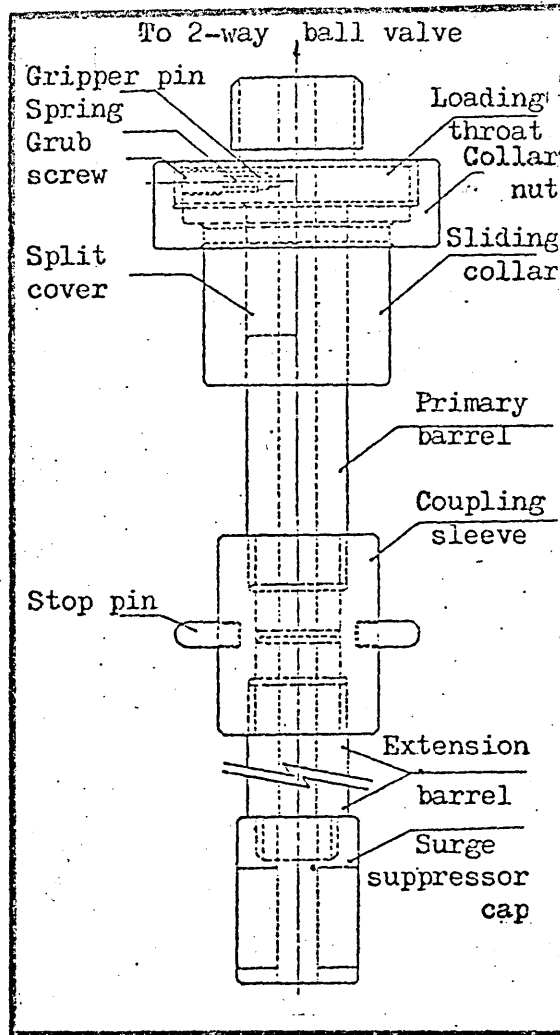


Fig.4 Line diagram of barrel and loading unit in assembled condition.

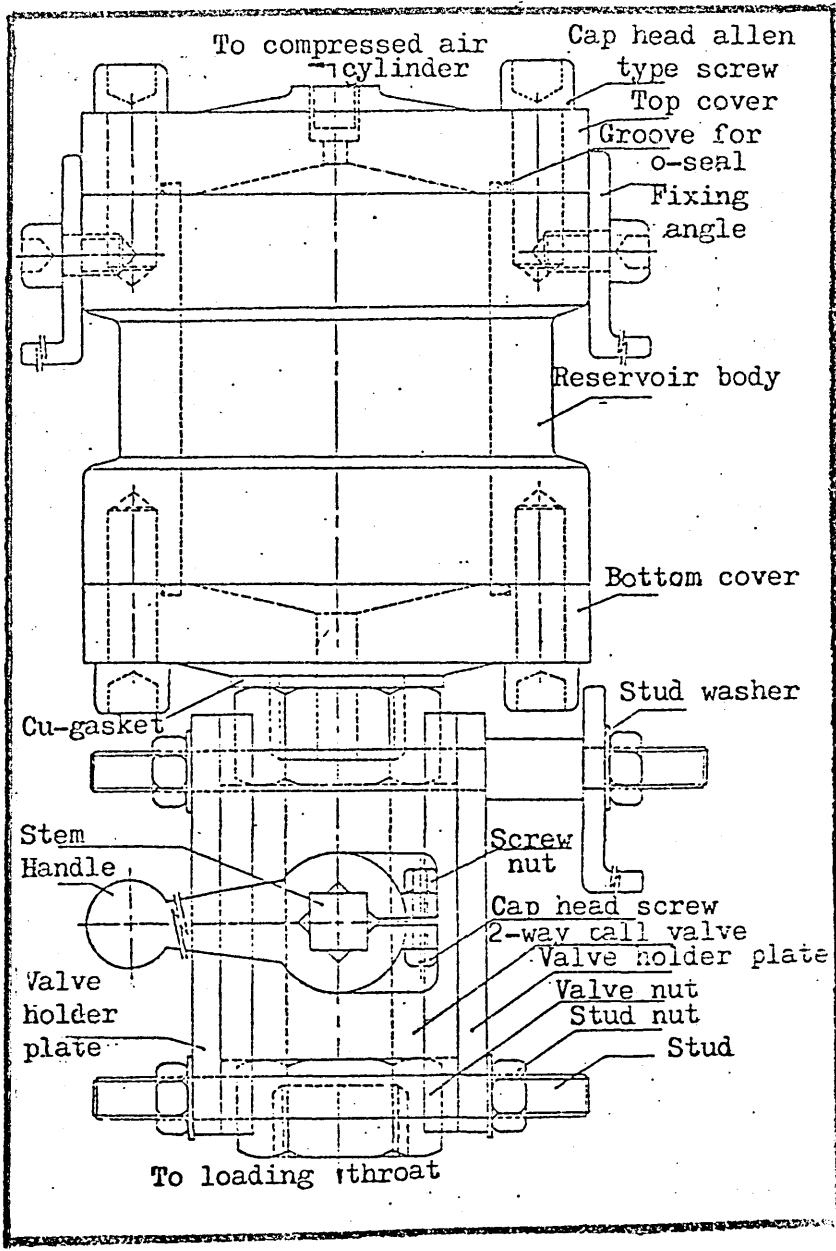


Fig.5 Line diagram of valve and reservoir unit in assembled condition.

Fig. 6 Showing details of (a) stud, (b) base plate and (c) back-up anvil.

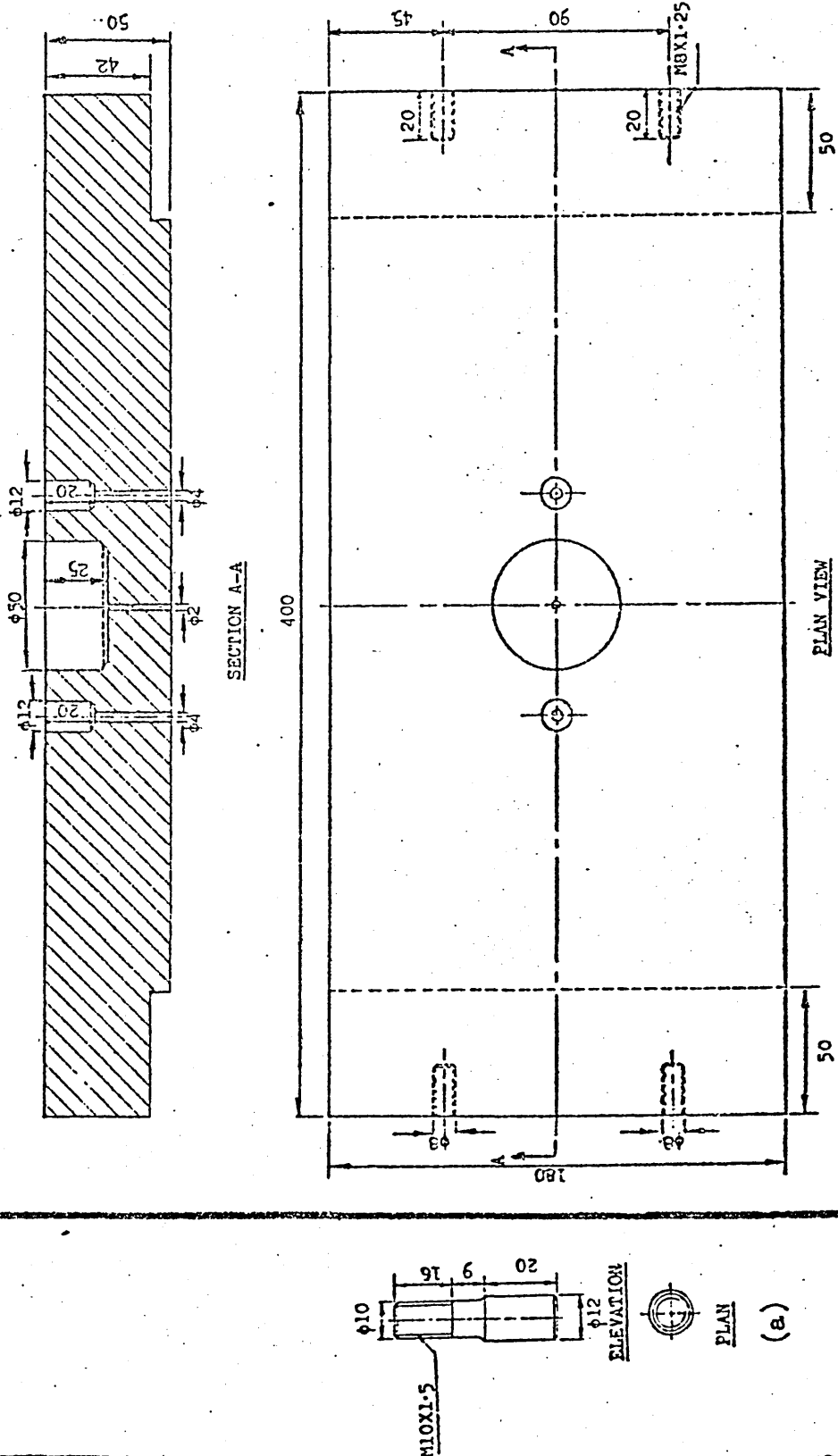


Fig. 7 Showing details of (a) cover plate, (b) holder plate, (c) top anvil, (d) middle anvil and (e) pressure bar.

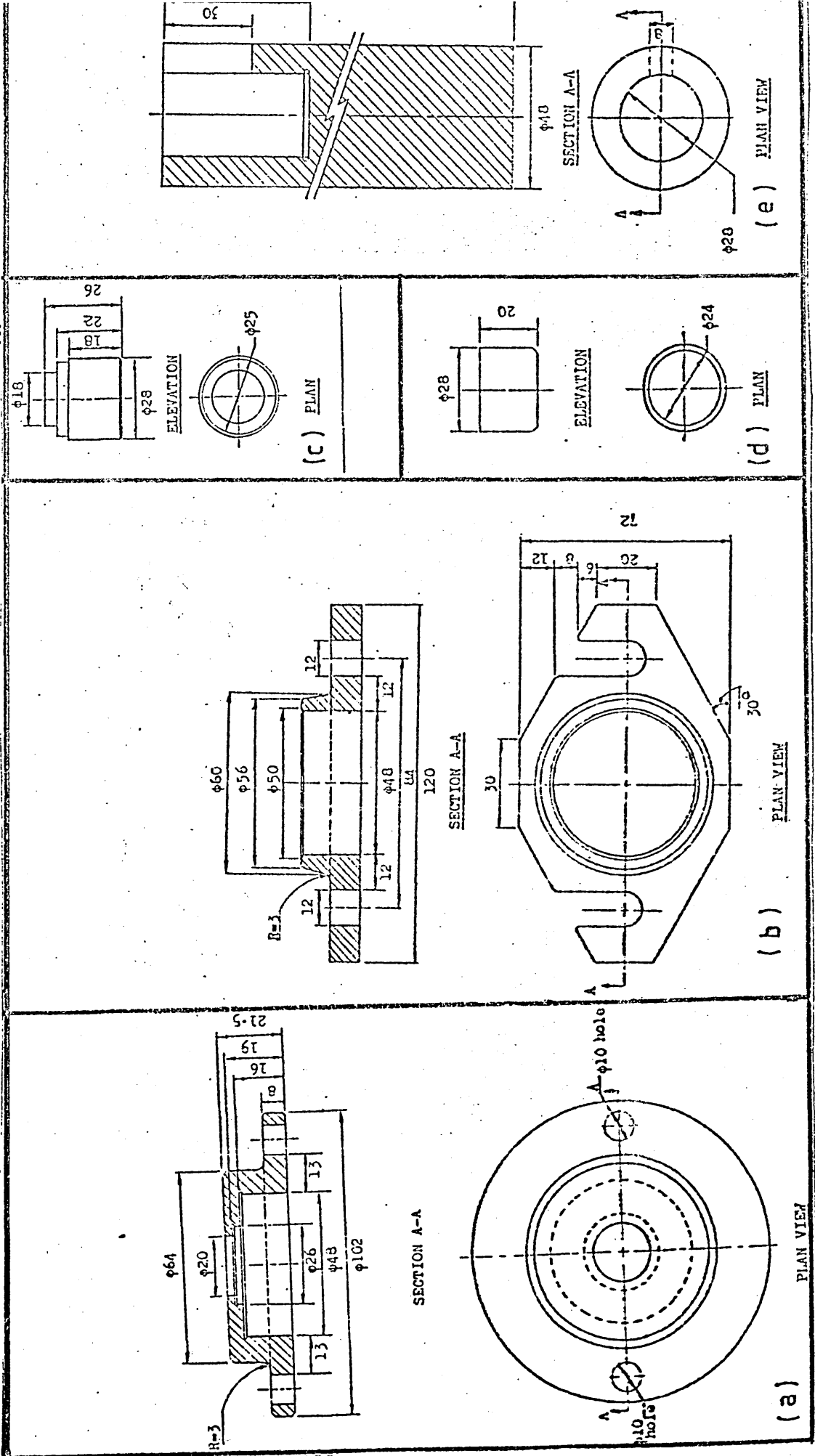
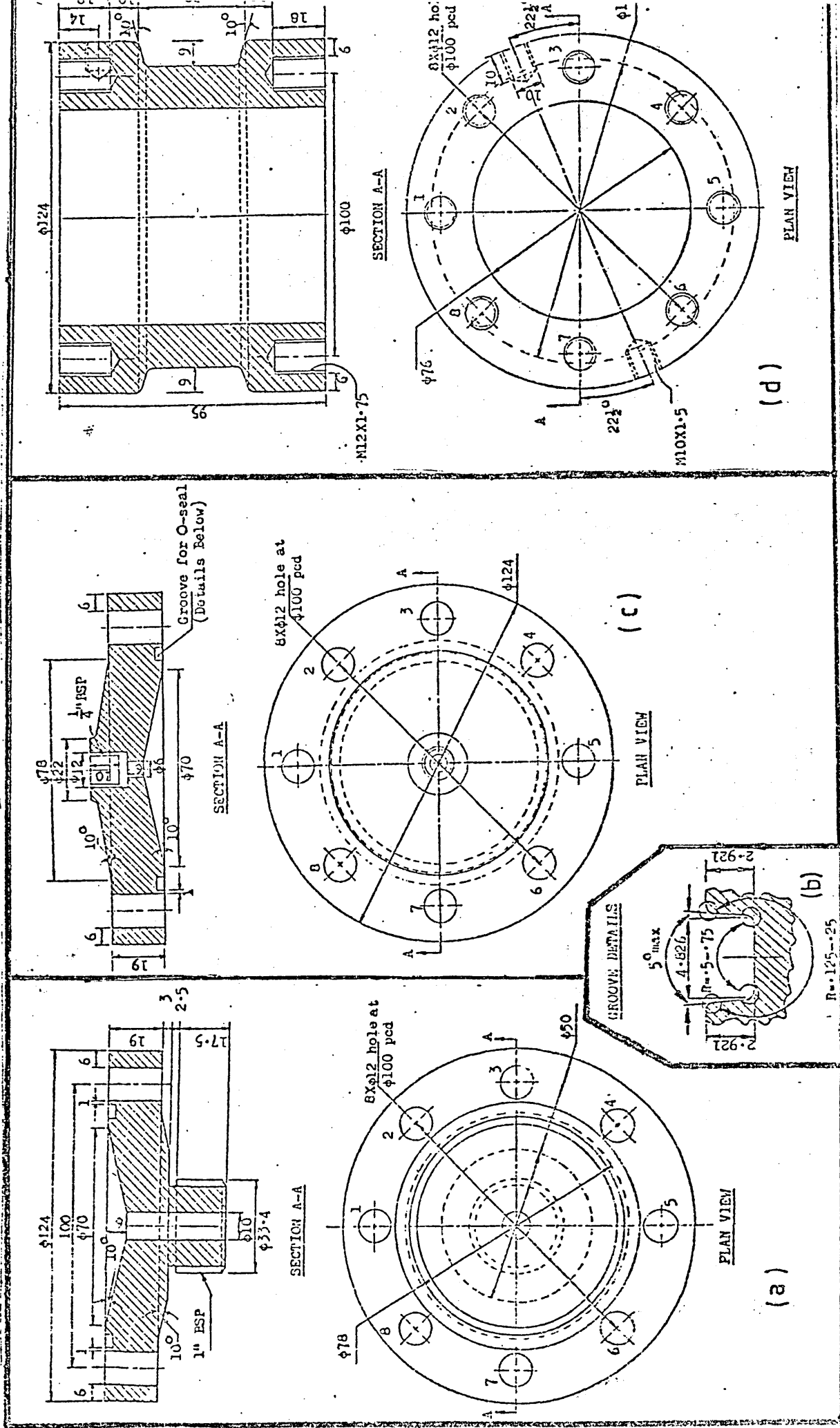






Fig.10 Showing details of (a) bottom cover, (b) groove for o-seal, (c) top cover and (d) reservoir body.



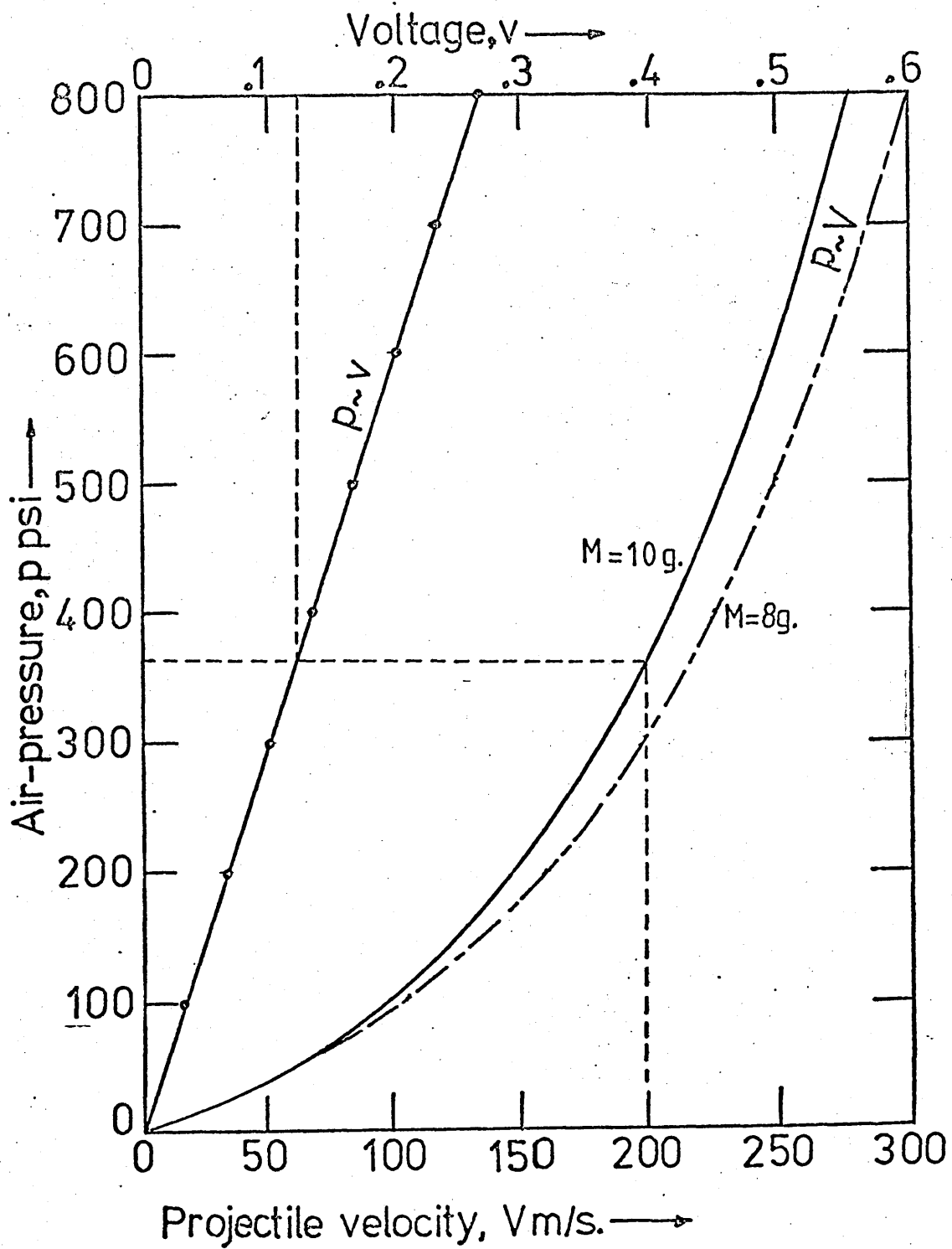
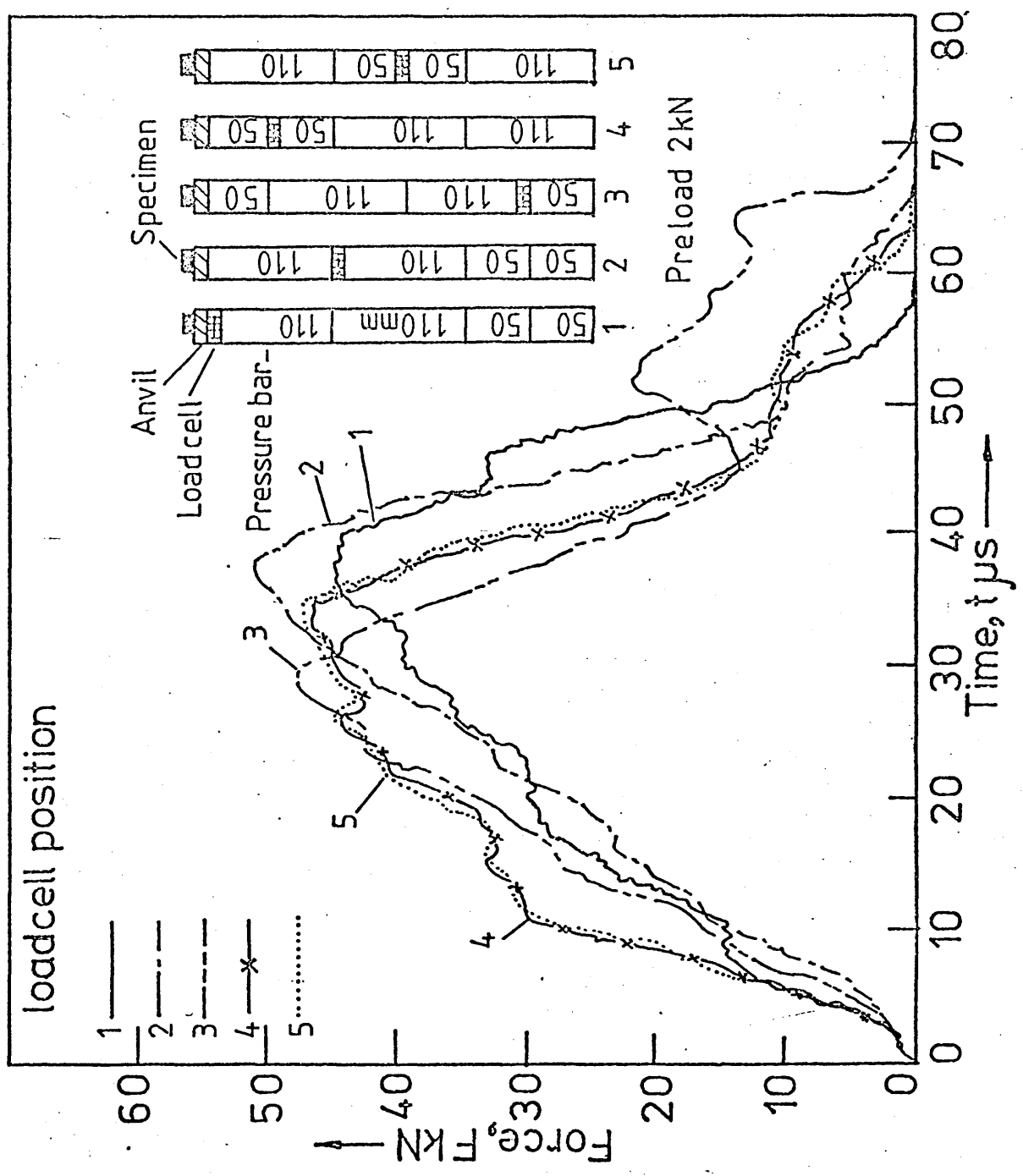


Fig.11 Showing air - gun calibration chart.

Fig.12 Showing load-time histories at various positions of load cell within the composite pressure bar.



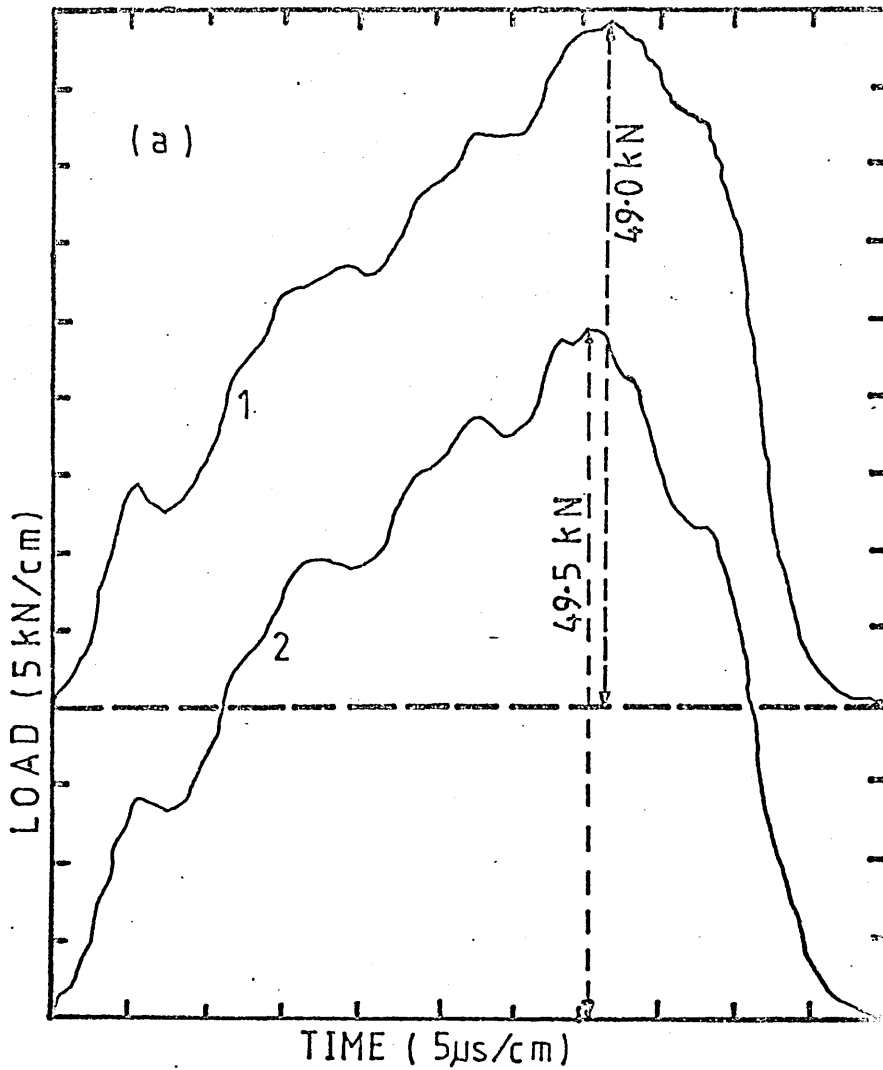


Fig.13 Showing repeatability of the load-time traces during impact by same projectile of 19.07 mm length.

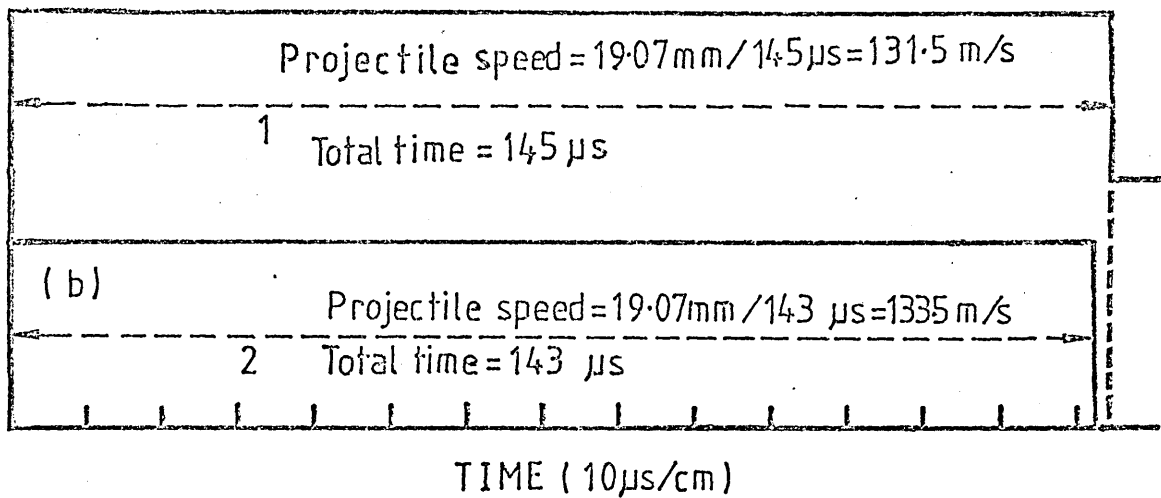


Fig.14 Showing repeatability of elapsed time during which the laser beam remains obstructed by 19.07 mm long projectile.

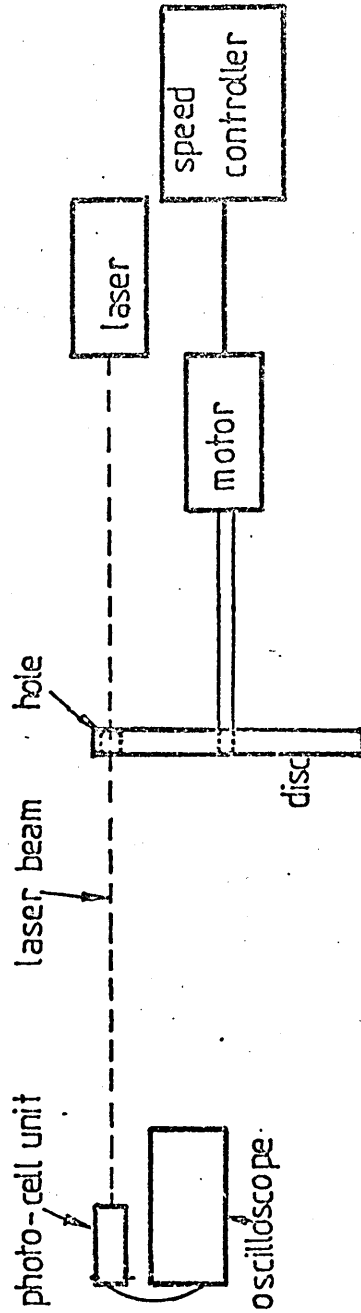
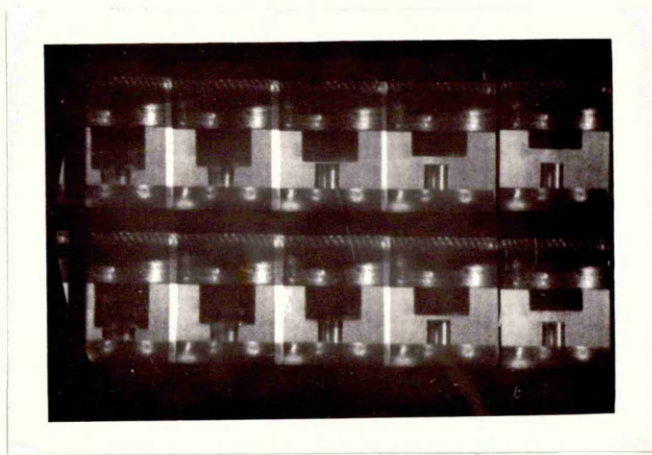
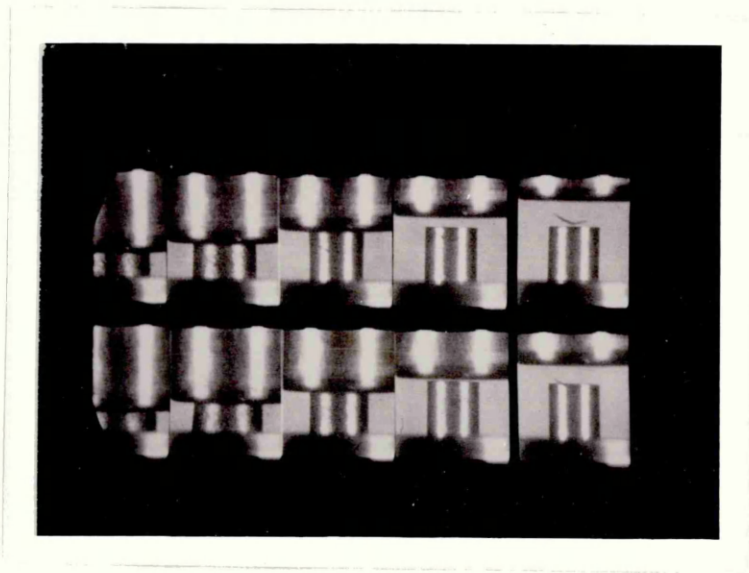


Fig.15 Schematic diagram of speed calibration arrangement.



(a)



(b)

Fig.16 Showing the sequence of events taken by the IMACON camera with framing mode (a) initial and (b) magnified.

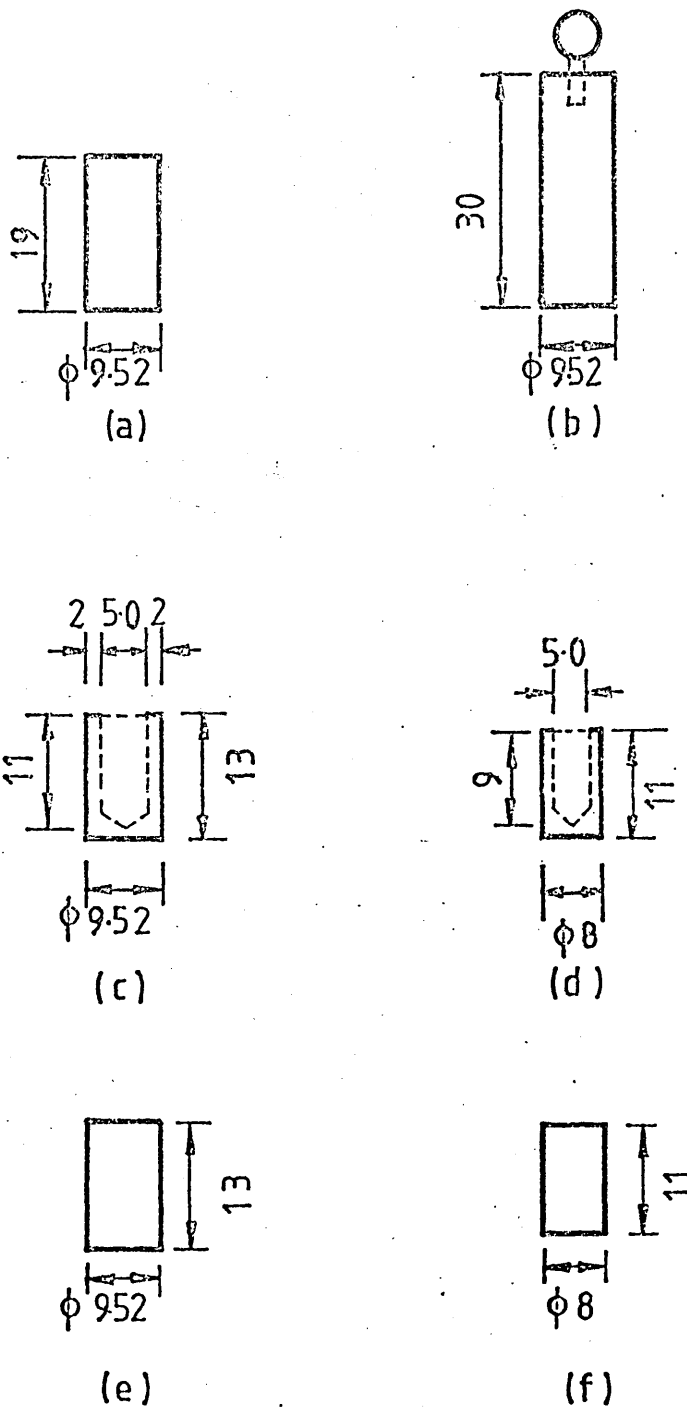
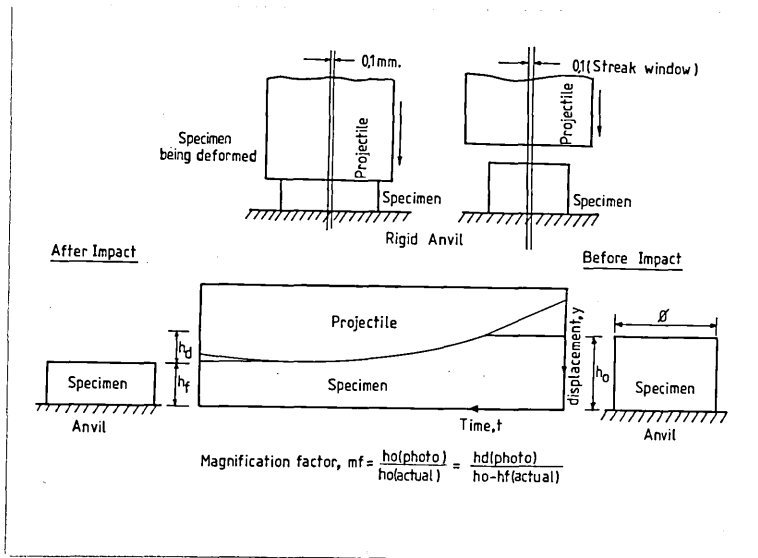
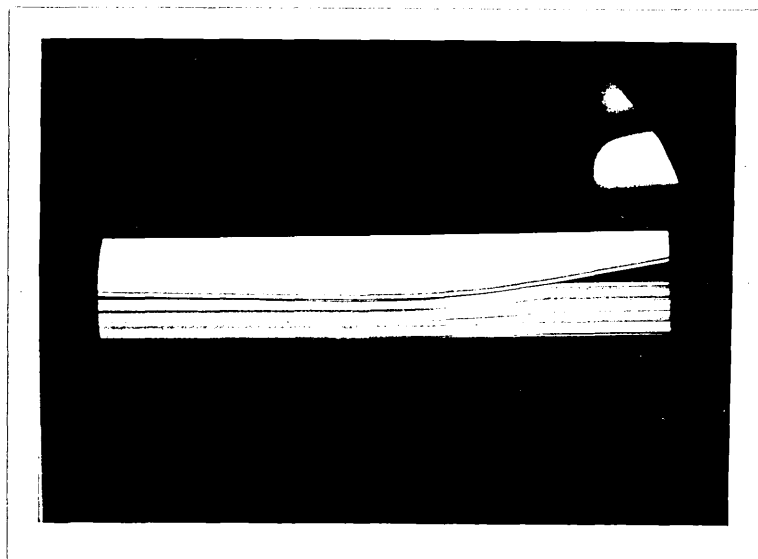


Fig.17 Line diagrams of projectiles of different masses (dimensions are in mm), (a) 10.20 gms, (b) 16.40 gms, (c) 5.20 gms, (d) 3 gms, (e) 8 gms and (f) 4.60 gms.



(a)



(b)

Fig.18 Showing the principle of streak photography  
(a) line diagram and (b) actual record.

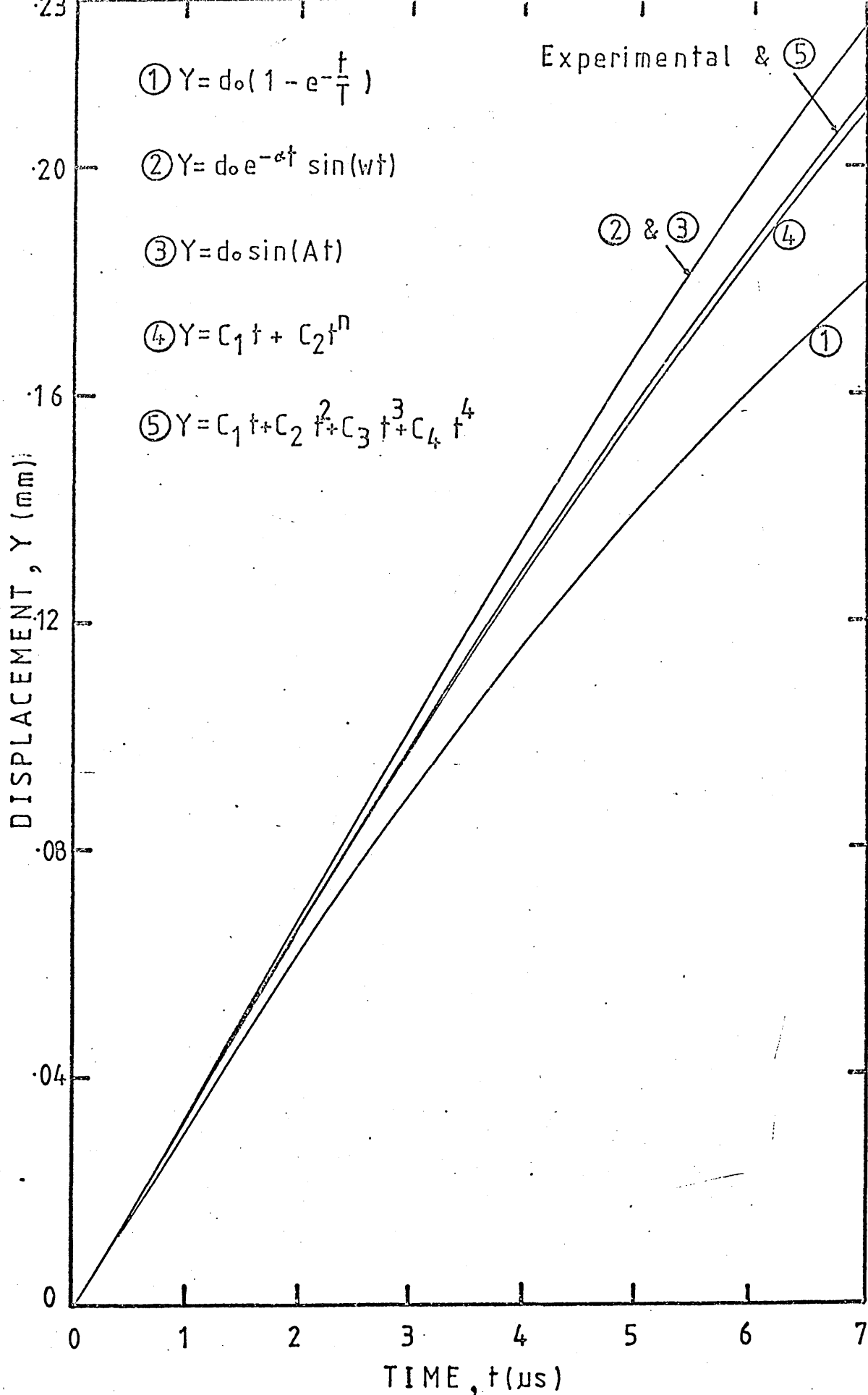


Fig.19 Showing the comparison of displacement-time data obtained by different curve fitting equations with those obtained experimentally during deformation.

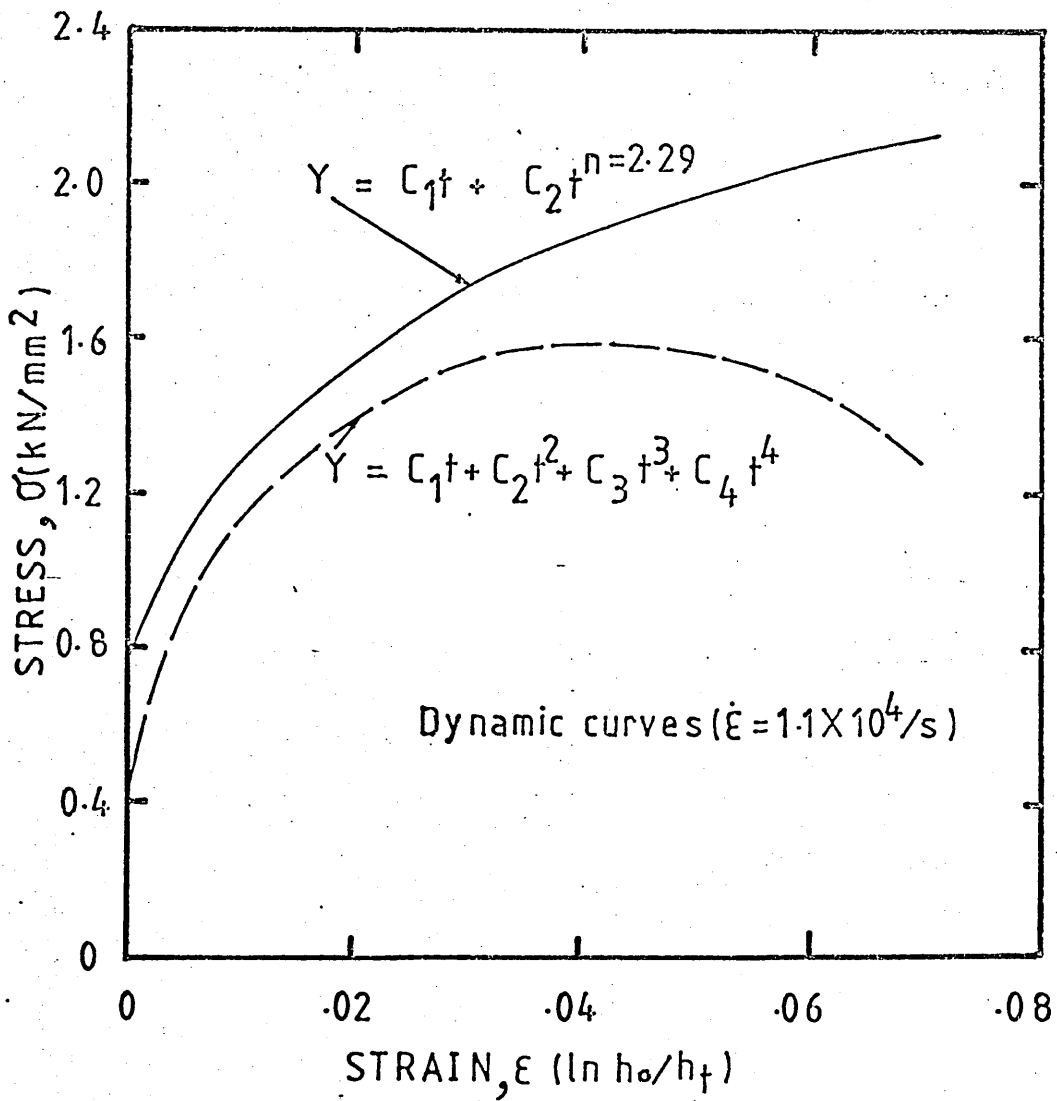


Fig.20 Showing comparison of stress-strain curves obtained by two equations (before friction correction).

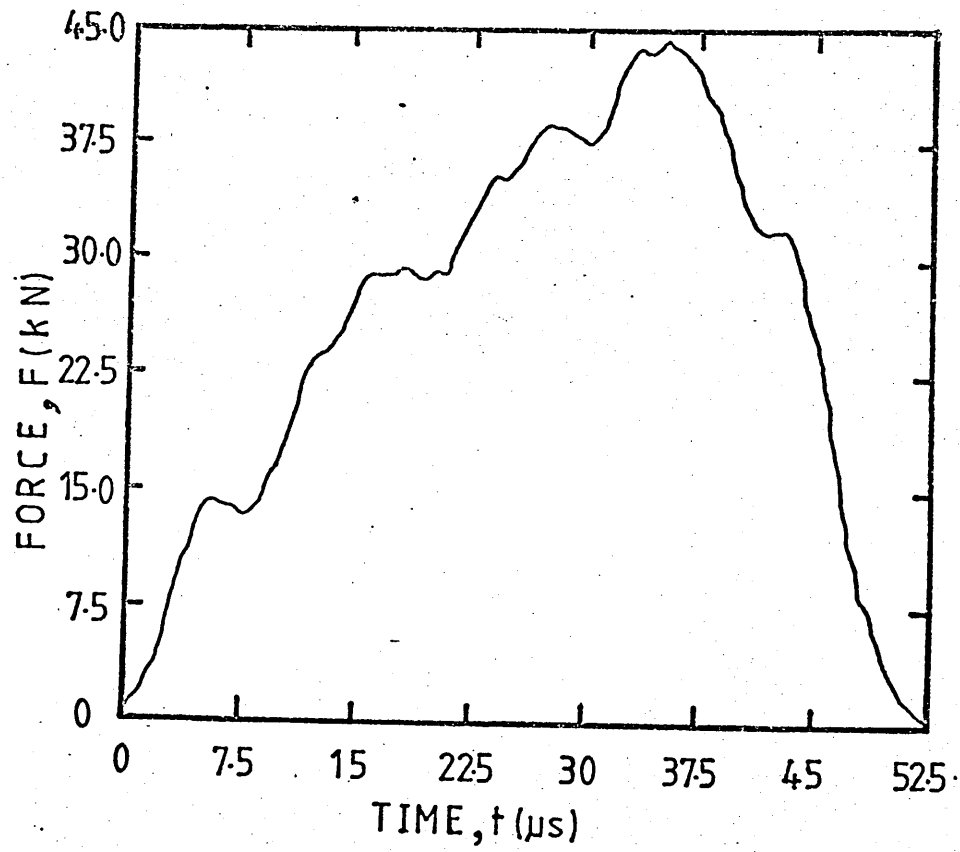
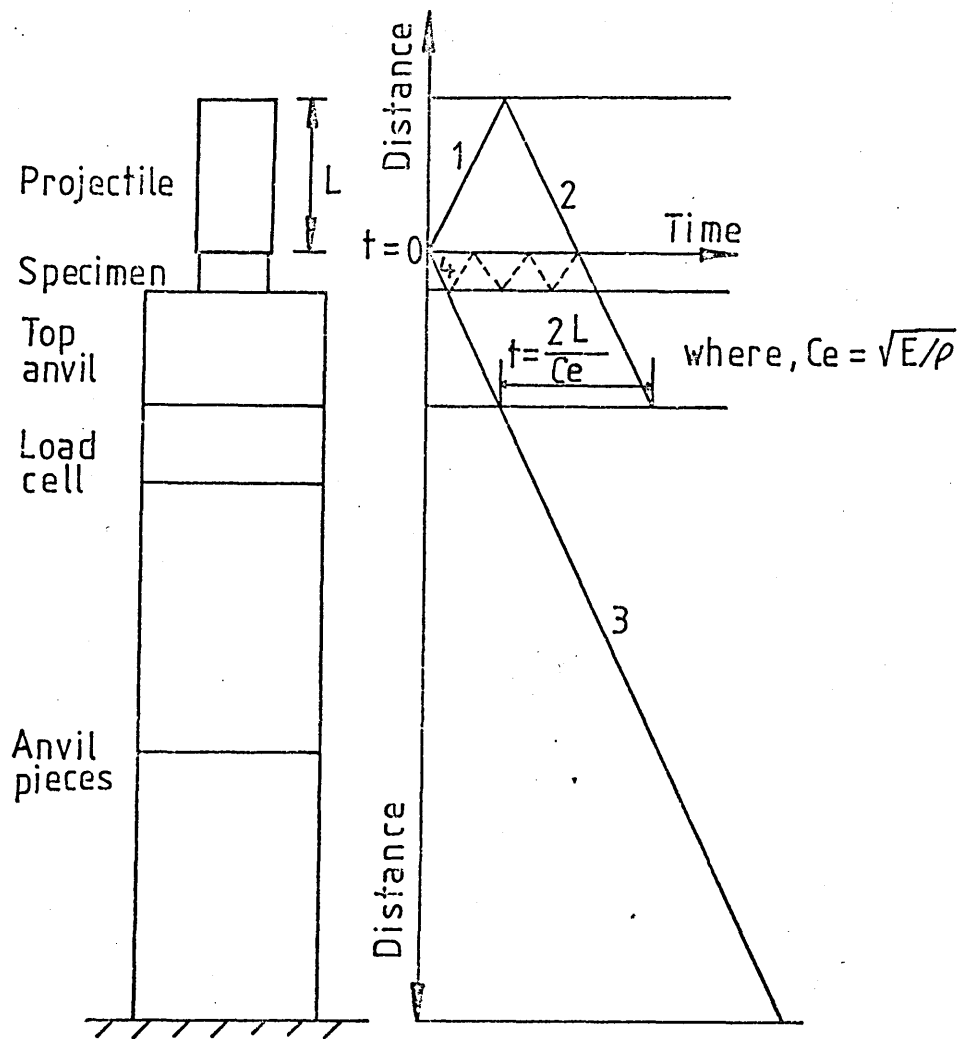


Fig.21 Showing the load-time (measured) with composite pressure bar arrangement.



- 1- Compressive wave through projectile.
- 2- Reflected tensile unloading wave through projectile, specimen and top anvil.
- 3- Incident compressive wave through specimen, top anvil, load cell and anvil pieces.
- 4- Minor reflected waves through specimen.

Fig.22 Showing a typical stress wave space-time diagram.

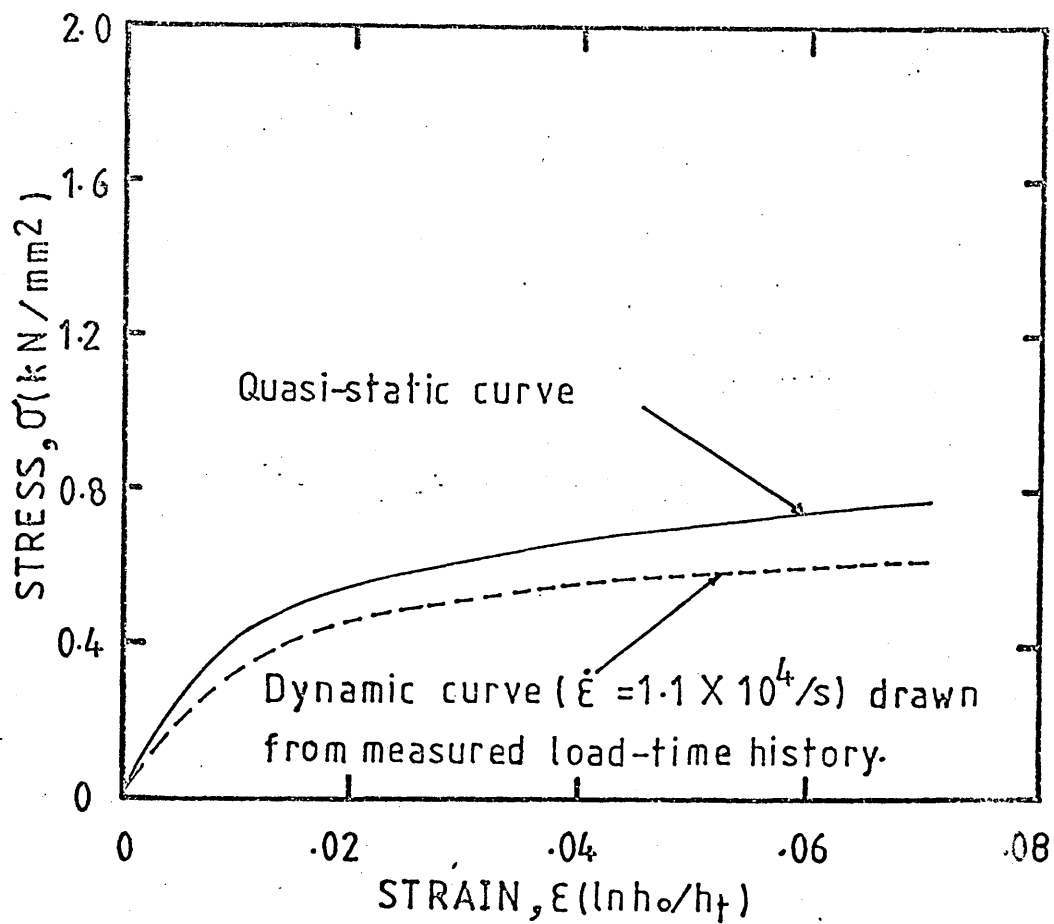


Fig.23 Showing the comparison of stress-strain curves using measured load-time history during impact test with those obtained quasi-statically. (before friction correction).

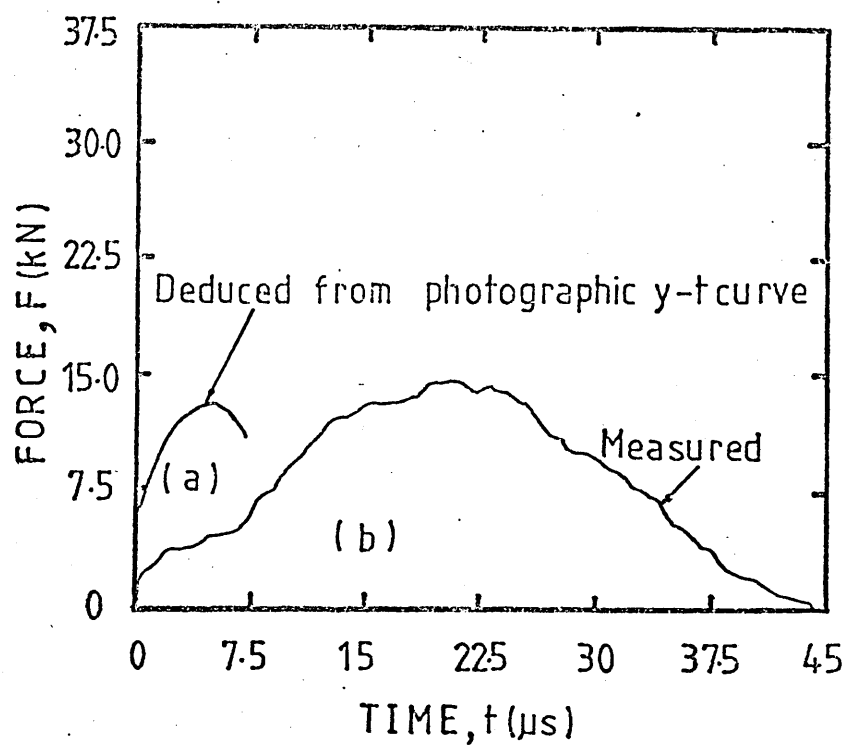


Fig.24 Showing comparison of load-time histories derived from (a) photographic record and (b) measured using load cell with new pressure bar arrangement.

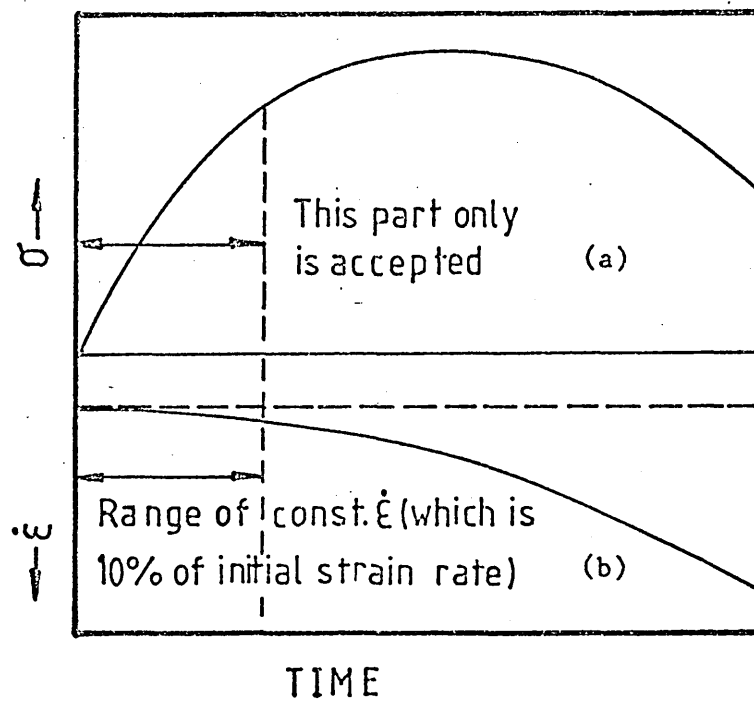


Fig.25 Showing (a) stress-time and (b) strain rate-time histories for a single test.

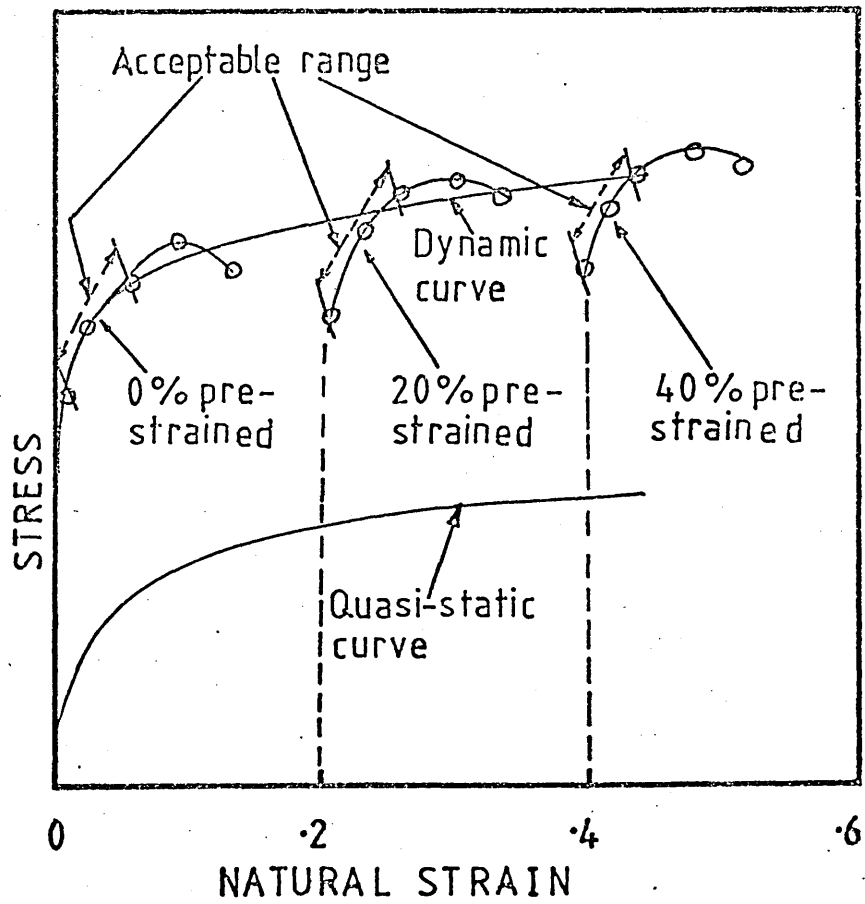


Fig.26 Illustrating construction of dynamic stress-strain curve for constant strain rate from the results of different pre-strained specimens.

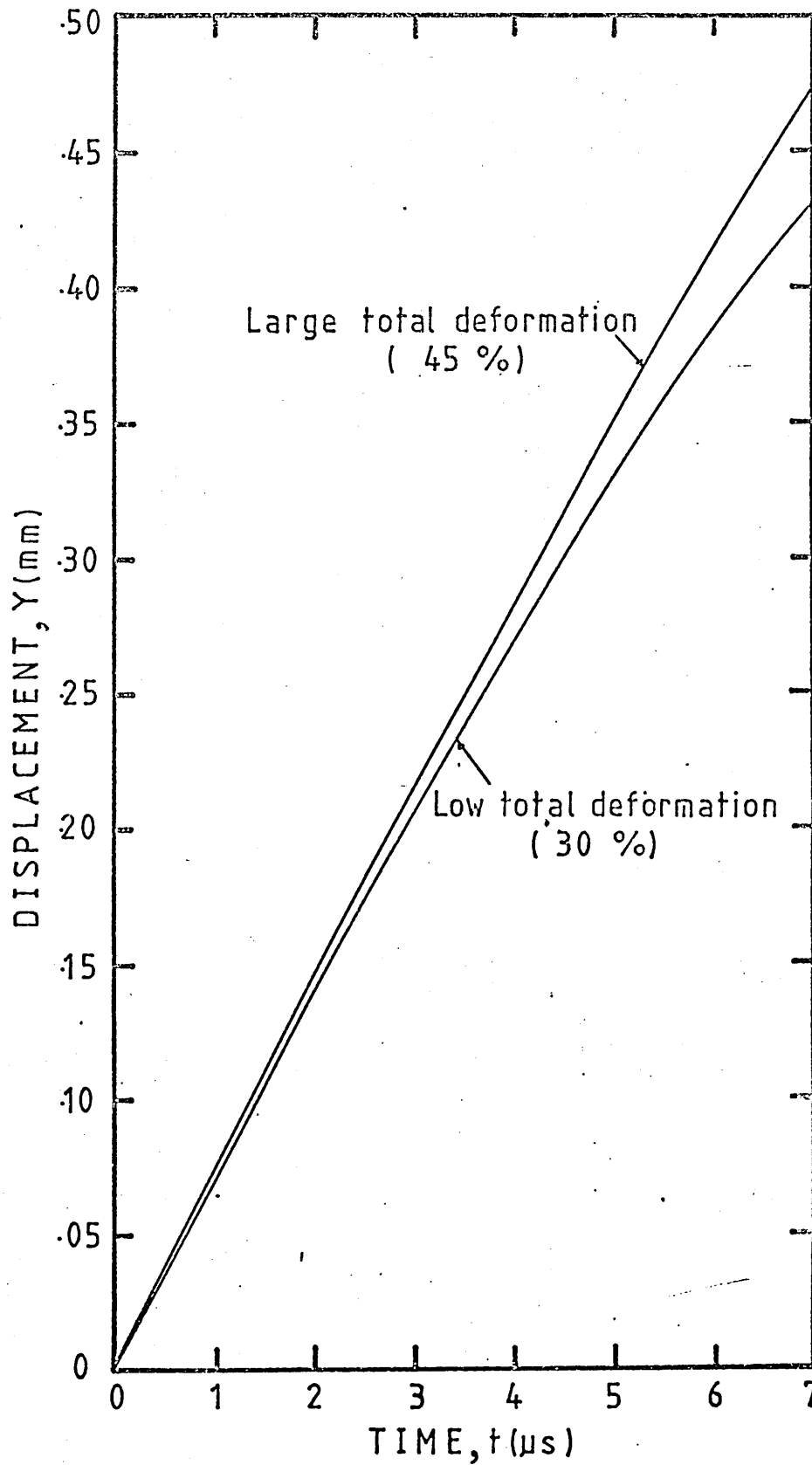


Fig.27 Showing the effect of total deformation on displacement-time curves for a single test.

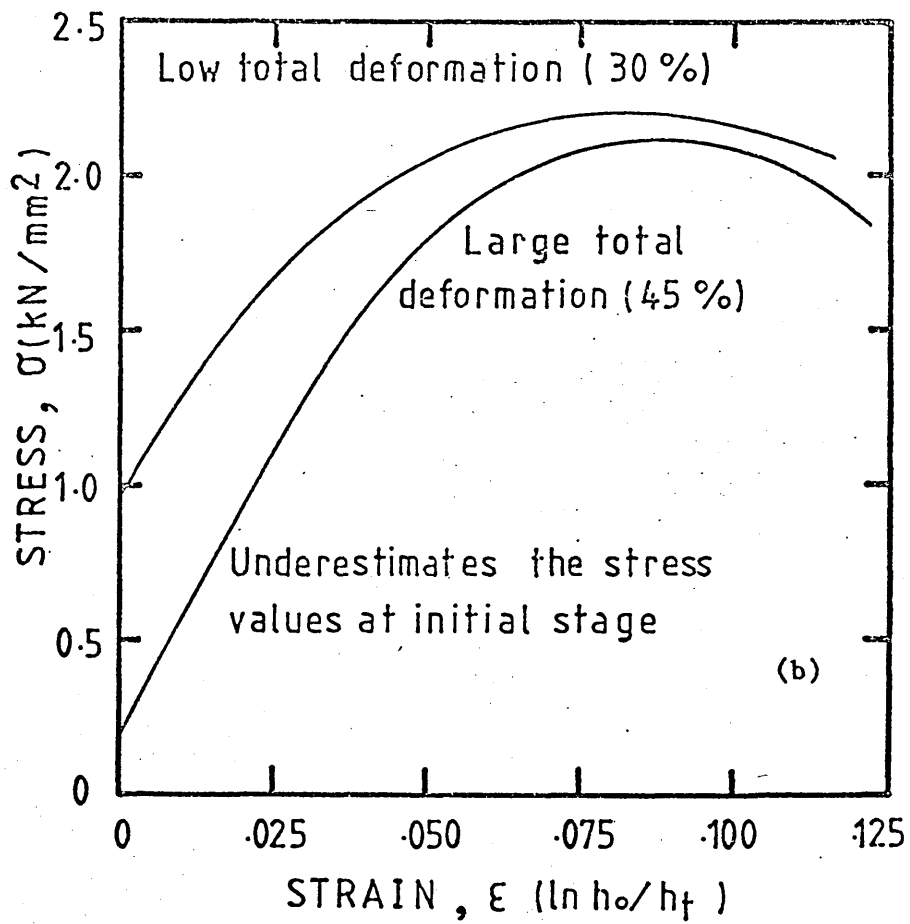
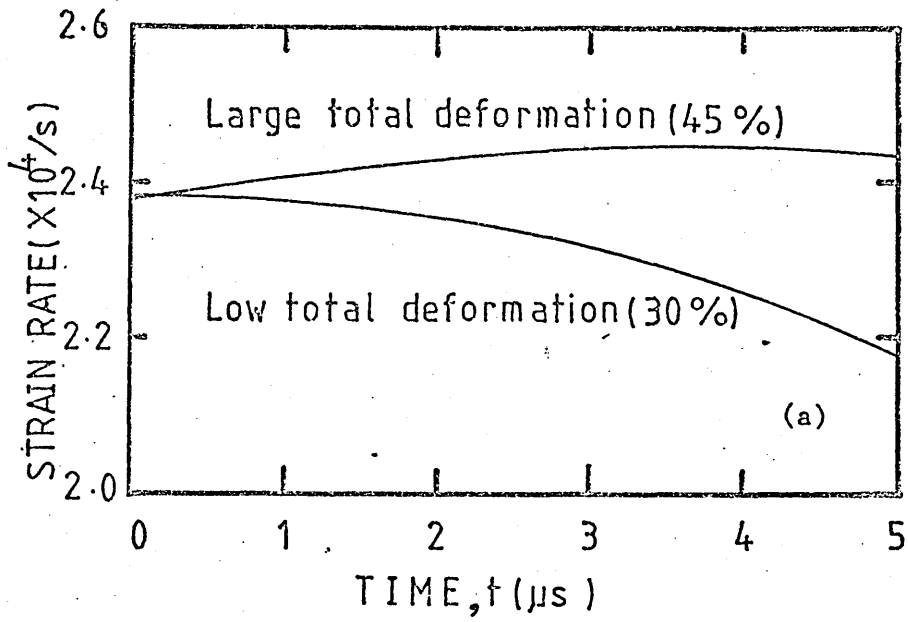


Fig.28 Showing the effect of total deformation on (a) strain rate - time and (b) stress-strain curves for a single test.

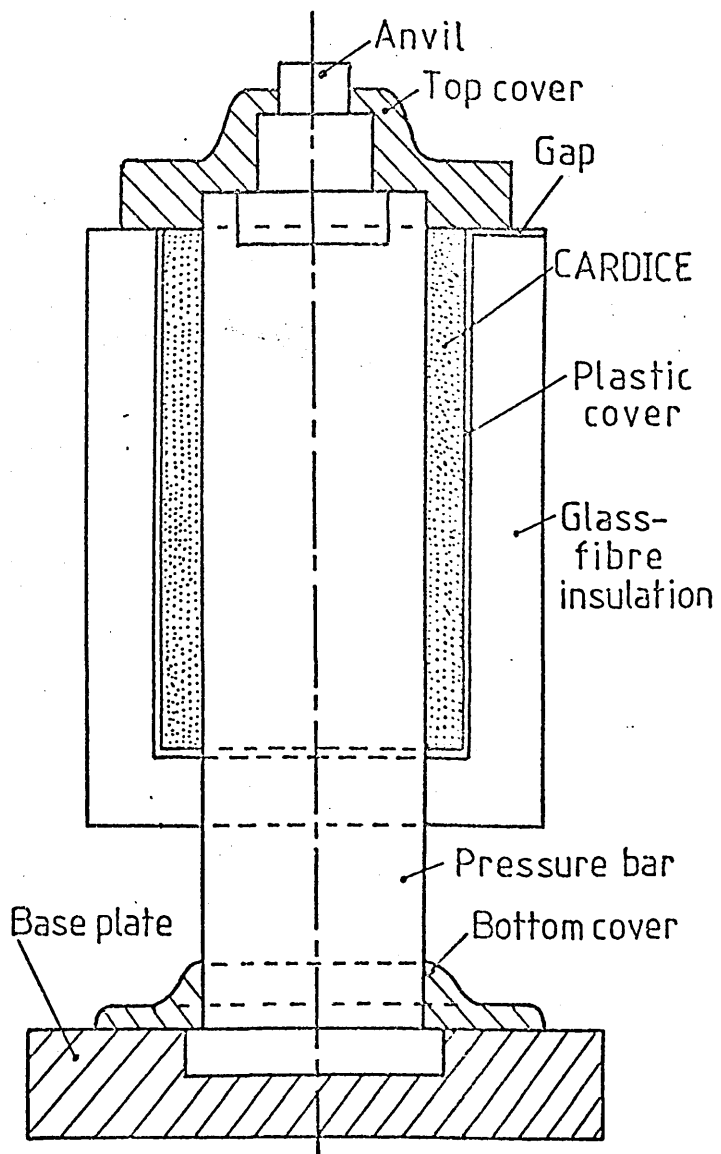


Fig.29 Showing cooling arrangement for pressure bar and top anvil.

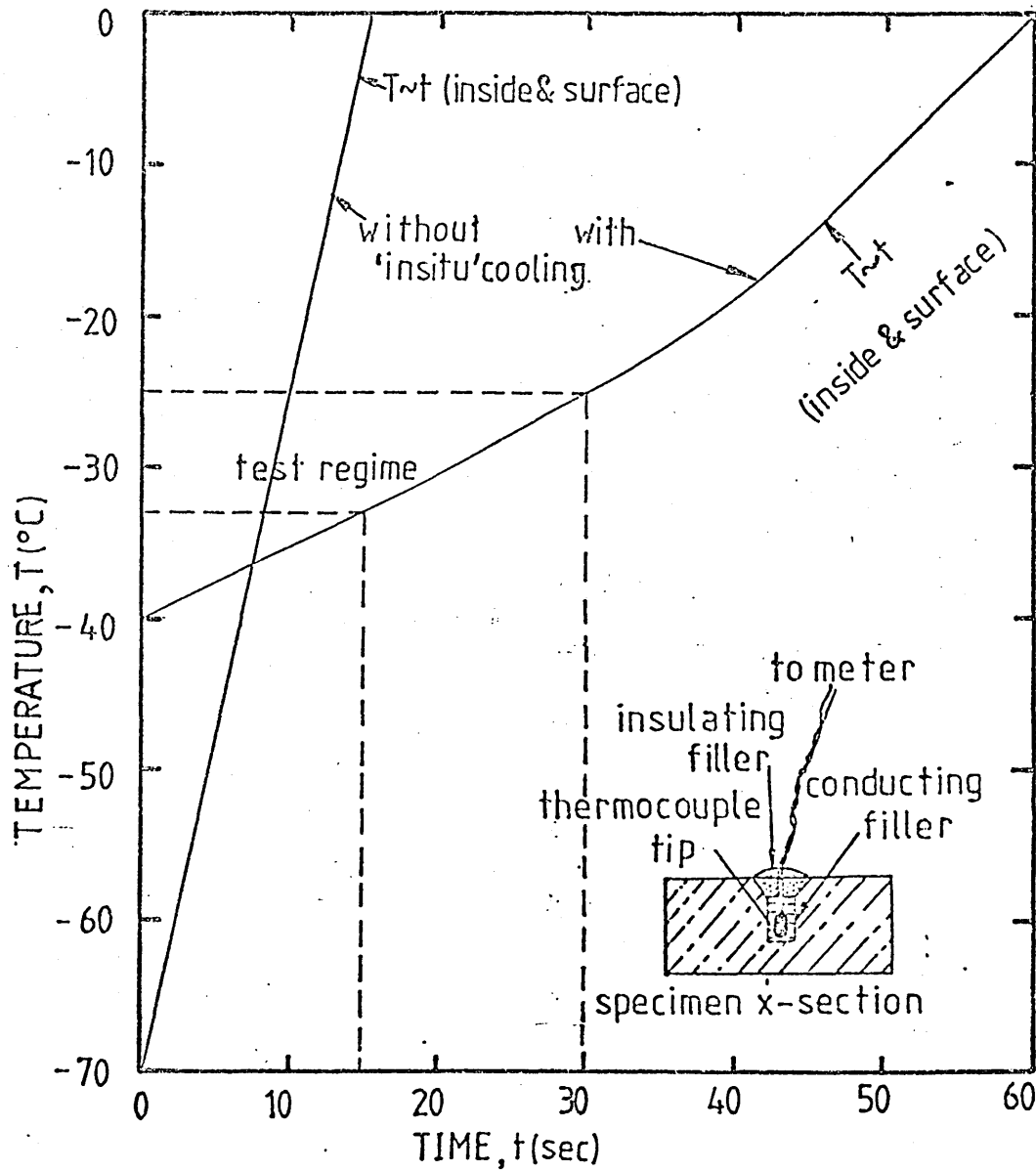


Fig.30 Showing time versus temperature rise curves during impact tests at sub-zero temperature.

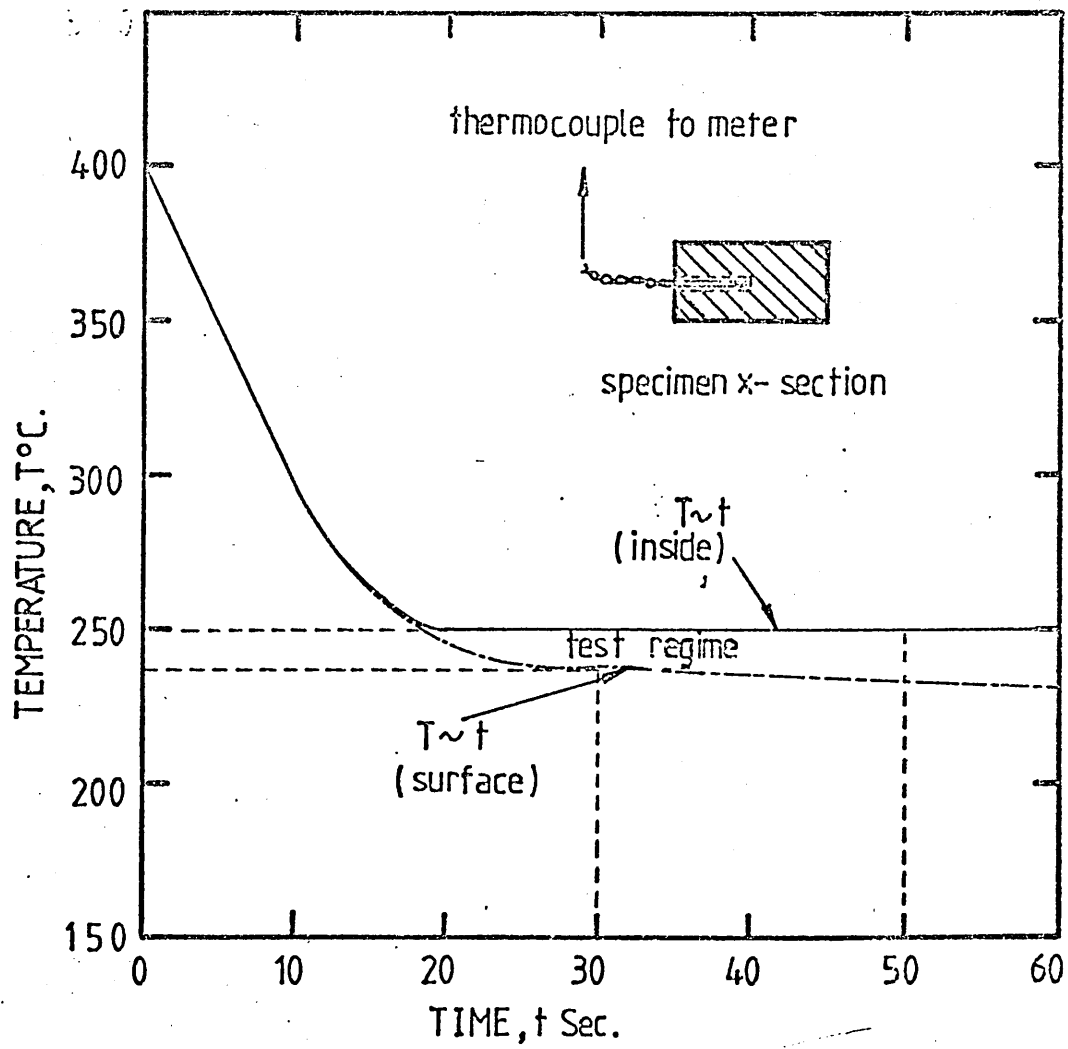


Fig.31 Showing time versus temperature fall curves during impact tests at warm temperature.

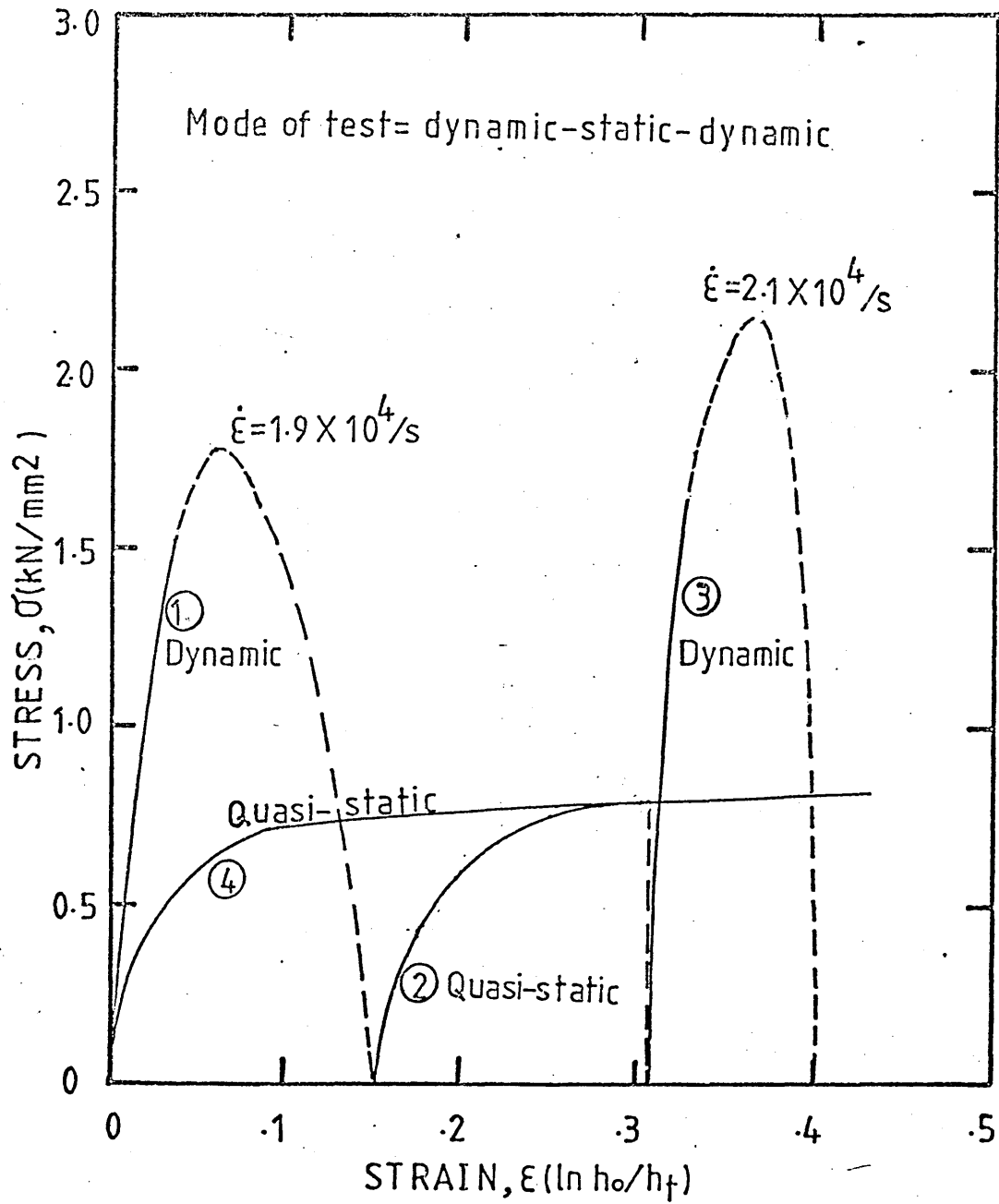


Fig. 32 Stress-strain characteristics of structural steel from D-S-D test sequence on a single specimen.

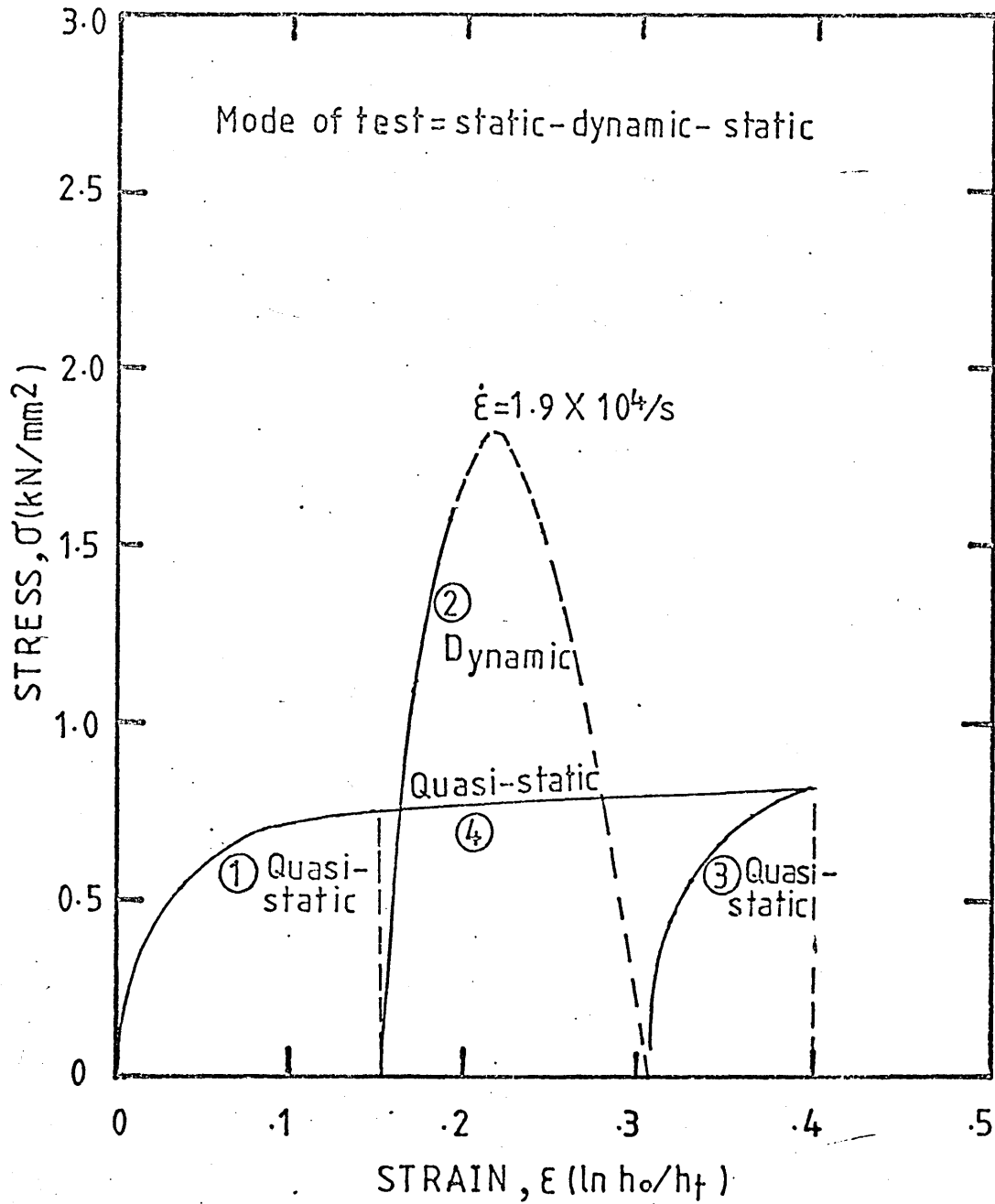
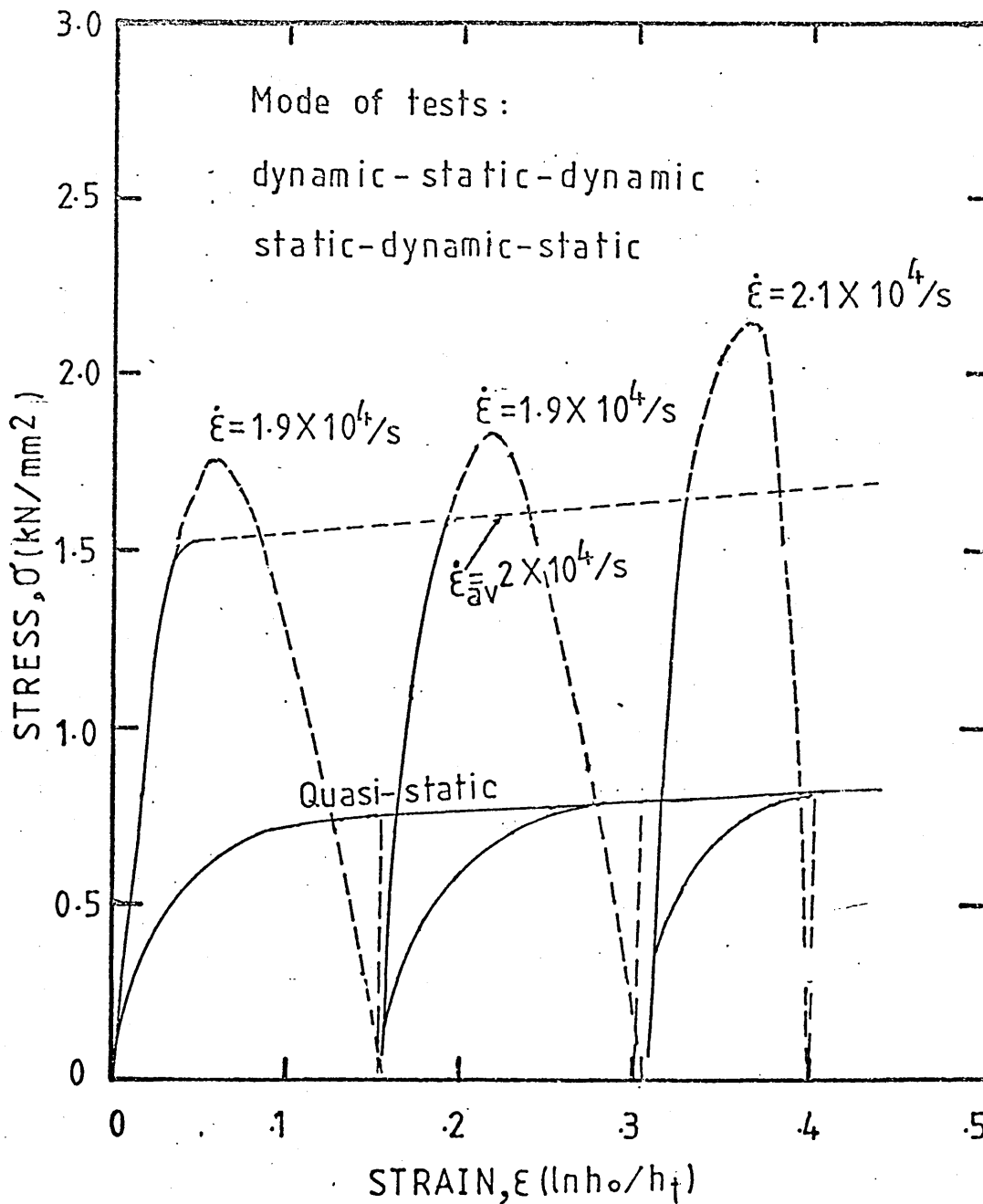


Fig.33 Stress-strain characteristics of structural steel from S-D-S test sequence on a single specimen.

Fig.34 Stress-strain characteristics of structural steel from D-S-D and S-D-S testing sequences on two dimensionally similar specimens.



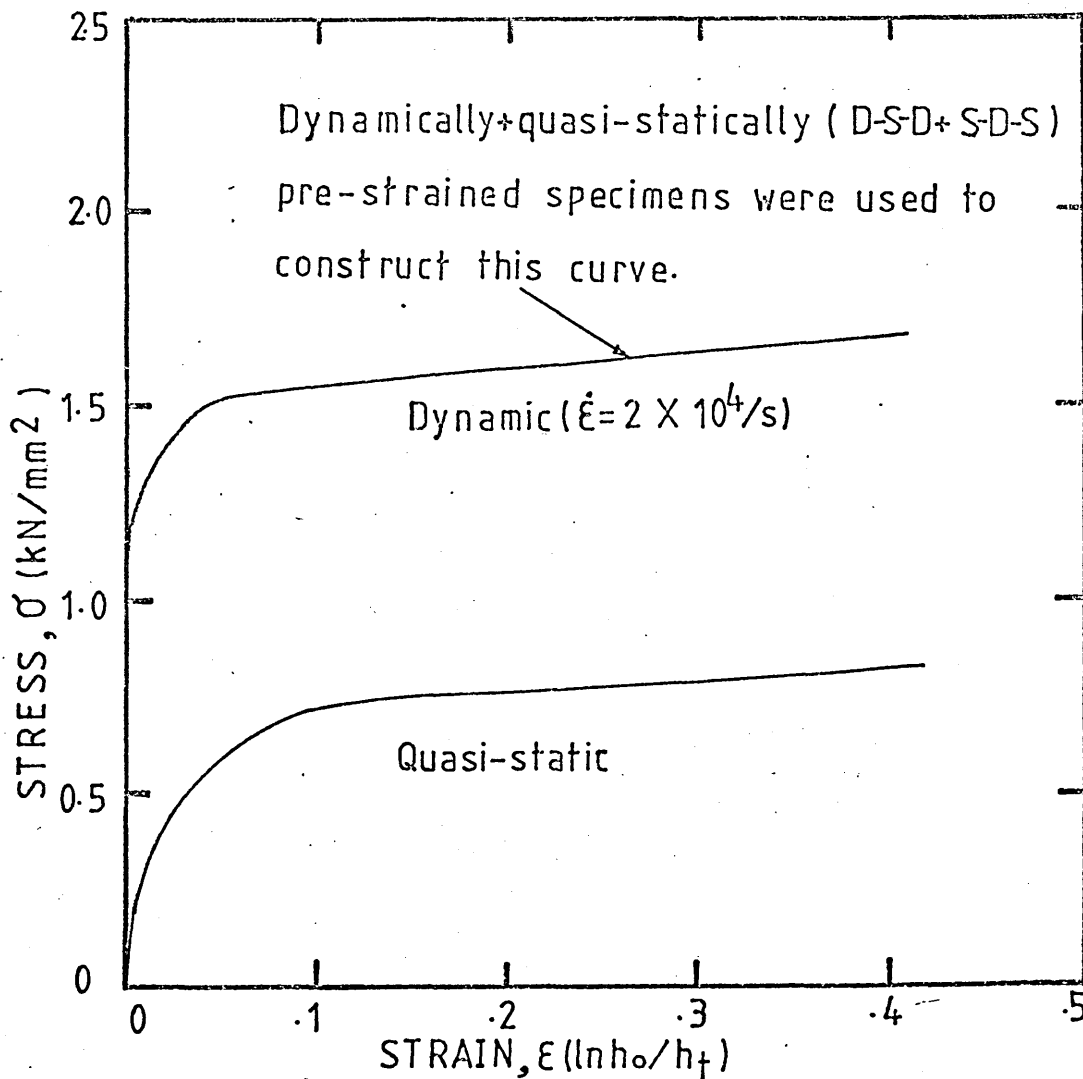


Fig.35 Showing the stress-strain characteristics of structural steel obtained from two dimensionally similar specimens deformed in D-S-D and S-D-S testing sequences.

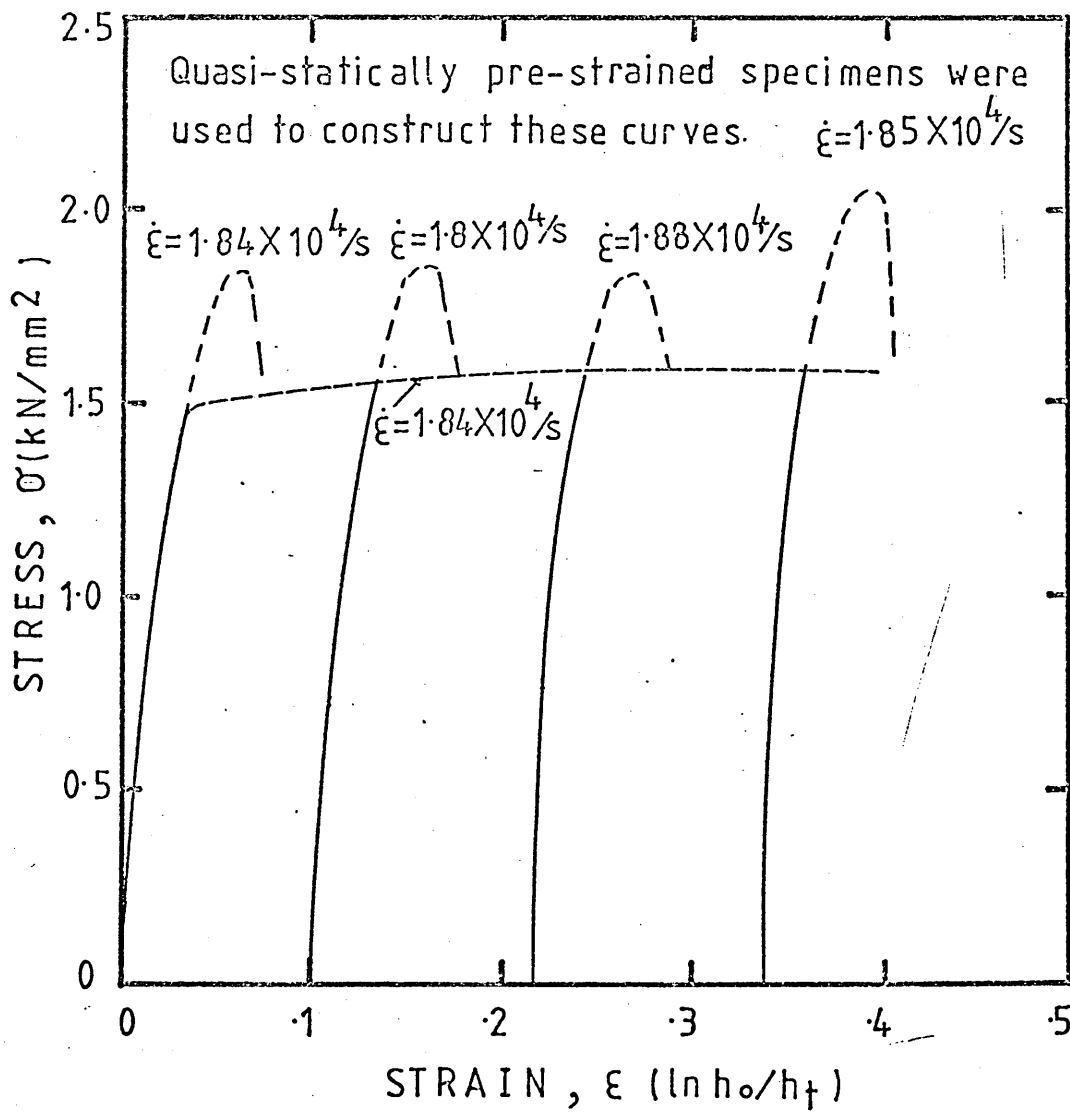


Fig.36 Construction of stress-strain curves for structural steel from quasi-statically pre-strained specimens.

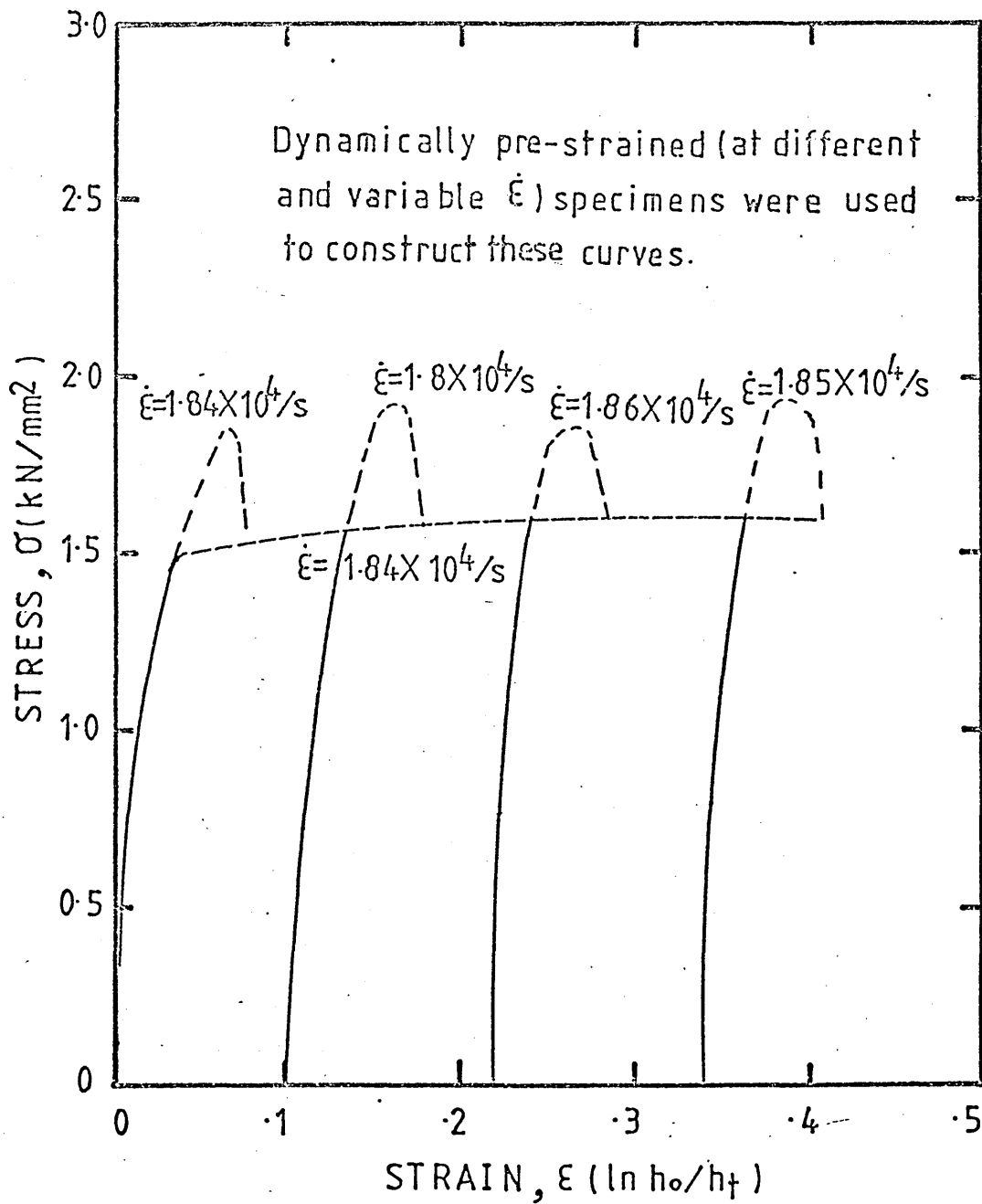


Fig.37 Construction of stress-strain curves for structural steel from dynamically pre-strained specimens.

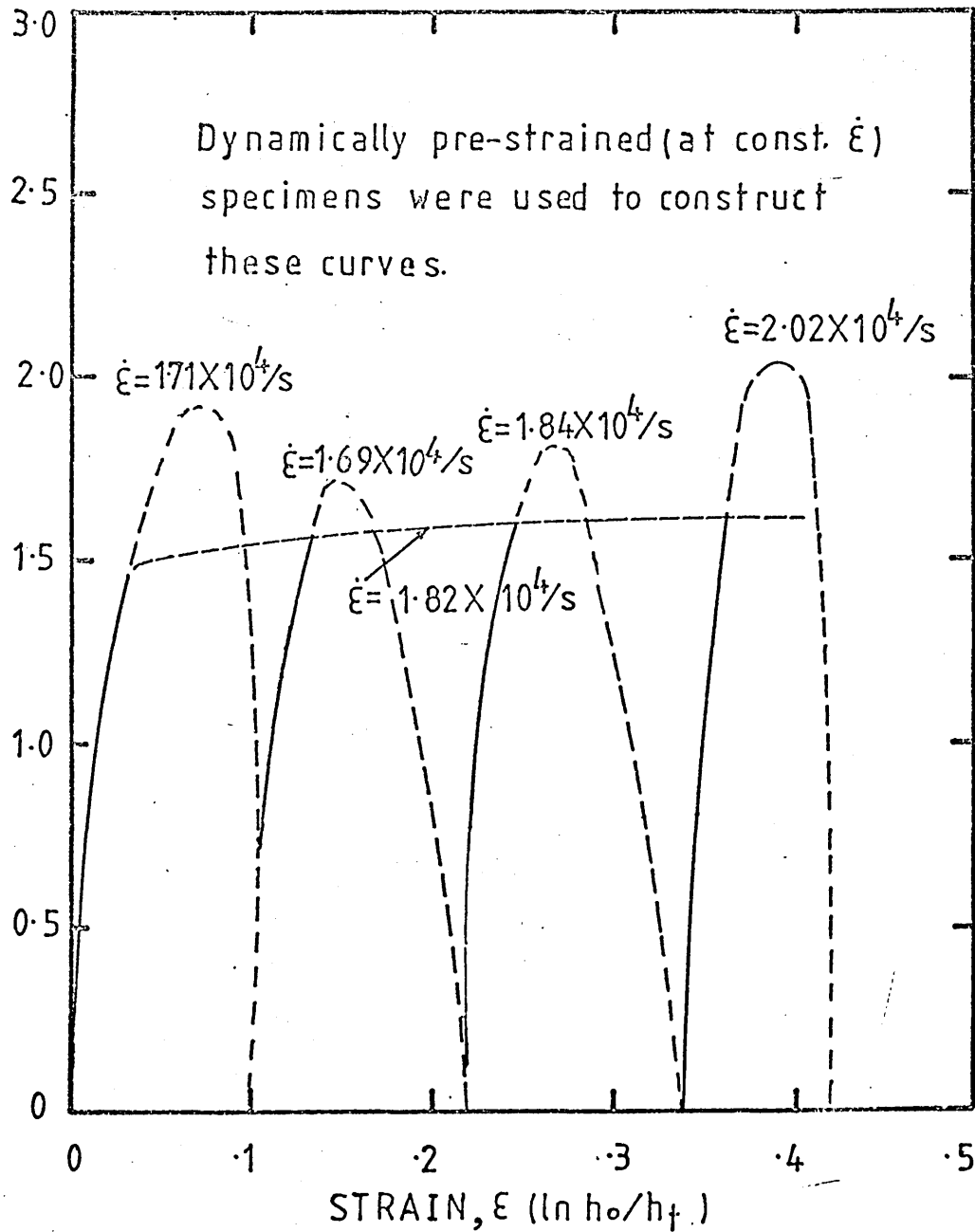


Fig.38 Construction of stress-strain curves for structural steel from dynamically pre-strained specimens deformed at constant strain rate.

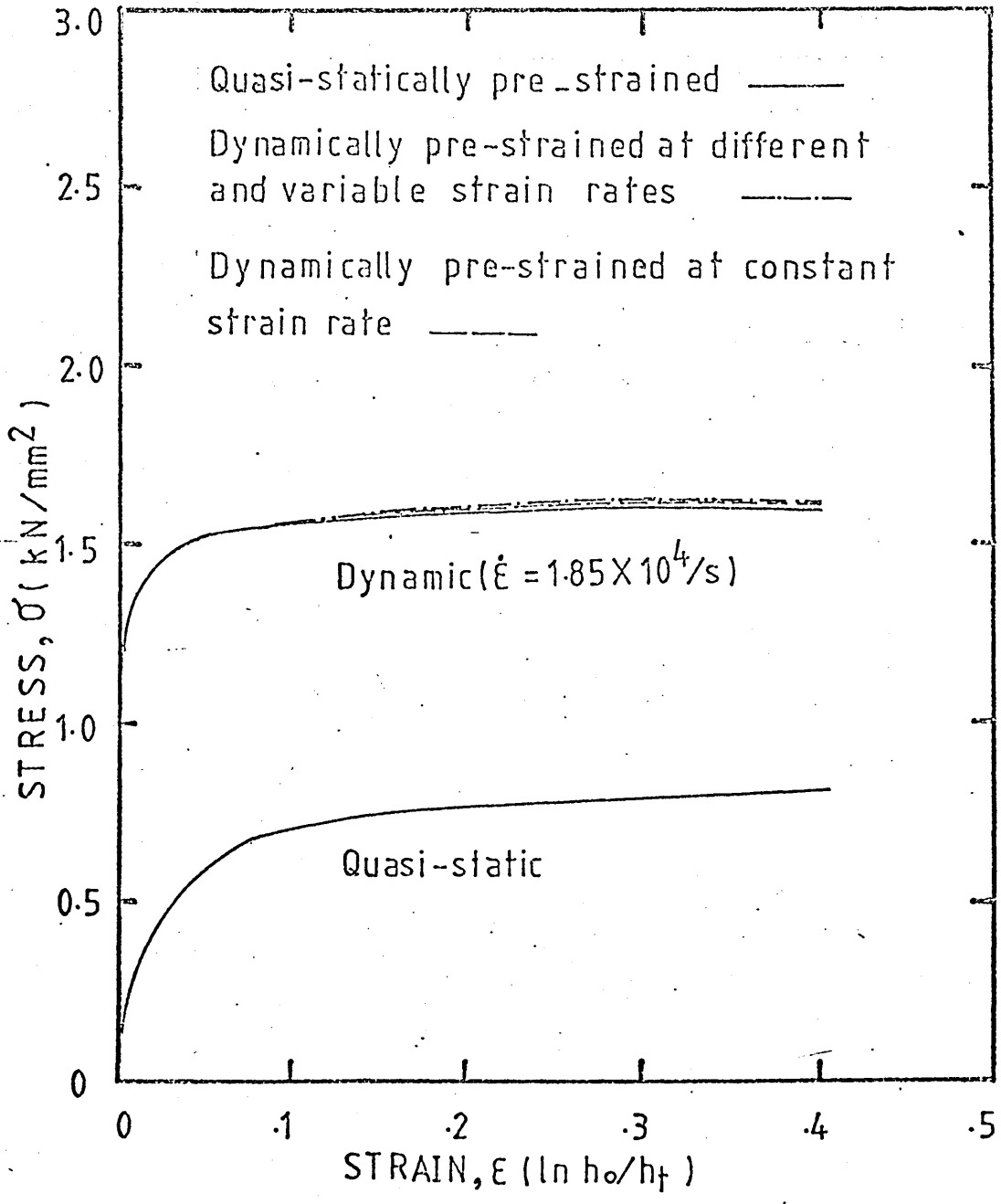


Fig. 39 Showing the effect of strain rate history on the stress-strain characteristics of structural steel.

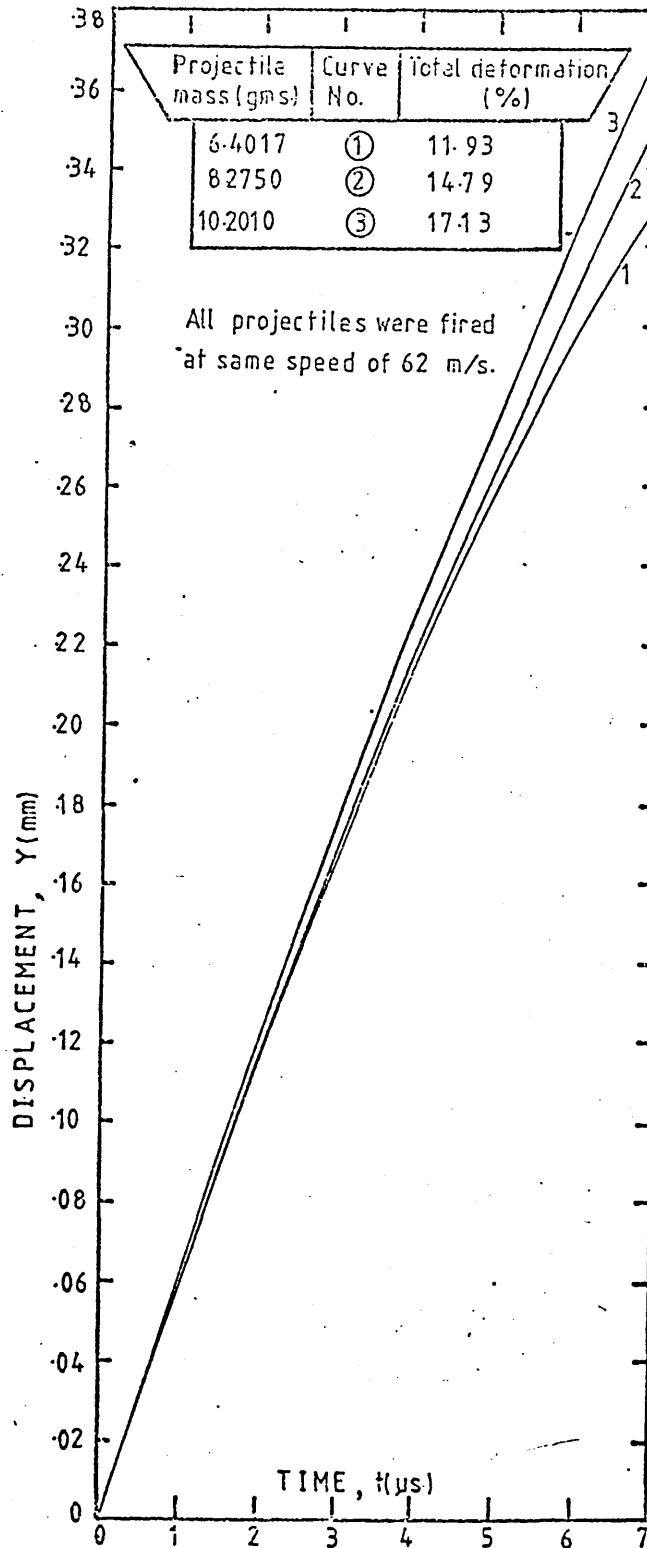


Fig.40 Showing the displacement-time curves of structural steel as affected by projectiles of different masses during deformation.

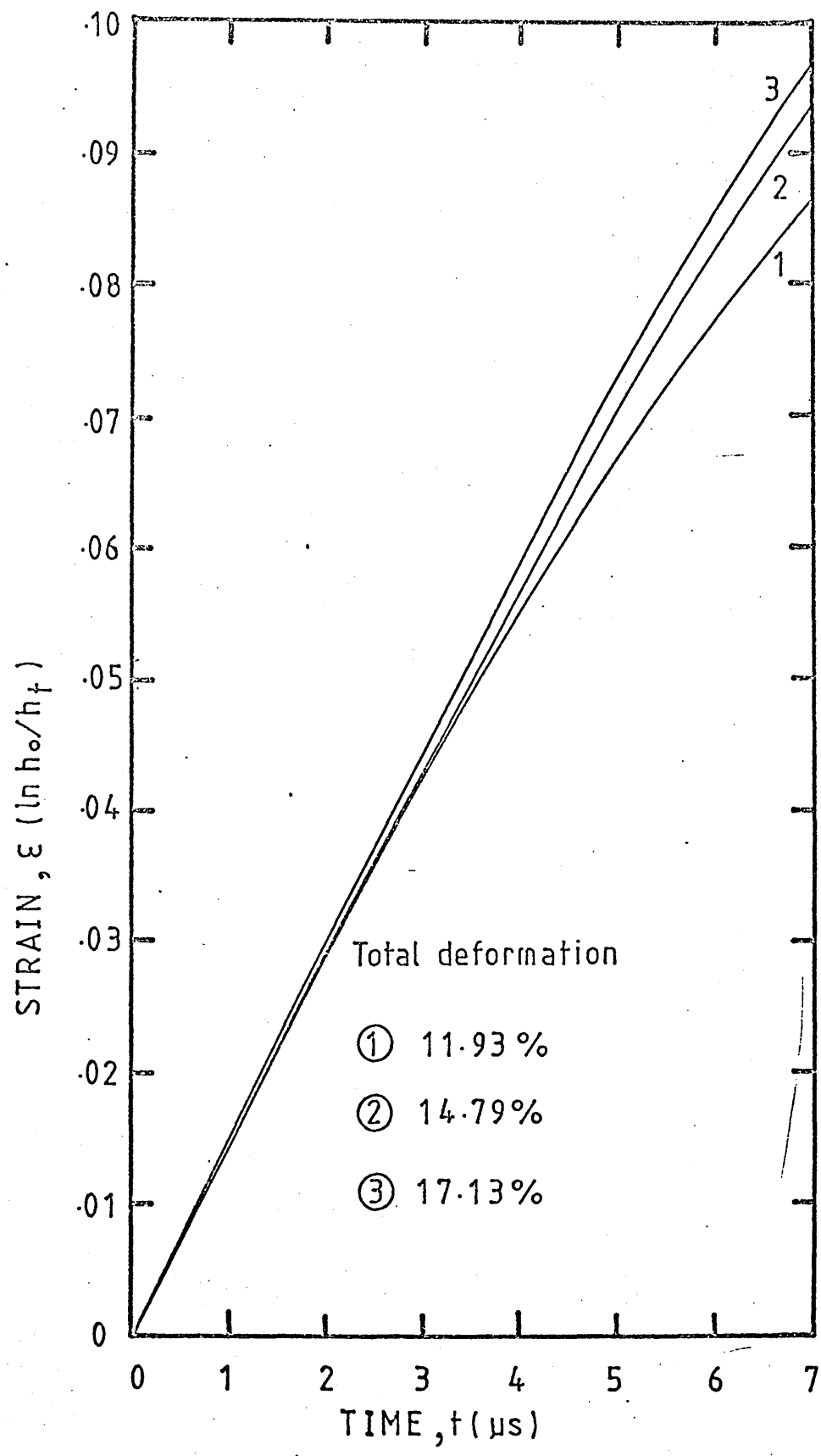


Fig.41 Showing strain-time histories due to different total deformation impact test.

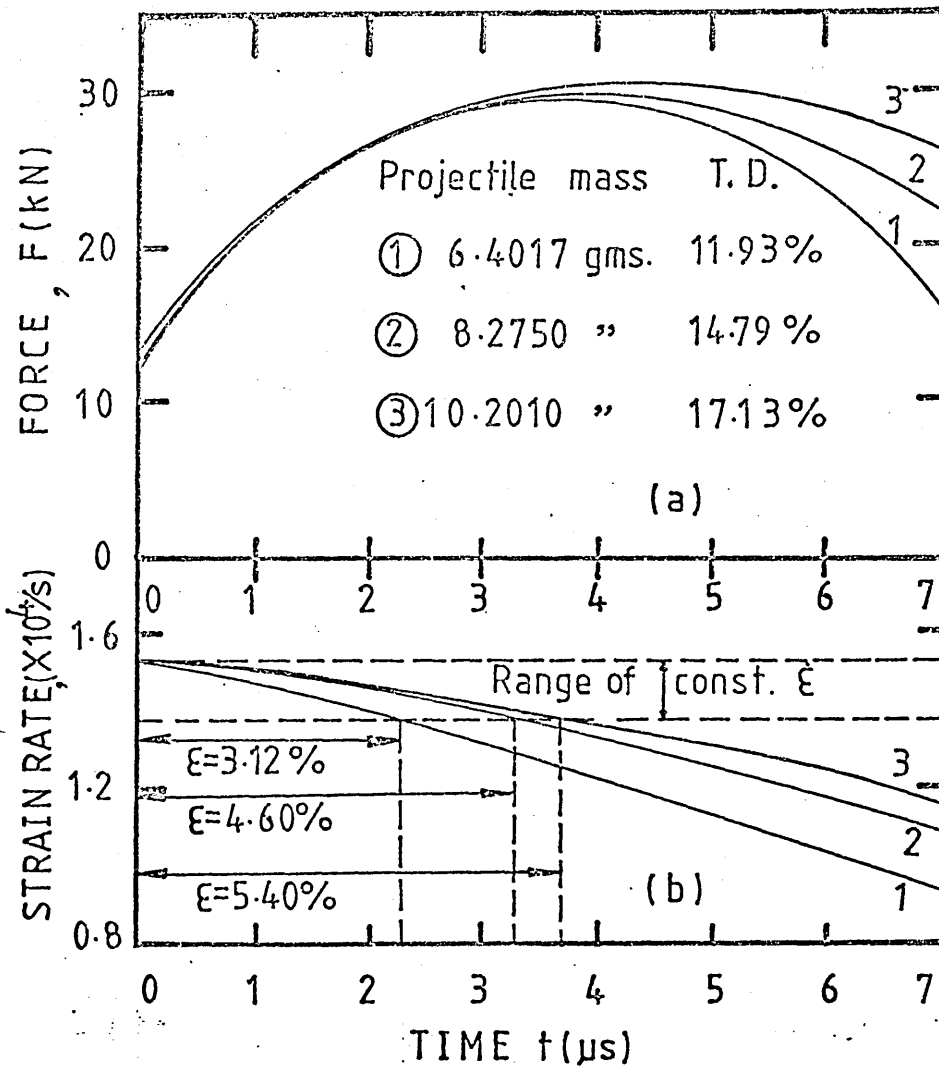


Fig.42 Showing the effect of total deformation on (a) force-time and (b) strain rate-time histories during impact test.

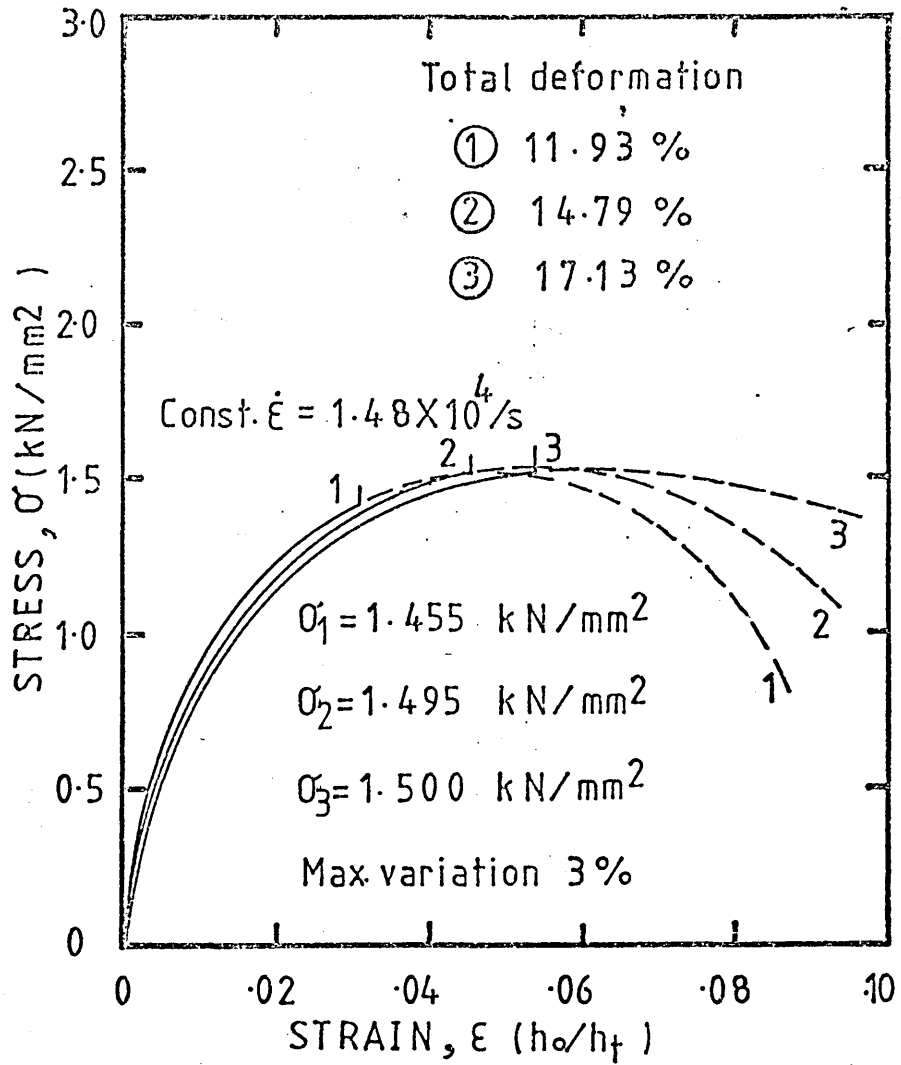
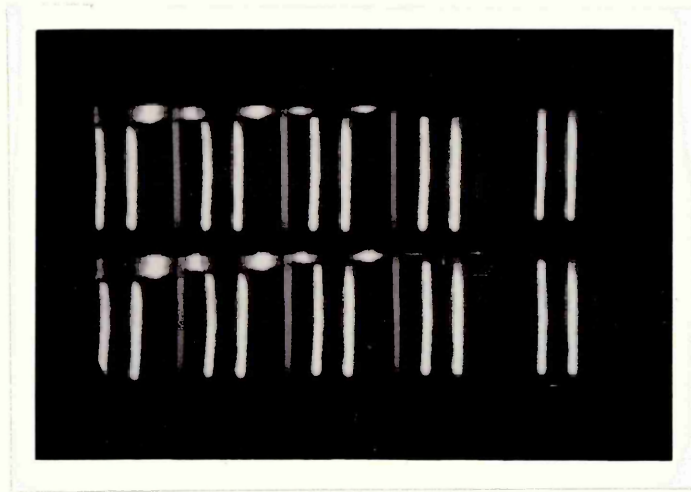
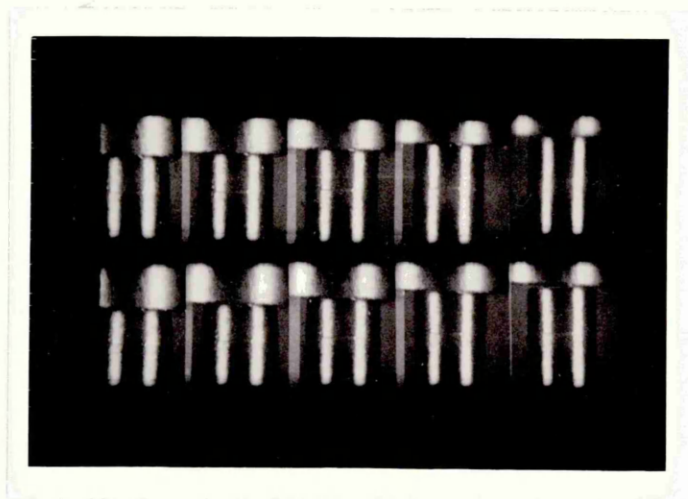


Fig.43 Showing the effect of total deformation on the stress-strain characteristics of structural steel.

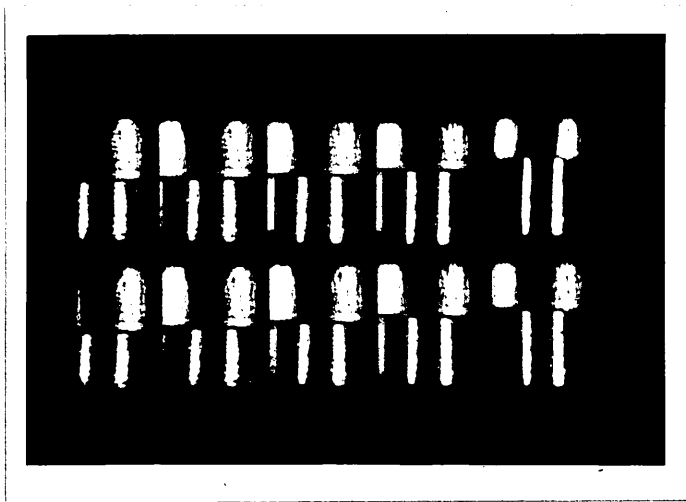


(a)

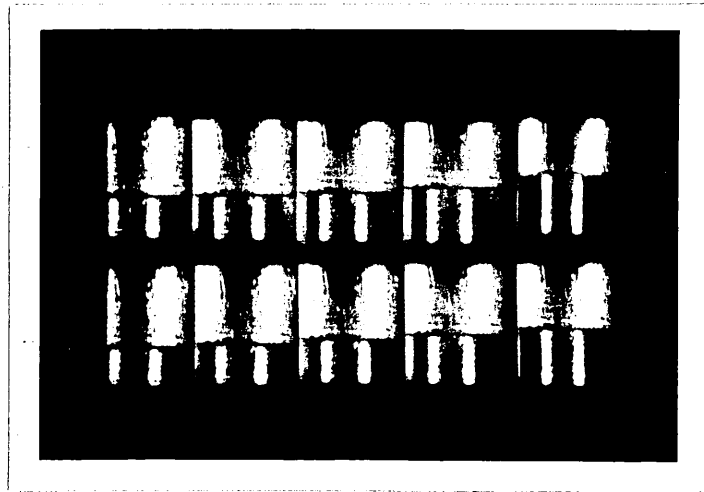


(b)

Fig.44 Showing the sequence of events with time during deformation,  $2 \mu\text{s}/\text{frame}$ , projectile speed = 100 m/s, specimen dimensions: (a) diameter = 4.00 mm, height = 6.00 mm ie aspect ratio 1.50 and (b) diameter = 4.00 mm, height = 5.00 ie aspect ratio 1.25.



(a)



(b)

Fig.45 Showing the sequence of events with time during deformation,  $2 \mu\text{s}/\text{frame}$ , projectile speed = 100 m/s, specimen dimensions: (a) diameter = 4.00 mm, height = 4.00 mm ie aspect ratio 1.00 and (b) diameter = 4.00 mm, height = 3.00 mm ie aspect ratio 0.75.

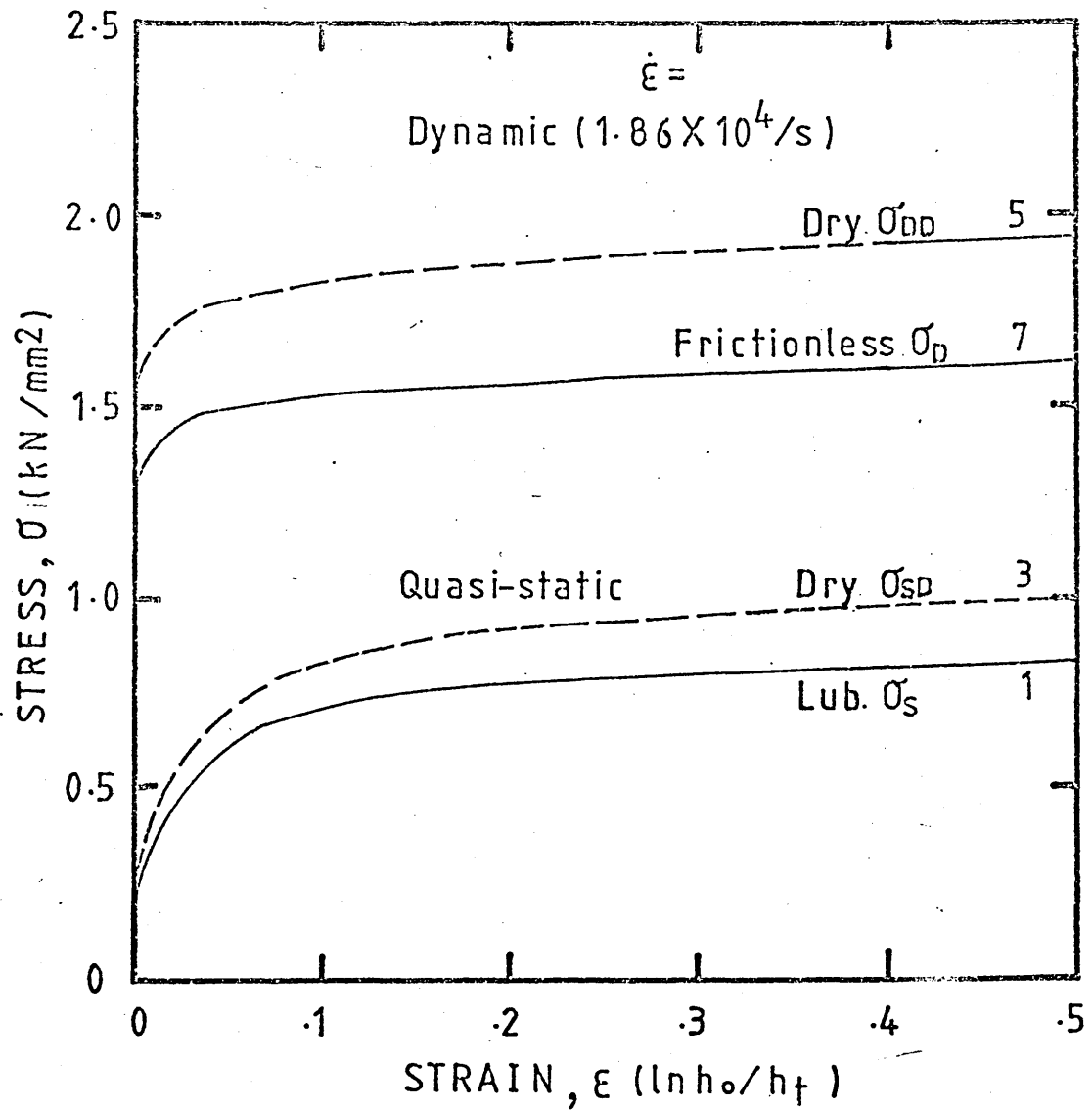


Fig.46 Stress-strain characteristics of structural steel under dry and frictionless condition for the specimen deformed at room temperature.

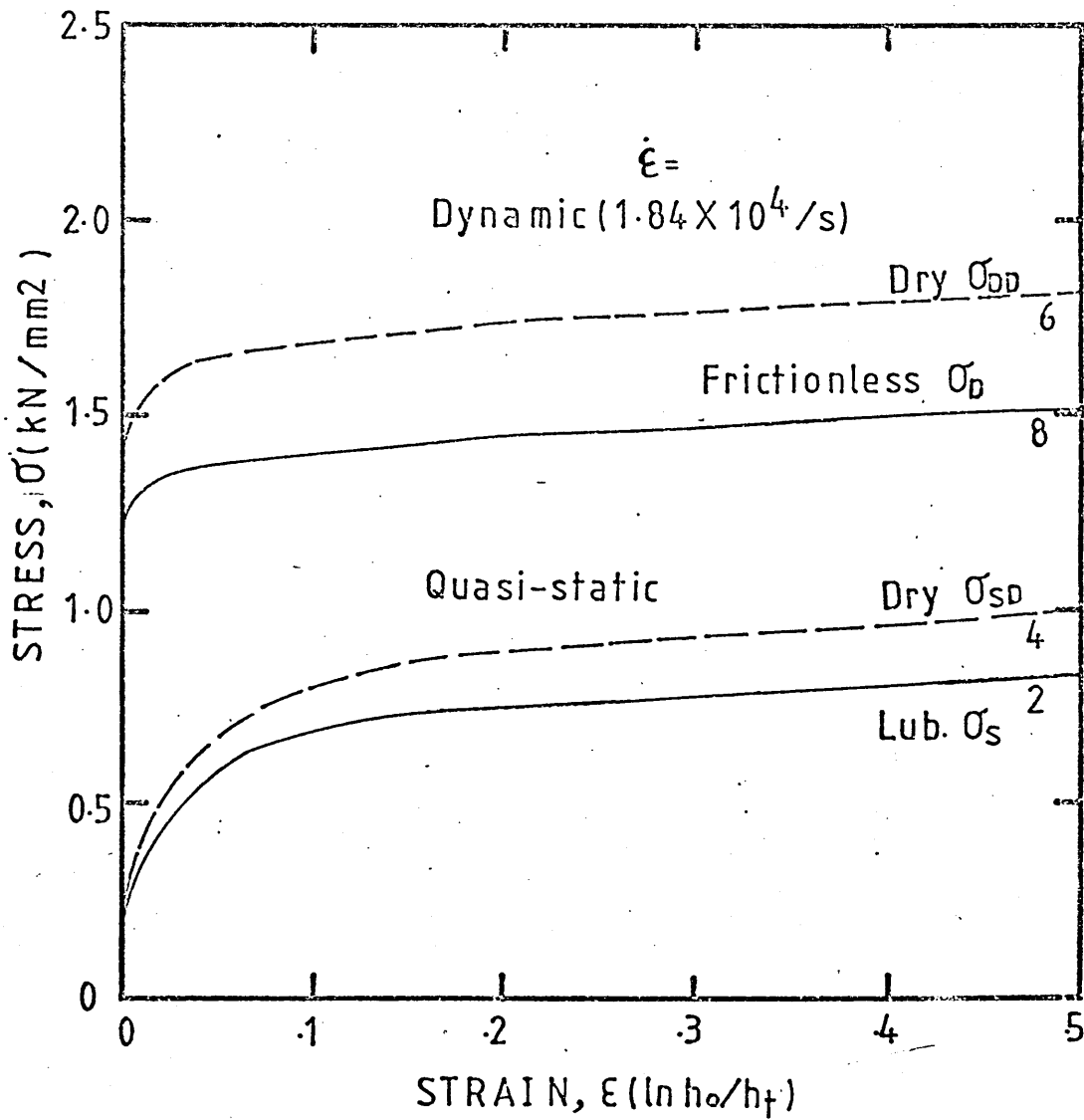


Fig.47 Stress-strain characteristics of structural steel under dry and frictionless condition for the specimen deformed at 235°C.

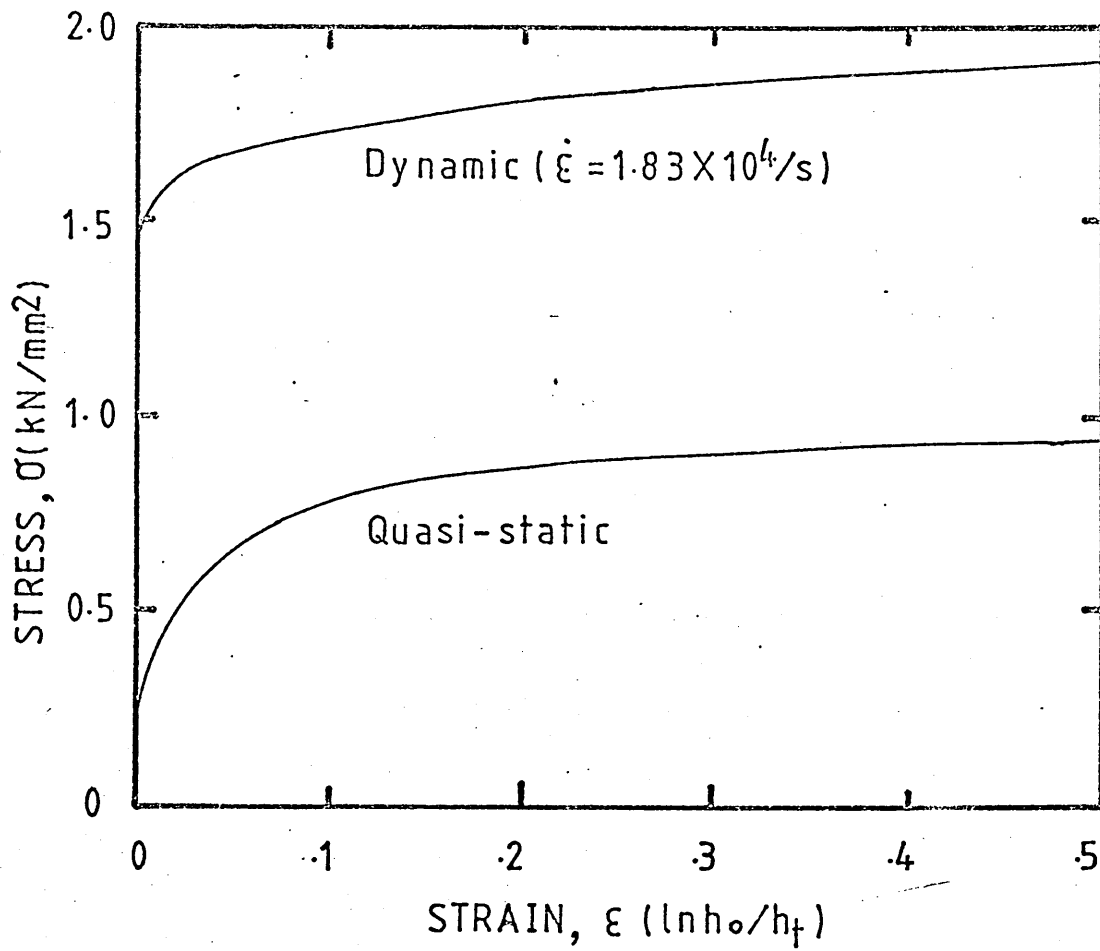


Fig.48 Showing the stress-strain characteristics of structural steel deformed at  $-30^{\circ} C$ .

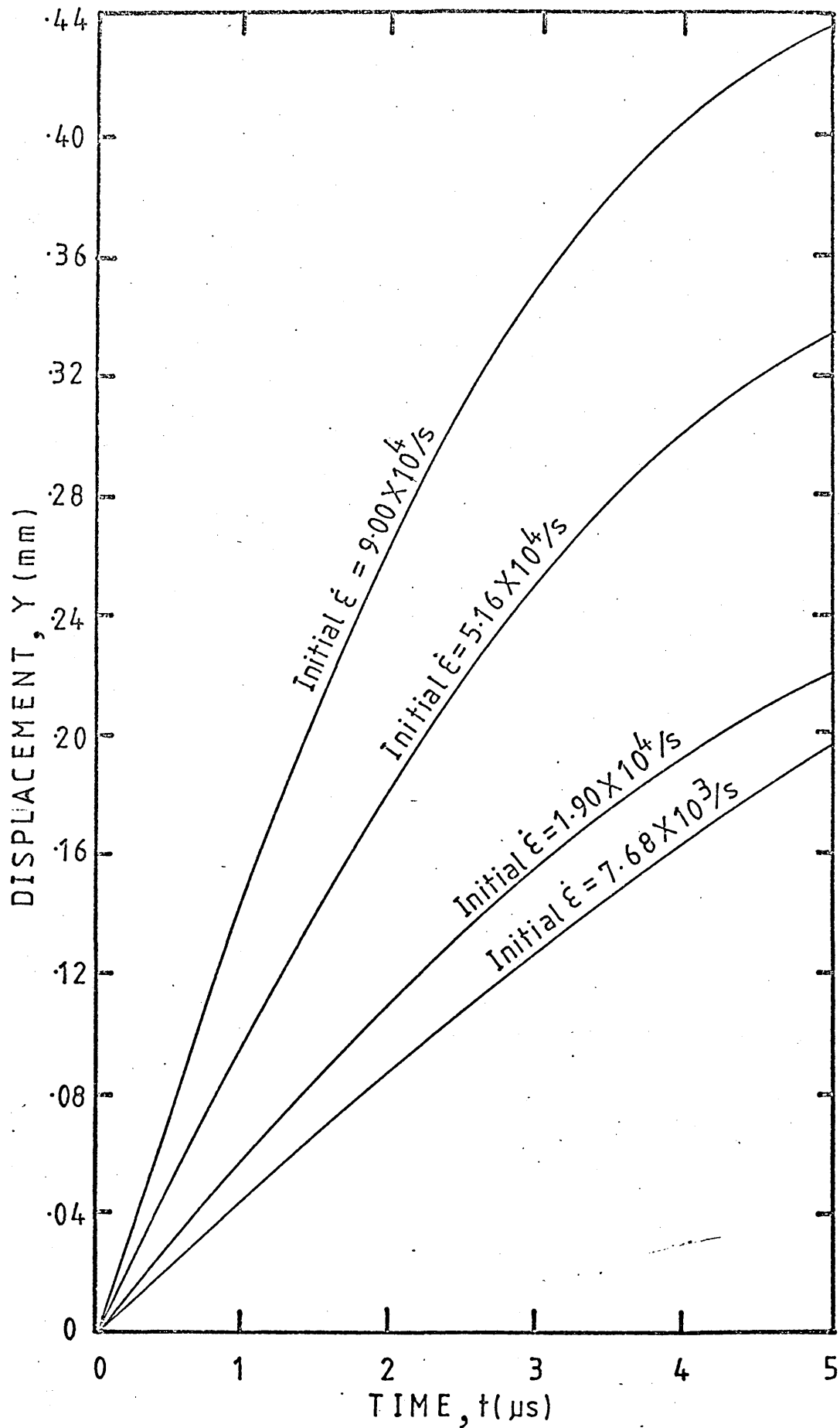


Fig.49 Showing displacement-time histories of structural steel deformed at different initial strain rates at room temperature.

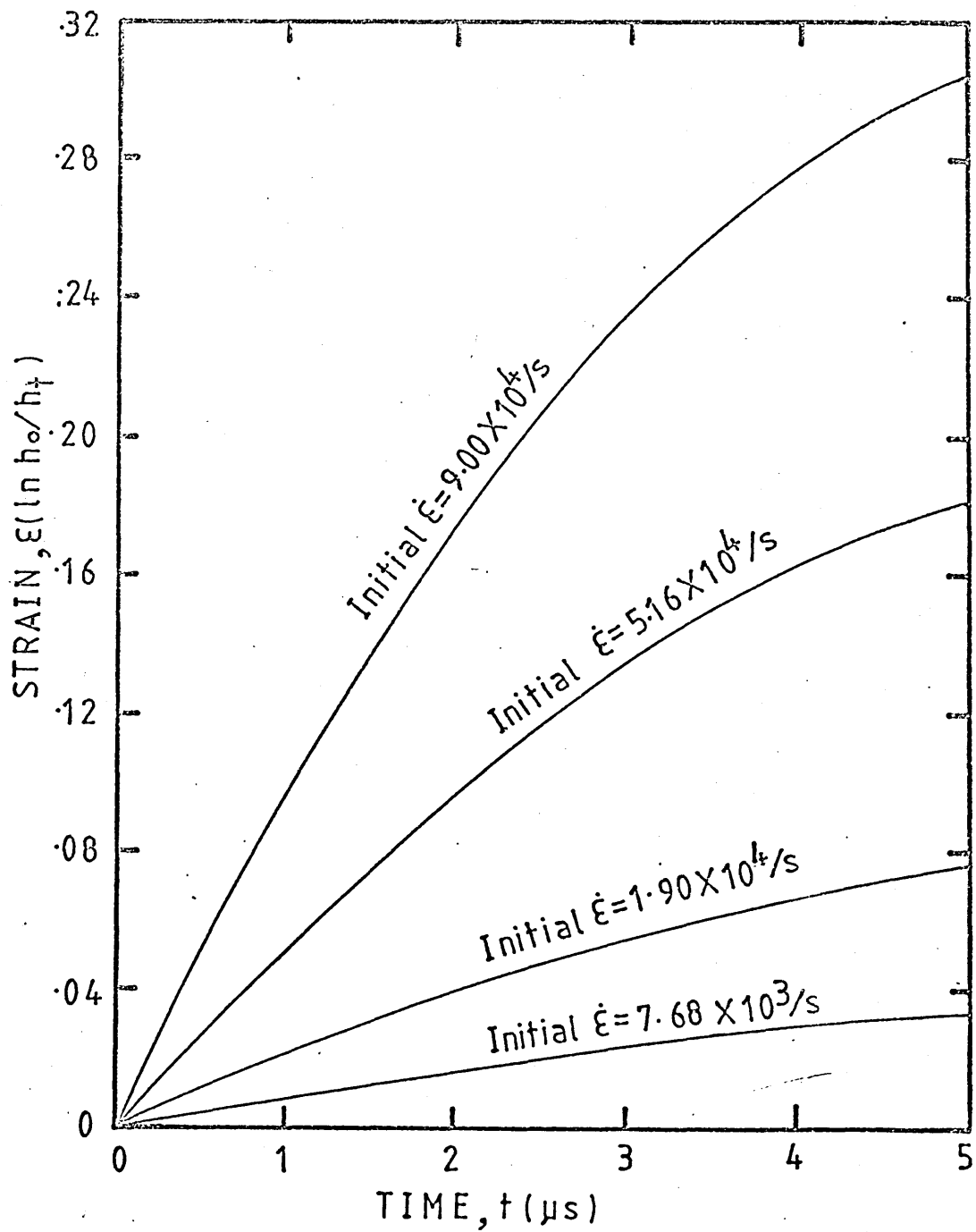


Fig. 50 Showing strain-time histories of structural steel deformed at different initial strain rates at room temperature.

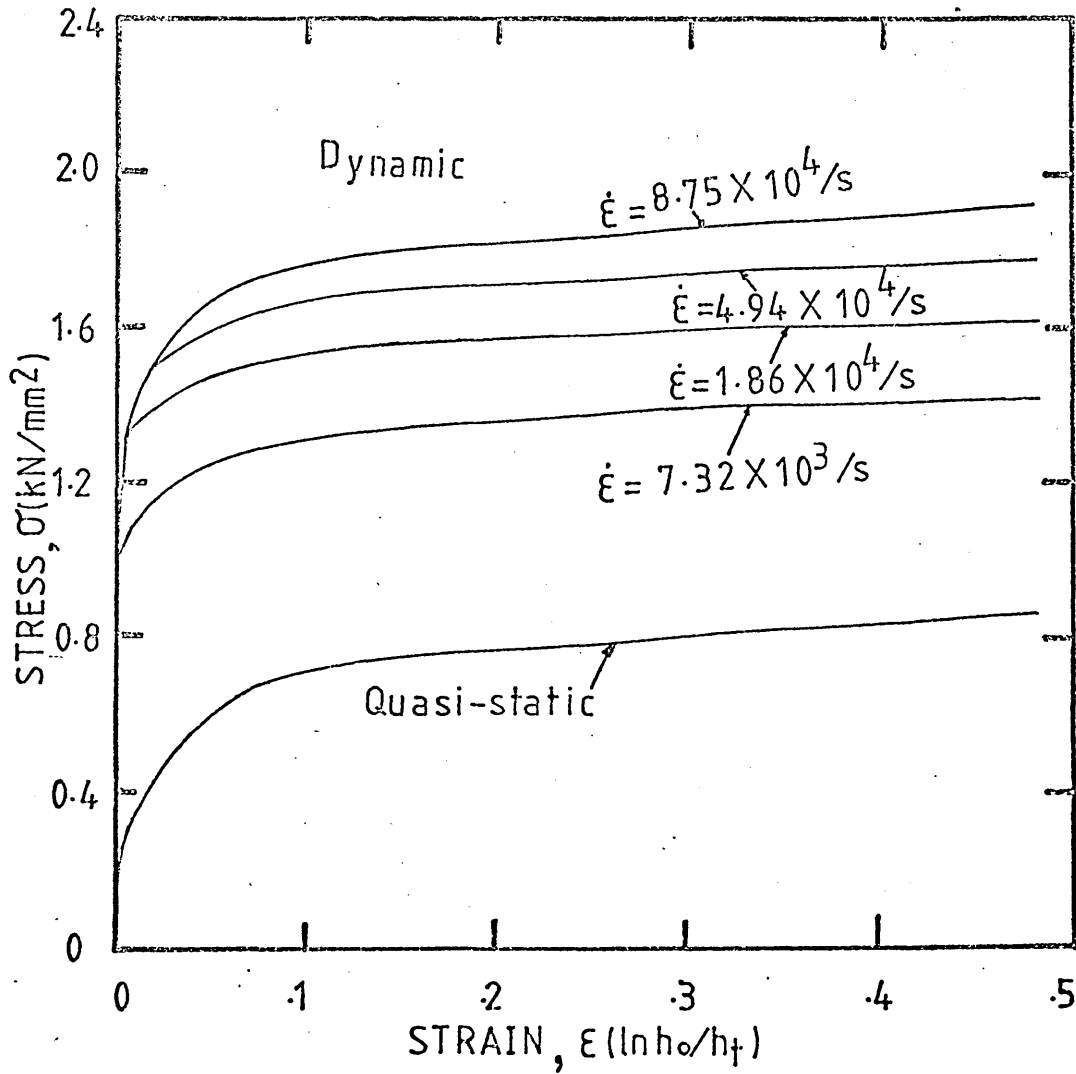


Fig.51 Stress-strain characteristics of structural steel deformed at different strain rates at room temperature.

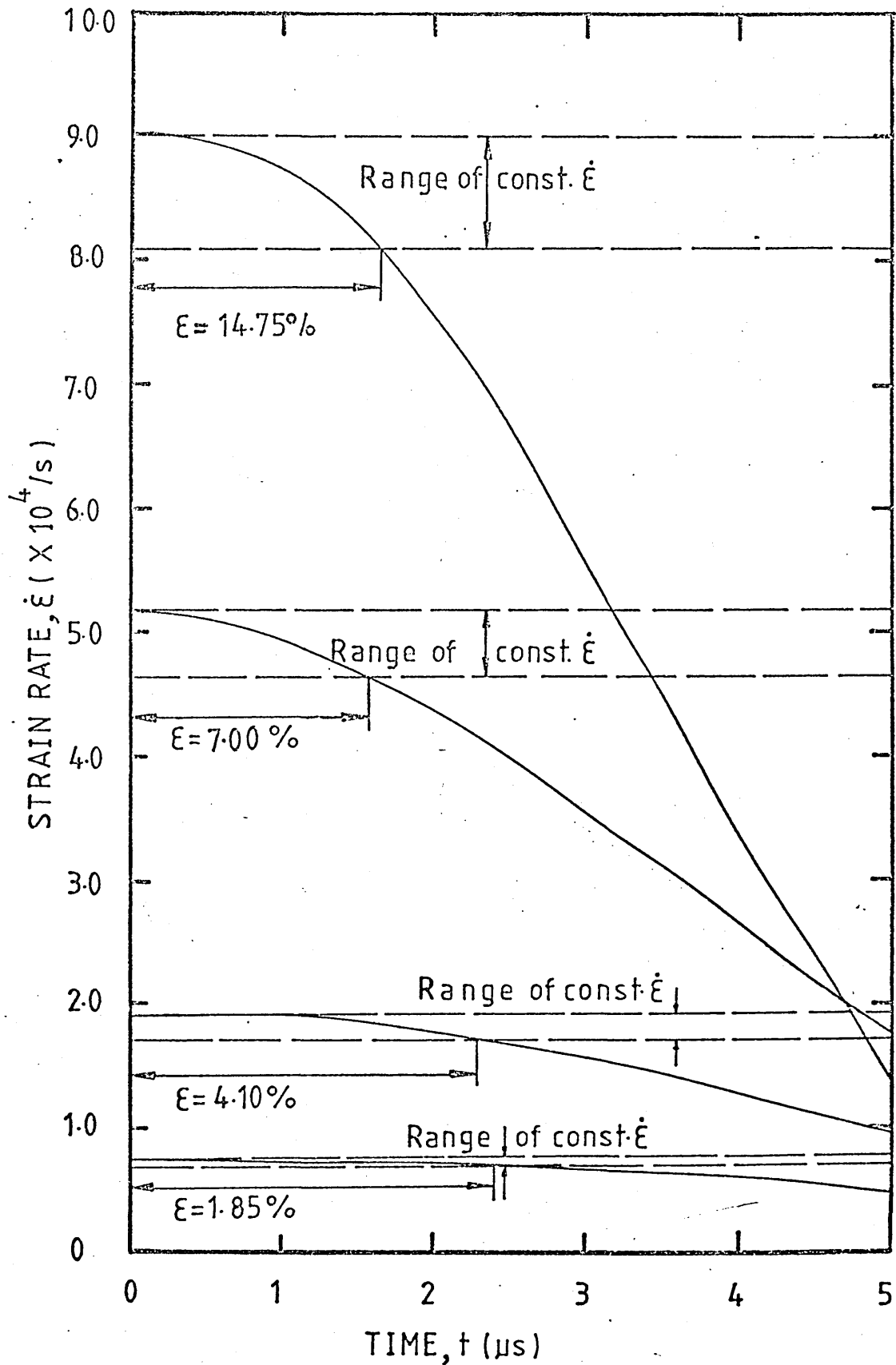


Fig.52 Showing strain rate-time histories of structural steel deformed at different initial strain rates at room temperature.

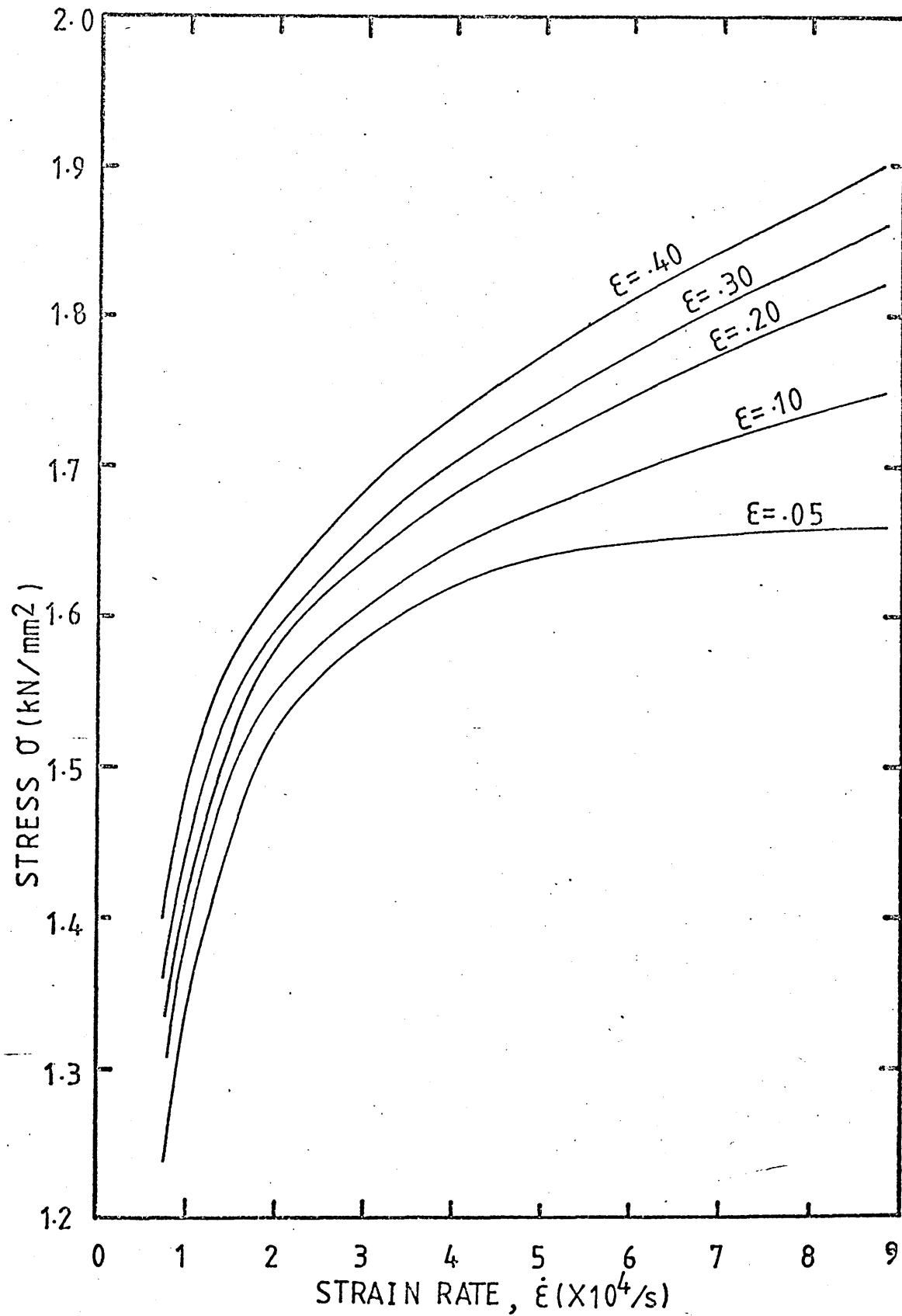


Fig.53 Showing variation of stress with strain rate at different strains at room temperature for structural steel.

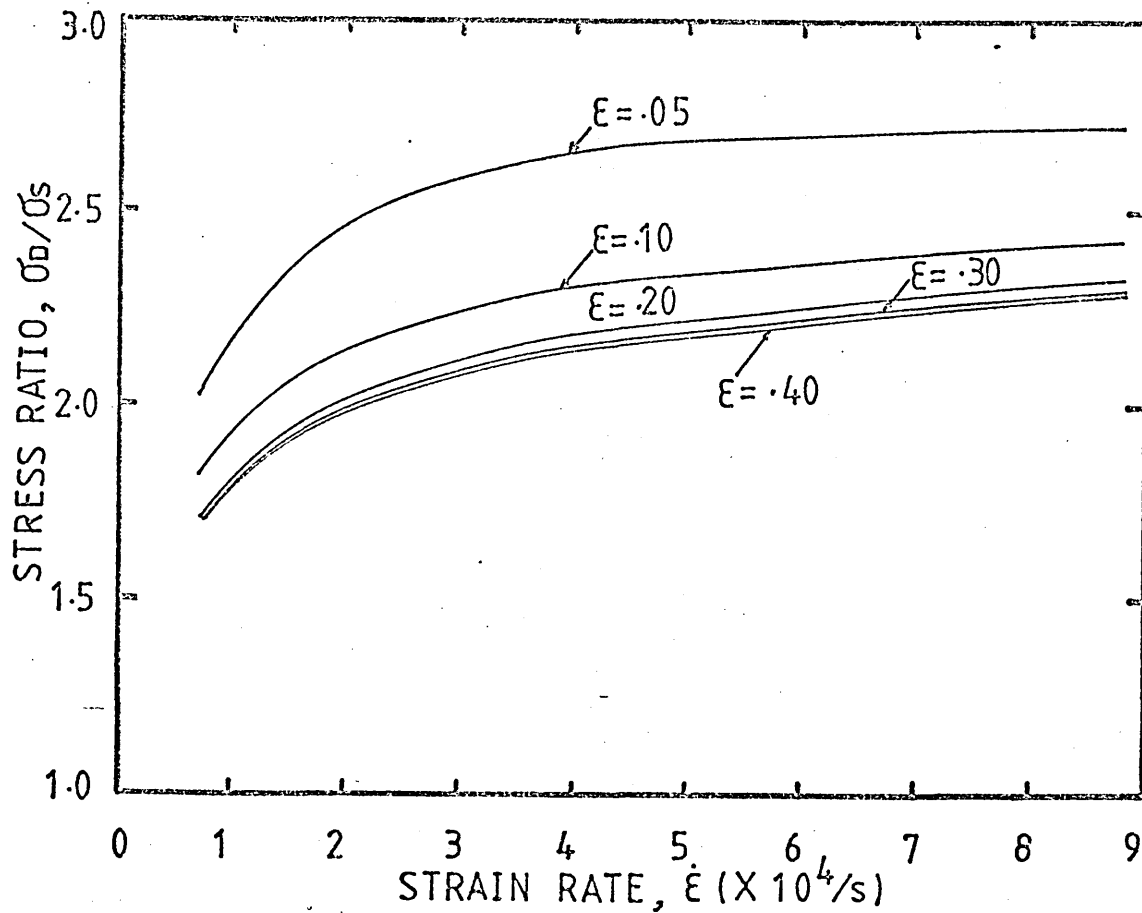


Fig.54 Showing variation of stress ratio with strain rate at different strains at room temperature for structural steel.

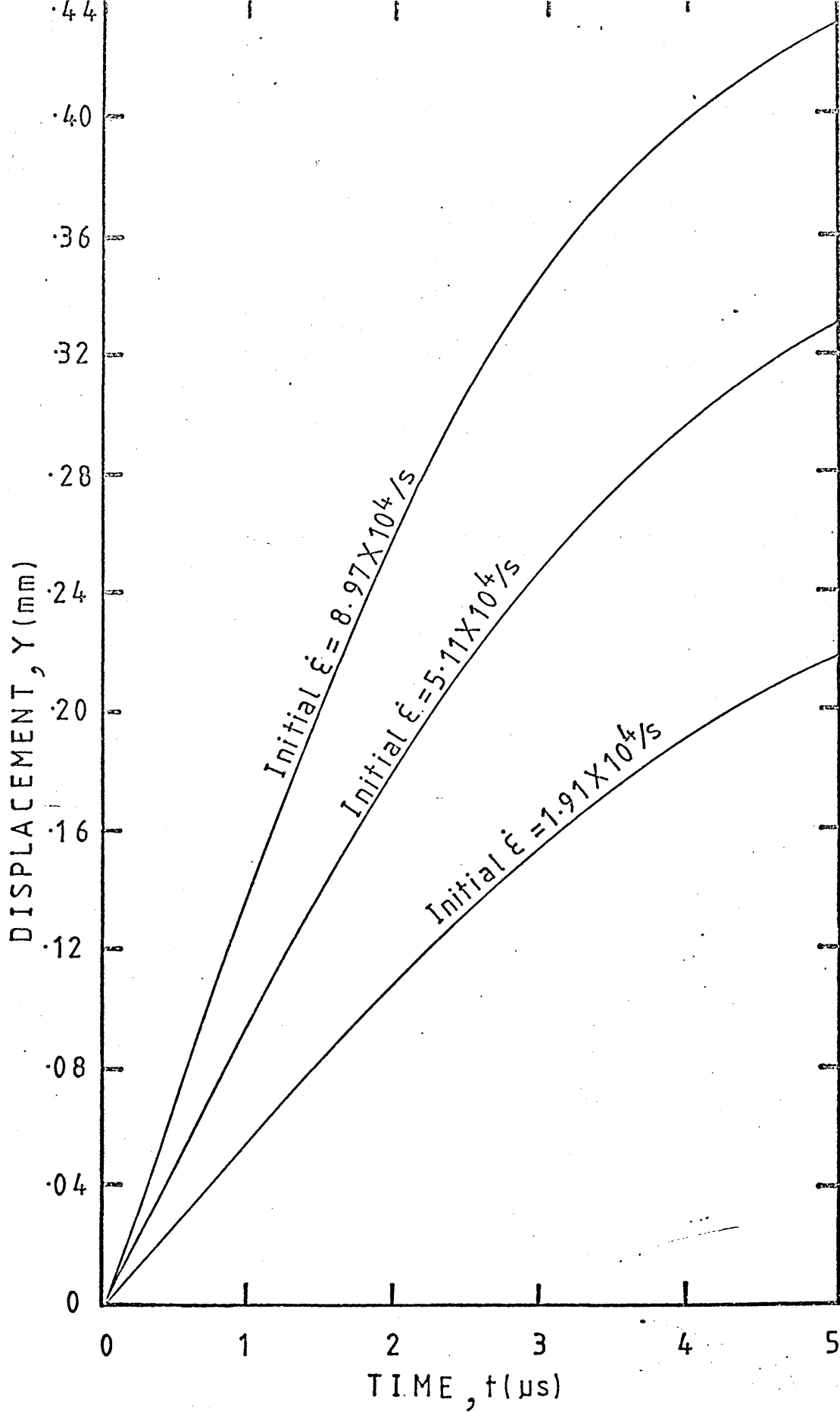


Fig.55 Showing displacement-time histories of structural steel deformed at different initial strain rates at  $-30^{\circ}\text{C}$ .

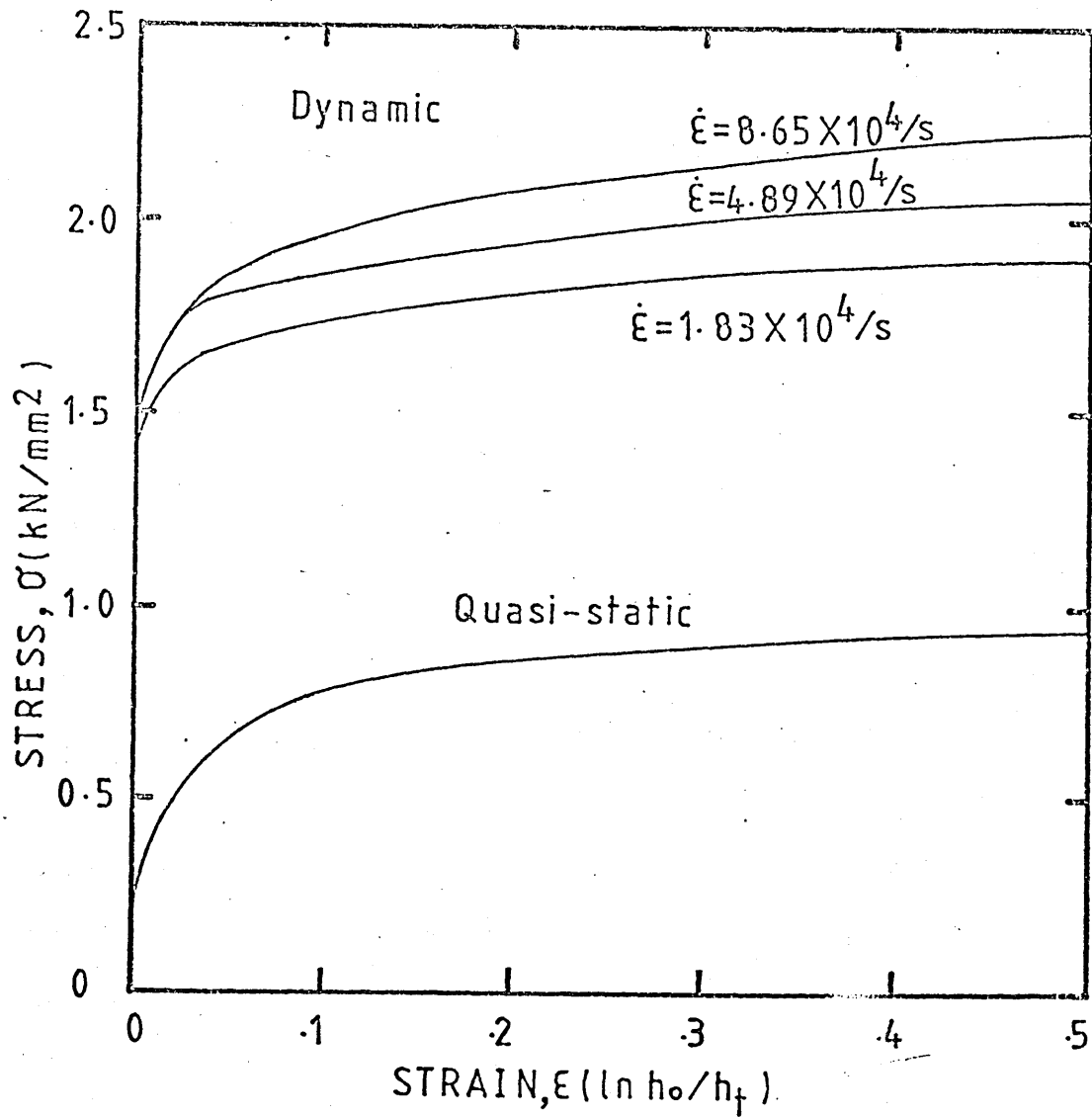


Fig.56 Stress-strain characteristics of structural steel deformed at different strain rates at -30° C.

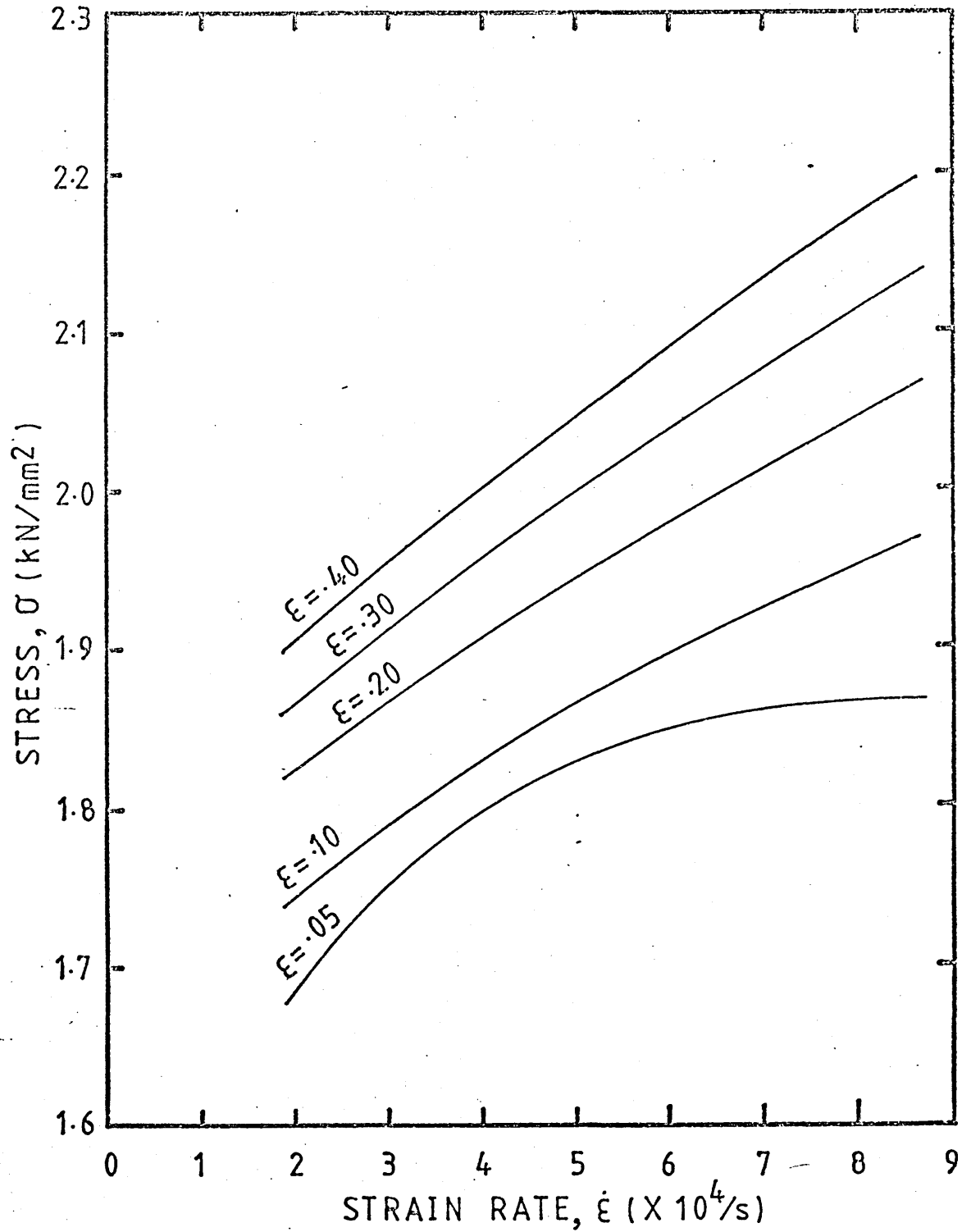


Fig.57 Showing variation of stress with strain rate at different strains at  $-30^{\circ}\text{C}$  for structural steel.

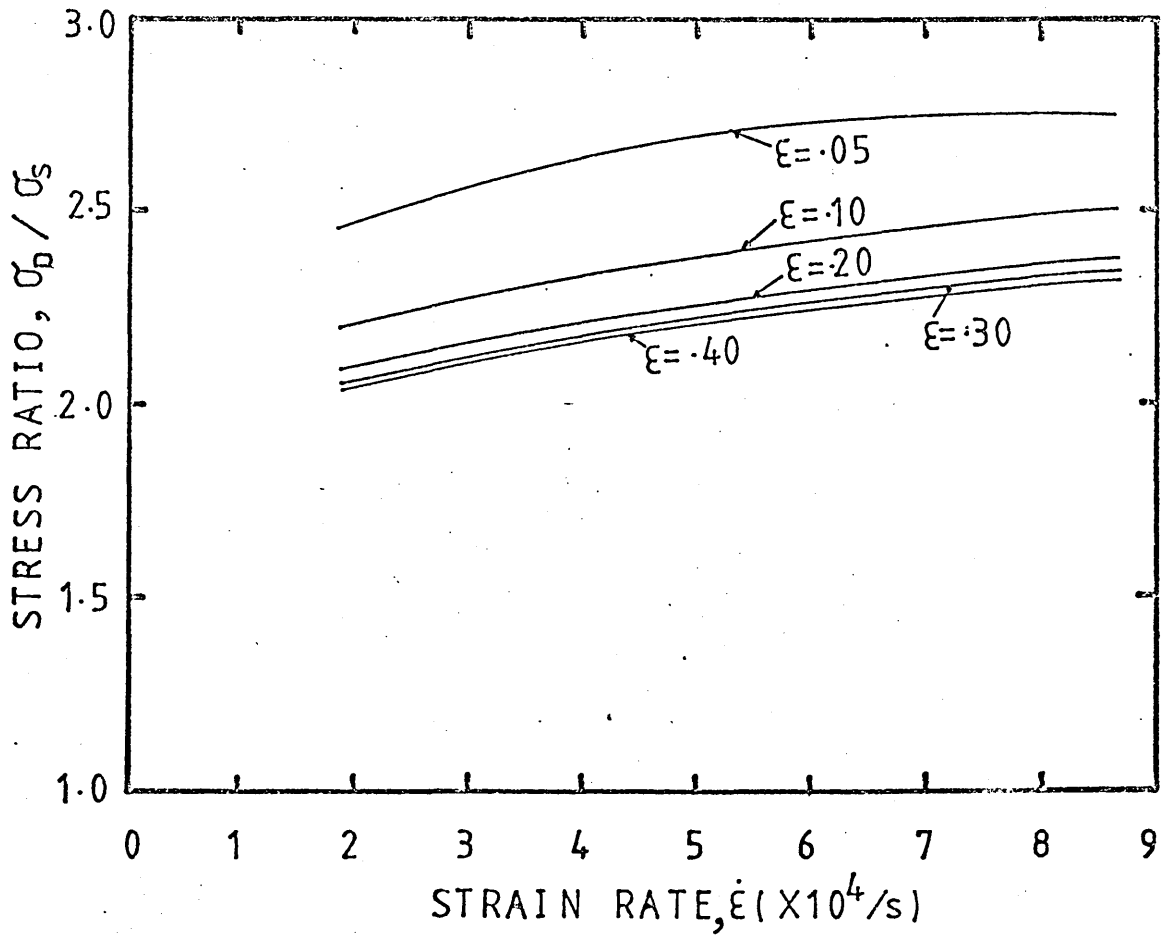


Fig.58 Showing variation of stress ratio with strain rate at different strains at  $-30^{\circ}\text{C}$  for structural steel.

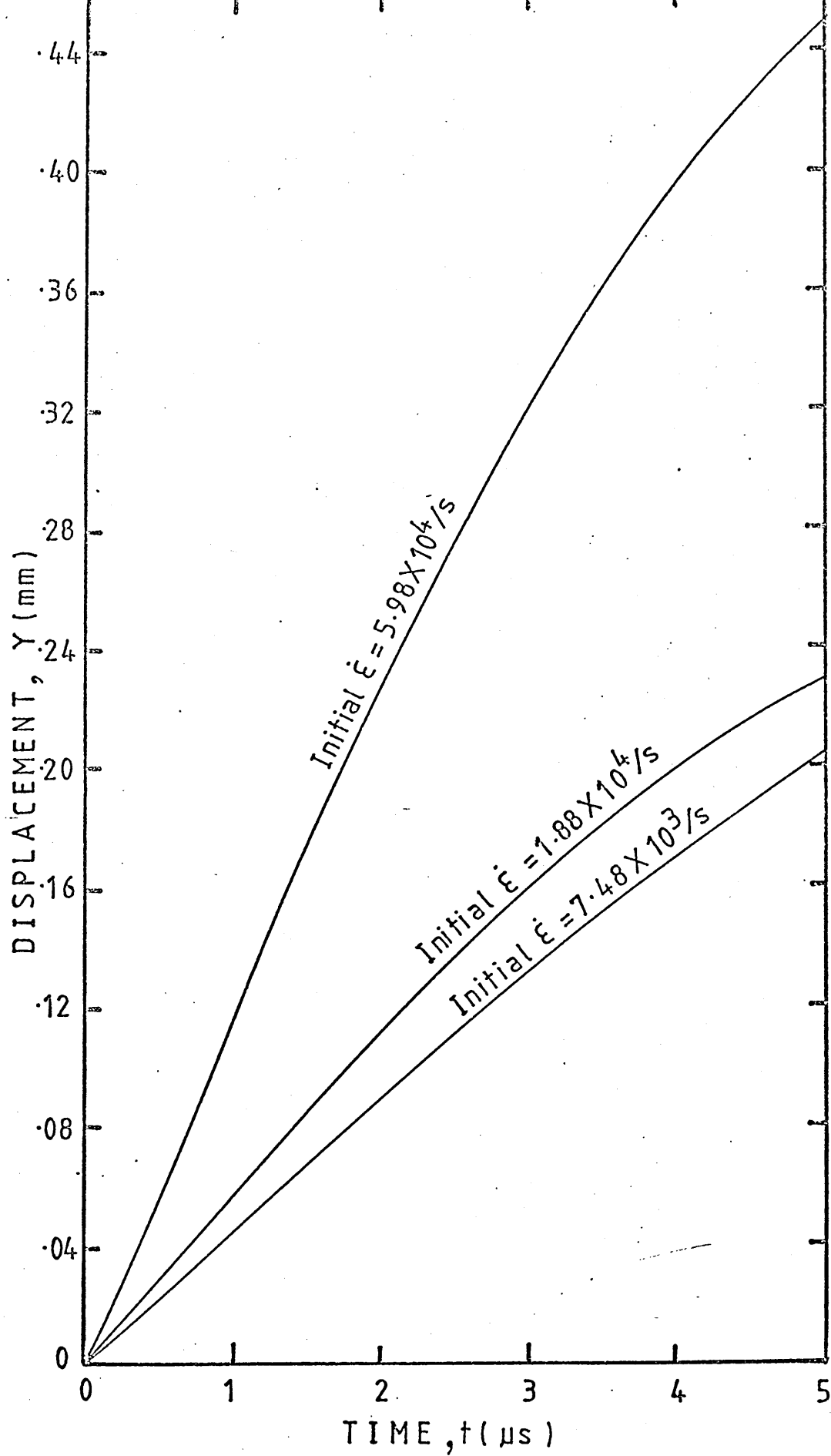


Fig.59 Showing displacement-time histories of structural steel deformed at various strain rates at 235° C.

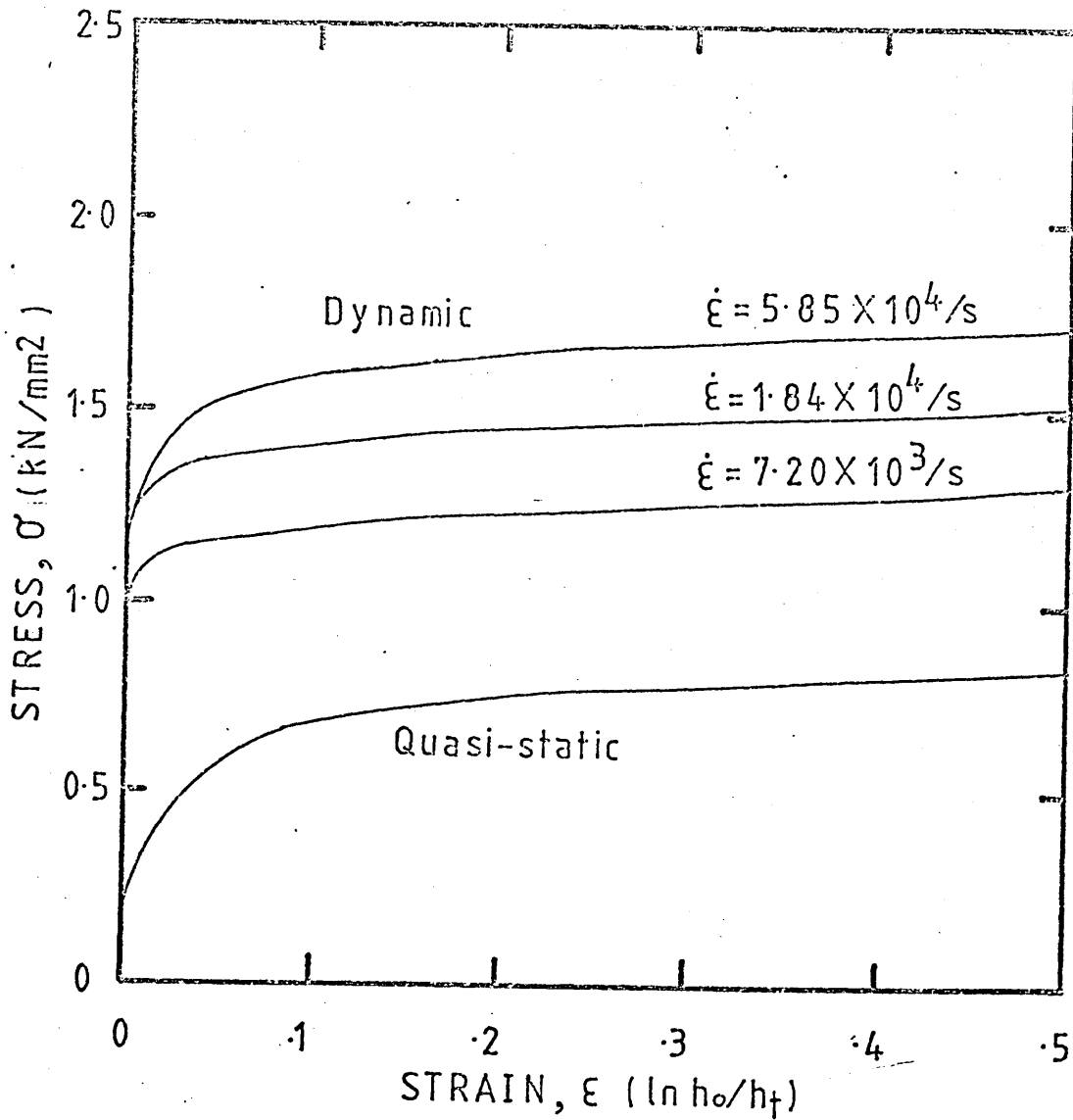


Fig.60 Stress-strain characteristics of structural steel deformed at different strain rates at 235° C.

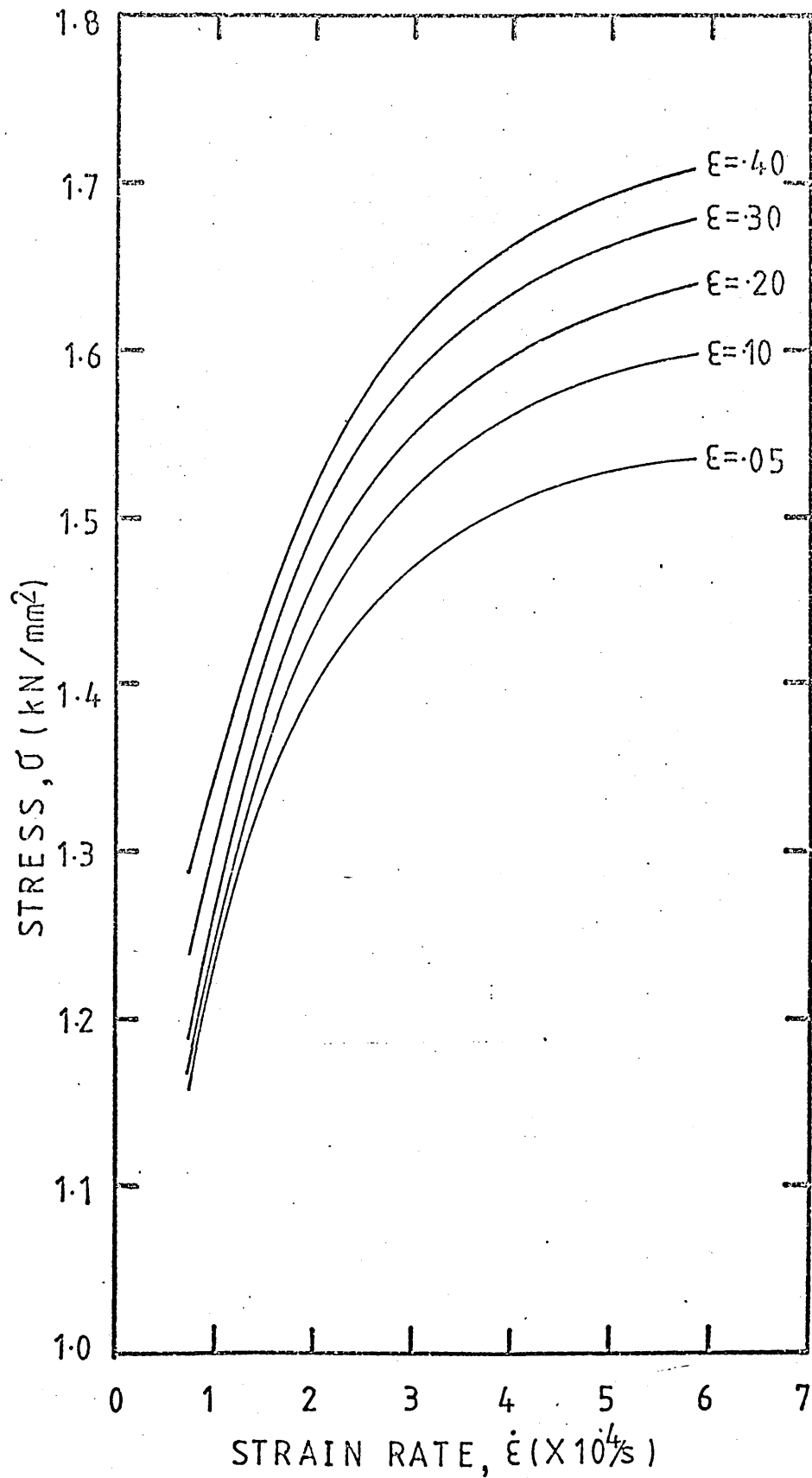


Fig.61 Showing variation of stress with strain rate at different strains at 235° C for structural steel.

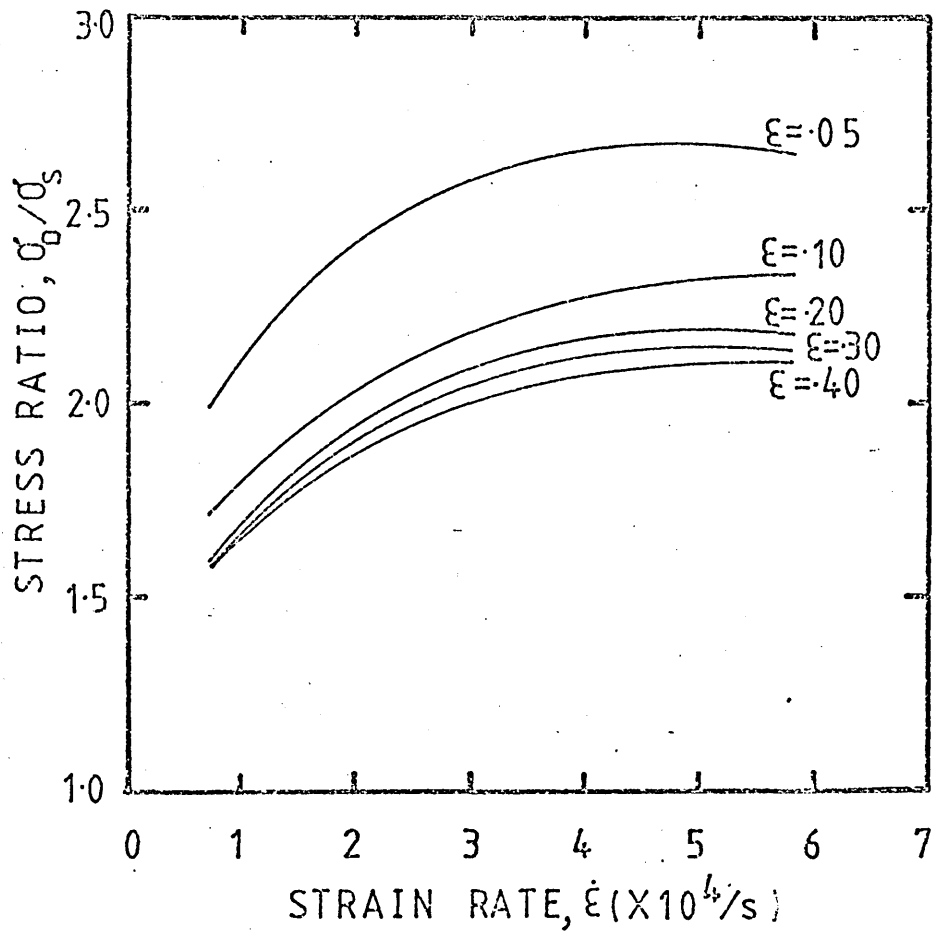


Fig.62 Showing variation of stress ratio with strain rate at different strains at 235° C for structural steel.

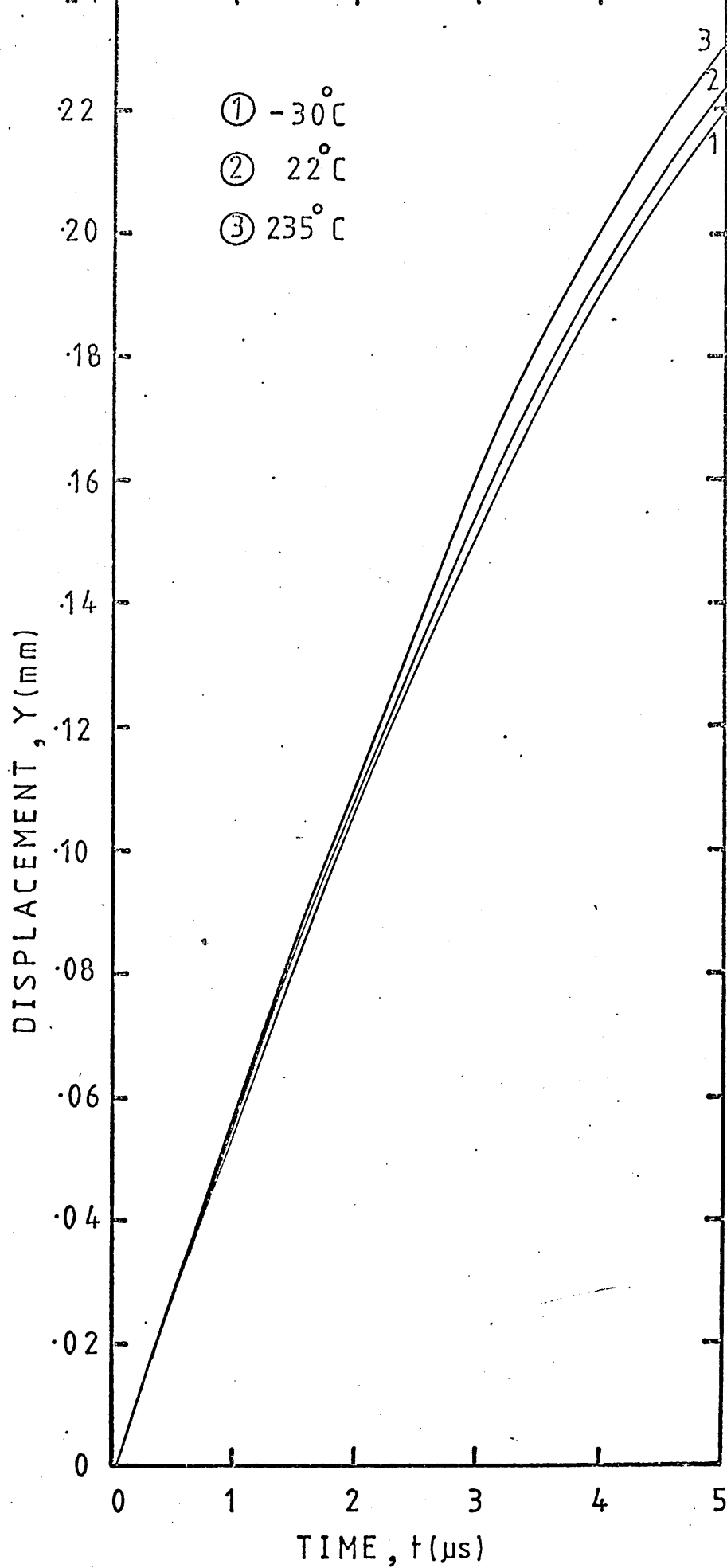


Fig.63 Showing displacement-time curves for structural steel deformed at strain rate of about  $1.8 \times 10^4/\text{s}$  at different temperatures.

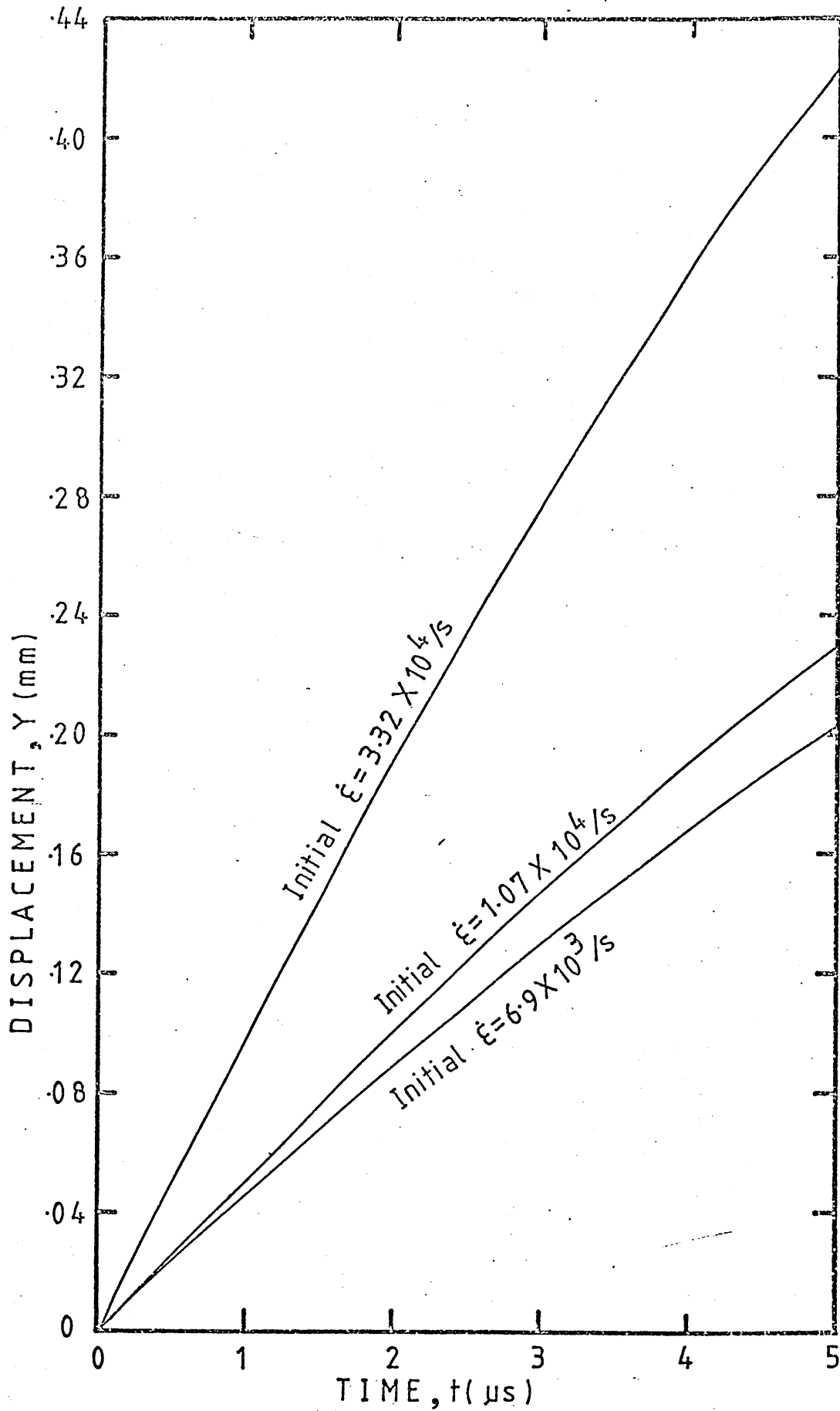


Fig.64 Showing displacement-time histories of as-received aluminium deformed at various initial strain rates at room temperature.

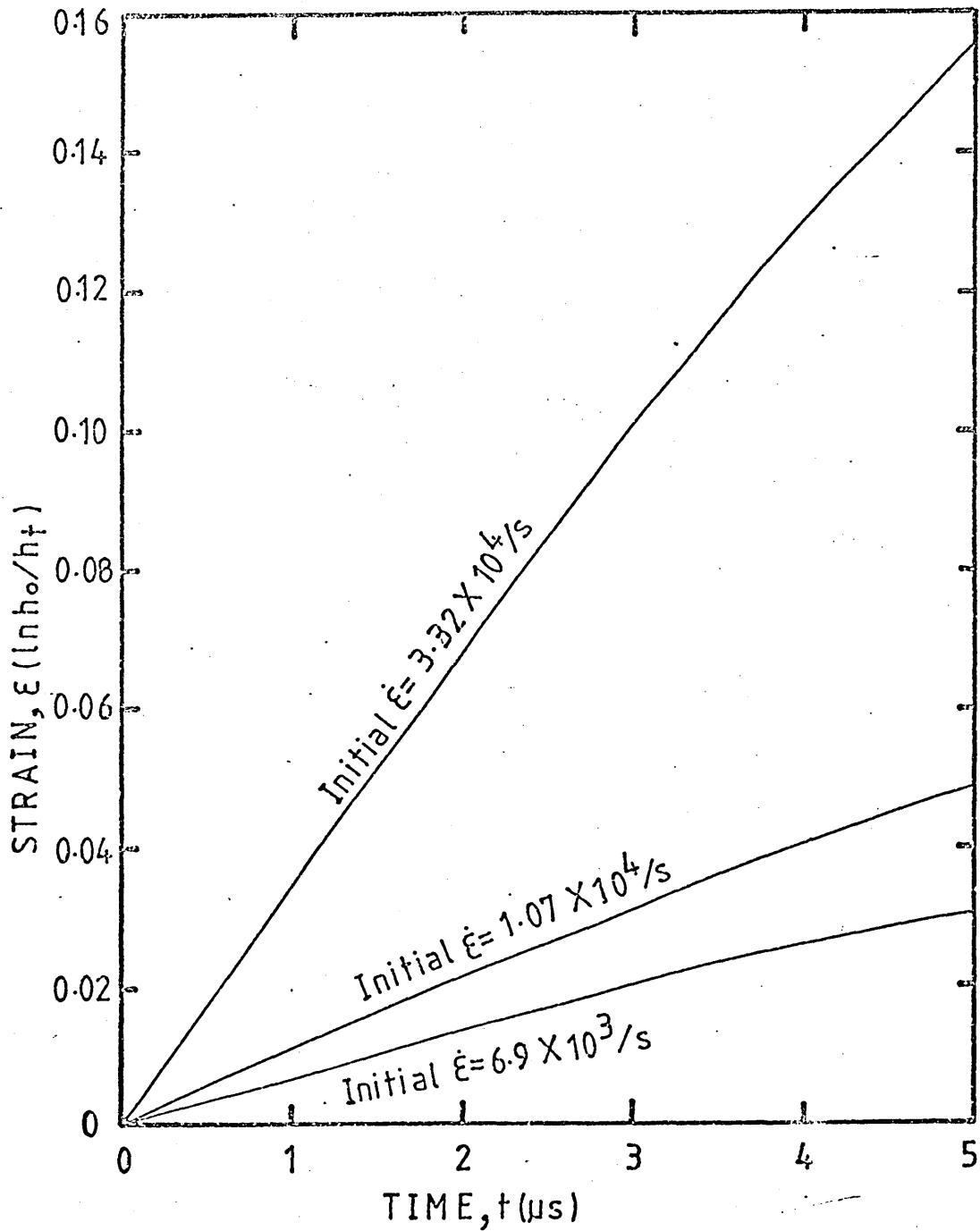


Fig.65 Showing strain-time histories of as-received aluminium deformed at various strain rates at room temperature.

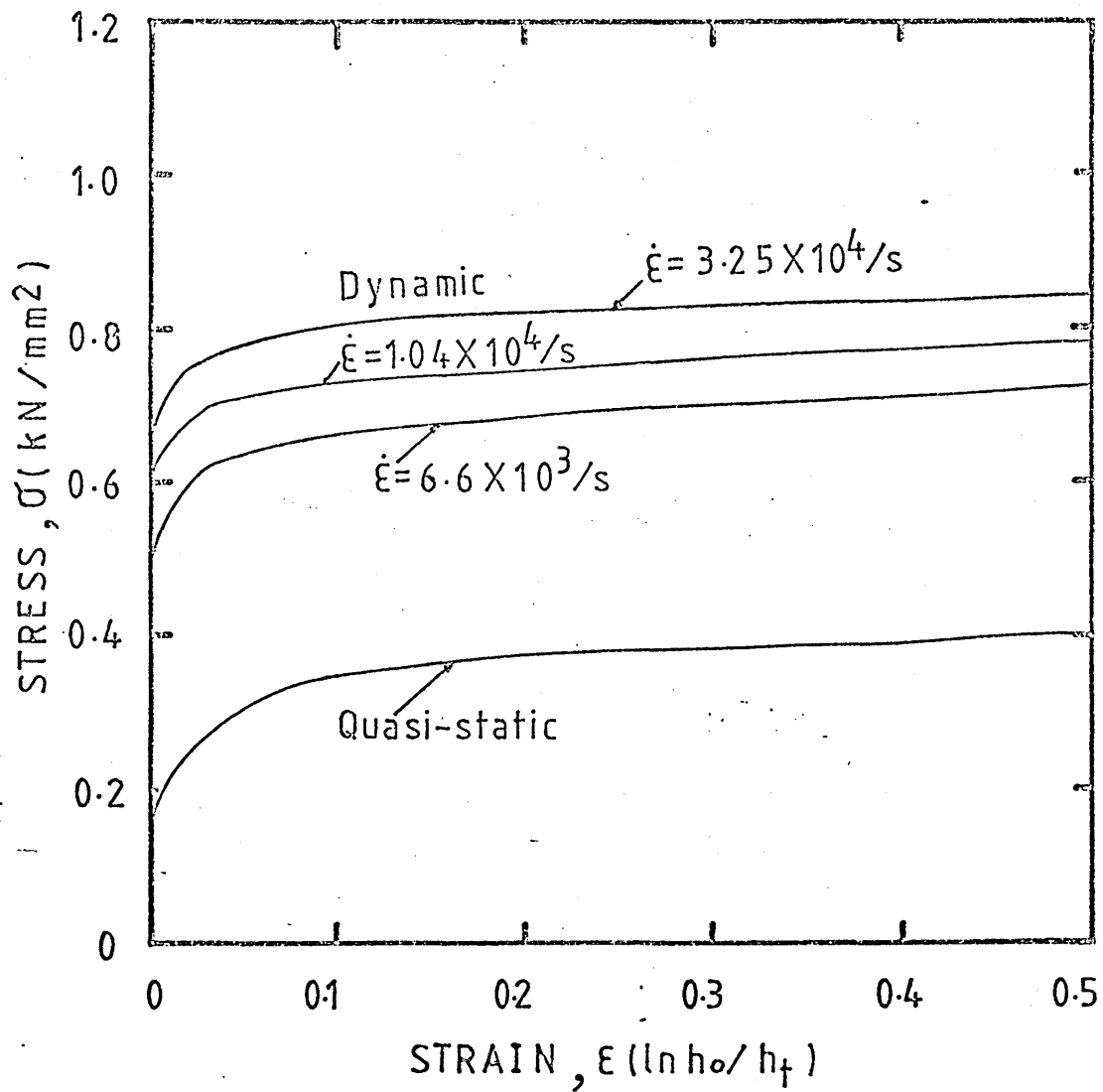


Fig.66 Showing stress-strain characteristics of as-received aluminium deformed at various strain rates at room temperature.

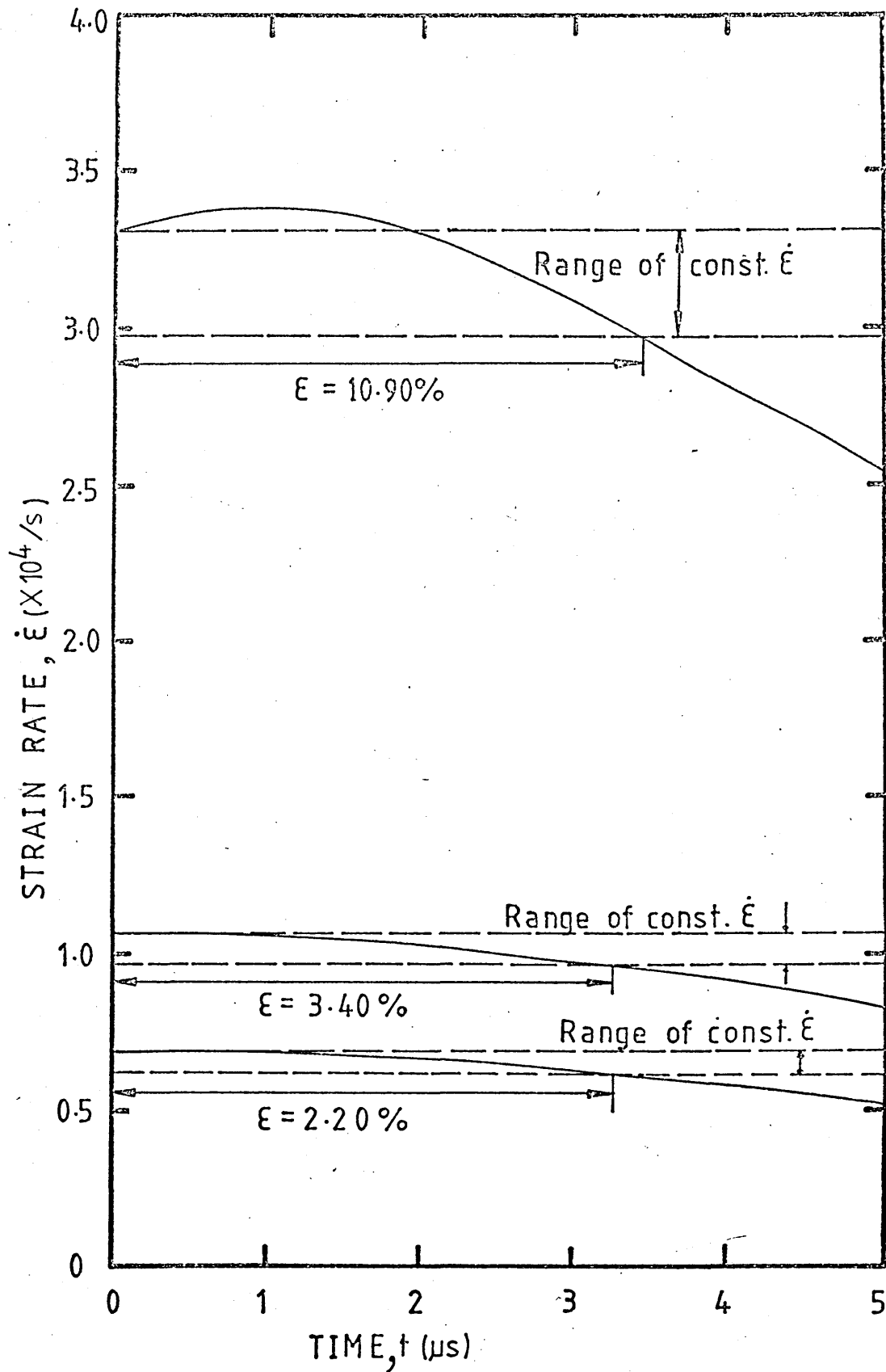


Fig.67 Showing strain rate-time histories of as-received aluminium during deformation at various strain rates at room temperature.

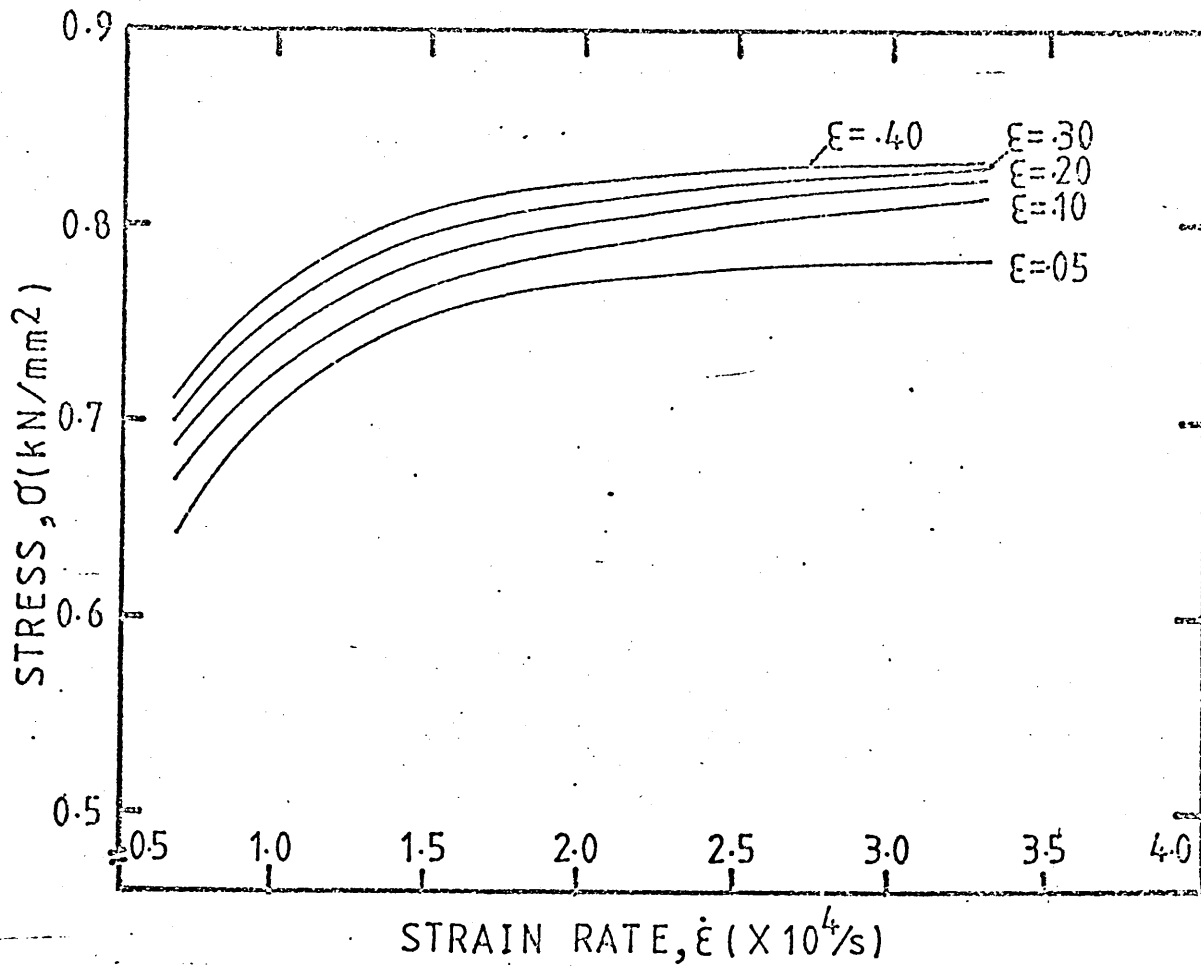


Fig.68 Showing variation of stress with strain rate at different strains at room temperature for aluminium.

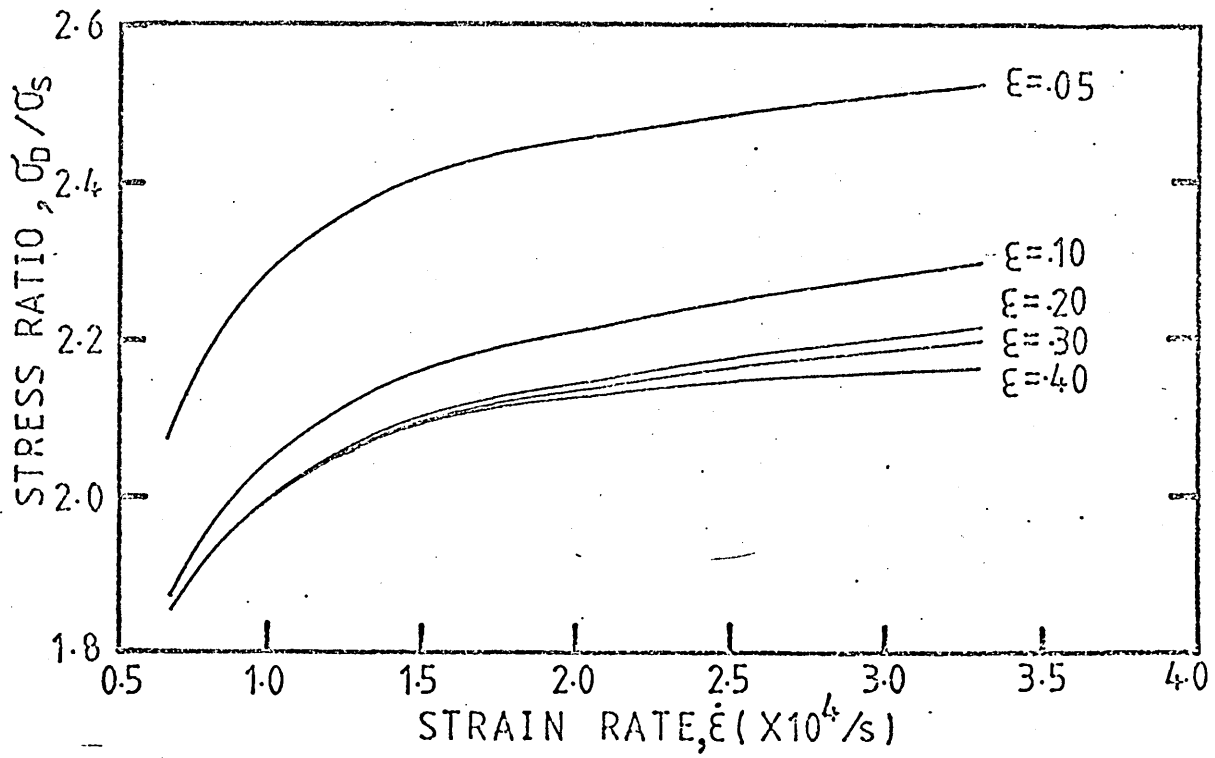


Fig.69 Showing variation of stress ratio with strain rate at different strains at room temperature for aluminium.

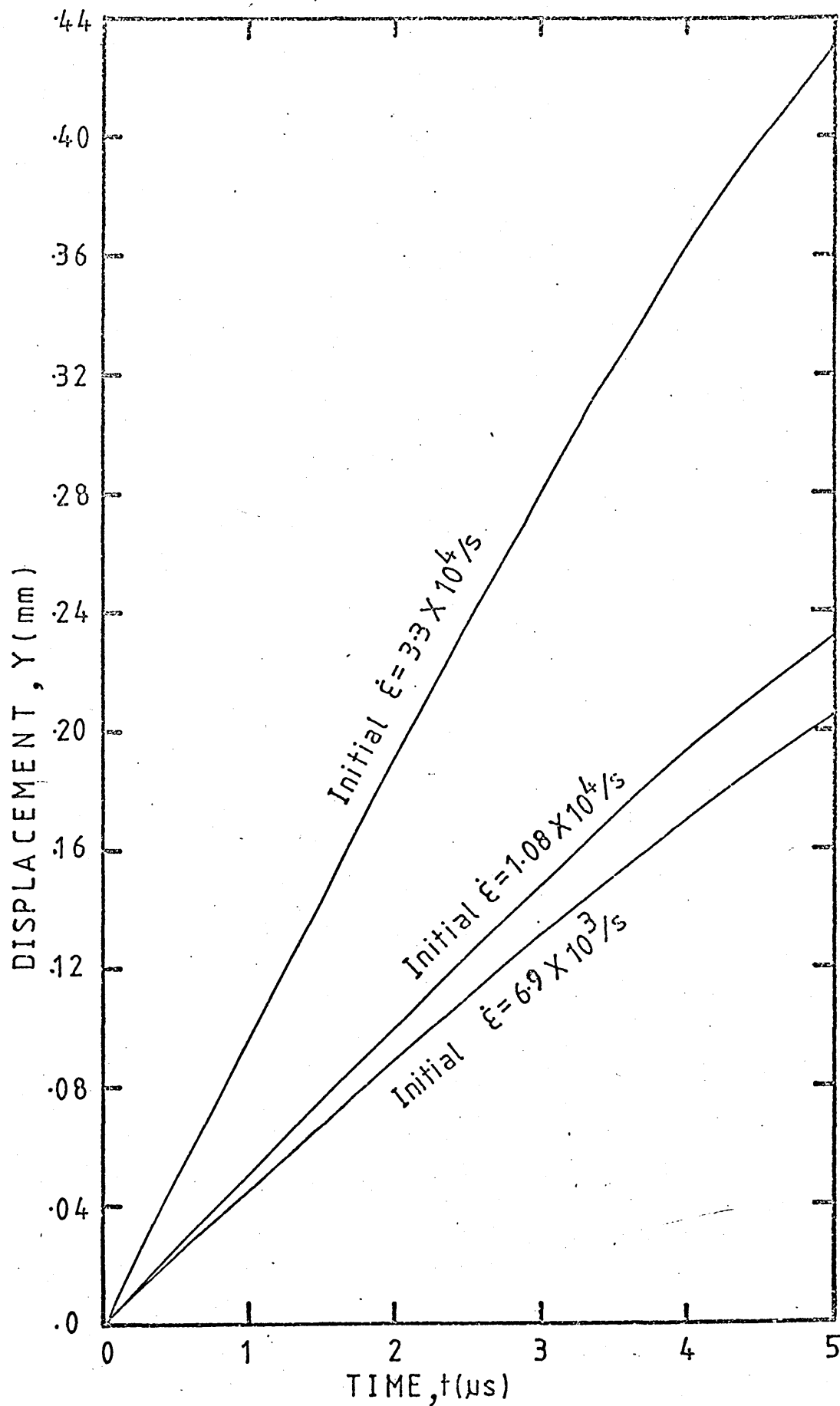


Fig.70 Showing displacement-time histories of as-received copper deformed at various strain rates at room temperature.

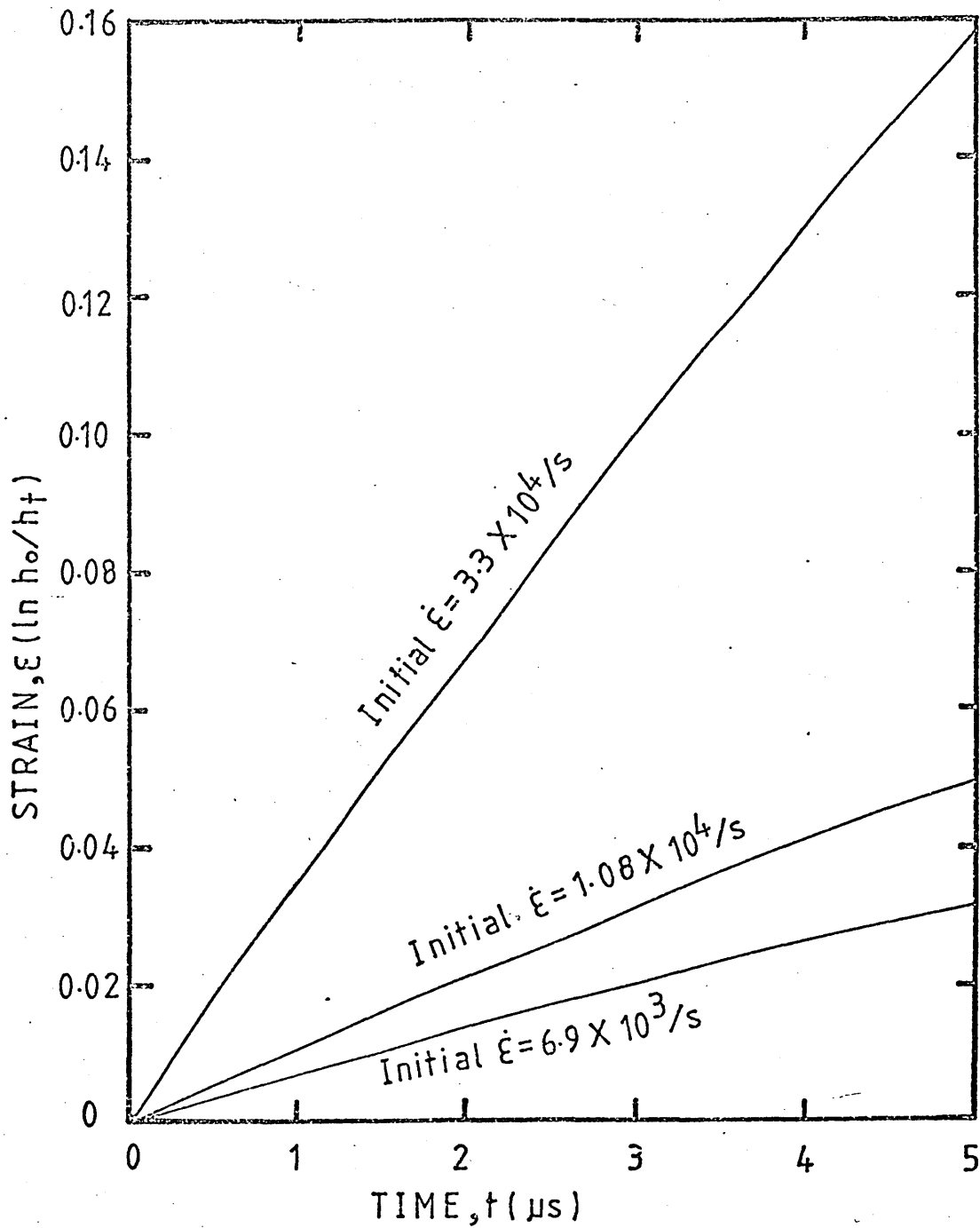


Fig.71 Showing strain-time histories of as-received copper deformed at various strain rates at room temperature.

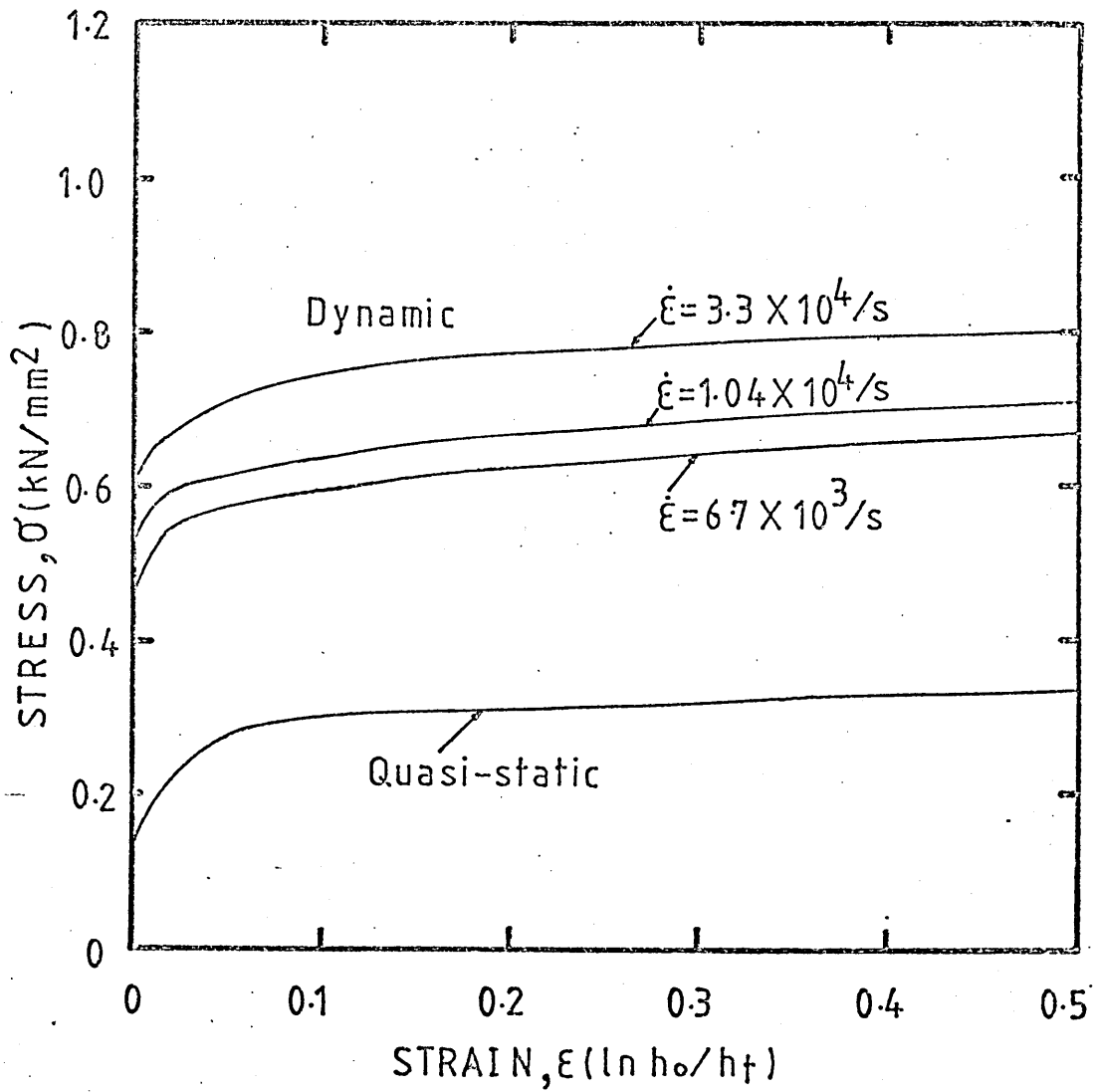


Fig. 72 Stress-strain characteristics of as-received copper deformed at various strain rates at room temperature.

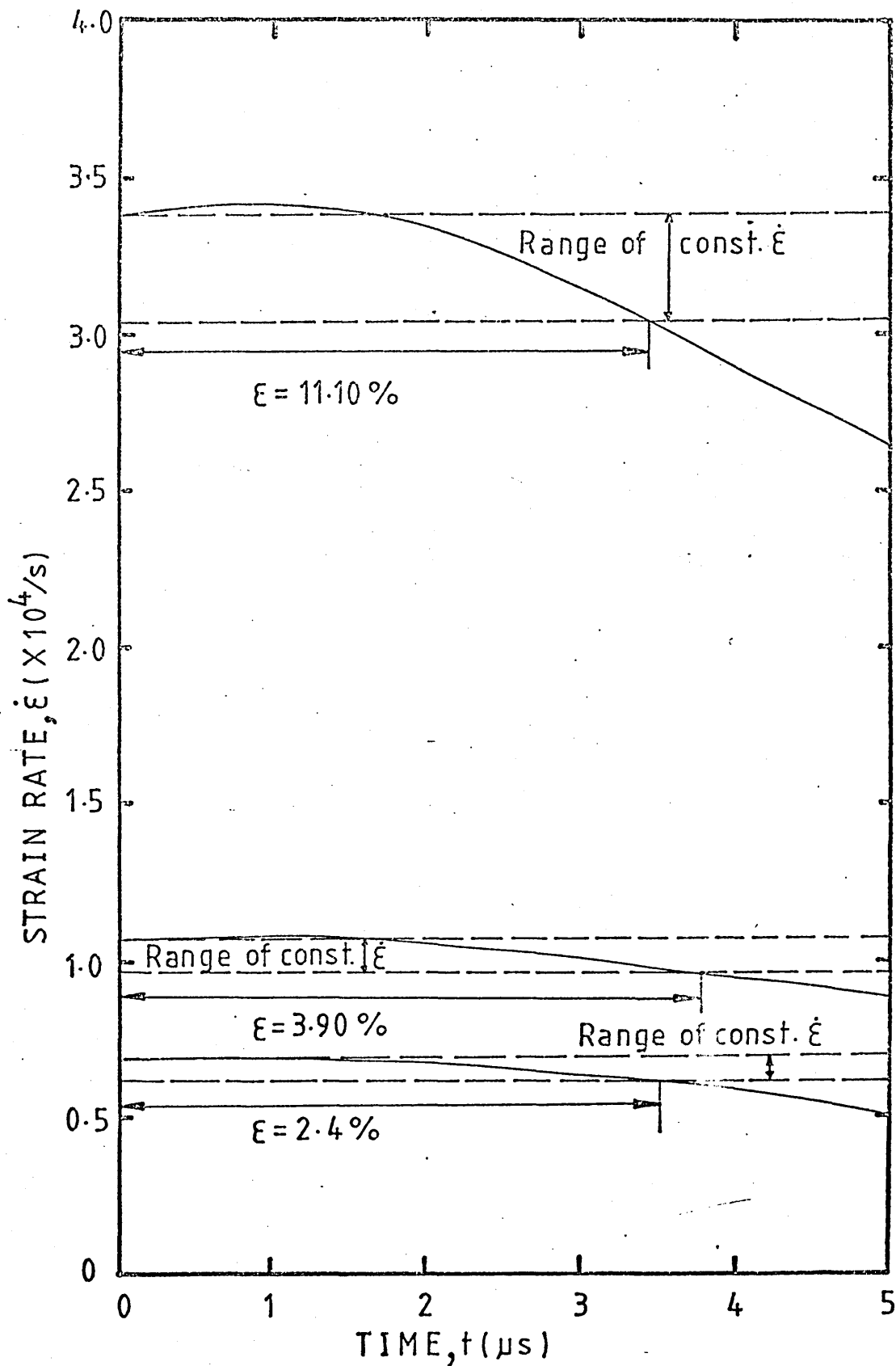


Fig.73 Showing strain rate-time histories of as-received copper during deformation at various strain rates at room temperature.

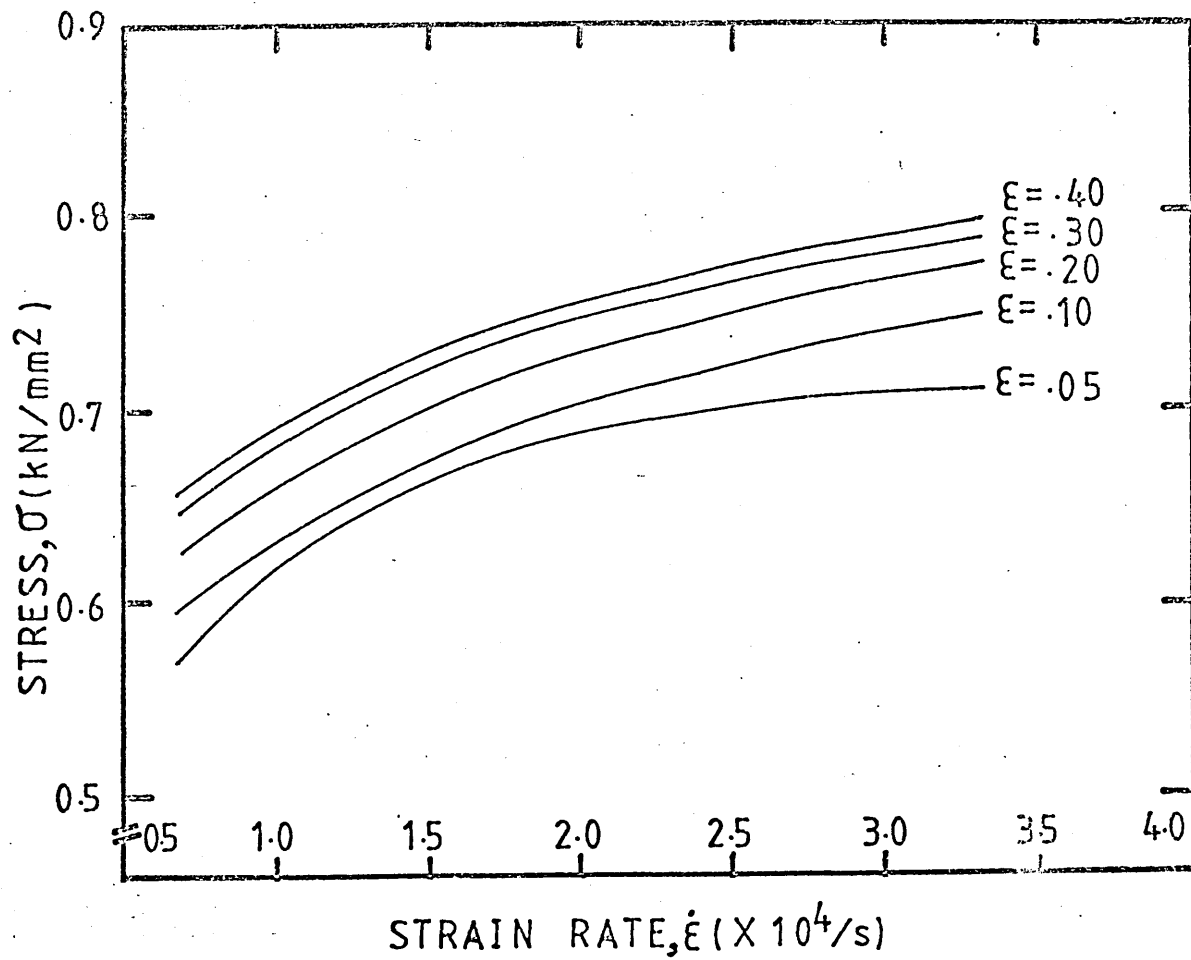


Fig.74 Showing variation of stress with strain rate at different strains at room temperature for copper.

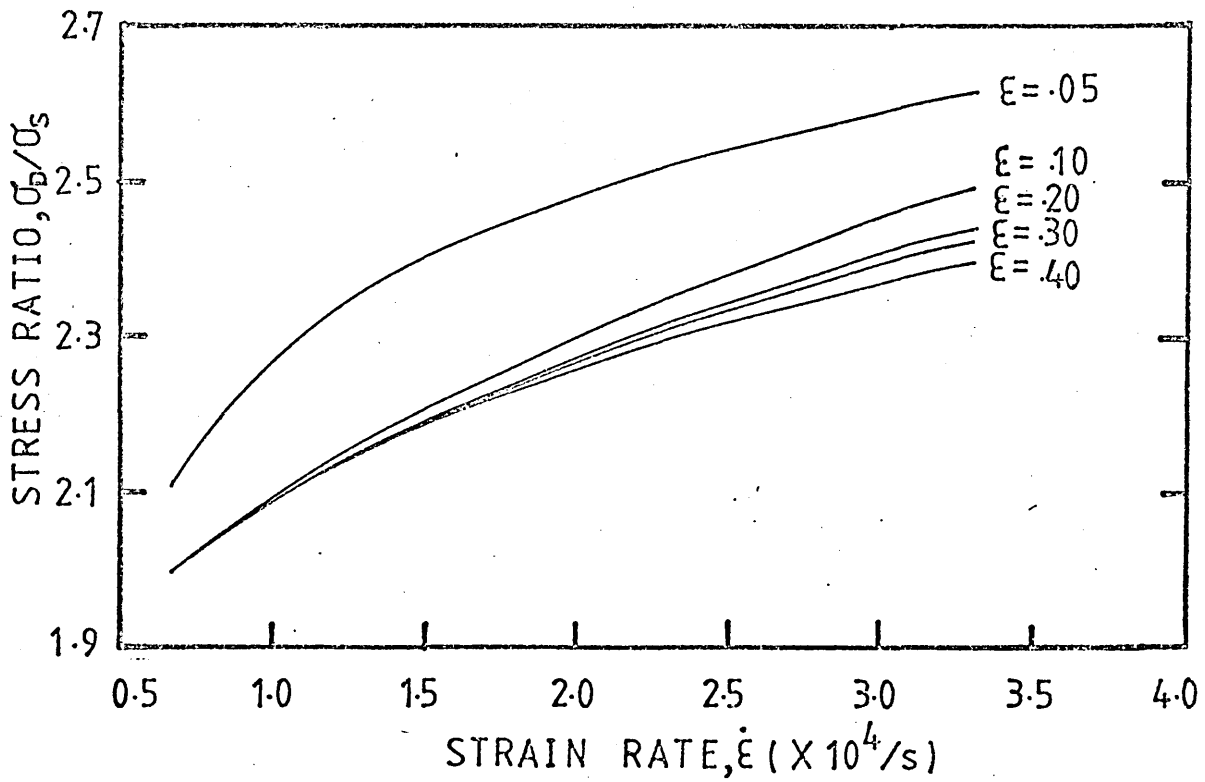


Fig.75 Showing variation of stress ratio with strain rate at different strains at room temperature for copper.

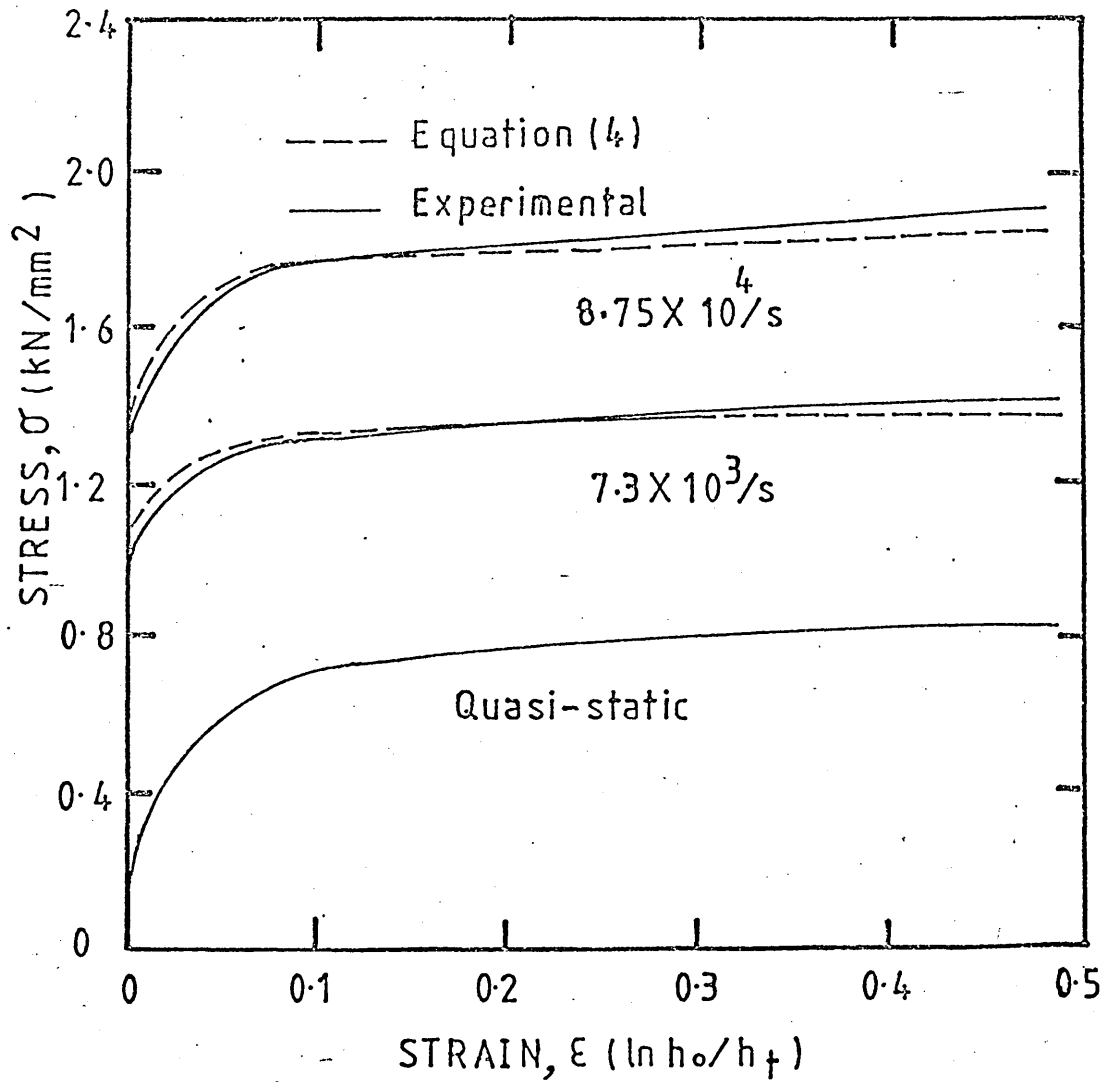


Fig. 76 Showing comparison of the dynamic stress-strain curves obtained by using proposed equation with those obtained experimentally at room temperature for structural steel.

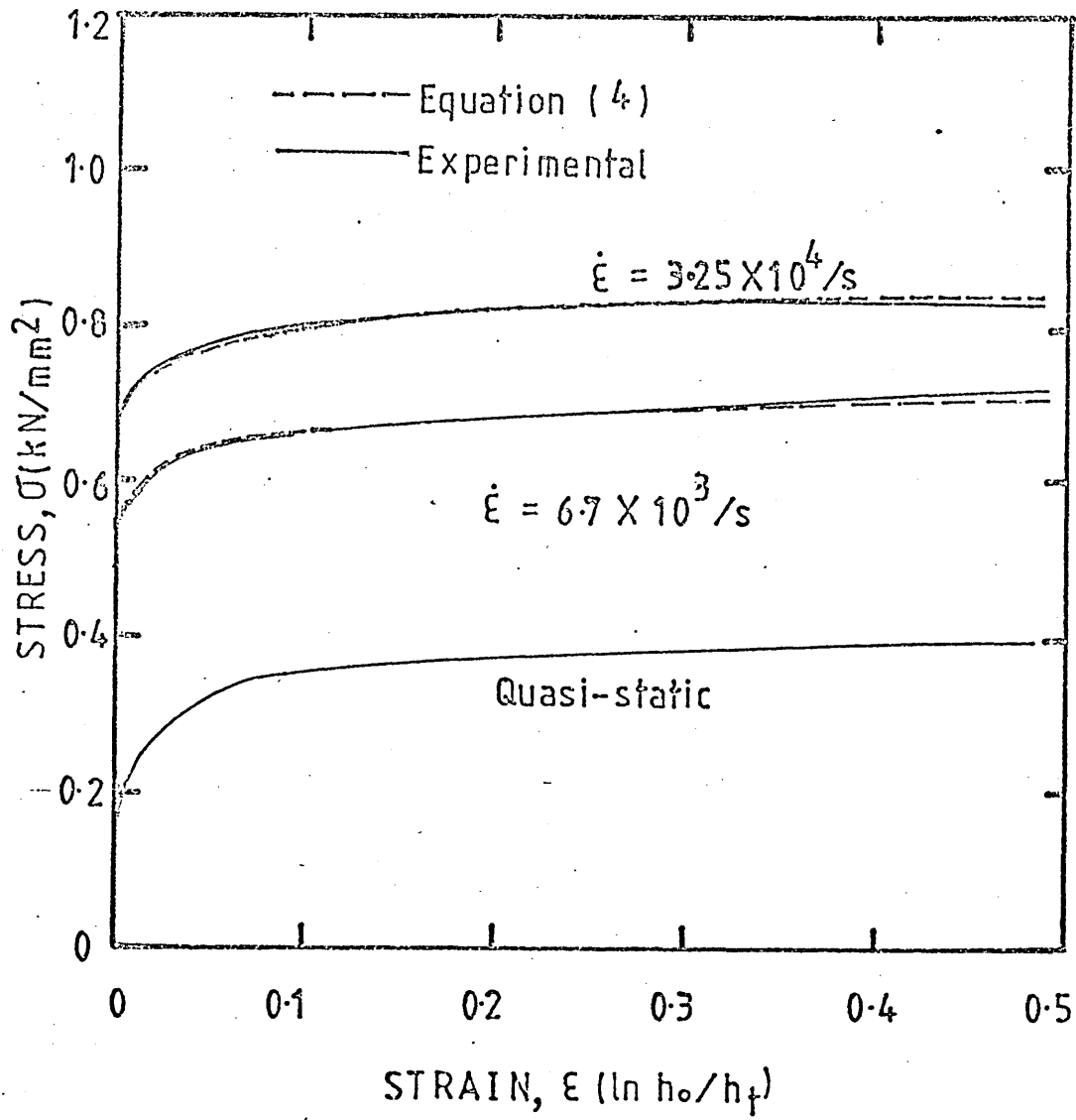


Fig.77 Showing comparison of the dynamic stress-strain curves obtained by using proposed equation with those obtained experimentally at room temperature for aluminium.

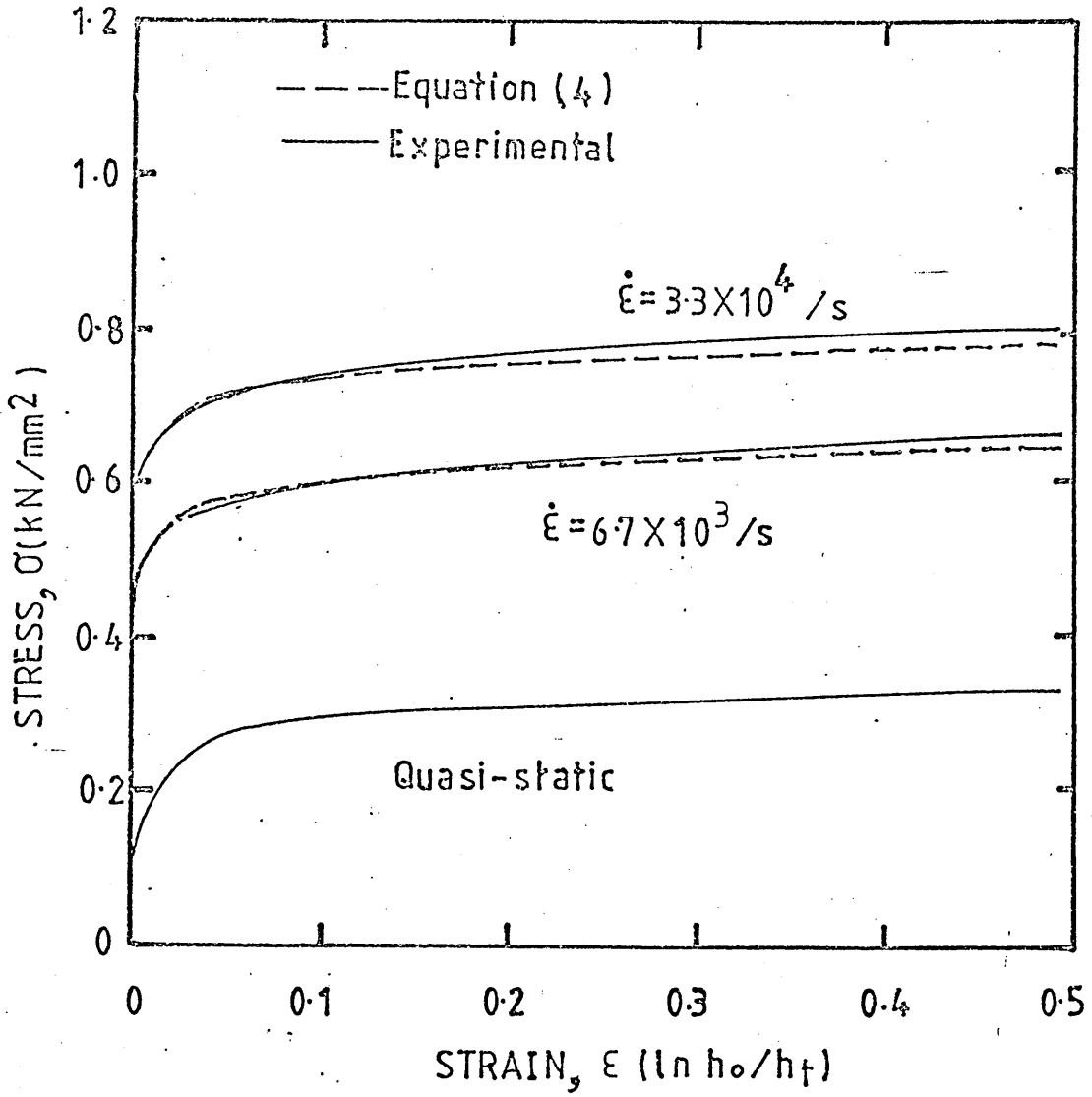


Fig.78 Showing comparison of the dynamic stress-strain curves obtained by using proposed equation with those obtained experimentally at room temperature for copper.

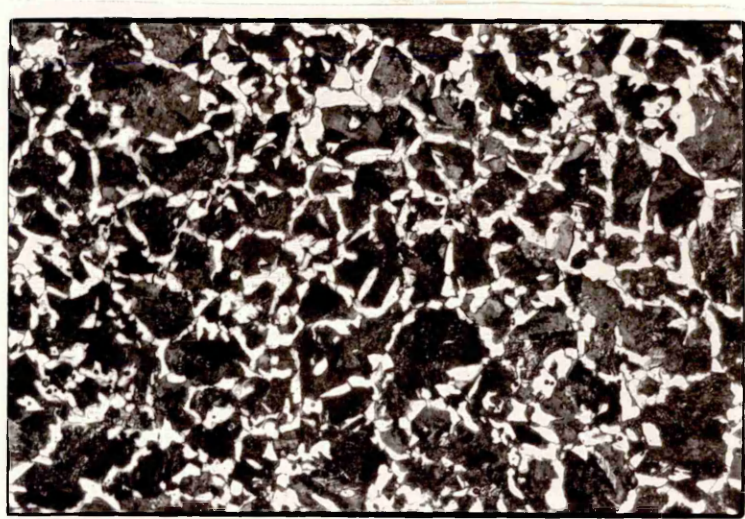
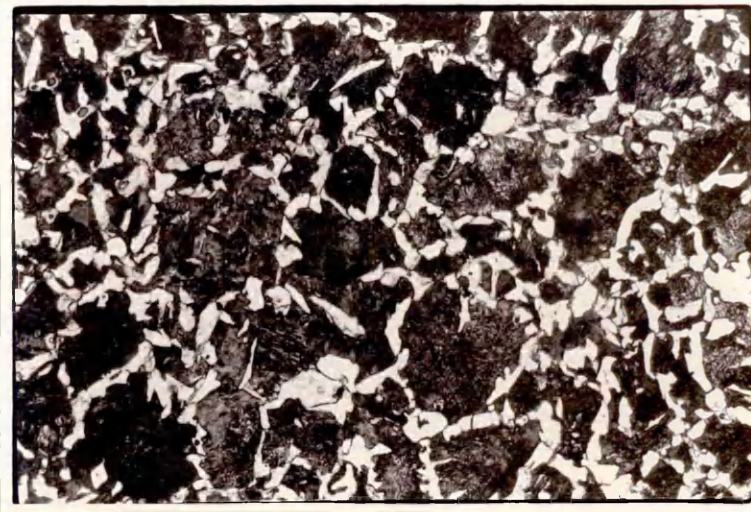
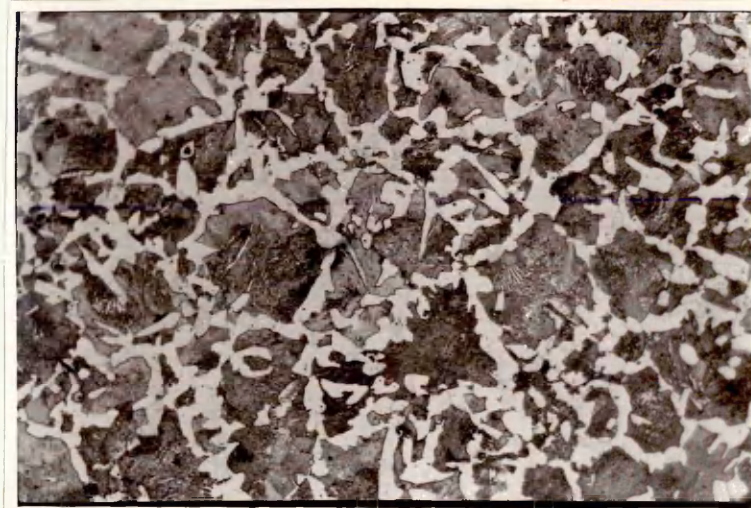


Fig.79 Normal micro-structure of as-received En-8 steel,  
showing ferrite (white) and pearlite (black),  
T-section, X 200.

(a)



(b)



(c)

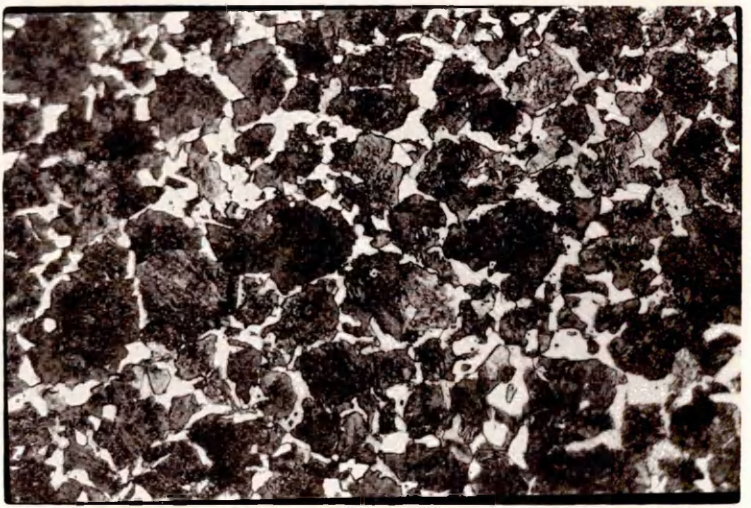
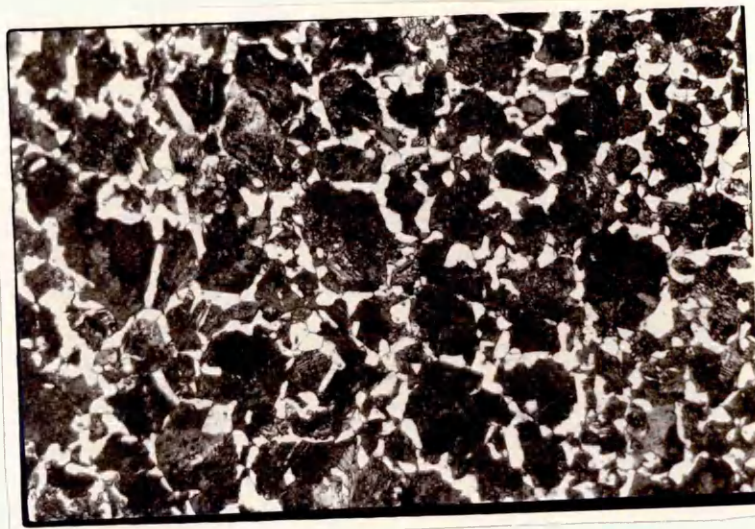
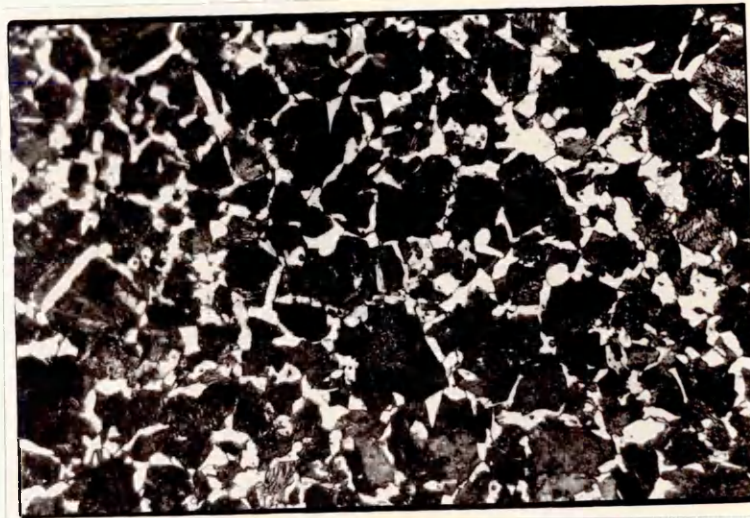


Fig.80 Showing structure of En-8 steel, deformed quasi-statically at (a) 22°C, (b) -30°C and (c) 235°C, total reduction about 20%, T-section, X 200.

(a)



(b)

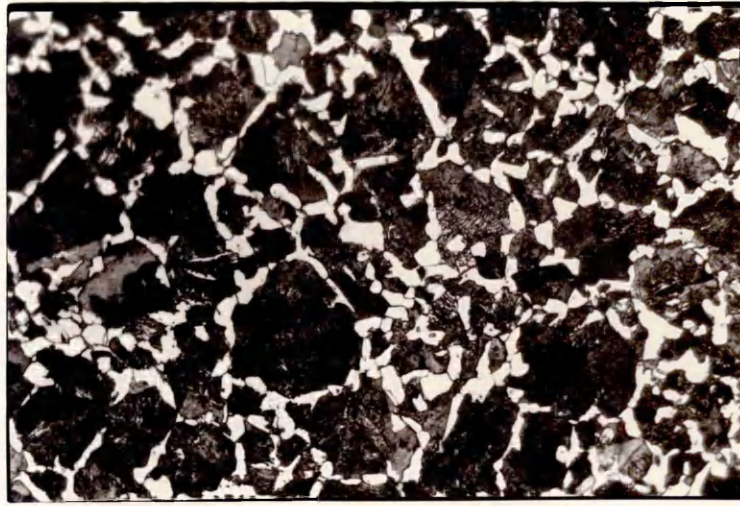


(c)

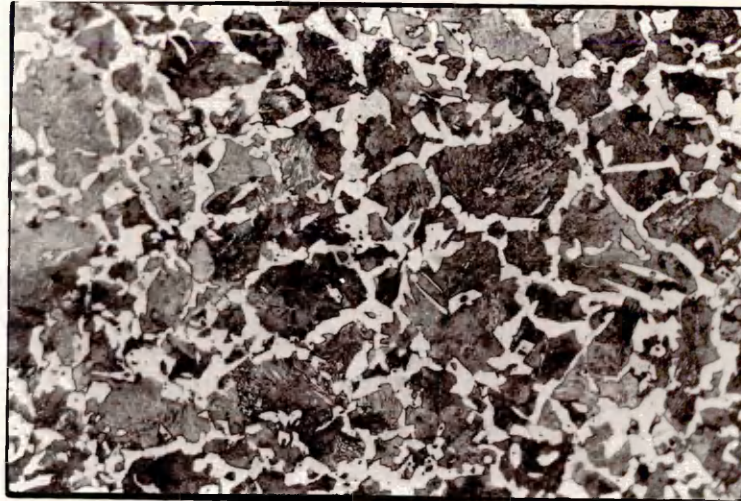


Fig.81 Showing structure of En-8 steel, deformed dynamically ( $\xi = 7 \times 10^3/s$ ) at (a) 22°C, (b) -30°C and (c) 235°C, total reduction about 10 %, T-section, X 200.

(a)



(b)



(c)

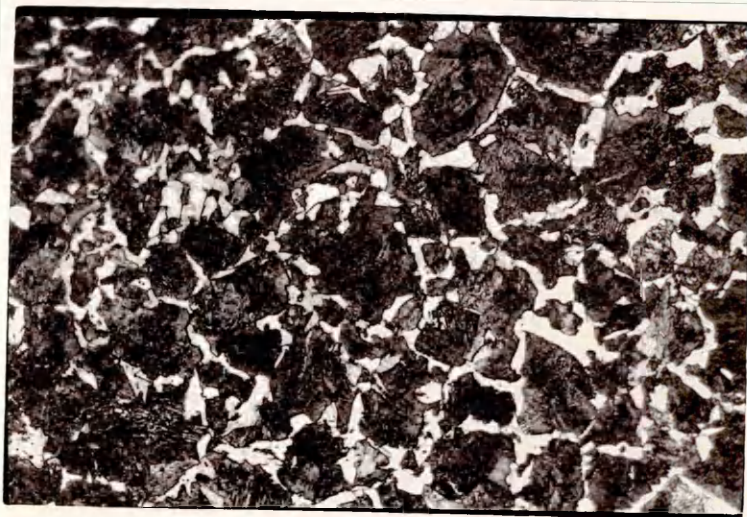
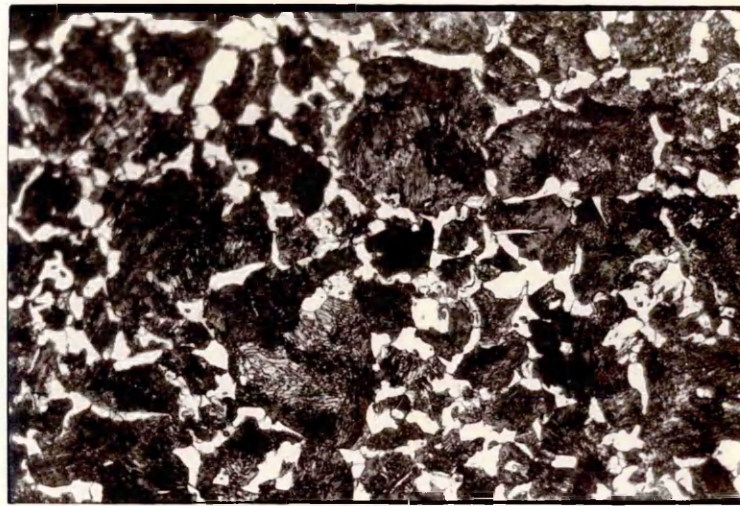
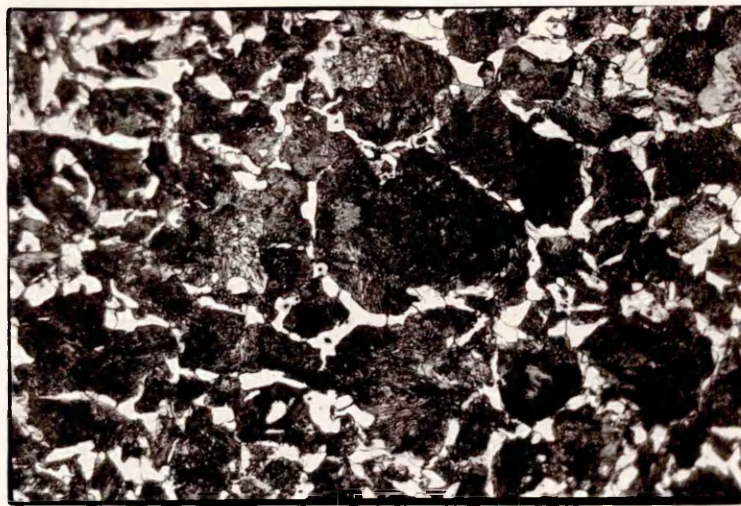


Fig.82 Showing structure of En-8 steel, deformed dynamically ( $\dot{\epsilon} = 2 \times 10^4/s$ ) at (a) 22°C, (b) -30°C and (c) 235°C, total reduction about 20%, T-section, X 200.

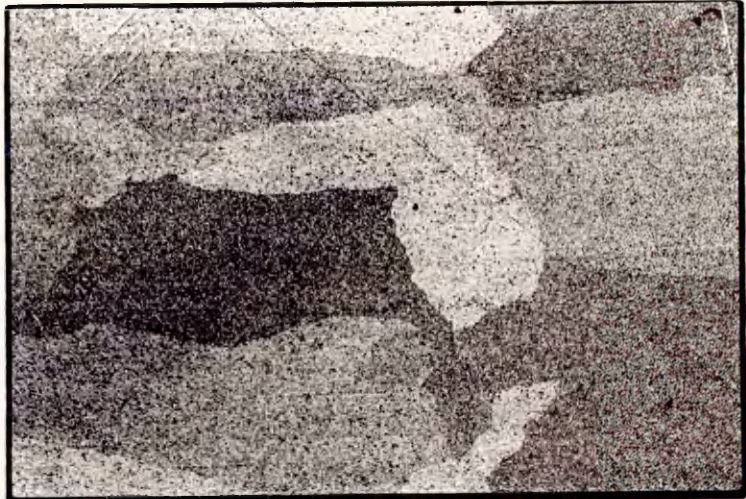


(a)



(b)

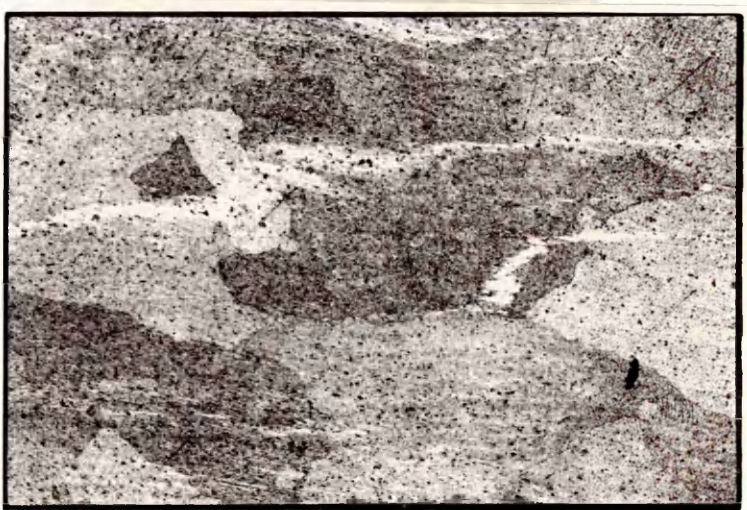
Fig.83 Showing structure of En-8 steel, deformed dynamically ( $\dot{\epsilon} = 10^5/s$ ) at (a)  $22^\circ C$  and (b)  $-30^\circ C$ , total reduction about 30 %, T-section, X 200.



(a)

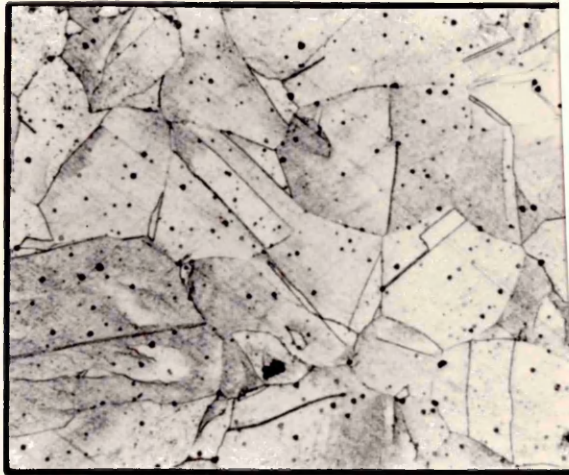


(b)

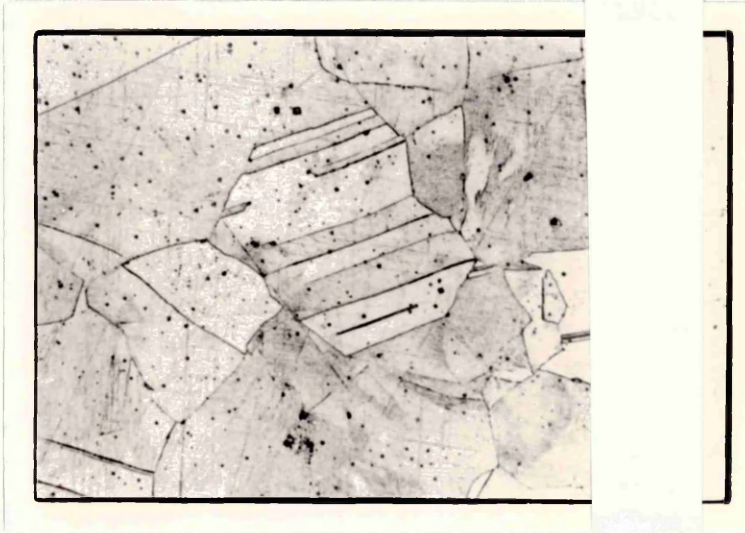


(c)

Fig.84 Showing structure of (a) as-received aluminium, (b) quasi-statically deformed and (c) dynamically ( $\dot{\epsilon} = 3.3 \times 10^4/s$ ) deformed, total reduction for (b) and (c) about 22 %, L-section, X 50.



(a)



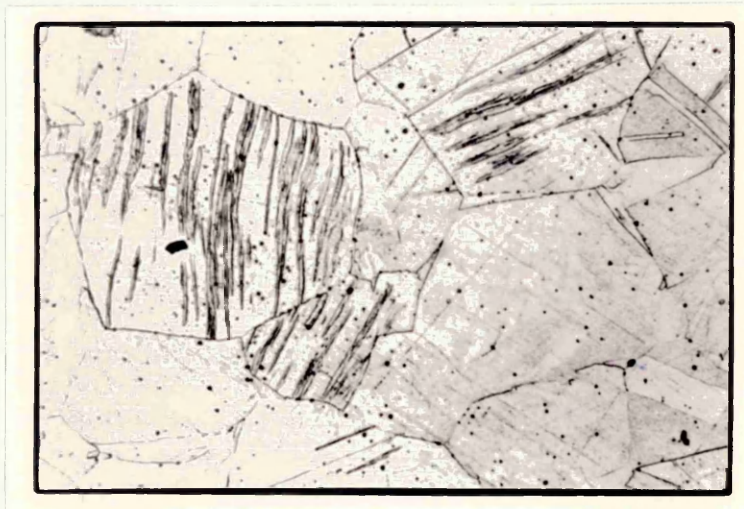
(b)

Fig.85 Structure of (a) as-received copper and deformed specimen, total reduction about 50%, showing grains, twinned grains and dispersion of particles (dark dots), T-section, X 2000

quasi-statically deformed specimen showing equiaxed grains and dispersion of particles (dark dots)



(a)



(b)

Fig.86 Structure of as-received copper deformed at (a)  $\dot{\epsilon} = 6.7 \times 10^3/s$  and (b)  $\dot{\epsilon} = 3.3 \times 10^4/s$ , total reduction about 24 %, showing mechanical twins in both structures, T-section, X 200.

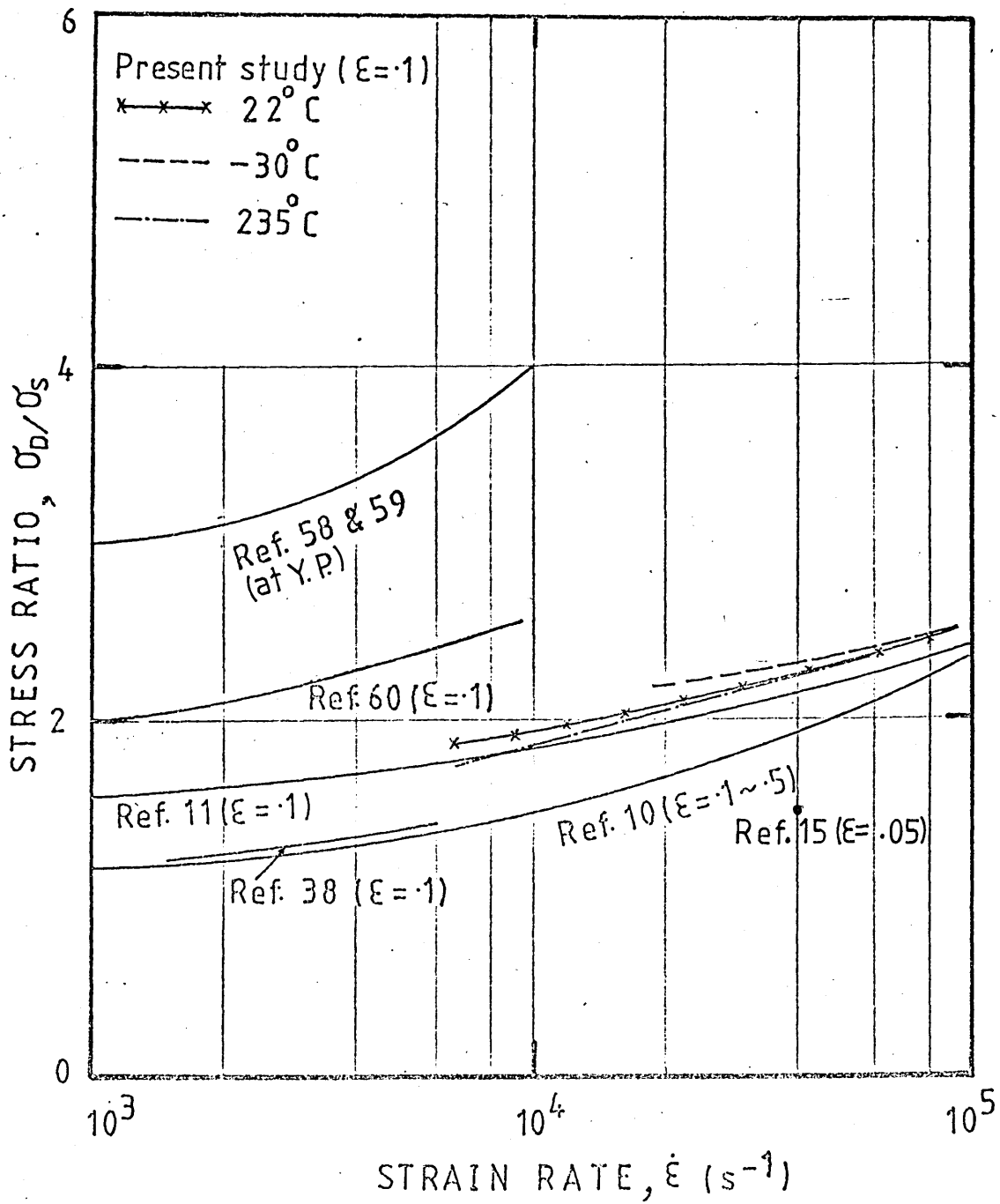


Fig.87 Showing the comparison of strain rate sensitivity of steel determined in the present study and those reported elsewhere.

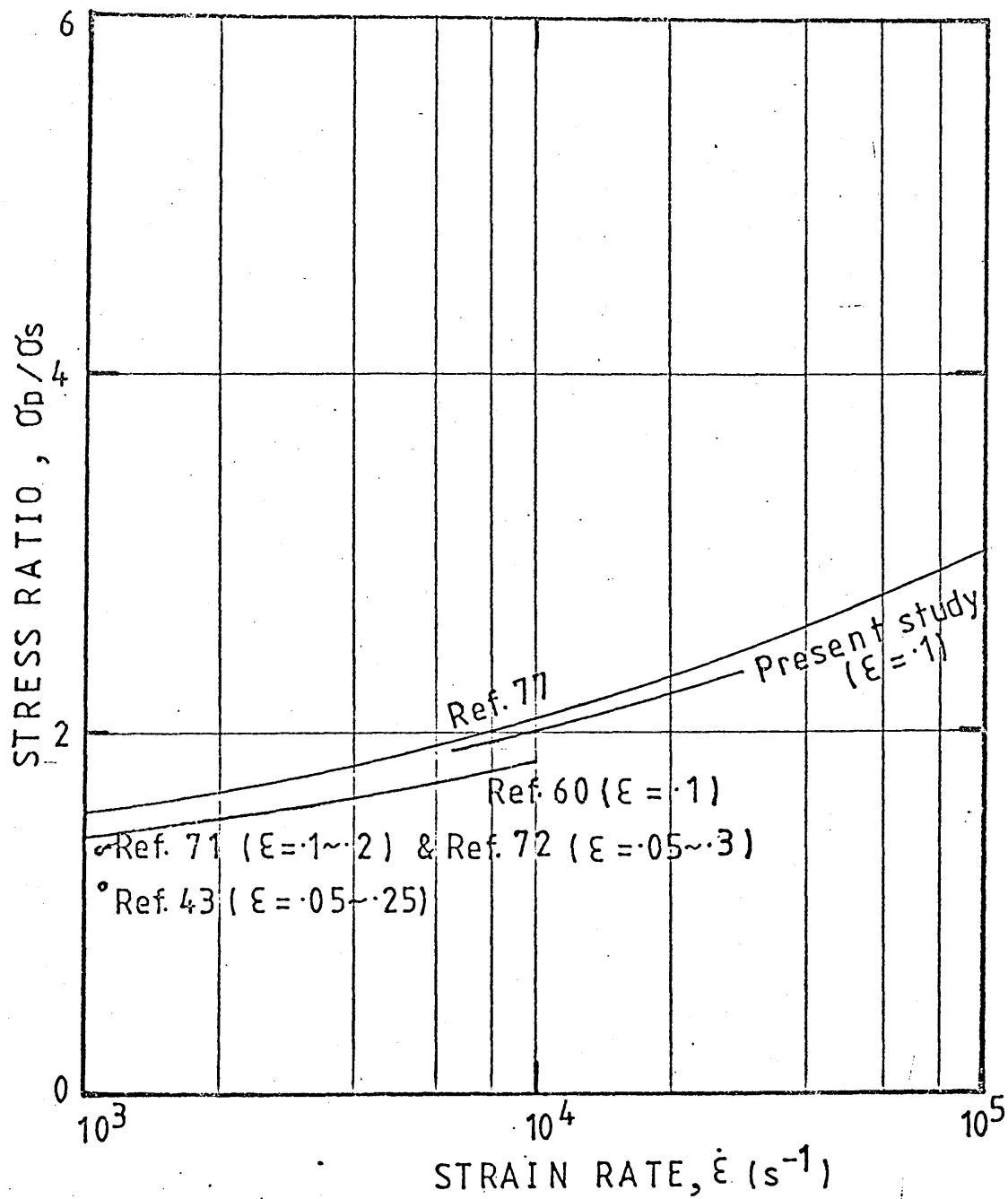


Fig.88 Showing the comparison of strain rate sensitivity of aluminium determined in the present study and those reported elsewhere.

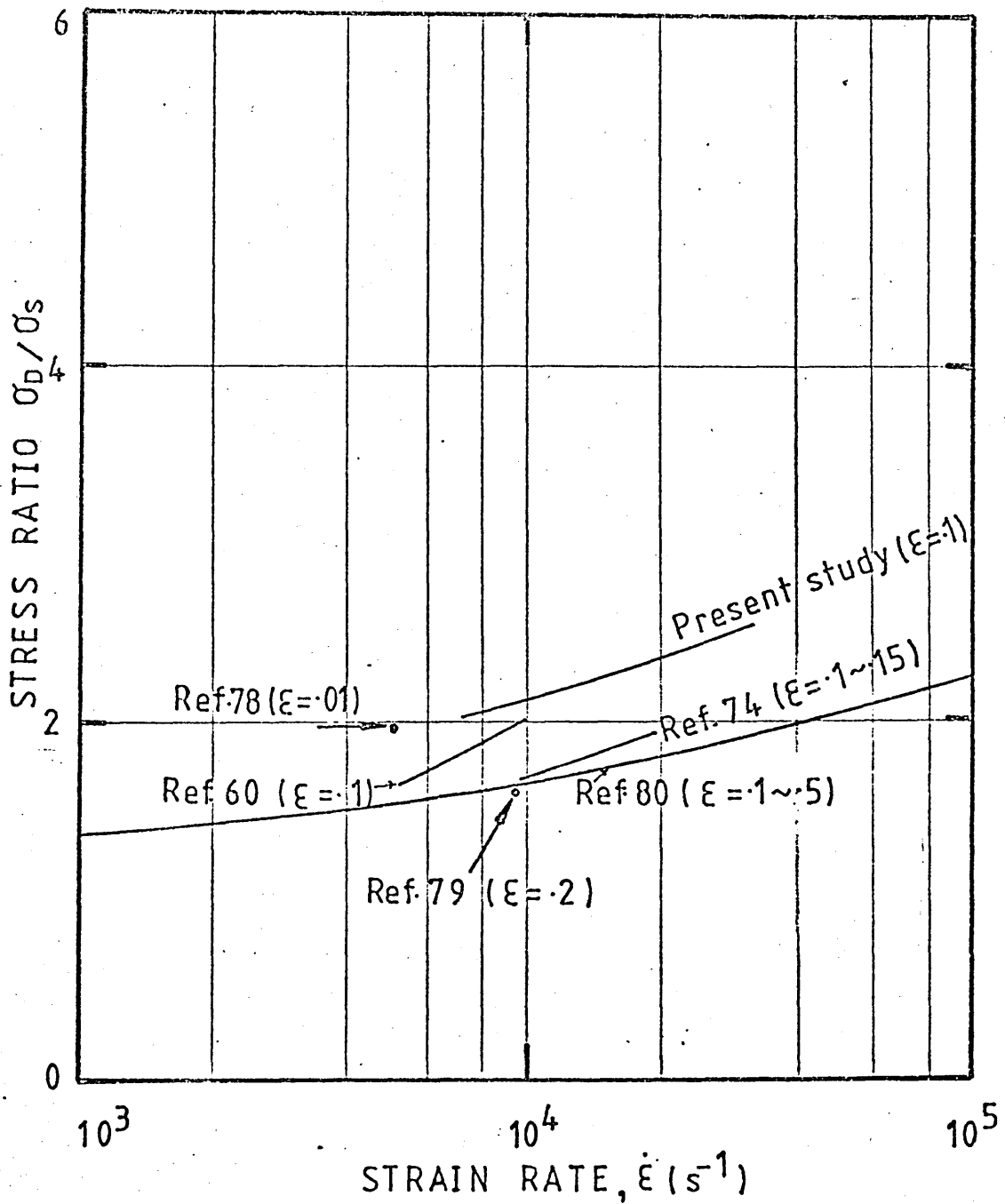


Fig.89 Showing the comparison of strain rate sensitivity of copper determined in the present study and those reported elsewhere.

## REFERENCES

1. J. Harding and J. Huddart, "The Use of the Double-Notch Shear Test in Determining the Mechanical Properties of Uranium at very High Rates of Strain", Inst. Phys. Conf. Ser. No. 47, 49, 1979.
2. W. Johnson, "Applications: Processes Involving High Strain Rates", Inst. Phys. Conf. Ser. No. 47, 337, 1979.
3. C. R. Johansson and P. A. Persson, "Detonics of High Explosives", New York, Academic Press, 1970.
4. N. G. Ohlson, "Determination of Crack Initiation at High Strain Rates", Inst. Phys. Conf. Ser. No. 47, 215, 1979.
5. A. Kandeil, J. P. Immariagon and W. Wallace, N R C Canada Aero. Rep. L R-595, 1978.
6. S. Clyens and W. Johnson, Mater. Sci. Engng., Vol. 30, 121, 1977.
7. G. Sachs, Spanlose Formung, 67, 1930.
8. E. Siebel, Steel, Vol. 93, 22, 1933.
9. G. Sachs, J. Inst. Met., Vol. 64, 261, 1939.
10. M. S. J. Hashmi, "A Technique of Assessing Strain Rate Sensitivity of a Mild Steel at Room Temperature and Strain Rates of Upto  $10^5$  per Second", J. of Strain Analysis, Instn. of Mech. Engrs., Vol. 15, 201, 1980.

11. P. L. B. Oxley and M. G. Stevenson, "Measuring Stress-Strain Properties at Very High Strain Rates Using a Machining Test", J. Inst. of Metals, Vol. 95, 308, 1967.
12. H. Kolsky, "An Investigation of the Mechanical Properties of Materials at Very High Rates of Loading", Proc. of the Physical Soc., London, Sec. B, Vol. 62, 676, 1949.
13. B. Lengyel and M. Mohitpour, "Dynamic Stress-Strain Data to Large Strains", J. Inst. Metals, Vo. 100, 1, 1972.
14. A. J. Holzer and R. H. Brown, "Mechanical Behaviour of Metals in Dynamic Compression", A S M E Trans., Vol. 101, 238, July 1979.
15. D. A. Gorham, "Measurement of Stress-Strain Properties of Strong Metals at Very High Rates of Strain", Inst. Phys. Conf. Ser. No. 47, 16, 1979.
16. A. C. Whiffin, "The Use of Flat Ended Projectiles for Determining Dynamic Yield Stress, Part-2, Test on Various Metallic Materials", Proc. Roy. Soc. A, Vol. 194, 300, 1948.
17. J. B. Hawkyard, D. E. Eaton and W. Johnson, "The Mean Dynamic Yield Strength of Copper and Low Carbon Steel at Elevated Temperatures from Measurements of the Mushrooming of Flat-ended Projectiles", Int. J. Mech. Sci., Vol. 10, 929, 1968.

18. S. K. Samanta, "Resistance to Dynamic Compression of Steel at Elevated Temperatures and at High Strain Rates", C I R P Conf. Paris, Sept. 1966.
19. C. E. N. Sturgess and M. G. Jones, "Estimation of Dynamic Forces in High Speed Compression Using a Free Flight Impact Forging Device", Int. J. Mech. Sci., Vol. 13, 309, 1961.
20. E. D. H. Davies and S. C. Hunter, "The Dynamic Compression Testing of Solids by the Method of the Split Hopkinson Pressure Bar", J. Mech. Phys. Solids, Vol. 11, 155, 1963.
21. A. L. Wingrove, "A Note on the Structure of Adiabatic Shear Bands in Steel", J. Aust. Inst. Metals, Vol. 16, 67, 1971.
22. S. A. Manion and T. A. C. Stock, "The Measurement of Strain in Adiabatic Shear Bands", J. Aust. Inst. Metals, Vol. 14, 190, 1969.
23. B. Lengyel and D. C. Stamelos, "On the Stress Strain Curves of Materials for Hydrostatic Cold Extrusion", Ann. C I R P, Vol. 19, 219, 1971.
24. N. C. Pandya and C. S. Shah, "Elements of Machine Design", Charotar Book Stall, Anand (India), 7th Ed., 173, 1978.
25. V. L. Doughtie, A. Vallance and L. F. Kreisle, "Design of Machine Members", McGraw-Hill Book Company, New York, 4th Ed., 134, 1964.

26. E. Siebel, "Principles for Calculating the Work and Energy Requirements in Forging and Rolling", Stahl and Eisen, Vol. 43, Pt. II, 1295, 1923.
27. A. B. Watts and H. Ford, "An Experimental Investigation of the Yielding of Strip Between Smooth Dies", Proc. Instn. Mech. Engrs. (B), 1B, 448, 1952.
28. D. R. Barraclough and C. M. Sellars, "Mechanical Properties at High Rates of Strain", Inst. Phys. Conf. Ser. No. 21, 111, 1974.
29. M. L. Wilson, R. H. Hawley and J. Duffy, Brown University, Rep. N S F - E N G 75-18532/8, 1979.
30. R. C. Smith, "Studies of Effect of Dynamic Preloads on Mechanical Properties of Steel", Expt. Mech., Vol. 1, 153, 1961.
31. T. Nicholas, "Strain Rate and Strain Rate History Effect in Several Metals in Torsion", Expt. Mech. Vol. 11, 153, 1971.
32. J. D. Campbell and J. Doby, "The Yield Behaviour of Mild Steel in Dynamic Compression", Proc. Roy. Soc., London, Ser. A, Vol. 236, 24, 1956.
33. J. D. Campbell and W. G. Ferguson, "The Temperature and Strain Rate Dependence of the Shear Strength of Mild Steel", Phil. Mag., Vol. 21, 63, 1970.

34. N. G. Ohlson, "The Effect of Strain History on Crack Initiation Under Dynamic Loading in Shock-wave and High Strain Rate Phenomena in Metals", Edited by M. A. Meyers and L. E. Murr, Plenum Press, New York, 193, 1981.
35. G. G. Brown and J. D. Watson, "The Tensile Properties of Pre-torsioned Steel Bars", Metals Forum, Vol. 5(4), 195, 1982.
36. M. Cook and E. C. Larke, "Resistance of Copper and Copper Alloys to Homogeneous Deformation in Compression", J. Inst. Metals, Vol. 71, 371, 1945.
37. S. K. Samanta, "Resistance to Dynamic Compression of Low Carbon Steel and Alloy Steels at Elevated Temperatures and at High Strain Rates", Inter. J. Mech. Sci., Vol. 10(8), 613, 1968.
38. R. L. Woodward and R. H. Brown, "Dynamic Stress - Strain Properties of a Steel and a Brass at Strain Rates Upto  $10^4$  per Second", Proc. Instn. Mech. Engrs., Vol. 189, 107, 1975.
39. K. K. Ray and A. K. Mallik, "On the Determination of Flow Properties from Compression Tests", Met. Trans., Vol. 14A, 155, 1983.
40. R. A. C. Slater, "Engineering Plasticity", The Macmillan Press Ltd., London, 272, 1977.

41. C. J. Maiden and S. J. Green, "Compressive Strain Rate Tests on Six Selected Materials at Strain Rates from  $10^{-3}$  to  $10^4$  in/in/Sec", J. of Appl. Mech., Trans. A S M E, 496, Sept. 1966.
42. S. K. Samanta, "Dynamic Deformation of Aluminium and Copper at Elevated Temperatures", J. Mech. Phys. Solids, Vol. 19, 117, 1971.
43. U. S. Lindholm, "Some Experimentals with the Split Hopkinson Pressure Bar", J. Mech. Phys. Solids, Vol. 12, 317, 1964.
44. K. Osakada, "A Mechanism of Lubrication Trapping in Slow Speed Compression", Inter. J. Mech. Sci., Vol. 19, 413, 1977.
45. P. J. Thompson and G. R. Symmons, "A Plasto-hydrodynamic Analysis of Disc Forging", Proc. Inter. Machine Tool Design and Research Conf., 587, Sept. 1976.
46. G. W. Rowe, 'Principles of Industrial Metal Working Processes', Edward Arnold, London, 291, 1977.
47. A. T. Male, Ph.D Thesis, University of Birmingham, Birmingham, U.K., 1962.
48. M. Mohitpour and B. Langyel, "Temperature Rise in the High Speed Compression of Right Cylindrical Billets", Proc. 2nd North American Metal Working Conf., Soc. Manuf. Enginrs., 48, 1974.

49. G. D. Lahoti and T. Altan, "Prediction of Temperature Distributions in Axisymmetric Compression and Torsion", Trans. A S M E, J. Engg. Mater. Tech., Vol. 97(2), 113, 1975.
50. W. S. Farren and G. L. Taylor, "The Heat Developed during Plastic Extension of Metals", Proc. Royal Soc., Series A, Vol. 107, 422, 1925.
51. R. N. Richardson and W. F. Hastings, "Predicting Tool-life and Build-up Edge Occurance when Machining Plain Carbon Steel with High Speed Steel Cutting Tools", Aust. Conf. on Manuf. Engg., 47, August 1977.
52. A. Nadai and M. J. Manjoine, "High Speed Tension Tests at Elevated Temperatures - Pt. II and III", J. of Appl. Mech. Vol. 8A, 77, June 1941.
53. T. Muller, "High Strain Rate Behaviour of Iron and Nickel", J. of Mech. Engg. Sci., Vol. 14(3), 161, 1972.
54. Abdel-Salam M. Eleiche, "Strain Rate History and Temperature Effects on the Torsional Shear Behaviour of a Mild Steel", Exptl. Mech. p-285, August 1981.
55. H. Conrad, "The Cryogenic Properties of Metals", in High Strength Materials, Wiley and Sons, New York, 436, 1964.
56. L. S. Costin, E. E. Crisman, R. H. Hawley and J. Duffy, "On the Localisation of Plastic Flow in Mild Steel Tubes under Dynamic Torsional Loading", Inst. Phys. Conf. Ser. No. 47, Edited by J. Harding, 90, 1979.

57. J. E. Hockett and E. G. Zukas, "The Response of Iron to Dynamic Compression", Inst. Phys. Conf. Ser. No. 21, 53, 1974.
58. P. S. Symonds, "Survey of Methods of Analysing for Plastic Deformation of Structures under Dynamic Loadings", Brown University, Report BU/NSRDC/1-67, 1967.
59. P. S. Symonds, "Visco-plastic Behaviour in Response of Structures to Dynamic Loading", Edited by N. J. Huffington, A S M E, 106, 1967.
60. A. R. Dowling, J. Harding and J. D. Campbell, "The Dynamic Punching of Metals", J. Inst. of Metals, Vol. 98, 215, 1970.
61. J. D. Campbell, R. H. Cooper and T. J. Fischhof, "The Dynamics of Nonuniform Plastic Flow in Low Carbon Steel", in Dislocation Dynamics, Edited by A R Rosenfield et al, McGraw-Hill Book Co., New York, 723, 1968.
62. W. C. Leslie, R. J. Sober, S. G. Babcock and S. J. Green, "Plastic Flow in Binary Substitutional Alloys of BCC Iron - Effects of Strain Rate, Temperature and Alloy Content", Trans. A S M, Vol. 62, 690, 1969.

63. N. Nagata, S. Yoshida and Y. Sekino, "Strain Rate, Temperature and Grain Size Dependence of the Lower Yield Stress of Polycrystalline Iron", Trans., I S I J., Vol. 10, 173, 1970.
64. K. Tanaka and T. Nojima, "Effects of the Strain Rate on the Strength of Steels", Proc. 22nd Cong. Mater. Res., Kyoto, Japan, Sept. 1978; Published by Soc. of Mater. Sci., Kyoto, Japan, 26 March 1979.
65. K. J. Marsh and J. D. Campbell, "The Effect of Strain Rate on the Post-yield Flow of Mild Steel", J. of Mech. Phys. Solids, Vol. 11, 49, 1963.
66. K. Tanaka and T. Nojima, "Dynamic and Static Strength of Steels", Inst. Phys. Conf. Ser. No. 47, Edited by J. Harding, 166, 1979.
67. J. A. Nock, Jr., in Physical Metallurgy of Aluminium Alloys, Edited by W. L. Fink, ASM, Metals Park, Ohio, 1949.
68. W. Helling et al, Metall., Vol. 5, 424, 1951.
69. E. Nachtingall, Aluminium, Vol. 31, 341, 1955.
70. J. E. Tomlinson, quoted by Pearson, Phillips, in Met. Rev., Vol. 2, 305, 1957.
71. P. E. Senseny, J. Duffy and R. H. Hawley, "Experiments on Strain Rate History and Temperature Effects during the Plastic Deformation of Close-Packed Metals", Trans. A S M E, J. of Appl. Mech., Vol. 45, 60, 1978.

72. S. Yoshida and N. Nagata, "Deformation of Polycrystalline Aluminium at High Strain Rates", Trans. Japan Inst. Metals, Vol. 7, 273, 1966.
73. A. E. Carden, P. E. Williams and R. R. Karp, "Comparison of the Flow Curves of 6061 Aluminium Alloy at High and Low Strain Rates", in Metallurgical Effect at High Strain Rates, Edited by R. W. Rohde et al, Plenum Press, New York, London, 37, 1981.
74. G. Sundararajan and P. G. Shewman, "The Use of Dynamic Impact Experiments in the Determination of the Strain Rate Sensitivity of Metals and Alloys", Acta Metallurgica, Vol. 31 (1), 101, 1983.
75. G. L. Wulf, "Dynamic Stress - Strain Measurements at Large Strains", Inst. Phys. Conf. Ser. No. 21, 48, 1974.
76. G. L. Wulf, "The High Strain Rate Compression of 7039 Aluminium", Int. J. Mech., Vol. 20, 609, 1978.
77. N. Jones and T. Wierzbicki, "Structural Crashworthiness" Butterworths & Co Ltd., London, 322, 1983.
78. I. M. Hutchings and T. J. Obrien, Int. J. Mech. Sci., Vol. 23, 255, 1981
79. J. Shiori, K. Satoh and K. Nishimura, I U T A M Symposium on High Velocity Deformation of Solids, Tokyo, Japan, 51, 1977.

80. M. S. J. Hashmi, "Strain Rate Sensivity of Commerically Pure Copper at Room Temperature and Strain Rates of Upto  $10^6$  per Second", Sheffield City Polytechnic Report No. SCP/MPE/R-106, October 1978.
81. W. C. Leslie, "Microstructural Effects of High Strain Rate Deformation", in Metallurgical Effect at High Strain Rates, Edited by R. W. Rohde et al, Plenum Press, New York, London, 571, 1973.
82. M. A. Meyers and L. E. Murr, "Defect Generation in Shock - Wave Deformation", in Shock - Wave and High Strain Rate Phenomena in Metals", Edited by M A Meyers and L E Murr, Plenum Press, New York, 487, 1981.
83. A. R. Champion and R. W. Rohde, "Hugoniot Equation of State and the Effect of Shock Stress Amplitude and Duration on the Hardness of Hadfield Steel", J. Appl. Phys., Vol. 41, 2213, 1970.
84. G. A. Stone, R. N. Orava, G. T. Gray and A. R. Pelton, "An Investigation of the Inlfuence of Shock-Wave Profile on the Mechanical and Thermal Response of Polycrystalline Iron", Final Technical Report, U.S. Army Research Office, Grant No: DAA 629-76-0181.
85. R. W. Rohde, "Dynamic Yield Behaviour of Shock-loaded Iron from 76 to  $573^{\circ}\text{K}$ , Acta Metallurgica, Vol. 17, 353, 1969.

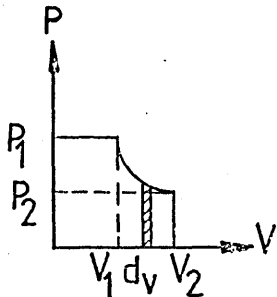
86. J. S. Erickson and J. R. Low, "The Yield Stress Temperature Relation for Iron at Low Temperature", Acta Metallurgica, Vol. 5, 405, 1957.
87. T. Muller, "The Visco-plastic Dynamic Behaviour of Iron and Nickel at Elevated Temperatures", Acta Metallurgica, Vol. 19, 691 1971.
88. L. E. Murr, H. R. Vydyanath and J. V. Foltz, "Comparison of the Substructures and Properties of Ni, TD - Ni, Chromel - A, Inconel 600, and TD - NiCr Following Explosive - Shock Deformation", Met. Trans. Vol. 1, 3215, 1970.
89. R. N. Orava, "Metallurgical Effects of High Energy Rate Forming", in Metallurgical Effects at High Strain Rates, Edited by R. W. Rohde et al, Plenum Press, New York, London, 129, 1973.
90. G. F. Bolling and R. H. Richman, "The Effect of Solute on Slip and Mechanical Twinning in Iron Alloys", Can. J. Phys. Vol. 45, 541, 1967.
91. D. A. Shockey and D. C. Erlich, "Metallurgical Influences on Shear Band Activity", in Shock-Wave and High Strain Rate Phenomena in Metals, Edited by M. A. Meyers and L. E. Murr, Plenum Press, New York, 249, 1981.
92. A. G. Dhere, H. J. Kestenback and M. A. Meyers, "Int. J. Mater. Sci. and Engg.", Vol. 54, 113, 1982.

93. R. J. DeAngelis and J. B. Cohen, "Effects of Shock Loading on Copper, Pt. III", J. of Metals, Vol. 15, 681, 1963.
94. O. Johari and G. Thomas, "Substructures in Explosively Deformed Copper and Copper - Aluminium Alloys", Acta Metallurgica, Vol. 12, 1153, 1964.
95. D. C. Brillhart, R. J. DeAngelis, A. G. Preban, J. B. Cohen and P. Gordon, "Quantitative Study of the Substructure and Properties of Shock-loaded Copper", Trans. AIME, Vol. 239, 836, 1967.
96. J. George, "An Electron Microscope Investigation of Explosively Loaded Copper", Phil. Mag., Vol. 15, 497, 1967.
97. F. I. Grace, "Shock-Wave Strengthening of Copper and Nickel", J. Appl. Phys., Vol. 40, 2649, 1969.

APPENDIX-A

The following fundamental calculations on the basis of which the design data were accepted to prepare the rig components.

Energy equations:



$P_1$  = Initial pressure of air,

$P_2$  = Final pressure of air,

$V_1$  = Initial volume of air,

$V_2$  = Final volume of air =  $V_1 + V_e$

where,

$V_e$  = Expanded volume ie volume of the barrel (primary barrel + extension barrel).

$$P_1V_1 = P_2V_2 = \text{Constant}, C = RT = PV, \text{ therefore } P = \frac{C}{V}$$

$$\text{Work done, } W = \int_{V_1}^{V_2} P \, dV = \int_{V_1}^{V_2} \frac{C}{V} \, dV = C \int_{V_1}^{V_2} \frac{dV}{V} = C \ln \frac{V_2}{V_1}$$

$$= P_1V_1 \ln \left( \frac{V_1 + V_e}{V_1} \right) = P_1V_1 \ln \left( 1 + \frac{V_e}{V_1} \right)$$

In accelerating a mass,  $m$  of the projectile from rest to a velocity,  $v$  the energy supplied =  $\frac{1}{2} mv^2$ , now using work-energy principle, it can be written as follows:

$$P_1V_1 \ln \left( 1 + \frac{V_e}{V_1} \right) = \frac{1}{2} mv^2$$

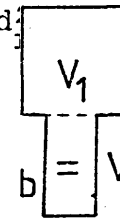
or 
$$P_1 = \frac{\frac{1}{2} mv^2}{V_1 \ln \left( 1 + \frac{V_e}{V_1} \right)} \dots\dots\dots (1)$$

Assumed dimensions of the reservoir and the barrel

(a) Assumed volume of the reservoir,  $V_1 = \frac{\pi}{4} d_r^2 l_r$  where,

$d_r$  = diameter of the reservoir = 76 mm,

$l_r$  = length of the reservoir = 100 mm.



Therefore,  $V_1 = \frac{\pi}{4} (76)^2 \times 100 \text{ (mm)}^3$   $V \text{ m}^3 / e$

or  $V_1 = 442000 \text{ (mm)}^3 = 4.42 \times 10^{-4} \text{ m}^3$

(b) Assumed volume of the barrel,  $V_b = \frac{\pi}{4} d_b^2 l_b$  where,

$d_b$  = diameter of the barrel = 10 mm,

$l_b$  = length of the barrel = 1000 mm.

Therefore,  $V_b = V_e = \frac{\pi}{4} (10)^2 \times 1000 \text{ (mm)}^3$ ,

or, assumed expanded volume,  $V_e = 7.85 \times 10^{-5} \text{ m}^3$

(c) Assumed volume of the projectile,  $V_p = \frac{\pi}{4} d_p^2 l_p$  where,

$d_p$  = diameter of the projectile = 9.5 mm,

$l_p$  = length of the projectile = 19 mm.

Therefore,  $V_p = \frac{\pi}{4} (9.5)^2 \times 19 \text{ (mm)}^3$

or  $V_p = 1347 \text{ (mm)}^3 = 1.35 \times 10^{-6} \text{ m}^3$

Mass,  $m$  of the projectile =  $\rho \times V_p$  where,

$\rho = 7.8 \times 10^3 \text{ Kg/m}^3$

Therefore,  $m = 7.8 \times 10^3 \times 1.35 \times 10^{-6} \text{ Kg} = 10^{-2} \text{ Kg}$

(d) Assumed velocity,  $v$  of the projectile = 400 m/s

Therefore, Energy supplied =  $\frac{1}{2} mv^2 = \frac{1}{2} \times 10^{-2} \times (400)^2$   
 $= 8 \times 10^2 \text{ J}$

Now required reservoir pressure,  $P_1$  can be calculated from equation (1):

$$P_1 = \frac{\frac{1}{2} mv^2}{V_1 \ln \left( 1 + \frac{V_e}{V_1} \right)} \text{ pascal}$$

$$\text{Therefore, } P_1 = \frac{8 \times 10^2}{7.226 \times 10^{-5}} \text{ pa}$$

$$\begin{aligned} \text{or} \quad &= \frac{8 \times 10^2}{7.226 \times 10^{-5} \times 6.9 \times 10^3} \text{ psi} \\ &= 1605 \text{ psi} \end{aligned}$$

This pressure has been counter checked by Newton's Second Law of Motion: Force,  $F = \text{Mass, } m \times \text{Acceleration, } a$ ; Acceleration, 'a' can be calculated from the following equation: (assuming constant acceleration throughout)

$$v^2 = u^2 + 2as \text{ where,}$$

$$v = \text{final velocity of the projectile} = 400 \text{ m/s}$$

$$u = \text{initial velocity} = 0$$

$$s = \text{distance} = 1 \text{ m}$$

$$\text{Therefore, acceleration 'a'} = ((400)^2/2)\text{m/sec}^2 = 8 \times 10^4 \text{ m/sec}^2$$

$$\text{Hence, } F = ma \approx 8 \times 10^2 \text{ N}$$

Therefore, reservoir pressure ' $P_1$ ' =  $F/A$  where,

$$\begin{aligned} A &= \text{cross-sectional area of the barrel} = \frac{\pi}{4} d_b^2 \\ &= \frac{\pi}{4} \times 10^2 \times 10^{-6} \text{ m}^2 \end{aligned}$$

Therefore,  $P_1 = 10.2 \times 10^6 \text{ pa} = 1478 \text{ psi}$  and hence the previous one is acceptable.

Assuming expanded volume constant throughout all the

following calculations, the available air pressure is again checked with varying  $V_1$  as shown in the following table.

$\frac{V_e}{V_1}$	$V_1$ (m <sup>3</sup> )	$V_1 \ln \left( 1 + \frac{V_e}{V_1} \right)$	$P_1 = \frac{\frac{1}{2} m v^2}{V_1 \ln \left( 1 + \frac{V_e}{V_1} \right)}$ pa	$P_1$ (psi)
0.1	$7.85 \times 10^{-4}$	$7.482 \times 10^{-5}$	$1.02 \times 10^7$	$1.478 \times 10^3$
0.2	$3.93 \times 10^{-4}$	$7.156 \times 10^{-5}$	$1.118 \times 10^7$	$1.620 \times 10^3$
0.3	$2.62 \times 10^{-4}$	$6.865 \times 10^{-5}$	$1.165 \times 10^7$	$1.688 \times 10^3$

Therefore, it is clear from above table that the assumed volume of the reservoir (about  $4 \times 10^{-4}$  m<sup>3</sup>) would be acceptable for the required air pressure (ie for 1600 psi).

#### APPENDIX-B

##### Design of thick walled close ended pressure vessel:

Clavarino's equation (for ductile material):

$$\text{Wall thickness, } t = \frac{d_i}{2} \left[ \sqrt{\frac{S_{t'} + (1 - 2\mu) p_i}{S_{t'} - (1 + \mu) p_i}} - 1 \right] \dots (2)$$

where,  $d_i$  = internal diameter in inch = 3" (assuming),

$S_{t'}$  = permissible working stress in tension, psi,

$\mu$  = Poisson's ratio = 0.3 and

$p_i$  = internal pressure = 2000 psi

For En-16 steel,  $S_{t'} = \frac{\sigma_{ut}}{\text{safety factor}}$

where,  $\sigma_{ut}$  = allowable ultimate tensile stress = 45 tsi

and taking factor of safety 3,  $S_{t'}$  comes

about 15 tsi ie about  $30 \times 10^3$  psi.

Therefore, from equation (2), the wall thickness 't' comes out about 0.090345 inch ie about 2.3 mm.

Birnie's equation for open cylinders:

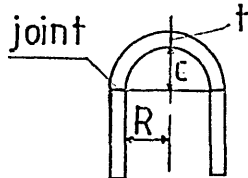
$$\text{Wall thickness, } t = \frac{d_i}{2} \left[ \sqrt{\frac{S_{t'} + (1 - \nu) p_i}{S_{t'} - (1 + \nu) p_i}} - 1 \right] \dots(3)$$

According to this equation, the wall thickness comes about 2.686 mm.

APPENDIX-C

Design of End Covers:

The thickness of the curved ends is given by the following equation, taken from ref (24):

$$\text{Thickness, } t = p \left( \frac{R^2 + C^2}{4\sigma t' C} \right) \dots\dots\dots(4)$$


where, R = radius of the reservoir  
 = 38 mm = 38 x 10<sup>-3</sup> m.

C = mean curvature of the end cover  
 = 7 mm = 7 x 10<sup>-3</sup> m.

p = internal pressure = 2000 psi  
 = 2000 x 6.9 x 10<sup>3</sup> N/m<sup>2</sup>.

σt' = allowable tensile stress of the end material and for En-16 steel, it is taken about 30 x 10<sup>3</sup> psi  
 = 30 x 10<sup>3</sup> x 6.9 x 10<sup>3</sup> N/m<sup>2</sup>

Therefore, thickness of the end cover comes about 3.55 mm.

APPENDIX-D

Design of Reservoir Bolts:

For 2000 psi air tight joints, bolts of diameter less than  $\frac{1}{2}$ " are not suitable as they yield on initial tightening. For a gas tight joint, a tightening load of about  $(16000 \times D)$  lb is usually required (25) where, D is the nominal bolt diameter. Therefore, initial tightening stress,

$$\sigma_i = \frac{\text{Initial load}}{\text{Root area}}$$

The stressing area (ie root area) of the bolt,

$$A_r = \frac{\pi}{4} (d_r)^2 \text{ where, } d_r = \text{root diameter}$$

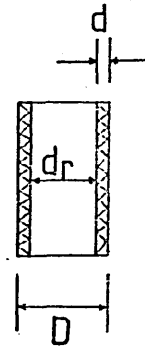
$$= 84.66 \text{ mm}^2$$

$$= 0.1313 \text{ in}^2.$$

$$= D - 2d \text{ where,}$$

$$D = \text{nominal diameter} = 12 \text{ mm.}$$

$$d = \text{depth of thread} = 0.8088 \text{ mm.}$$



$$\text{Therefore, } \sigma_i = \frac{16000 \times 12/25.4}{0.1313} = 57,604.5 \text{ psi.}$$

For high pressure air tight joint, high quality bolt material is to be selected. Therefore, SAE-2320 or Equivalent En-22 nickel steel (hardened and oil quenched condition) was chosen, which gives the following stress value:

$$\text{Ultimate tensile stress, } \sigma_u = 110,000 \text{ psi}$$

$$\text{Tensile yield stress, } \sigma_y = 85,000 \text{ psi}$$

Now subtracting the initial tightening stress from yield stress, it will give the available stress for gas

load.

$$\begin{aligned}\text{Hence, available stress, } \sigma_a &= \sigma_y - \sigma_i \\ &= (85,000 - 57,604) \text{ psi} \\ &= 27,396 \text{ psi}\end{aligned}$$

Here taking factor of safety as 2, the available load capacity per bolt over the stressing area,  $F_a$

$$\begin{aligned}&= A_r \times \sigma_a / 2 \\ &= 0.1313 \times 27,396 / 2 \\ &= 1797.5 \text{ lb}\end{aligned}$$

Total gas load on the end cover plate,  $F_t$

$$\begin{aligned}&= \frac{\pi}{4} (76/25.4)^2 \times 2000 \text{ lb} \\ &= 14,062.64 \text{ lb}\end{aligned}$$

Therefore, No. of bolts required:  $N = F_t / F_a$

$$\begin{aligned}&= 14,062.64 / 1797.5 \\ &= 8 \text{ (approximately)}\end{aligned}$$

The probable stress in each bolt is given by the following equation, taken from ref. (25):

$$= \sigma_i + \frac{KF_t}{NA_r} \dots\dots\dots(5)$$

where  $K$ , = gasket factor = 0.75 for soft gasket.

Therefore, probable stress,  $\sigma$

$$= 57,604 + \frac{0.75 \times 14062}{8 \times 0.1313} \text{ psi}$$

= 67651 psi which is about 80% of the yield stress

and therefore, should be satisfactory.

Hence, reservoir bolt should be of the following specifications:

Bolt size: M 12 x 1.75

No. of bolts: 8

Material: SAE-2320 or En-22 (hardened and oil quenched).

### APPENDIX-E

#### Design of Pressure Column:

According to American Institute of Steel Construction, safe working stress,  $\sigma_w$  of a steel column whose  $l/k < 120$  is given by:

$$= 119 - 0.0034 (l/k)^2 \text{ and}$$

max. safe load,  $P_c = \sigma_w \times A$  where,

$l$  = length of the column

$$= 300 \text{ mm} = 0.3 \text{ m}$$

$k$  = radius of gyration w.r.t. an axis

(here X---X)

$$= \sqrt{I_{XX}/A} \text{ where, } I_{XX} = \text{second moment of}$$

area

$$= \pi r^4 / 4 \text{ where, } r = \text{radius of the column}$$

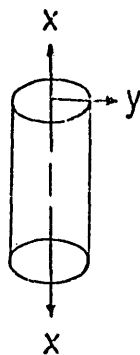
$$= 24 \text{ mm and}$$

$A$  = cross-sectional

area of the column

$$= \pi r^2$$

$$= 1810 \times 10^{-6} \text{ m}^2$$



$$\text{Therefore, } k = \sqrt{I_{XX}/A} = \sqrt{\frac{\pi r^4 / 4}{\pi r^2}} = r/2 = 12 \text{ mm}$$

Hence,  $1/k = 300 \text{ mm}/12 \text{ mm} = 25$

$$\begin{aligned} \text{Safe working stress, } \sigma_w &= 119 - 0.0034 \times (25)^2 = 119 - 2.125 \\ &= 116.875 \text{ MPa} = 116.875 \times 10^3 \text{ kN/m}^2 \end{aligned}$$

Therefore, maximum safe load,  $P_c$

$$= 116.875 \times 10^3 \text{ kN/m}^2 \times (1810 \times 10^{-6})^2 = 211.5 \text{ kN}$$

Hence, the column should be safe to withstand maximum load upto 211.5 kN.

#### APPENDIX-F

In formulating the constitutive equation for the results obtained in this study, a number of equations were attempted. The following are typical examples of these:

$$\sigma_D = A\epsilon^n \left( \ln \frac{\dot{\epsilon}}{\dot{\epsilon}_0} \right)^m \dots\dots\dots(1)$$

$$\sigma_D = A\epsilon^n \left[ 1 + \ln \frac{\dot{\epsilon}}{\dot{\epsilon}_0} \right] \dots\dots\dots(2)$$

$$\sigma_D = A\epsilon^n \left[ 1 + (b - c\epsilon) \ln \frac{\dot{\epsilon}}{\dot{\epsilon}_0} \right] \dots\dots\dots(3)$$

$$\sigma_D = A\epsilon^{n\alpha} (1 + Bf^3) \dots\dots\dots(4)$$

where,  $\alpha = e^{-f \cdot 25}$  and  $f = \ln (\dot{\epsilon}/\dot{\epsilon}_0)$

The stress-strain curves obtained using equations (1) to (3) did not fit closely with the experimental results due to the fact that the strain hardening index 'n' was also found to be influenced by strain rate. Hence the equation (4) was finally attempted which accommodated

variation of the index 'n' and gave closer results with those obtained experimentally.

Hence, when  $\dot{\epsilon} = 7.32 \times 10^3/s$ , (putting  $\dot{\epsilon}_0 = \text{const.} 1/s$ )  
then,  $\ln (7.32 \times 10^3) = \ln 7.32 + 3 \ln 10 = 1.99 +$   
 $6.9 = 8.89$

i.e.  $f = 8.89$  and  $f^3 = 703$ .

Similarly, when  $\dot{\epsilon} = 8.75 \times 10^4/s$ , then

$\ln (8.75 \times 10^4) = 11.37$ , i.e.  $f = 11.37$  and  $f^3 = 1470$ .

The values of the constants A, n and B for structural steel were found to be as follows:

$$A = 1 \text{ kN/mm}^2, n = 0.18, B = 5.85 \times 10^{-4}$$

Now, putting these values to the equation (4), the dynamic stress value at  $\dot{\epsilon} = 7.32 \times 10^3$  per second and at  $\epsilon = .05$  was calculated as follows:

$$\sigma_D = \left[ 1 \times (.05)^{.18} e^{-(8.89) \cdot .25} \times \right. \\ \left. (1 + 5.85 \times 10^{-4} \times 703) \right] \text{ kN/mm}^2$$

$$= \left[ (.05)^{.032} \times (1 + 0.411255) \right] \text{ kN/mm}^2$$

$$= (0.9085 \times 1.411255) \text{ kN/mm}^2$$

$\approx 1.28 \text{ kN/mm}^2$  and when  $\epsilon = .40$ , the dynamic stress was found to be  $1.37 \text{ kN/mm}^2$ .

Similarly, when  $\dot{\epsilon} = 8.75 \times 10^4/s$ , the dynamic stress values were found to be as follows:

$$\sigma_D = 1.70 \text{ kN/mm}^2, \text{ when } \epsilon = .05$$

$$\sigma_D = 1.82 \text{ kN/mm}^2, \text{ when } \epsilon = .40.$$

APPENDIX-G

$$\text{Total force, } F = \pi r^2 Y + \pi r^2 Y I$$

where,  $I = \frac{3}{16} \rho \frac{V^2}{Y} \left( \frac{r}{h} \right)^2$ , a dimensionless parameter.

Inertia contribution to the total force,  $F$  can be calculated as

$$= \frac{\pi r^2 Y I}{\pi r^2 Y (1 + I)} = \frac{I}{1 + I}$$

Value of  $I$  for strain rate of about  $7.3 \times 10^3 \text{ sec}^{-1}$  at 2% strain (upto acceptable range of constant strain rate) was calculated as:

$$V = 45 \text{ m/s, therefore, } V^2 = 2025 \text{ m}^2/\text{s}^2$$

$$Y = 1.2 \text{ kN/mm}^2 = 1200 \text{ N/mm}^2 = 1200 \times 10^6 \text{ N/m}^2$$

$$\text{Since, } 1\text{N} = \text{Kg. m/s}^2$$

$$\text{Therefore, } Y = 1200 \times 10^6 \text{ Kg/s}^2\text{m}$$

$$\text{Density, } \rho = 7.862 \times 10^3 \text{ Kg/m}^3$$

$$\text{Initial radius of the specimen} = 3.25 \text{ mm}$$

$$\text{Initial height of the specimen} = 6.00 \text{ mm}$$

Strain,  $\epsilon = \ln \frac{h_0}{h} = 0.02$  where,  $h$  = current height of the specimen.

$$\text{Therefore, } \frac{h_0}{h} = e^{.02} \text{ ie } h_0 = h \times e^{.02}$$

Therefore, current height of the specimen,  
 $h = h_0 \times e^{-.02} = 6.0 \times e^{-.02} = 5.881192 \text{ mm.}$

$$\text{Volume, } V_0 = \pi r_0^2 \times h_0 = \pi r^2 \times h$$

$$\text{Therefore, } r = \sqrt{\frac{r_o^2 \times h_o}{h}} = \sqrt{\frac{(3.25)^2 \times 6.0}{5.881192}} = 3.28266 \text{ mm}$$

$$\text{Hence, } \left(\frac{r}{h}\right)^2 = \left(\frac{3.28266}{5.88119}\right)^2 = 0.31154$$

$$\begin{aligned} \therefore I &= \frac{3}{16} \times (7.862 \times 10^3 \text{ Kg/m}^3) \times (2025 \text{ m}^2/\text{s}^2) \\ &\times \left(\frac{1 \times \text{s}^2 \text{ m}}{1200 \times 10^6 \text{ Kg}}\right) \times (0.31154) \\ &= 0.000775 \end{aligned}$$

Therefore, Inertia effect comes out about 0.0007744 ie about 0.08%.

For strain rate of about  $9 \times 10^4$  per second, the strain upto acceptable range of constant strain rate = 14.75%.

Initial radius of the specimen = 3.25 mm

Initial height of the specimen = 1.65 mm

Current height at 14.75% strain found about 1.4237 mm and current radius found about 3.4987 mm.

$$\left(\frac{r}{h}\right)^2 = 6.039$$

$$V = 148 \text{ m/s}$$

$$Y = 1.8 \text{ kN/mm}^2 = 1800 \times 10^6 \text{ Kg/ms}^2$$

Therefore, value of I found to be about 0.1076 which gave the value of  $\left(\frac{I}{1+I}\right)$  about 0.097 ie 9.7%.

Therefore, inertial effect found to be about 9.7%.

APPENDIX-H

The coefficient of friction,  $\mu_D$ , during dry quasi-static test was found by:

$$\mu_D = \left[ \frac{\sigma_{SD}}{Y} - 1 \right] / \frac{2}{3} \cdot \frac{r}{h} \quad \text{where, } Y = \sigma_S / \left( 1 + \frac{2}{3} \mu \frac{r}{h} \right)$$

Initial radius of the specimen = 3.50 mm

Initial height of the specimen = 3.00 mm

Current height of the specimen at strain of 40% found to be about 2.0109mm and that of the radius found to be about 4.2749 mm.

Therefore, the ratio of current radius to current height = 2.1258. Hence, the frictionless flow stress, Y, at room temperature was calculated as follows:

$$\sigma_S = 0.8205 \text{ kN/mm}^2$$

$$\mu = 0.01$$

$$Y = 0.8205 / \left[ 1 + \frac{2}{3} \times 0.01 \times 2.1258 \right] = 0.809 \text{ kN/mm}^2$$

$\sigma_{SD} = 0.9725 \text{ kN/mm}^2$  at room temperature and therefore  $\mu_D$ , at room temperature was found to be about 0.14.

Similarly, value of Y at 235°C was calculated to be about 0.7986 kN/mm<sup>2</sup> when  $\sigma_S = 0.8100 \text{ kN/mm}^2$ .

$\sigma_{SD} = 0.9635 \text{ kN/mm}^2$  at 235°C and hence,  $\mu_D$ , at 235°C was found to be about 0.15.

APPENDIX-I

Temperature rise during deformation was calculated using following equation:

$$\Delta T = \frac{0.865}{\rho S} \times A \text{ where, } A = \int_0^{\epsilon_f} \sigma d\epsilon$$

Area, A, under the true stress - true strain curve, was calculated for strain rate of about  $10^5$  per second, in the following way:

The stress value corresponding to 14.75% strain (ie upto acceptable range of constant strain rate) was found to be about 1.80 kN/mm<sup>2</sup>. This corresponds to an area of 3050 mm<sup>2</sup> under the shaded curve, A.

Therefore, 0.2 kN/mm<sup>2</sup> x 0.1475 (true strain) = 0.0295 kN/mm<sup>2</sup> represents about 10 x 37 ie 370 mm<sup>2</sup> in the shaded curve.

Since, 370 mm<sup>2</sup> represents 0.0295 kN/mm<sup>2</sup>

∴ 1 mm<sup>2</sup> represents 0.0295 kN/mm<sup>2</sup>/370

∴ 3050 mm<sup>2</sup> represents  $\frac{0.0295 \times 3050}{370}$  kN/mm<sup>2</sup>

= 0.2431 kN/mm<sup>2</sup>

Therefore A = 0.2431 kN/mm<sup>2</sup> = 0.2431 x 10<sup>3</sup> N/mm<sup>2</sup>

= 0.2431 x 10<sup>9</sup> N/m<sup>2</sup>

Specific heat, 'S', was calculated from the following equation:

$$S(\text{J/Kg}^\circ\text{K}) = 420 + 0.504T \text{ where, } T \text{ in } ^\circ\text{C}.$$

At room temperature ie at 22<sup>o</sup>C, the specific heat was found to be about 431.088 J/Kg<sup>o</sup>K.

$$\rho = 7862 \text{ Kg/m}^3$$

$$\Delta T = \frac{0.865 \times 0.2431 \times 10^9 \text{ N/m}^2}{(7862 \text{ Kg/m}^3) \times (431.000 \text{ J/kg}^\circ\text{K})}$$

$$= 62 \text{ (Nm/J)}^\circ\text{K}$$

$$= 62^\circ\text{K, since } J = \text{Nm}$$

